UNIVERSITY OF SOUTHAMPTON
FACULTY OF PHYSICAL SCIENCES AND ENGINEERING
SCHOOL OF ELECTRONICS AND COMPUTER SCIENCE

Design and Optimisation of User-Centric Visible-Light Networks

by

Xuan Li
B.Eng

A doctoral thesis submitted in partial fulfilment of the
requirements for the award of Doctor of Philosophy
at the University of Southampton

August 2016

SUPERVISOR:
Prof. Lajos Hanzo
FREng, FIEEE, FIEE, DSc, EIC of IEEE Press
Chair of Southampton Wirelss Group
and
Dr. Rong Zhang
School of Electronics and Computer Science
University of Southampton
Southampton SO17 1BJ
United Kingdom

Dedicated to my family

UNIVERSITY OF SOUTHAMPTON

ABSTRACT

FACULTY OF PHYSICAL SCIENCES AND ENGINEERING
SCHOOL OF ELECTRONICS AND COMPUTER SCIENCE

Doctor of Philosophy

Design and Optimisation of User-centric Visible-Light Networks

by Xuan Li

In order to counteract the explosive escalation of wireless tele-traffic, the communication spectrum has been gradually expanded from the conventional radio frequency (RF) band to the optical domain. By integrating the RF band relying on diverse radio techniques and optical bands, the next-generation heterogeneous networks (HetNets) are expected to be a potential solution for supporting the ever-increasing wireless tele-traffic. Owing to its abundant unlicensed spectral resources, visible light communications (VLC) combined with advanced illumination constitute a competent candidate for complementing the existing RF networks. Although the advantages of VLC are multi-fold, some challenges arise when incorporating VLC into the classic RF HetNet environments, which may require new system architectures. This motivates our research on the system design of user-centric (UC) VLC.

Our investigations are focused on system-level design of VLC and it is constituted by three major aspects, namely 1) by the cooperative load balancing (LB) in hybrid VLC and wireless local area network (WLAN) as discussed in Chapter 2; 2) by the UC cluster formation and multiuser scheduling (MUS) of Chapter 3; 3) as well as by the energy-efficient scalable video streaming design example of Chapter 4. Explicitly, we first study VLC as a complementary extension of the existing WLAN. In Chapter 2 we study various conventional cell formations invoked for networks in order to tackle the significant inter-cell interference (ICI) problem, including the traditional unity/non-unity frequency reuse (FR) techniques as well as the advanced combined transmission (CT) and vectored transmission (VT) schemes. Then a distributed LB algorithm is proposed for a hybrid VLC and WLAN network, which is then evaluated from various perspectives.

In order to further mitigate the ICI in VLC networks, we focus our attention on novel UC-VLC cluster formation techniques in Chapter 3 and Chapter 4. The concept of UC cluster formation is a counterpart of the conventional network-centric (NC) cell formation, which is dynamically constructed according to the users' location. Relying on graph theory, the joint cluster formation and MUS problem is solved in Chapter 3. Furthermore, another important optimisation aspect in most wireless networks is the achievable energy efficiency (EE). Hence, we design an energy-efficient scalable video streaming scheme for our UC-VLC network, which achieves superior performance compared to the NC cells in terms of its throughput attained, EE as well as the quality of service (QoS).

Declaration of Authorship

I, **Xuan Li**, declare that the thesis entitled **Design Optimisation of User-Centric Visible-Light Networks** and the work presented in it are my own and has been generated by me as the result of my own original research. I confirm that:

- This work was done wholly or mainly while in candidature for a research degree at this University;
- Where any part of this thesis has previously been submitted for a degree or any other qualification at this University or any other institution, this has been clearly stated;
- Where I have consulted the published work of others, this is always clearly attributed;
- Where I have quoted from the work of others, the source is always given. With the exception of such quotations, this thesis is entirely my own work;
- I have acknowledged all main sources of help;
- Where the thesis is based on work done by myself jointly with others, I have made clear exactly what was done by others and what I have contributed myself;
- Parts of this work have been published.

Signed: ..... Date: .....

Acknowledgements

First of all, I would like to give the greatest gratitude to both of my supervisors Dr. Rong Zhang and Prof. Lajos Hanzo. I really appreciate their generous and insightful guidance as well as wise advice in the past four years of my PhD study, which encouraged me to build my own career that I am so passionate about. I appreciate that they shared with me their valuable experiences, not only in science, but also in life.

Secondly, I would also like to thank all the other colleagues in Southampton Wireless Group for their help and supports. In particular, I wish to express my appreciation to Dr. Wei Liang, Dr. Dandan Liang, Dr. Jing Zuo, Dr. Shaoshi Yang, Dr. Jie Hu, Dr. Jia Shi, Dr. Jiankang Zhang, Dr. Junyi Jiang, Mr. An Li, Ms. Siyao Lu and Mr. Xiaoyu Zhang for their kindly help and valuable encouragement. I am very grateful for the collaboration with Dr. Fan Jin, Dr. Yongkai Huo and Miss. Simeng Feng.

Thirdly, I would like to thank my parents, Mr. Zhexiong Li and Mrs. Chunyan Gao, as well as my parents in law, Mr. Hongjun Zhang and Mrs. Shuqin Jiang for their endless love and full support on my PhD study.

Last but not the least, I would like to express my deepest appreciation to my husband, Mr. Haojie Zhang. Thanks for his love, understanding and support.

List of Publications

Journal Papers

1. **Xuan Li**, Rong Zhang and Lajos Hanzo, "Cooperative load balancing in hybrid visible light communications and WiFi", *IEEE Transactions on Communications*, vol. 63, no. 4, pp. 1319-1329, April 2015.

2. **Xuan Li**, Fan Jin, Rong Zhang, Jiaheng Wang, Zhengyuan Xu and Lajos Hanzo, "Users first: user-centric cluster formation for interference-mitigation in visible-light networks", *IEEE Transactions on Wireless Communications*, vol. 15, no. 1, pp. 39-53, January 2016.

3. **Xuan Li**, Yongkai Huo, Rong Zhang and Lajos Hanzo, "User-centric visible light communications for energy-efficient scalable video streaming", *Submitted to IEEE Journal on Selected Areas in Communications*.

4. Simeng Feng, **Xuan Li**, Rong Zhang, Ming Jiang and Lajos Hanzo, "Hybrid positioning for the amorphous-cell assisted user-centric visible light downlink", *IEEE Access* , vol. 4, pp. 2705-2713, May 2016.

5. Fan Jin, **Xuan Li**, Rong Zhang and Lajos Hanzo, "Resource Allocation Under Delay-Guarantee Constraints for Visible-Light Communication", *IEEE Access (Early access)*, May 2016.

Conference Papers

1. **Xuan Li**, Rong Zhang, Jiaheng Wang and Lajos Hanzo, "Cell-centric and user-centric multi-user scheduling in visible light communication aided networks", *2015 IEEE International Conference on Communications (ICC 2015)*, 8-12 June, London, UK.

2. **Xuan Li**, Fan Jin, Rong Zhang and Lajos Hanzo, "Joint cluster formation and user association under delay guarantees in visible-light networks", *2016 IEEE Global Communications Conference (GLOBECOM 2016)*, 4-8 December, Washington, DC USA.

Contents

List of Symbols

General Conventions

- The superscript $\underline{(.)}$ indicates the symbol sequences.
- The superscript ^{T} is used to indicate matrix transpose operation. Therefore, $\mathbf{a}^T$ represents the transpose of the matrix $\mathbf{a}$.
- The superscript ^{H} is used to indicate complex conjugate transpose operation. Therefore, $\mathbf{a}^H$ represents the complex conjugate transpose of the matrix $\mathbf{a}$.

Mathematical Operators and Functions

$[\cdot]_{a\times b}$	The matrix having a rows and b columns.
$\exp(\cdot)$	The exponential operation.
$\sum$	The sum operation.
$var[\cdot]$	The variance of a variable.
$\log_2(\cdot)$	Logarithm to base 2.
$\min(\cdot)$	The minimum value among a number of variables.
$\max(\cdot)$	The maximum value among a number of variables.

Specific Symbols

a	The index of the VLC AP.
u	The index of the UE.
ϕ_d	The angle of irradiance in the LoS link.

ϕ_r	The angle of irradiance in the first-reflection link.
ψ_d	The angle of incidence in the LoS link.
ψ_r	The angle of incidence in the first-reflection link.
$h_d[u, a]$	The LoS optical channel's total DC attenuation from a VLC transmitter a to the receiver u.
w	The Lambert index.
$\phi_{1/2}$	The semi-angle at half-illuminance of the source.
D_{PA}	The detector's physical area for a PD.
ψ_{F}	Half of the receiver's FoV.
$T_s(\psi_d)$	The gain of the optical filter.
$g(\psi_d)$	The gain of the optical concentrator .
n_r	The refractive index of a lens at a PD.
$dh_r[u, a]$	The channel's DC attenuation on the first reflection.
l_1	The distance between the transmitter and a reflective point.
l_2	The distance between the reflective point and the receiver.
ρ	The reflectance factor.
dD_{wall}	The reflective area.
β_1	The irradiance angles to the reflective point.
β_2	The irradiance angles to the receiver.
P_t	The transmitted optical power.
P_r	The optical power received.
γ	The PD's responsivity.
B	The modulation bandwidth.
ξ	The SINR received.
N_0	The noise power spectral density.
n_a	The number of APs in a merged cell.
U	The number of users are within the overlapping area in a merged cell.

H	Channel matrix.
G	TPC matrix.
I	The interference imposed by neighbouring APs.
β_u	The actual throughput allocated to a user u.
$\mathcal{G}$	The graph model of the VLC down-link.
N_A	The total number of VLC APs.
N_U	The total number of UEs.
n	The index of the UC cluster.
$\mathbb{Q}$	The independent component of the graph.
$\mathcal{V}$	The vertex set of the graph model.
$\mathcal{E}$	The edge set of the graph model.
$\mathcal{C}$	The UC cluster/The VLC cell.
$r_{a,u}$	The achievable data rate of the UE u from the AP a.
$\hat{r}_u$	The long-term average throughput of the UE u.
$\mathcal{V}_A$	The VLC AP set.
$\mathcal{V}_U$	The UEs set.
$\mathcal{V}_W$	The WiFi AP set.
$\omega(e_{a,u})$	The weight of a particular link.
P_b	The LoS blocking probability.
$d_{a,u}$	The mutual distances between any AP-UE pair.
$d_{u,u'}$	The mutual distances between any pair of UEs.
d_α	The distance constraint for the APs within a single cluster.
d_μ	The distance constraint for the UEs within a single cluster.
c_n	The cluster centre.
l	The index of the video layer.
M	The number of AM modes.

m	The index of the AM mode.
r^m	The data rate provided by the AM mode m.
ξ^m_{thr}	The SINR threshold of the AM mode m.
$p^m_{u,l}$	The power allocated to the l-th video layer of the UE u associated with the AM mode m in the electronic domain.
$p^{\mathsf{tx}}_{\mathsf{max}}$	The maximum optical transmit power allowed for each optical AP.
$p^{\mathsf{tx}}_{u,l}$	The electronic transmit power for the l-th video layer of the UE u.
$t^m_{u,l}$	The time required for transmitting the lth video layer to the UE u using the AM mode m.
$S_{u,l}$	The length of the lth video layer.
T	The frame time.
$\bar{p}_u$	The average power allocated to the UE u.
$\mathbb{E}^m_{u,l}$	The EE of the UE u receiving the video layer l.
$\Delta^m_{u,l}$	The utility of the UE u receiving the video layer l.
$E_{u,\hat{l}}(t)$	The achievable EE when transmitting all the video layers up to $\hat{l}$ to the UE u under the time constraint t.
$E_{a,\hat{u}}(p^{\mathsf{tx}})$	The achievable EE when supporting $\hat{u}$ UEs under the power constraint p^{tx}.
$\mathcal{M}_u$	The AM mode assignment matrix for the UE u.
E_u	The achievable EE matrix of the UE u.
K_u	The number of frames during a single optimisation slot for the UE u.

Chapter 1

Introduction

1.1 Background

As a truly revolutionary paradigm shift [1], wireless technology relying on radio waves has become an integral part of our everyday life, facilitating basic services, such as making a phone call or sending a message, as well as radio reception on near-field-communication-enabled mobile payment. As shown in Figure 1.1, the radio waves occupy the 3 kHz∼300 GHz electromagnetic band, which has been widely used for communication purposes. However, with the huge increase of tele-traffic, the radio frequency (RF) band is becoming more and more crowded. Following the launch of the global 5G research initiatives [2] conceived for tackling the explosive escalation of wireless tele-traffic, the horizon of communication bands has been expanded from the conventional RF band both to the millimetre wave [3] and to the visible light [4] frequency band spanning from 400 to 800 THz.

The earliest known use of visible light communications (VLC) dates back to 1880, when Bell developed a photophone transmitting voice by employing sunlight [5]. With the development of solid-state lighting, white light-emitting diodes (LEDs) were invoked for constructing VLC systems in the early 2000s for the dual function of illumination and communications by Tanaka *et al.* in Japan [6]. In VLC, the intensity of light is modulated and transmitted by a light source, which

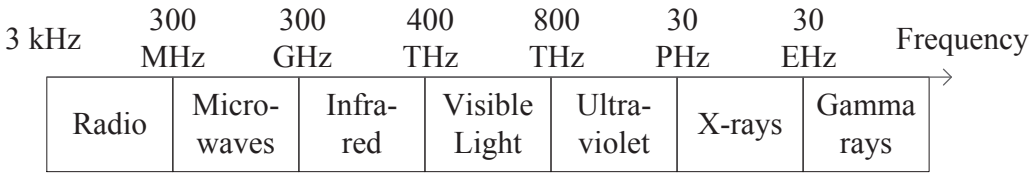

Figure 1.1: Stylised partitioning of the electromagnetic spectrum.

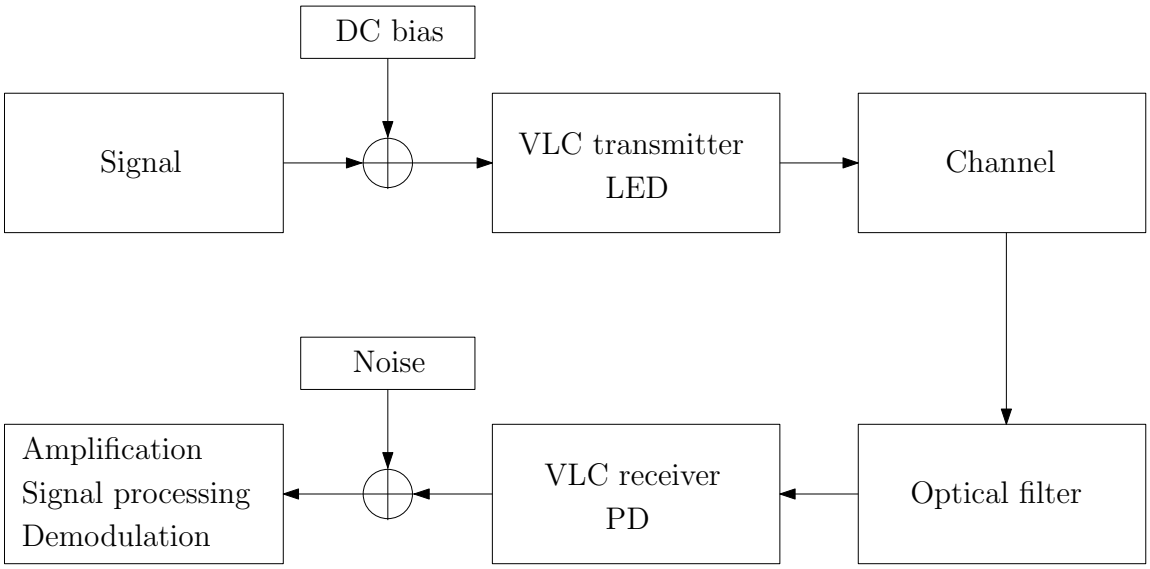

Figure 1.2: A general VLC link structure.

flickers above the fusion-frequency of the human eye. As a benefit of their high switching rate and energy efficiency, LEDs may be the best choice for indoor VLC systems, which are capable of serving the dual function of illumination and communications. In the rest of this chapter, point-to-point VLC links will be introduced in Section 1.2 including the devices and other components, the VLC channels as well as the physical layer techniques. An overview of VLC networks will be presented in Section 1.3. Furthermore, the applications and the open challenges of VLC-based systems will be discussed in Section 1.4 and Section 1.5, respectively. Finally, in Section 1.6, the contributions and the outline of this thesis will be summarised.

1.2 VLC Links

A general VLC link structure is shown in Figure 1.2. The optically modulated signal is superimposed on the average direct current (DC) level, which drives the LED and converts the electrical signals into intensity modulated optical signals. The received optical signal arrives at the optical filter and it is focused on a photodetector (PD), where the optical signal is converted back to electrical signal. Due to the thermal agitation of charge carriers and owing to the ambient light, noise is imposed. In Figure 1.2, only the electronic domain noise is shown, although noise is accumulated at every stage. Relying on the process of amplification, signal processing and demodulation, etc. the transmitted signals are then recovered. In this section, VLC is treated as a *point-to-point* data transmission technique. Its transmitter and receiver, its channel model as well as the applicable modulation techniques will be introduced. Additionally, since the primary function of light luminaries is to provide illumination in indoor environments, adjustable dimming and safety to the human eye should also be considered as constraints, when integrating VLC with indoor lighting systems.

1.2.1 Devices and Components

1.2.1.1 VLC Transmitter: Light-Emitting Diode

Owing to the rapid development of solid-state lighting, which refers to the fact that light is emitted by solid-state electro-luminescence as opposed to incandescent bulbs or fluorescent tubes, VLC using LEDs as the data 'transmitters' has intensified during the past decade or so. Exhibiting the dual function of illumination and data transmission, the advantages of LEDs are multi-fold, such as low heat generation [7], low power consumption [8], high energy conversion efficiency/luminous efficacy [9] as well as a potentially high bandwidth [10], etc. Diverse types of LEDs have been developed, which are available in commercial markets, including phosphor converted LEDs (PC-LEDs) [11], multi-chip LEDs (MC-LEDs) [12], organic LEDs (OLEDs) [13] and micro-LEDs [14].

Apart from the study of the specific types of LEDs mentioned above, the basic characteristics of white LEDs have been widely investigated in [8, 10, 15–17], for the sake of constructing a VLC system. Since LEDs perform dual functions in indoor environments, the typical characteristics of LEDs are usually studied from two perspectives, namely in terms of their photometric parameters and radiometric parameters. The photometric parameters quantify the LEDs characteristics in terms of indoor illumination, while the radiometric parameters describe the radiated electromagnetic energy of the light, which are related to the communication characteristics of LEDs. Let us now provide a brief description of the most important parameters:

- *luminosity function* $V(\lambda)$: the function reflecting the human eyes' sensitivity to different colours, which provides design guidelines for the associated lighting technology [18];
- *spectral power distribution* $S_p(\lambda)$ [W/nm]: the function reflecting the power of the LED at all wavelengths in the visible light spectrum [19];
- *luminous flux* Φ [lumen]: calculating the power emitted by an LED, which can be perceived by the human eye [20];
- *luminous intensity* $I_{\mathcal{L}}$ [candelas]: a parameter defined as the luminous flux per unit solid angle, which describes the brightness of an LED;
- *semi-angle at half power*: the angle at which the luminous intensity in candelas decreases to half of the intensity at 0° solid angle, etc.

To elaborate further, the luminous flux Φ may be characterised as

$$\Phi = V_m \int_{\lambda_1}^{\lambda_2} V(\lambda) S_p(\lambda) \mathrm{d}\lambda, \tag{1.1}$$

where V_m is the maximum visibility, which is around 683 lm/W at $\lambda = 555$ nm. Furthermore, according to its definition, the luminous intensity $I_{\mathcal{L}}$ may be written as $I_{\mathcal{L}} = \mathrm{d}\Phi/\mathrm{d}\theta$, where θ is

the spatial angle. In order to calculate the illuminance of an illuminated surface, from a different perspective, we may also calculate $I_{\mathcal{L}}$ in angle ϕ as

$$I_{\mathcal{L}}(\phi) = I_{\mathcal{L}}(0) \cdot \cos^{w}(\phi), \tag{1.2}$$

where $I_{\mathcal{L}}(0)$ is the centre luminous intensity of an LED and ϕ is the angle of irradiance. Furthermore, w denotes the order of Lambertian emission [1] and is given by $w = \ln 2 / \ln(\cos \phi_{1/2})$, where $\phi_{1/2}$ is the semi-angle at half-illuminance of the LED. Now we are ready to calculate the illuminance $E_{\mathcal{L}}$ at a certain point of the illuminated surface, which is given as

$$E_{\mathcal{L}} = I_{\mathcal{L}}(0) \cdot \cos^{w}(\phi) / d_{a,u}^{2} \cdot \cos(\psi), \tag{1.3}$$

where $d_{a,u}$ is the distance between the LED transmitter and the receiver's surface, while ψ is the angle of incidence.

Since illumination is the primary function of LEDs, the illumination requirements should be considered before invoking their communication function. As an example, we investigate the illumination distribution of a typical 15 m $\times$ 15 m room covered by 8$\times$8 uniformly distributed LED-array transmitters at a height of 2.5m. Our simulation parameters are summarized in Table 2.1. Figure 1.3 shows the illuminance distribution of the room model for different VLC transmitters arrangements. In Figure 1.3(a), 8$\times$8 LED-array transmitters are uniformly distributed on the ceiling, while 4$\times$4 uniformly distributed transmitters are assumed in Figure 1.3(b). Furthermore, the total transmitted optical power is the same in both settings. The illuminance range is between 300-1500 lx in Figure 1.3(a), which satisfies the lighting standard of a typical room. However, the illuminance may be excessively bright for human eyes in some areas in Figure 1.3(b). since it is as high as 1600 lx.

1.2.1.2 VLC Receiver: Photodetector

PDs are widely used as the receivers in VLC systems. A PD is a semiconductor device, which converts the information-bearing optical radiation into the equivalent electrical signal with the aim of recovering the transmitted information [21]. In particular, the electrical signal power is generated proportionally to the square of the instantaneous received optical power. A relevant parameter to characterise a PD is termed as quantum efficiency, which may be defined as the ratio of the number of the electron-hole pairs [2] and that of the incident photons in a given time. Apart from the quantum efficiency, the speed of response and the bandwidth of a PD are also essential, which are dependent on the transit time through the depletion regions, the electronic frequency response and the slow diffusion outside the depletion regions, etc. Furthermore, when employing many PDs together as

[1] In Lambertian emission, the optical power radiated from a unit area into a unit solid angle is constant [21]. The maximum luminous intensity $I_{\mathcal{L}}(0)$ is perpendicular to the planar surface but reduced proportional by the cosine of the angle ϕ.

[2] An electro-hole is the phenomenon that an electron leaves its position in an atom or atomic lattice.

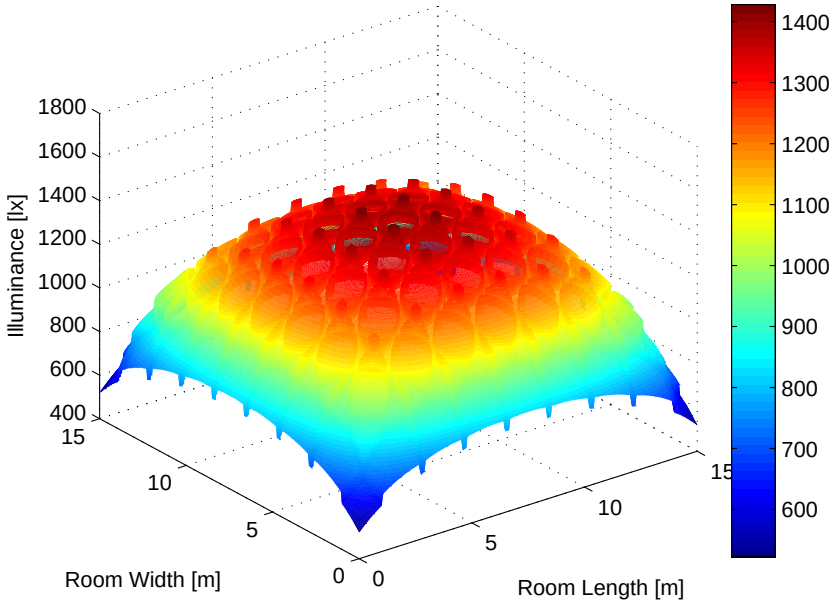

(a)

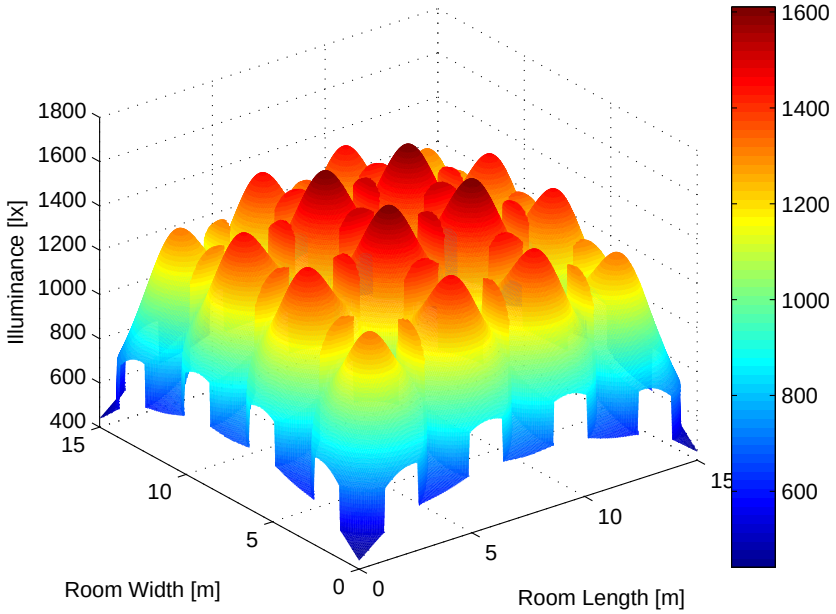

(b)

Figure 1.3: (a) Illuminance distribution of a 15 m $\times$ 15 m room covered by 8$\times$8 uniformly distributed LED-array transmitters at a height of 2.5m, where the transmitted optical power is 9 W per LED array. Min. 520.2 lx, Max. 1430.0 lx, Ave. 1120.2 lx. (b) Illuminance distribution of the same room covered by 4$\times$4 uniformly distributed LED-array transmitters at a height of 2.5m, where the transmitted optical power is 36 W per LED array and the total power is the same as in (a). Min. 439.0 lx, Max. 1612.9 lx, Ave. 1157.0 lx.

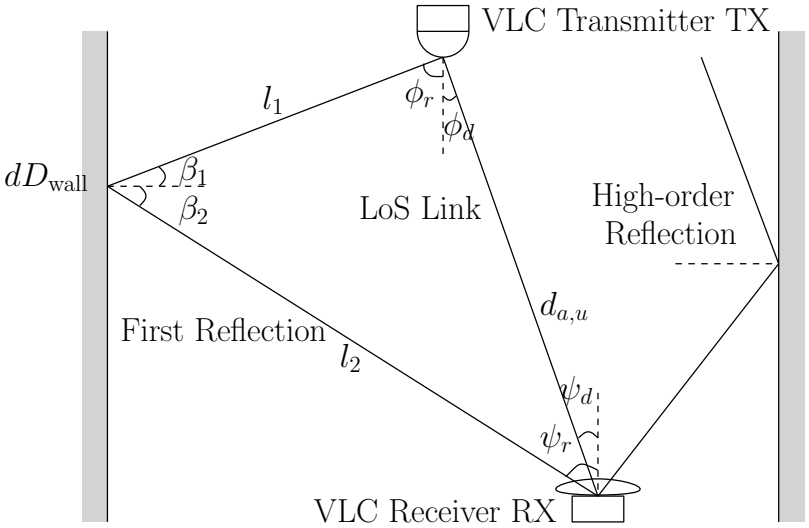

Figure 1.4: Propagation model of VLC links, including the LoS links, the first reflection as well as the kth reflection. However, the average received optical power from all links, which are reflected more than once, may be negligible according to [15].

an array, the imaging sensor can also be adopted as the VLC receiver. However, due to its low sampling rate, the achievable rate of an imaging sensor is much lower than that of a stand-alone PD [17].

1.2.2 VLC Channels

Figure 1.4 shows a stylised propagation model of VLC links, including the line-of-sight (LoS) links, the first reflection as well as the high-order reflections. However, the average optical power received from all links, which are reflected more than once, may be negligible according to [15]. In the model of Figure 1.4, a VLC transmitter TX located on the ceiling transmits data to a VLC receiver RX. The angles of irradiance in the LoS link and the first-reflection link are denoted as ϕ_d and ϕ_r, while correspondingly the angles of incidence in each link are denoted as ψ_d and ψ_r, respectively. The LoS optical channel's total DC attenuation $h_d[u,a]$ from a VLC transmitter TX to the receiver RX is given by [22, 23]

$$h_d[u,a] = \begin{cases} \dfrac{(w+1)D_{\text{PA}}}{2\pi d_{a,u}^2} \cdot \cos^w(\phi_d) \cdot T_s(\psi_d) \cdot g(\psi_d) \cdot \cos(\psi_d), & \psi_d \leq \psi_{\text{F}}, \\ 0, & \psi_d > \psi_{\text{F}}, \end{cases} \tag{1.4}$$

where the Lambert index w depends on the semi-angle $\phi_{1/2}$ at half-illuminance of the source, which is given by $w = -1/\log_2(\cos\phi_{1/2})$. D_{PA} is the detector's physical area for a PD and ψ_{F} represents half of the receiver's field-of-view (FoV). In a direct LoS path, the irradiant angle equals to the incident angle, where both the transmitter and the receiver point vertically. As shown by Figure 1.4, we have $\phi_d = \psi_d$. Still referring to Equation (1.4), $T_s(\psi_d)$ and $g(\psi_d)$ denote the gain of the optical filter and of the optical concentrator employed, respectively, while $g(\psi_d)$ can be

written as [22]

$$g(\psi_d) = \begin{cases} \dfrac{n_r^2}{\sin^2 \psi_d}, & 0 \leq \psi_d \leq \psi_{\mathrm{F}}, \\ 0, & \psi_d > \psi_{\mathrm{F}}, \end{cases} \tag{1.5}$$

where n_r is the refractive index of a lens at a PD.

Furthermore, according to [15], when the incidence angle ψ_r is no larger than the FoV, the channel's DC attenuation $dh_r[u,a]$ on the first reflection is given by

$$dh_r[u,a] = \frac{(w+1)D_{\mathrm{PA}}}{2\pi^2 l_1^2 l_2^2} \cdot \rho \cdot dD_{\mathrm{wall}} \cdot \cos^w(\phi_r) \cdot \cos(\beta_1) \cdot \cos(\beta_2) \cdot T_s(\psi_r) \cdot g(\psi_r) \cdot \cos(\psi_r), \tag{1.6}$$

where l_1 represents the distance between the transmitter TX and a reflective point, while l_2 is the distance between this point and the receiver RX. The reflectance factor and the reflective area are denoted by ρ and dD_{wall}, respectively. Additionally, β_1 and β_2 represent the irradiance angles to the reflective point and to the receiver, respectively. Our parameter values are summarized in Table 2.1.

1.2.3 PHY Techniques

1.2.3.1 Modulation Schemes

Modulation schemes constitute one of the most important physical-layer techniques in communication systems. This is especially true when jointly considering indoor illumination requirements, since the modulated signals can be used to switch on/off the LEDs, which conveys the on-off pattern-based binary information to the receiver. Since LEDs emit incoherent light, where photons have different wavelength and phase, it is an open challenge to collect appreciable signal power in a single electromagnetic mode in a practical low-cost VLC system. Hence, often the intensity modulation direct detection (IM-DD) scheme is employed, where the transmitted signal modulates the instantaneous optical power of the LEDs. Hence, IM-DD constitutes an attractive scheme and has been widely used in VLC systems.

Let us now elaborate a little further. The simple on-off keying (OOK) technique is realised by switching a LED, where the binary signals are transmitted as the presence or absence of light [15, 24]. In [25], an aggregate parallel data transmission rate of 1.5 Gb/s was achieved by employing OOK modulation. Furthermore, various pulse position modulation (PPM) schemes have been introduced into VLC systems for achieving different design objectives [26–28], where the basic concept is to map the modulated signal into 2^M legitimate time-slots for M-ary PPM [29]. Another bandwidth-efficient baseband modulation technique is constituted by pulse amplitude modulation (PAM) [22], which was also invoked and evaluated in VLC systems [10, 30]. However, the signals modulated by multiple intensity levels may suffer from nonlinear distortions due to the LEDs intensity-dependent luminous efficacy [16]. On the other hand, in order to provide high data rates, multiple-carrier techniques have also been applied in VLC systems, such as the quadrature ampli-

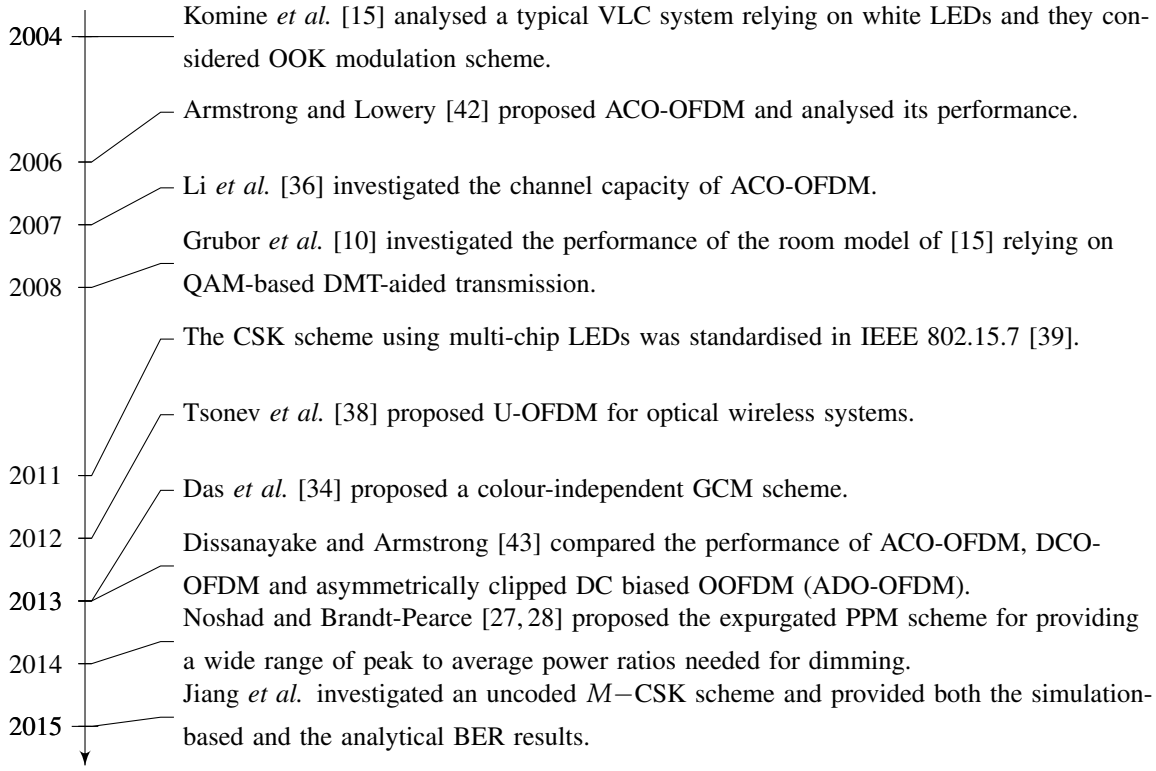

Figure 1.5: A brief summary of popular modulation schemes reported in VLC systems.

tude modulation (QAM)-based discrete multitone (DMT) transmission technique [10].

Apart from the widely known modulation schemes, some unique modulation techniques have also been developed for VLC systems, including colour shift keying (CSK) [31–33], generalised colour modulation (GCM) [34, 35], optical orthogonal frequency division multiplexing (OOFDM) [36–38], etc. Explicitly, the CSK scheme using multi-chip LEDs was standardised in the IEEE 802.15.7 recommendation [39], which may be a potential modulation scheme for future VLC systems, although it relies on sophisticated implementation. In [33], Jiang *et al.* investigated an uncoded M-CSK scheme relying on a joint maximum likelihood hard-detection based VLC system, where both simulation-based and analytical bit-error-rate (BER) results were derived. By contrast, a colour-independent GCM scheme was proposed in [34], which had the advantages of flicker-free operation, accurate dimming control and the ability to function independently of the number of LEDs at the transmitter or the PDs at the receiver [35]. Moreover, there are three popular types of OOFDM proposed for VLC systems, i.e. asymmetrically clipped OOFDM (ACO-OFDM) [36, 40], DC biased OOFDM (DCO-OFDM) [37, 41] as well as unipolar OFDM (U-OFDM) [38]. The milestones of popular modulation schemes in VLC systems are summarized in the timeline of Figure 1.5.

1.2.3.2 Dimming Control and Flicker Mitigation

According to [18], different levels of illuminance are required in different scenarios. Owing to the fact that an LED can be dimmed to an arbitrary level, integrating dimming control into VLC systems is required for the sake of saving energy [24]. The light should be dimmable arbitrarily in VLC systems, without the communications becoming interrupted, which means that the data should be modulated in such a way that any desired level of dimming is supported [17]. Numerous valuable modulation schemes supporting dimming control have been proposed for the LEDs, such as the variable OOK VOOK [24, 44], variable PPM (VPPM) [45], pulse width modulation with DMT (PWM-DMT) [46], etc.

When the light intensity changes, it should be flickering above the human eyes' fusion frequency, so that the human eye cannot perceive it. Otherwise, serious physiological problems may be caused. Hence, the speed of the changes in light intensity, termed as flickering, should be carefully considered when designing modulation schemes for VLC systems. As suggested by [39], flickering faster than 200MHz can avoid harmful effects to the human eye. In order to mitigate flickering, run length limited (RLL) codecs have been incorporated into modulation schemes for avoiding long runs of 0s and 1s, which is believed to be the most common reason of flickering.

1.3 VLC Networks

Beyond point-to-point links, VLC is also considered as a new member in the small-cell family of the heterogeneous networks (HetNets) landscape for complementing the overloaded radio frequency band [47]. In this section, the layout of the visible-light-aided networks is investigated, ranging from a regular network-centric cell-layout associated with different frequency reuse (FR) patterns to the radically new user-centric (UC) cluster formation employing advanced transmission schemes. Furthermore, the family of multiuser techniques such as multiuser signal processing, scheduling and resource management are reviewed.

1.3.1 Network-Centric versus User-Centric Cell-Structure

1.3.1.1 Network-Centric Optical Attocells

In a typical VLC down-link (DL) network, each optical access point (AP) illuminates only a small confined cell, as shown in Figure 1.6. The coverage of the single-AP optical cell is usually limited to room-size ($\sim$m) and it is considerably smaller than the coverage of the traditional RF cells ($\sim$km), which is referred to as an optical *attocell* [48], where atto means 10^{-18} in physics and mathematics. The concept of optical attocells is borrowed from the RF attocell, which was originally announced by the company Ubiquisys to represent the personal femtocell in 2011. Considering a specific optical attocell, its coverage is dependent both on the illumination requirements as well as on the

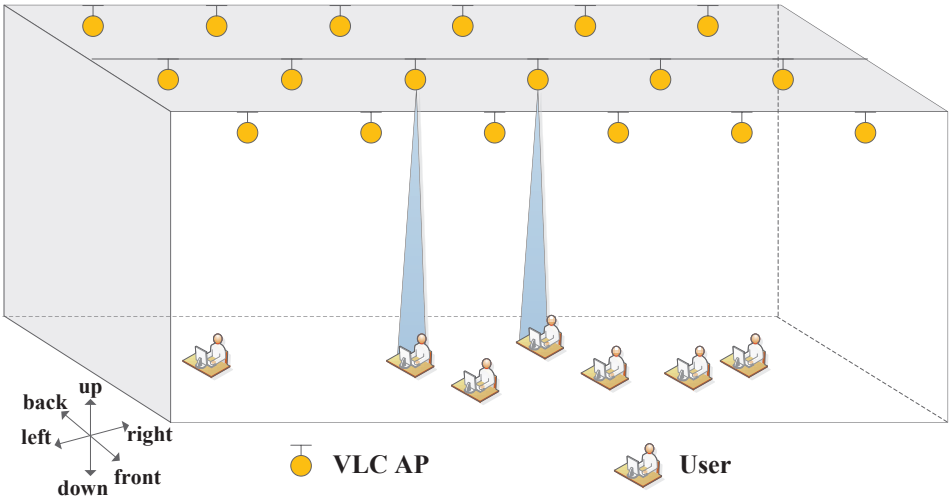

Figure 1.6: Example of an indoor LED-based VLC system.

FoV of the VLC receivers. Relying on these optical attocells, the indoor VLC network may be operated by assuming the full functionality of a RF cellular DL system. Note that the optical attocell is merely limited to the single-AP optical cell in the discussion of this section.

When there are multiple optical attocells in a VLC network, the inter-cell interference (ICI) imposed both by the LoS ray as well as by the non-LoS (NLoS) links has to be carefully treated, since the performance may become dramatically degraded at the cell edge due to ICI [49]. This degradation itself both in terms of the signal-to-interference-plus-noise ratio (SINR), the BER, the bandwidth efficiency, etc. and consequently vertical handovers may be frequently activated in VLC-based HetNets [50]. In order to reduce the effect of the ICI and to improve the performance, valuable research has been dedicated to

1) the initial design of the optical APs deployment [51–53],

2) the frequency planning within the optical spectrum available [54–57], as well as

3) the cell coordination between the multiple neighbouring optical attocells [58, 59].

To elaborate a little further, the ICI avoidance methods were considered at the preliminary design stage of the entire VLC-network design cycle by the authors of [51–53,56]. A novel VLC AP arrangement was advocated in [51], where 12 LEDs constitute a circle and 4 LEDs are placed in the corners, which are referred to here as the circular-LED arrangement and corner-LED arrangement, respectively, as shown in Figure 1.7. Compared to the arrangement of [15], where a single LED lamp is placed in the centre of the ceiling illuminating the entire room with the same total emitted optical power as in Figure 1.7, the arrangement proposed in [51] provides a much lower variance of the received signal-to-noise ratio (SNR) and of the received power at different locations in the room. Furthermore, the radius of the circle constituted by the circular-LED arrangement may be optimised according to the receivers' specific locations as well as to the various layouts of the room

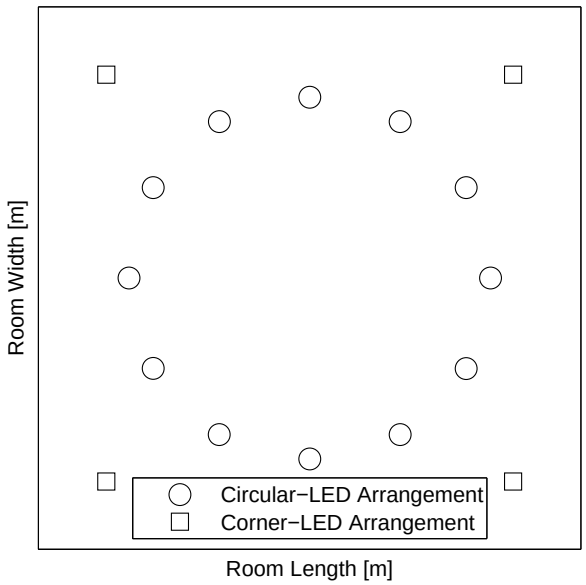

Figure 1.7: A novel VLC AP arrangement was advocated in [51], where 12 LED lamps constitute a circle and 4 LED lamps are placed in the corners, which are referred to here as the circular-LED arrangement and corner-LED arrangement, respectively.

considered. The optimisation problem of the LED-lamp placement was also formulated and solved in [52] for the sake of maximising the average area spectral efficiency [bits/s/Hz/m^2] [60]. Upon studying the optimum layout of two LED lamps with different FoV of the receiver, they found that the average area spectral efficiency is degraded, when imposing the classic lighting requirements on the communication performance maximisation problem. Moreover, instead of optimising the placement of the LED lamps, the authors of [53] investigated two LED deployment schemes, i.e. the single-LED-based deployment scheme and the array-LED-based deployment scheme. They used the classic particle swarm optimisation algorithm, in order to minimise the average outage area. Both of their proposed schemes are superior to the conventional random deployment scheme.

Following the traditional cellular design principle, FR is an appealingly simple solution for ICI mitigation. Marsh and Kahn [54] contributed one of the early studies investigating FR schemes conceived for optical communications, where an indoor infrared wireless communication system employing fixed-channel reuse for optical base stations was examined. In contrast to the static FR planning scheme, the resources are dynamically reused relying on a self-organising allocation mechanism in [55] and a scalable orthogonal frequency-division multiplexing access (OFDMA)-based VLC system is proposed in [56]. More recently, the authors of [57] designed a pair of fractional frequency reuse schemes for the DCO-OFDM-based optical attocell based networks, where strict fractional frequency reuse and soft frequency reuse were employed. However, although FR planning is an effective solution, the system has to obey the classic trade-off between having

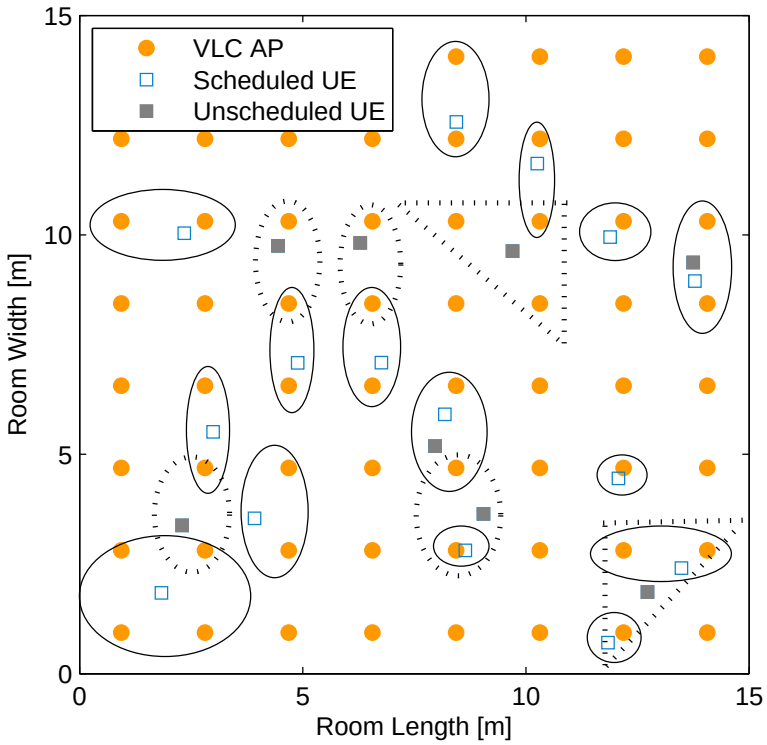

Figure 1.8: The amorphous UC multi-AP clusters constructed for jointly transmitting data to a single UE by employing CT, where the multiple APs convey the same information on the same visible carrier frequency and served a single UE at a time. When multiple UEs can receive data from the same AP, only one of them can be granted access for the sake of avoiding extra interference.

reduced bandwidth efficiency and an improved SINR. Furthermore, an inherent disadvantage of FR is that switching between optical frequencies every few meters degrades the user experience [47].

On the other hand, advanced cooperative transmission by multiple LEDs may be conceived by relying on the elegant time-of-arrival synchronisation advocated in [58], where multiple LEDs transmit simultaneously to the same receiver. In [59], three modulation techniques, namely OOK, PPM and pulse width modulation, were employed in the neighbouring optical cells and this scheme was expected to achieve a data rate of 71 Mb/s whilst providing seamless coverage. The milestones of the ICI mitigation schemes in VLC systems are summarised in the timeline of Figure 1.10. Broadly speaking, most techniques conceived for ICI avoidance and performance improvement in VLC networks were designed from a *network-centric* perspective, where fixed-shape regular optical attocells were investigated. By contrast, the amorphous user-specific cluster formation philosophy exemplified in Figure 1.8 is designed from the *user-centric* perspective discussed in the next subsection.

1.3.1.2 User-Centric Cluster Formation

Against the above-mentioned network-centric design philosophy, a UC cluster formation regime is proposed and studied in [47, 61–66], as a beneficial counterpart of the existing network-centric cells. By definition, UC design is different from the network-centric design, where the network configuration is fixed, regardless of the tele-traffic. First the so-called combined transmission (CT) technique is employed in each UC cluster, where multiple APs jointly convey the same information mapped to the same visible carrier frequency, while serving a single user equipment (UE) at a time. Considering the example seen in Figure 1.8, each hollow square and multiple APs (sometimes a single AP) constitute a UC cluster. When multiple UEs can receive data from the same AP, only one of them can be granted access for the sake of avoiding extra interference, as discussed in [62]. For example, the solid square on the bottom right of Figure 1.8 and the other two neighbouring hollow squares can receive information from the same APs, while the solid square is not scheduled during the current slot. Its potential cluster is surrounded by a dashed ellipse. All the disjoint groups seen in Figure 1.8 are scheduled in a parallel manner upon using the scheduling algorithm of [62].

In order to further improve the bandwidth efficiency and serve multiple UEs at the same time, the so called vectored transmission (VT)-aided UC cluster formation philosophy was proposed in [47,63], where each user-centric-vectored-transmission-aided (UC-VT) cluster is served by a set of VLC APs, which simultaneously serve multiple UEs by employing VT. An example of two APs serving two UEs by using VT will be shown and discussed in the context of Figure 2.2(d). More explicitly, a UC-VT cluster includes a set of APs and UEs as well as the transmission links between them. The concept of cluster formation is different from the concept of cell formation. Explicitly, the former may be defined as forming a UC cluster, where a set of VLC APs simultaneously serve multiple users by employing the advanced VT scheme of [49], which will be discussed in the context of Figure 4.2. However, the concept of cell formation is more conventional, which may be defined as combining several optical APs to form a large multi-AP cell and to transmit data cooperatively, as shown in Figure 2.2(c).

Figure 1.9 portrays the conventional cell formation structure (left) and the amorphous UC cluster formation (right) for a 15m$\times$15m indoor VLC system having 8$\times$8 APs (marked by squares) and 20 UEs (marked by circles) under three typical scenarios, where the UEs' positions are drawn from a uniform random distribution. Conventional cells typically have a fixed shape. For example, we may partition the 15m$\times$15m indoor environment into four square-shaped cells having (4$\times$4) = 16 APs per cell, where the users are associated with cells depending on the UEs' positions relative to the square-shaped boundary amongst the cells. We may switch off the communications function of the specific APs having no LoS links to the users in their vicinity (indicated by hollow small squares), in order to improve the energy efficiency. The related examples may be seen in the left of Figure 1.9. Note that the number of APs per cell may be pre-set as any feasible number.

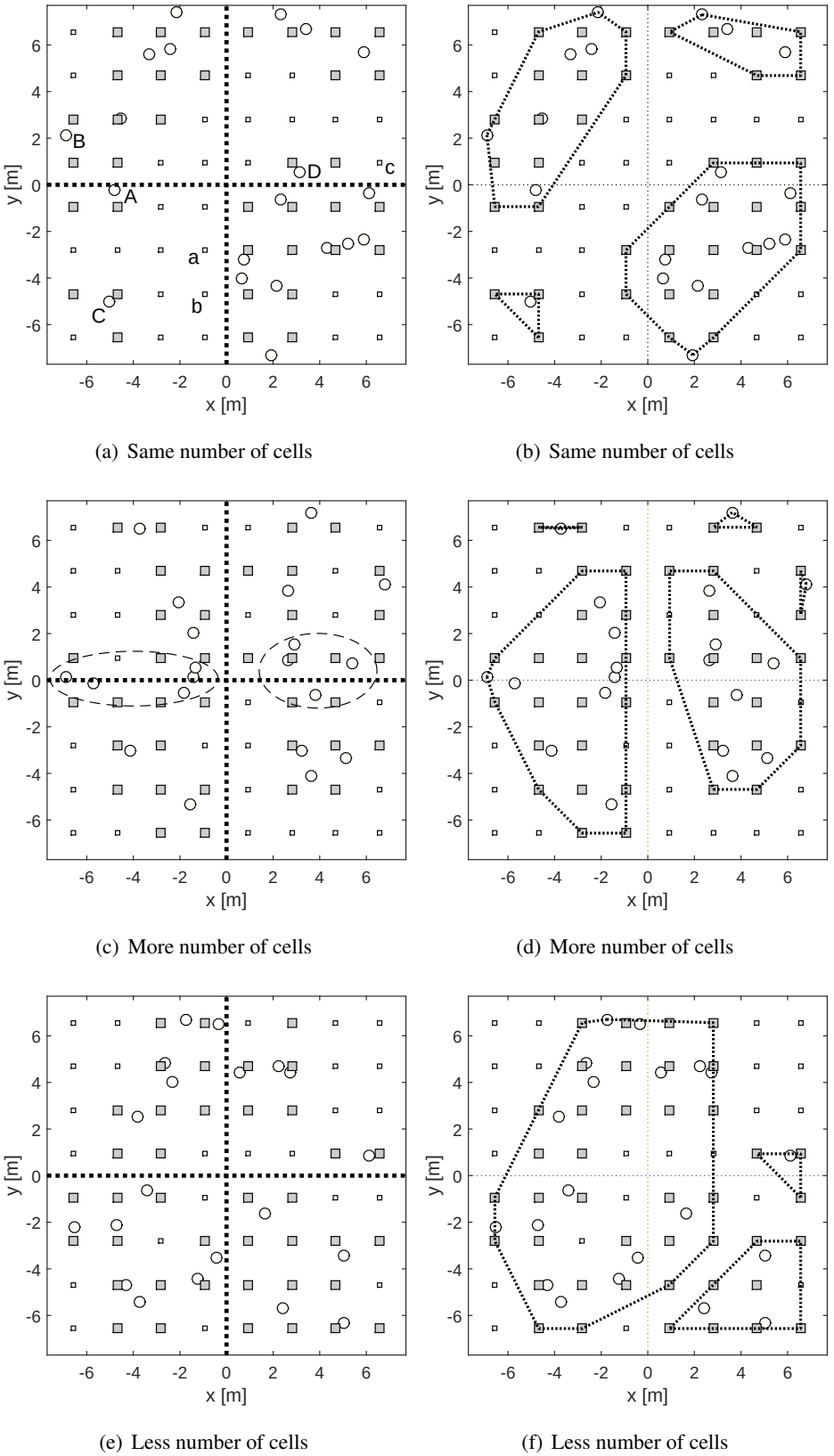

(a) Same number of cells

(b) Same number of cells

(c) More number of cells

(d) More number of cells

(e) Less number of cells

(f) Less number of cells

Figure 1.9: Illustration of the conventional (left) and the amorphous structure (right) for VLC indoor systems. The active VLC APs are marked by solid squares, while the idle APs are marked by hollow squares. The UEs are marked by circles.

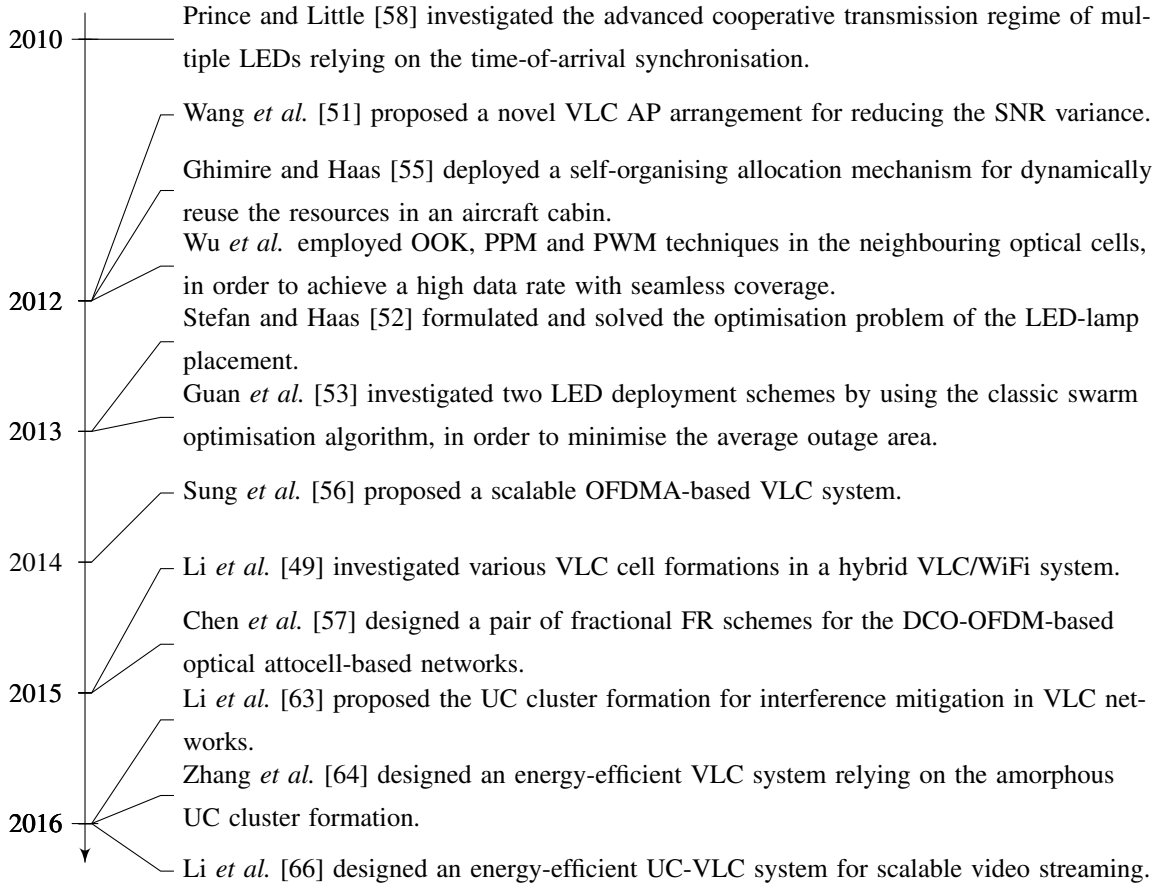

Figure 1.10: A brief summary of ICI mitigation schemes in VLC systems.

Observe from the left subfigures of Figure 1.9 that this arrangement may not be the most appropriate one. For example, in the bottom-left corner of cell of Figure 1.9(a), the 'boundary UE' 'A' is clearly far from UE 'C' in the same cell, but it is more close to UE 'B' in the neighbouring cell. This is good reason for UE 'A' to be separated from user 'C' and to join UE 'B', as seen in Figure 1.9(b) of the distance-based UC cluster. This is also true for the 'boundary UE' 'D' in Figure 1.9(a), since it is more close to the UEs located in the bottom-right cell, than to the rest of the distant UEs in the same cell. More examples are shown in Figure 1.9(c), where two clusters of boundary users - namely those highlighted by ellipses - join the UC clusters of Figure 1.9(d). In addition to a different UE-to-AP association, the status of APs is also different, where for example, APs ('a','b','c') were switched from idle mode in the conventional cells of Figure 1.9(a) to active mode in the UC clusters of Figure 1.9(b), since they have LoS connections to the associated UEs. Hence, the proposed UC cluster formation is capable of rearranging the conventional boundaries, leading to five and three AP-UE clusters in Figure 1.9(d) and Figure 1.9(f), whilst in Figure 1.9(b) there are four clusters. Hence, without a dynamic cell boundary, the UC cluster formation is updated to include the users moving in, arriving at or departing from the system, which leads to a flexible, "breathing" and evolving cell structure.

1.3.2 Multiuser Signal Processing

In order to support multiple UEs simultaneously, multiuser signal processing techniques have to be invoked for UC cluster formation. Let us hence embark on a brief review of the multiuser signal processing techniques proposed for VLC systems.

Multiple input multiple output (MIMO) systems are capable of offering an increased data rate compared to the single input single output (SISO) systems. Hence, the research of advanced MIMO transmission techniques has also been intensified in the optical domain [67–77]. In particular, the authors of [67] and [68] investigated the free-space optical MIMO systems equipped with multiple lasers and PDs, while the treatises [69, 70, 72, 74] are based on VLC systems. Explicitly, Zeng *et al.* [69] studied and compared the non-imaging and imaging MIMO techniques [3], which provided deep insights concerning optical MIMO systems. An experimental 2×2 imaging-based MIMO system was reported in [70], but the illumination requirements were not given any cognisance. In addition, a MIMO system using an imaging receiver relying on a hemispherical lens was designed and analysed in [74] for improving the spatial diversity order. Relying on the wide FoV achieved by using the hemispherical lens, the optical signals received are effectively separated. Hence, the correlations between the elements of the channel matrix are relatively low, which provides a beneficial spatial diversity gain for the efficient decoding of the signal in a MIMO system. Furthermore, a transmission rate of 1 Gb/s was achieved by an imaging MIMO system, as reported in [72].

In contrast to the above single-user MIMO systems, the family of multiuser-multiple-input-single-output (MU-MISO) techniques designed for VLC systems have also attracted much attention [73, 75–77]. In [73], a transmit precoding and biasing scheme was designed for the transmitter of a MU-MISO broadcast system. As a further advance, the MU-MISO transceiver designed for VLC systems was improved by considering the LED's optical power constraints in [75]. Furthermore, optical-OFDM schemes were also studied in a multi-user MIMO (MU-MIMO) system [76], while Shen *et al.* [77] optimised the achievable data rate of the VLC DL in a MU-MISO system.

1.3.3 Multiuser Scheduling and Resource Management

When multiple UEs are present in the VLC system, fair and efficient multiuser scheduling (MUS) and resource management constitutes one of the salient problems, which in fact affects all multiuser networks. The problem has been lavishly studied in the context of RF networks [79–82], but in VLC-based networks the problem has remained to a large extent hitherto unexplored in the

[3] In a conventional non-imaging MIMO system, each of the multiple LED transmitters conveys an independent data stream simultaneously and an individual non-imaging optical concentrator is used by each receiver, where the desired signal, delayed multipath components, ambient light noise, and co-channel interference are combined into a single electrical signal. By contrast, in an imaging MIMO system, light propagates from each LED as before, but is projected onto a detector array [78]. The projected images may activate a single pixel or a group of pixels on the array, where each pixel of the detector array represents a receiver [69].

open literature. Nonetheless, recently some valuable studies were disseminated in the context of network-centric single-AP VLC cells [77, 83–90].

In particular, Bykhovsky and Arnon [83] proposed a heuristic scheme for beneficially allocating sub-carriers in a VLC multiple access system relying on DMT modulation, in order to improve the aggregate throughput. Biagi *et al.* [84] designed a logical framework aiming for localizing, accessing, scheduling and transmitting in VLC systems, which was capable of achieving a substantial throughput at a modest complexity. However, similar to most of the literature studying resource allocation in VLC-based systems, both [83] and [84] endeavoured to improve the attainable throughput without giving any cognisance to the fairness experienced by the UEs. By taking fairness into account, Huang *et al.* [85] proposed an incremental scheduling scheme, where the global scheduling phase is responsible for assigning the resources to the UEs, while the local scheduling phase regularly adjusts the resource allocation by tracking the UEs' movements. Since the VLC APs are sending beacon frames periodically, the users can send a response message whether they have received the beacons. Then the scheduler can find the moving users according to the feedback information. Furthermore, Babatundi *et al.* [86] proposed a proportional fairness (PF) based scheduling algorithm for a centrally controlled VLC system, which outperformed the maximum-rate scheduling policy in terms of balancing the achievable throughput against the fairness experienced by the UEs. Additionally, compared to RF communications, VLC has some unique features, which should be carefully treated. Specifically, blocking is one of the most significant physical characteristics of VLC. Kim *et al.* [87] proposed three resource-allocation-based service modes for the VLC DL, in order to maintain both a high system throughput as well as satisfying the lighting requirements. Moreover, considering the nonnegativity of the intensity-modulated signals as another distinguishing feature of VLC, Park *et al.* [88] designed an optical MIMO system and proposed an optical power allocation (PA) scheme for the sake of maximising the system's spectral efficiency.

1.4 Applications and Extensions of VLC

As a promising complimentary extension to the well-established RF networks, VLC is becoming a promising enabler for providing indoor coverage, owing to its energy-efficient nature, whilst simultaneously supporting both communications and illumination. In this section, we focus our attention on the application of VLC-based systems, including video streaming, VLC-based HetNets as well as its broader extension to the Internet of Things (IoT).

1.4.1 Video Streaming

According to the global mobile data traffic statistics recently released by Cisco [91], video streaming is and will continue to be the most dominant form of tele-traffic, which will account for three quarters of all tele-traffic in 2020, as seen in Figure 1.11. As one of the 'killer'-applications in

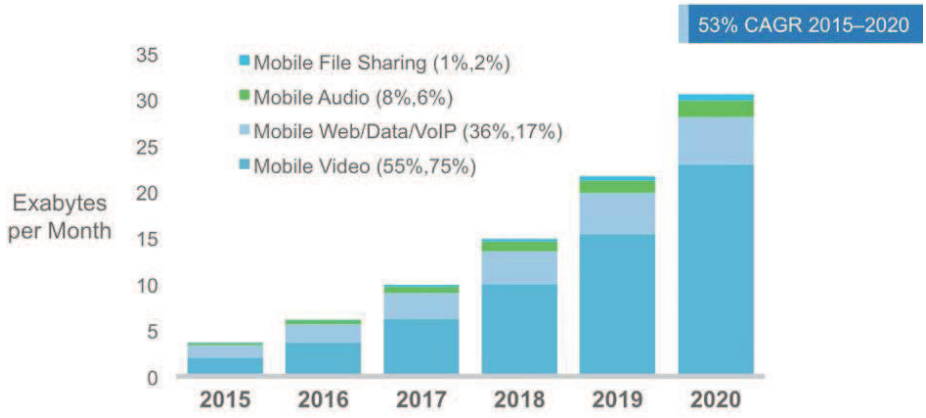

Figure 1.11: The global mobile data traffic forecast for 2015-2020 [91].

contemporary wireless communications systems [92–94], video streaming has become a popular research topic, including efficient compression standards [95–97], error-concealment/error-resilient streaming techniques [93, 98, 99], as well as reliable transmission schemes [100–102], etc.

In order to meet the requirements of the various transmission scenarios in the era of the Internet and of mobile networks, the advanced scalable extension of the so-called high-efficiency video coding (SHVC) techniques [97] has emerged and gained popularity, as a benefit of its scalable nature. Explicitly, this scheme is capable of offering diverse visual qualities by promptly adapting to the time-variant channel conditions of different UEs. The SHVC-based layered video stream is constituted by multiple unequal-importance layers, which are generated by using carefully designed source codecs [103, 104] as well as adaptive modulation and channel coding schemes [105, 106]. According to [107], if a carefully constructed subsets of the original video sequence may lead to video reconstruction either at a reduced picture size or at a reduced frame rate compared to the original one, then this video scheme is deemed to exhibit either spatial or temporal scalability, respectively. Another popular scalability mode is the so-called quality-scalability, where the subsets of bits may provide a reduced video fidelity. Explicitly, the fidelity is often represented in terms of the peak signal-to-noise ratio (PSNR). As a further advance, the afore-mentioned modes of scalability may be supported by a single scalable video sequence. The benefits of scalable video are multi-fold, amongst others, allowing for example the video decoder to progressively refine the reconstructed visual quality, as the channel-quality improves. The hierarchical structure of the video-stream also facilitates energy-efficient video communications by jointly considering the scalable video quality and the power consumption, as demonstrated for traditional RF networks in [108–110]. This motivated us to support energy-efficient scalable video streaming in the radically new context of UC-VLC networks.

1.4.2 VLC-aided Heterogeneous Networks

In order to support the rapidly increasing demand improved wireless data rates, as shown in Figure 1.11, both industry and academia are dedicated to seeking effective solutions, since we are practically approaching the theoretical limit of the RF channel capacity [111]. Exploiting new spectral bands may be expected to be one of the radical solutions, such as for example the millimetre-wave [3] and the optical wireless/VLC band [4]. In this thesis, we focus our attention on the family of VLC systems, which is deemed to be a promising complementary extension to the well-established indoor RF networks. On the other hand, a stand-alone VLC system may exhibit several potential disadvantages, such as the lack of up-link transmission, poor performance in NLoS scenarios and small coverage for a single VLC AP. Hence, its RF counterpart may be invoked as a cooperative 'partner' in order to realise seamless communications. Although this integration may be an effective solution for satisfying the increasing throughput demand, there are some open challenges, such as for example the conception of cooperative load balancing and of efficient handovers.

1.4.2.1 Load Balancing

The concept of load balancing (LB) is interpreted in [112] as matching the demand for resources ('load') with the supply of resources ('capacity'), which constitutes one of the fundamental problems in many fields of engineering, logistics and economics. Moreover, the LB problem also affects all cooperative multi-rate HetNets. Substantial related work has been undertaken based on the LB problem in RF networks [2, 113–119]. In particular, Andrews *et al.* [112] investigated diverse technical approaches to the LB problems of HetNes and furthermore provided valuable design guidelines for OFDMA-based cellular systems. As also suggested in [112], the primary approaches included centralized optimisation, game theory, Markov decision processes and the family of cell range expansion techniques.

Broadly speaking, the LB problem can be formulated as the constrained optimisation of a carefully selected utility function [120], while satisfying the users' quality of service (QoS) requirements, which may be written as the generic optimisation problem formulated below:

$$\max_{\boldsymbol{x}} \quad U_0(\boldsymbol{x}) \tag{1.7}$$

$$\text{s.t.} \quad f_i^c(\boldsymbol{x}) \leq C_i \quad 1 \leq i \leq m, \tag{1.8}$$

$$f_j^t(\boldsymbol{x}) \geq T_j \quad 1 \leq j \leq k, \tag{1.9}$$

where $\boldsymbol{x} \in \mathbb{R}^n$ is the independent variable and U_0 is the selected utility function. Furthermore, f_i^c is the ith cost function and C_i is the corresponding ith AP/network resource limit, while f_j^t denotes the jth UEs achievable data throughput and T_j corresponds to its throughput requirement. If Equation (1.7)-Equation (1.9) are all convex [4], the problem is a convex optimisation problem

[4] A function f: $\mathbb{R}^n \to \mathbb{R}$ is convex if, $\forall \boldsymbol{x}$, $\forall \boldsymbol{y} \in$ dom f and $\theta \in [0,1]$, $\theta\boldsymbol{x} + (1-\theta)\boldsymbol{y} \in$ dom f (i.e. the domain is a convex set) and $f(\theta\boldsymbol{x} + (1-\theta)\boldsymbol{y}) \leq \theta f(\boldsymbol{x}) + (1-\theta)f(\boldsymbol{y})$.

[120]. However, due to the coupled relationship between the user association and scheduling, the problem of Equation (1.7)-Equation (1.9) is usually NP-hard and may not be directly computable in a centralised manner. Since the subject of convex optimisation has been widely studied [121, 122], a straightforward way is to relax the optimisation problem Equation (1.7)-Equation (1.9) and make it convex. For example, with the aid of the classic dual decomposition approach, the authors of [118] developed a distributed resource allocation algorithm for the UEs associated with multi-homing capability in HetNets. Furthermore, by using the dual decomposition approach, Ye *et al.* [119] proposed a low-complexity near-optimal algorithm for the essential user association and LB problem after relaxing the binary variable. In Chapter 2, we will provide more details about the dual decomposition approach and propose a related distributed algorithm for VLC-based HetNets.

1.4.2.2 Efficient Handover

When considering a mobile user coming in a hybrid VLC/RF network, it may experience a high QoS in the centre of the VLC AP, while the QoS will be dramatically degraded, when it moves to the cell edge or when the LoS transmission is blocked. In this scenario, vertical handover (VHO) to the over-sailing RF cell should be invoked to maintain a smooth service quality. On the other hand, a VHO also occurs, when a RF user receives a stronger VLC signal and thus changes its connection from RF to VLC. Apart from the VHO, when the VLC APs are densely deployed, a user may experience several horizontal handovers between different VLC APs within a few dozen of metres.

Similarly to the existing RF-based HetNets, there are some potential problems, when invoking handovers in hybrid RF/VLC networks. Let us consider a user switching its connection from VLC to RF. When a new user arrives, the load of the RF AP is increased and the resources should be reallocated. Consequently, some of the existing users served by this RF AP only granted a reduced data throughput, while others may be assigned to the VLC network or to another RF AP. Conversely, in the specific VLC AP, where a user terminates his/her session, more resources become available for enhancing the QoS of its users. This is referred to as the knock-on handover effect [123]. Another problem is caused by transient LoS link blockages, which results in the user switching back and forth between the RF and VLC networks, hence increasing the system's signalling overhead. This is the so-called ping-pong effect [124]. In order to mitigate the adverse effects of frequent handovers, efficient handover techniques are essential for the success of VLC-based HetNets.

Although there is plenty of valuable research on handovers in RF networks [124–126], handover techniques conveived for VLC-based HetNets have remained to a large extent hitherto unexplored. In [127], the horizontal handovers between multiple VLC APs were studied in both non-overlapping spotlighting and in overlapping uniform lighting scenarios. Rahaim *et al.* [128] investigated the VHO criteria of a hybrid VLC/wireless fidelity (WiFi) network in order to improve

both the service quality and the total throughput. As a further development, Liang *et al.* [129] proposed an advanced VHO algorithm relying on the prediction of transfer delay in a hybrid VLC/LTE system, which may be determined by service interruption duration, message size, access delay, etc. Wang and Haas [50] optimised the LB by taking into account the handover signalling overhead of a hybrid VLC/WiFi system. Furthermore, the classic decision-making algorithms, such as the fuzzy-logic decision making approach [130] as well as the Markov decision process [131], were also introduced into VLC-based HetNets for designing effective handover schemes. In particular, Hou and O'Brien [130] proposed a fuzzy-logic-based VHO algorithm by jointly considering a pair of VHO techniques. Specifically, for their immediate handover scheme, there is no dwell time and the VHO is immediately triggered when the optical channel is interrupted. By contrast, for their dwell-based handover scheme, the dwell time is set to the maximum tolerable duration of a short service interruption, after which the VHO will be triggered. Moreover, Wang *et al.* [131] formulated the VHO problem as a Markov decision process and solved it in a dynamic manner in a VLC/RF system at a low signalling cost without any obvious system performance degradation.

1.4.3 Internet of Things

HetNets relying on a diverse spectrum allocation constitute an integral part of the IoT, where VLC provides a vast supply of unregulated spectrum and plays an important role. Let us now discuss two significant applications of VLC techniques in IoT scenarios, namely in indoor positioning and vehicular communications.

Location-aware technologies will revolutionise many aspects of the commercial and public services, as well as the military sectors, and are expected to spawn numerous unforeseen applications [132]. Although the global positioning system (GPS)-based outdoor localisation has been widely utilised, the accuracy of the indoor localisation techniques may not be satisfactory. Compared to the metre-level accuracy of the outdoor localisation, the error range of the indoor environment should be much lower, since the area of the indoor environment is usually limited to dozens of square metres. The straightforward approach is to use low-cost WiFi-based indoor localisation [133], but the achievable accuracy is low, on the order of 3-6 meters provided by the conventional WiFi-based localisation approach. As a member of the indoor communication family, VLC is also expected to provide indoor localisation services. It was shown in [134] that the number of LED lamps is usually more than that of the WiFi APs, which is a potential advantage of the triangulation based indoor localisation technique. A practical VLC-based localisation scheme was proposed in [134], where the localisation accuracy is around $\sim$0.4 m. Valuable research has also been undertaken related to VLC-based positioning in [65, 135–141].

Apart from the indoor localisation applications, VLC techniques have also been employed in outdoor vehicle to vehicle (V2V) and vehicle to infrastructure (V2I) communication scenarios [142–150]. One of the most important applications of VLC-based vehicular communications

is related to road traffic safety, where the traffic lights broadcast signals and approaching vehicles send hazard warnings. In these processes, the undesirable interference imposed by ambient light may not be negligible, as exemplified by street lights and the light emanating from the buildings. This problem was discussed in most of the relevant literature. On the other hand, the advantages of employing VLC for vehicular communications are multi-fold. Specifically, as a benefit of the self-positioning capability, the real-time information of neighboring vehicles is readily available for sharing and the drivers can adjust their driving conditions accordingly, which is capable of dramatically reducing the risk of collisions. Furthermore, LED lamps have already been routinely installed on vehicles, which reduces the extra cost of communications compared to deploying RF-based devices.

1.5 Open Challenges

Since the uplink transmission from the mobile devices relying on VLC may be wasteful in terms of its energy-consuming and may impose visual disturbances, most of the open literature focuses on the VLC DL transmission [49]. In order to solve this uplink problem, both RF- [128] and infrared-based [151] techniques may be employed. Furthermore, WiFi has been ubiquitously rolled out in indoor environments, which is capable of providing convenient uplink transmissions for VLC-based HetNets. In the meantime, WiFi can also ensure a seamless coverage and an uninterrupted service, when the VLC channel is poor or blocked [50].

Apart from the up-link transmission, the provision of a high-speed, low delay back-haul is another important design issue in VLC-based HetNets. The popular approaches rely on power-line and on fibre, respectively. Since power-line communication (PLC) uses the existing power-lines and the ubiquitous wires for communication, it may be readily employed. Various integrated VLC and PLC systems were proposed and investigated in [152, 153]. However, the highly dispersive and noisy nature of the power-line constitutes a bottleneck, limiting the achievable data rate of the VLC system. An alternative approach is the fibre-based system. Given the high-density deployment of LEDs, the cost of the fibre-based infrastructure may be deemed expensive. Hence, the most appropriate design of the VLC back-haul is still a challenging problem to explore.

Due to the random blockage of LoS by the users' movement or owing to obstructing objects, the received optical power may be dramatically reduced and the performance of VLC is consequently degraded. Frequently switching between the VLC and cooperative RF networks may result in the so-called ping-pong effect, as stated in Section 1.4.2.2. In order to mitigate the amount of control signalling and to reduce latency, a predictive handover decision should be adopted [154]. However, except for the preliminary study of [155], the research of the blockage patterns remains limited in the literature.

When the users are moving, mobility management constitutes another significant issue in VLC-

based HetNets. Within a single VLC cell, the mobile user will experience substantially varying channel quality between the cell centre and the cell edge. This effect should be taken into consideration, when deploying the VLC APs as well as designing link-level techniques. Furthermore, the overlapping areas of neighbouring VLC APs may be contaminated by ICI, which dramatically degrades the QoS. Hence, the transmission schemes conceived for these ICI-infested areas should be carefully designed for ensuring the service remains uninterrupted. Although various FR techniques have been proposed, an inherent disadvantage is that switching between different optical frequencies every few meters degrades the user experience. Therefore, seamless horizontal handover and VHO should be supported in VLC-based HetNets.

1.6 Contributions and Thesis Outline

1.6.1 Main Contributions

The novel research contributions provided by this treatise are summarised as follows:

- We investigate the *LB problem* in a hybrid VLC/WiFi DL, as part of next-generation HetNets, which relies on a hybrid combination of several VLC APs and a WiFi AP. The VLC system is capable of providing a high throughput, while the WiFi AP is capable of assisting the VLC DL both by supporting the uplink as well as when the light propagation is blocked, as well as when the VLC signals are ICI-contaminated or the VLC cell is overloaded. More explicitly, *a systematic solution* is provided, where the LB problem is carefully formulated as a network utility maximisation problem relying on the users' *proportional fairness* utility function. This joint *AP-association control* and *resource allocation* problem constitutes a mixed-integer non-linear programming (MINLP) problem. Upon discretizing the resources, we arrive at a near-optimal solution. Furthermore, by relaxing the original joint association-control and resource-allocation problem to a pure association control problem, we propose a distributed algorithm using dual decomposition. Upon invoking this dual decomposition technique, the solution approaches the optimal one within a low number of iterations, as it will be demonstrated in Section 2.4 with the aid of our simulation results. By using this distributed algorithm, each AP becomes capable of accomplishing its user association and resource allocation without the aid of a central resource manager. Furthermore, various *VLC cell formations* are considered, where the performances are investigated and compared in terms of the attainable area spectral efficiency (ASE), fairness, etc.

- We investigate the *MUS problem* relying on the UEs' PF as a measure by assigning each UE a specific scheduling priority, which is inversely proportional to its anticipated resource consumption [156] and then maximizing a carefully selected network utility function [157], in the meantime, considering amorphous UC-VT cluster formations for the VLC DL. More

explicitly, the optimal solution of this joint UC-based cluster formation and MUS problem is first found by a high-complexity exhaustive search, which may have an overwhelming complexity even for a modest-scale system. In order to reduce the computational complexity, the original problem is formulated as a *maximum weighted matching* (MWM) problem and multiple UEs are scheduled by solving the Kuhn-Munkres (KM) algorithm [158–162]. To further improve the grade of practicability, a greedy algorithm is proposed, which operates at a considerably lower complexity, despite taking into account the dynamics of the UC-VT clusters. Moreover, the computational complexity of both the exhaustive search and of the proposed schemes is analysed and various cluster formations are evaluated in terms of diverse VLC characteristics, such as the FoV, the LoS blocking probabilities, the optical AP arrangement, etc.

- We design *an energy-efficient scalable video system* relying on dynamic UC cluster formation in VLC networks, while jointly considering adaptive modulation (AM) mode assignment and power allocation. To be more specific, we propose *a distance-based localisation-aided UC cluster formation* technique and employ two different joint transmission schemes within the clusters, which we refer to as CT and VT. The beneficial construction of UC clusters constitutes the basis of an inherently energy-efficient VLC network. We propose *a heuristic 3-tier dynamic-programming-based algorithm* for solving our carefully formulated energy efficiency (EE) maximisation problem, including the user/layer-level AM mode assignment, the AP-level PA and the cluster-level EE optimisation, for maximising the *system-level EE* of our UC-VLC network. We evaluate the proposed EE scheme by transmitting a SHVC sequence and characterise our UC design in terms of its achievable EE, throughput and video quality in comparison to the conventional cells utilising FR. For our simulations results of the full video clips, please refer to `http://www.wireless.ecs.soton.ac.uk/`.

1.6.2 Thesis Outline

Let us now highlight the outline of this thesis, as explicitly shown in Figure 1.12. Chapter 1 is mainly constituted by four parts, namely by the portrayal of the VLC links, VLC networks, VLC applications as well as of the open challenges in VLC systems. The first two parts provide the preliminaries for the following chapters, which introduce some sedimentary knowledge concerning VLC systems. Then the VLC applications are extended as VLC-based HetNets, UC-VLC networks as well as scalable video streaming in Chapter 2, Chapter 3 and Chapter 4, respectively. Finally, Chapter 5 offers our conclusions based on the simulation results and outline our potential future work by jointly considering the open challenges discussed in Chapter 1. Let us continue with an overview of following chapters as follows.

- **Chapter 2: Cooperative load balancing in hybrid VLC and WiFi**

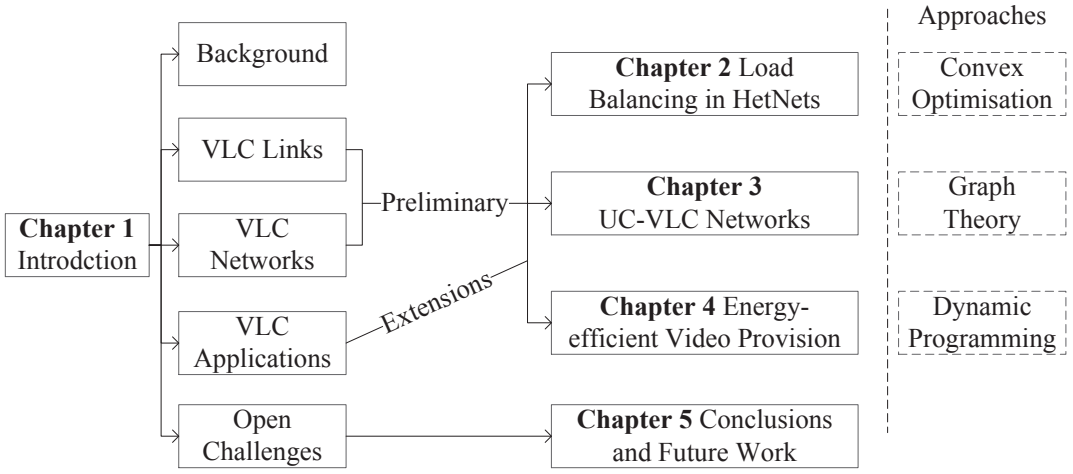

Figure 1.12: Organisation of this thesis.

In Chapter 2, as a complementary extension of the established RF Wireless Local Area Network (WLAN), VLC relying on commercially available LED transmitters offers a huge data rate potential in this license-free spectral domain, whilst simultaneously satisfying energy-efficient illumination demands. Various VLC cell formations, ranging from a regular cell-layout associated with different FR patterns to merged cells are investigated by employing advanced transmission schemes. Furthermore, a hybrid DL offering full RF-coverage by a WLAN and additionally supported by the abundant spectral resources of a VLC network is studied. Cooperative LB achieving PF is implemented by using both centralised and distributed resource-allocation algorithms. The performance of this hybrid RF/VLC system is analysed both in terms of its throughput and fairness in diverse cell formation scenarios. Our simulation results demonstrate that the VLC system advocated is capable of providing a high ASE and our hybrid RF/VLC system achieves the highest throughput and the highest grade of fairness in most of the scenarios considered.

- **Chapter 3: Users first: UC cluster formation for interference-mitigation in visible-light networks**

  VLC combined with advanced illumination may be expected to become an integral part of next generation heterogeneous networks. In order to mitigate the performance degradation imposed by the ICI, a UC cluster formation technique employing VT is proposed for the VLC DL system, where multiple users may be simultaneously supported by multiple APs. In contrast to the traditional network-centric (NC) design, the UC-VT cluster formation is dynamically constructed and adjusted, rather than remaining static. Furthermore, we consider the critical issue of MUS relying on maximizing the 'sum utility' of this system, which leads to a joint cluster formation and MUS problem. In order to find a practical solution, the original problem is reformulated as a MWM problem relying on a user-AP distance-based

weight and then a low-complexity greedy algorithm is proposed, which offers a suboptimal yet compelling solution operating close to the optimal value found by the potentially excessive-complexity exhaustive search. Our simulation results demonstrate that the proposed greedy MUS algorithm combined with the UC-VT cluster formation is capable of providing an average user throughput of about 90% of the optimal throughput, which is about three times the throughput provided by the traditional cellular design in some of the scenarios considered.

- **Chapter 4: UC VLC for energy-efficient scalable video streaming**

  An energy-efficient indoor VLC system relying on dynamic UC cluster formation is designed for scalable video streaming. Explicitly, the radically new UC cluster formation technique is based on an amorphous user-to-network association structure, which is ultimately the basis of our energy-efficient indoor VLC system. Furthermore, in order to optimise the system-level energy efficiency, our objective function is selected by jointly considering both the video quality and the power consumption. We then propose a 3-tier dynamic-programming-based algorithm for user/layer-level adaptive modulation mode assignment, for access-point-level power allocation and for cluster-level energy efficiency optimisation, respectively. Based on a scalable video coded sequence, our simulation results demonstrate the superior performance of our UC clusters compared to the conventional cell design in terms of its energy efficiency, throughput as well as video quality in most of the scenarios considered.

- **Chapter 5: Conclusions and future work**

  In Chapter 5, we summarise the major findings of this thesis and some potential research topics are outlined for future work as well.

Chapter 2

Cooperative Load Balancing in Hybrid Visible Light Communications and WiFi

As hypothesised in Chapter 1, VLC may be expected to become an integral part of the next-generation HetNets. In this chapter, the essential LB problem of a hybrid VLC/WiFi DL is investigated by taking into account various cell structures. Note that all the cell formations considered in this chapter are NC, while the radically new UC design principle will be introduced in Chapter 3 and Chapter 4. Figure 2.1 shows the organisation of this chapter, which commences with the motivation of the VLC and WiFi integration as well as with a brief review of the LB studies in RF HetNets in Section 2.1. After the discussion of the VLC link, in Section 2.2, various NC cell formations are presented and comparatively analysed with special emphasis on their area spectral efficiency. Our methodology of finding the optimum load balancing in the hybrid VLC/WiFi system, including both centralised as well as distributed LB, are critically appraised in Section 2.3 and Section 2.4, respectively. Finally, Section 2.5 offers our conclusions.

2.1 Chapter Introduction

2.1.1 Background of the Hybrid System

With the promise of gaining access to a huge unlicensed bandwidth, which is available in the optical domain of the electromagnetic spectrum, the research of optical wireless (OW) communications intensified during the past decade or so [4]. Apart from the substantial amount of research on the infrared region of the optical spectrum [22, 26], as a benefit of the rapid development of sol id-state lighting, high data rate VLC combined with advanced illumination has become a reality in indoor scenarios [10, 15, 21]. Specifically, the LEDs exhibit a high energy efficiency and additionally they are capable of exploiting a vast unregulated spectrum. Extensive investigations have been dedicated to the physical layer of VLC [43, 163–166], as also indicated by the IEEE 802.15.7 standard

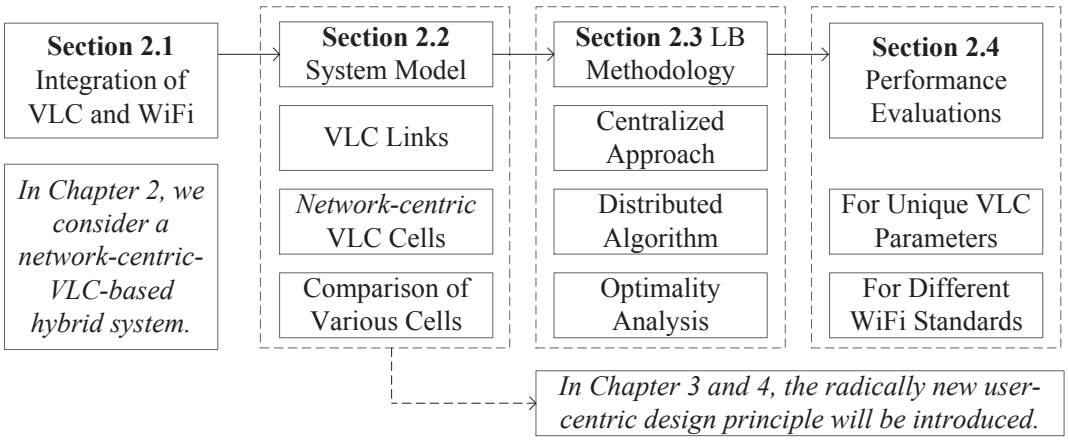

Figure 2.1: Outline of this chapter. Note that all the cell formations considered in this chapter are network-centric, while the radically new user-centric design principle will be introduced in Chapter 3 and Chapter 4.

ratified for short-range visible light wireless communication [39]. As far as the network level of our VLC system is concerned, stand-alone VLC networks may exhibit some potential drawbacks, such as for example: 1) VLC networks perform poorly in non-line-of-sight scenarios owing to the predominantly LoS propagation of light; 2) In VLC networks, each optical AP illuminates only a small confined cell compared to cellular RF networks; 3) VLC networks fail to provide convenient up-link coverage at the current-state-of-the-art. To overcome the above drawbacks, it is necessary to develop cooperative HetNets, which additionally rely on RF techniques as a complementary extension. As a result, the widely used WiFi network may be invoked as a cooperative partner of the VLC networks in indoor scenarios. As mentioned above, the proposed hybrid VLC/WiFi system is capable of providing high-data-rate connections as well as a seamless reliable coverage [4]. Compared to the traditional WiFi-only and VLC-only systems, the integration of VLC and WiFi is expected to significantly improve the aggregate throughput, which has been shown both by analytical and simulation results in [128] and the independent efforts disseminated in [167] led to similar conclusions. This motivates our research of the hybrid VLC/WiFi system by investigating fair and efficient cooperative LB, where a salient problem is the appropriate formation of VLC cells.

2.1.2 Related Works of Load Balancing in Radio Frequency Heterogeneous Networks

There is a paucity of studies on the formulation of VLC cells, although recently some valuable studies were disseminated in the context of a stand-alone VLC-only system. In particular, the authors of [168] discussed fractional frequency reuse for VLC cells and subsequently a joint transmission regime was derived in [169] for VLC cells. On the other hand, LB constitutes one of the fundamental problems, which in fact affects all cooperative multi-rate HetNets. Broadly speaking, this prob-

lem can be formulated as the constrained optimisation of a carefully selected utility function [120]. Substantial related work has been undertaken based on this problem in RF networks [2, 113–119]. Specifically, the authors of [2] investigated diverse technical approaches to the LB problems of HetNes and provided valuable design guidelines for OFDMA-based cellular systems. Moreover, the authors of [113–115] proposed centralised solutions, which rely on a centralised resource manager, while the authors of [116–119] addressed the LB problems of cellular networks with the aid of distributed algorithms. More particularly, Burchardt *et al.* [116] introduced a fuzzy logic based system, while Heliot *et al.* [117] proposed the employment of the Newton-Raphson-based method. However, both of them considered a homogeneous single-network scenario, rather than a VLC/RF HetNet scenario. As a further advance, in [118, 119] the LB problem of a RF-based HetNet was solved by using the dual decomposition approach and provided a near-optimal solution at a low complexity. However, the LB problem of VLC-based HetNets has remained to a large extent hitherto unexplored [170], especially when combined with various VLC cell formations.

2.1.3 Chapter Contributions

Against the above-mentioned background, in this chapter,

- we investigate the LB problem between several VLC APs and a WiFi AP relying on the users' PF as a measure;
- various VLC cell formations are jointly considered, ranging from the traditional cellular design philosophy to merged cells;
- the hybrid system's performance is analysed from the perspectives of both the unique VLC parameters as well as of the different WiFi standards.

2.2 Hybrid System Model

A hybrid VLC/WiFi DL system model is considered in this chapter, where the IEEE 802.11 WLAN is complemented by an optical network. The hybrid network has a set of VLC APs as well as a WiFi AP, but this scenario may be readily extended to other AP configurations. More explicitly, each VLC AP relies on an LED lamp constructed from several LEDs. Let us first discuss a range of VLC cell formations in this section before investigating our LB problems, as shown in Figure 2.1.

2.2.1 Link Characteristics

For a given transmitted optical power P_t of each VLC AP, the average optical power P_r received by a PD is the sum of the power received from all the corresponding transmitting VLC APs within its

vicinity, which is hosted in the set S and it is given as [1]

$$P_r = \sum_{a \in S} P_{r,i} = \sum_{a \in S} h_d[u,a] \cdot P_t. \tag{2.1}$$

According to [22,23], the optical channel's total DC attenuation from each VLC AP to the receiver u is given by Equation (1.4) and Equation (1.5). Our parameter values are summarised in Table 2.1.

According to [15], the average received power including *all* reflections may be negligible compared with the direct received average power of the LoS path. Therefore we may ignore the reflected optical power for simplicity and consider only the LoS-power as the desired received power. As a result, when the incoming optical radiation having an average power P_r impinging on a PD, the electronic current generated by the PD is given by

$$< i_{\text{PD}} >= \gamma \cdot P_r, \tag{2.2}$$

where γ [A/W] denotes the PD's responsivity and is assumed to be 0.53[A/W]. Let us now define the SINR as the aggregate electronic power received from signal set $S_S \subseteq S$ over the noise power in a bandwidth of B [MHz] [10] plus the sum of the electronic power received from other optical sources in interference set S_I, which is the complementary set of S_S. Since the corresponding electronic power is proportional to the square of the amplitude of the electronic current, we can write the SINR as

$$\xi = \frac{\gamma^2 \sum_{a \in S_S} P_{r,a}^2}{N_0 B + \gamma^2 \sum_{a \in S_I} P_{r,a}^2}, \tag{2.3}$$

where N_0 [A^2/Hz] is the noise power spectral density dominated by the shot noise N_{shot} [15], given as $N_0 \cong N_{\text{shot}} = qI_a(P_r) \sim 10^{-22}$, where q denotes the electron charge and $I_a(P_r)$ is the photo-current at the receiver [10], which relies on the received power. The expression in Equation (2.3) is in its common form and it will be different for each of the VLC cell formations, which are discussed next.

2.2.2 Regular Cell Formation

2.2.2.1 Unity Frequency Reuse

The most straightforward way of constructing a VLC cell is to simply assume that each VLC AP illuminates an individual cell, which corresponds to adopting unity FR (UFR) across all cells. Figure 2.2(a) shows the UFR design, where each single VLC AP illuminates an individual cell and the same frequency f is reused across all cells. The shaded areas represent the ICI imposed by the LoS ray conveying different information and arriving from the neighbouring cells at the cell edge.

[1] Since our major concern is that of investigating various VLC cell formations and finding an efficient LB solution for this hybrid system, some of the practical VLC channel characteristics have been simplified. The optical channel of Equation (1.4) may be widely adopted, when considering a Lambertian source in indoor optical wireless scenarios. Our algorithm is a generic one, which may be readily adapted to other types of optical channels.

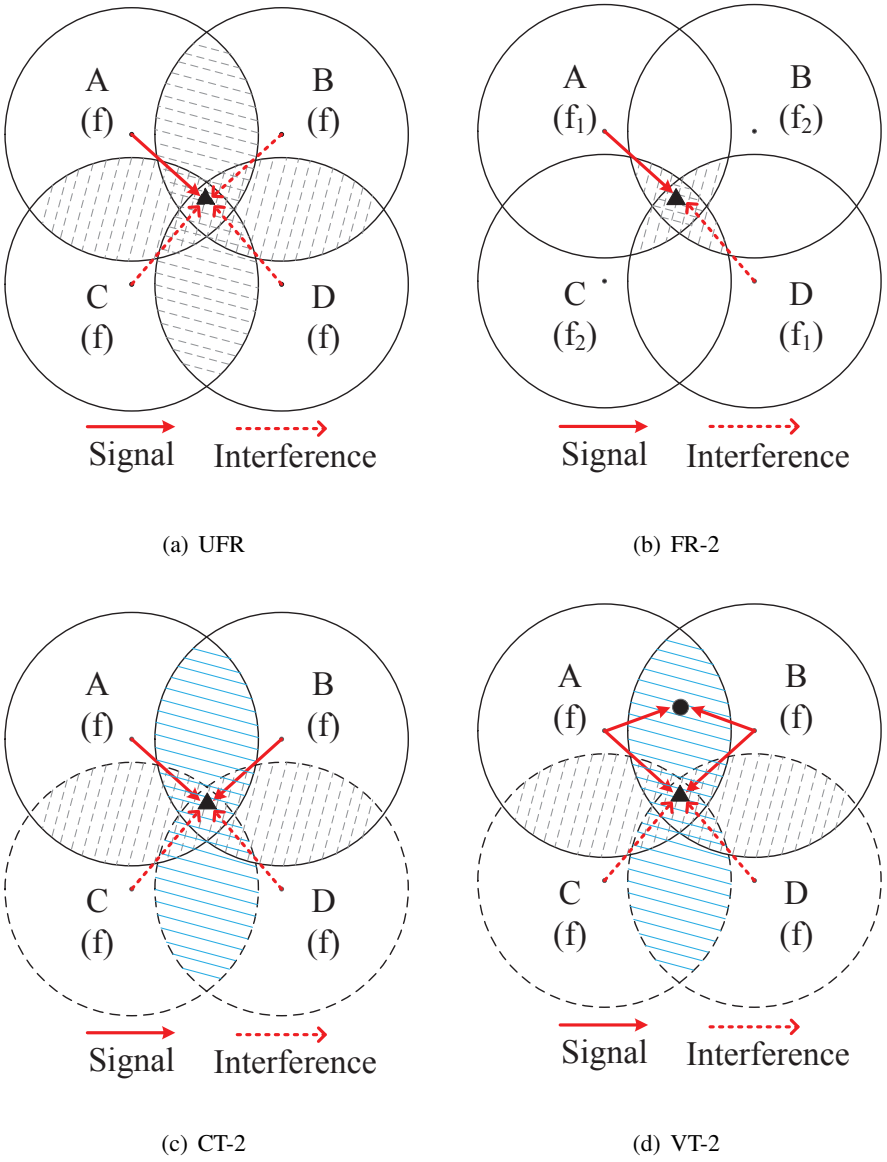

(a) UFR

(b) FR-2

(c) CT-2

(d) VT-2

Figure 2.2: Different cell formations. (a) is a regular cell formation, (b) has a FR factor of two, (c) represents two merged 2-AP cells with CT and (d) shows two merged 2-AP cells using VT. The triangle and circle denote certain points of reception. The shaded areas covered with dotted lines represent the ICI imposed by the LoS ray of neighbouring cells at the cell edge. The shaded areas covered by solid lines represent the overlapping areas within the merged 2-AP cells. In (a), (c) and (d), the entire frequency band f is used by each small cell, while in (b) orthogonal frequencies f_1 and f_2 are employed by neighbouring cells, where we have $f_1 = f_2 = f/2$.

VLC parameters	
Semi-angle at half power ($\phi_{1/2}$)	70°
Gain of an optical filter ($T_s(\psi)$)	1.0
Refractive index of a lens at a PD (n_r)	1.5
Modulation bandwidth (B) [10]	20 [MHz]
Detection area of a PD (D_{PA})	1.0 [cm^2]
O/E conversion efficiency (γ)	0.53 [A/W]
Half of the receiver's FoV (ψ_{F})	60°/62.5°
Room model parameters	
Room size	15m×15m×3m
Height of VLC APs	2.5m
Distribution of VLC APs	4×4
No. of users	50
Algorithmic parameters	
BER threshold	10^{-5}
Nyquist Roll-off factor (ρ)	1
Normalised WiFi capacity for DL (p_{DL})	0.8
Supply and demand gap (δ_{target})	1

Table 2.1: Simulation parameters of the hybrid VLC/WiFi system.

For the triangular point shown in Figure 2.2(a), the SINR is given by

$$\xi_{\text{UFR}} = \frac{\gamma^2 P_{r,\text{A}}^2}{N_0 B + \gamma^2 (P_{r,\text{B}}^2 + P_{r,\text{C}}^2 + P_{r,\text{D}}^2)}, \tag{2.4}$$

which shows that ICI arrives from all the other three neighbouring cells in this scenario. If the FoV was sufficiently narrow, the ICI may be mitigated since the user can only receive data from a single VLC AP. However, this would potentially lead to isolated 'coverage islands' and 'coverage holes', which consequently may result into frequent horizontal handovers and outage event, when the DL user is walking between VLC APs, since the user will experience dramatic performance degradation in the area without LoS coverage.

2.2.2.2 Non-Unity Frequency Reuse

Following the traditional cellular design principle, non-unity FR patterns may be employed for reducing the ICI, while each VLC AP still functions as an individual cell. Since the first-tier neighbouring cells contribute most of the ICI, while the second-tier cells generally have a negligible influence, an FR factor of two may be used. For the triangular point shown in Figure 2.2(b), the

SINR is given by

$$\xi_{\text{FR-2}} = \frac{\gamma^2 P_{r,\text{A}}^2}{N_0 B/2 + \gamma^2 P_{r,\text{D}}^2}. \tag{2.5}$$

Hence, the ICI emanating from the neighbouring cells B and C can be removed. Although this is an appealingly simple solution, when using an FR factor larger than one, the system has to obey the classic trade-off between reduced bandwidth efficiency (BE) and improved cell-edge SINR. In fact, supporting mobility is the most grave problem associated with non-unity FR during VLC cell formation, since switching between frequencies every few meters during the user's movement degrades the user experience. This is also the reason for not considering FFR [168], which exhibits a more elaborate frequency planning and triggers even more frequent handovers.

2.2.3 Merged Cell Formation

In order to reduce the size of the ICI-infested areas, whilst improving the mobility, several neighbouring cells can be merged into a large multi-AP cell, where advanced transmission techniques may be employed in their overlapping areas. In the following, we use UFR across multi-AP cells for simplicity, although non-unity FR might be also used.

2.2.3.1 Combined Transmission

In this arrangement, each individual VLC AP of a multi-AP cell conveys the same information on the same visible carrier frequency in their overlapping areas. In Figure 2.2(c), A and B are merged into a 2-AP cell and transmit identical signals in their overlapping area as a single source, which we refer to as CT. Thus the potential ICI is beneficially turned into useful signals which may be combined and the original cell edges of Figure 2.2(a) become the cell centers of Figure 2.2(c). For the triangular point shown in Figure 2.2(c), the SINR is given by

$$\xi_{\text{CT-2}} = \frac{\gamma^2 (P_{r,\text{A}}^2 + P_{r,\text{B}}^2)}{N_0 B + \gamma^2 (P_{r,\text{C}}^2 + P_{r,\text{D}}^2)}. \tag{2.6}$$

Although the SINR may be enhanced, CT results in a reduced BE, since only a single user is served at a time by several APs in the overlapping area within a merged cell.

2.2.3.2 Vectored Transmission

In order to eliminate the BE-reduction imposed by CT, zero-forcing ()-based VT techniques can be employed for serving multiple users at the same time in the overlapping area. The underlying principle of ZF-based VT is to totally eliminate the ICI at the multiple transmitters, so that the multiple users receive mutually interference-free signals.

To elaborate a little further, let n_a denote the number of APs in a merged n_a-AP cell and a vector of n_u users are served simultaneously within the overlapping area. Let further $\boldsymbol{x_t} \in \mathbb{R}^{n_u \times 1}$

and $\boldsymbol{y_r} \in \mathbb{R}^{n_u \times 1}$ denote the vectors of transmitted and received signals, respectively. By using VT, we have

$$\boldsymbol{y_r} = \gamma \cdot P_t \cdot \boldsymbol{H} \cdot \boldsymbol{G} \cdot \boldsymbol{\Omega} \cdot \boldsymbol{x_t} + \boldsymbol{n}, \tag{2.7}$$

where $\boldsymbol{n}$ includes both the noise and the ICI received from the neighbouring merged cells, while the channel-matrix $\boldsymbol{H} \in \mathbb{R}^{n_u \times n_a}$ hosts the DC attenuations between n_u users and n_a APs. Furthermore, the matrix $\boldsymbol{G} = \boldsymbol{H}^H(\boldsymbol{H}\boldsymbol{H}^H)^{-1}$ obeys the ZF criterion, which hence results in a beneficial ICI-free identity matrix for $\boldsymbol{H}\boldsymbol{G} = \boldsymbol{I}_{n_u}$. Finally, the matrix $\boldsymbol{\Omega}$ is introduced to enforce the per-AP power constraints. According to [171], we have

$$\boldsymbol{\Omega} = \omega \boldsymbol{I}_{n_u}, \quad \omega = \min_{a=1,2,\ldots,n_a} \sqrt{\frac{1}{\|\boldsymbol{G}(a,:)\|_F^2}}, \tag{2.8}$$

where $\boldsymbol{G}(a,:)$ is the ath row of $\boldsymbol{G}$. As a result, the SINR of a particular user may be written as [2]

$$\xi_{\text{JT}} = \frac{\gamma^2 P_t^2 \omega^2}{N_0 B + \gamma^2 \sum_{i \in S_I} P_{r,i}^2}. \tag{2.9}$$

In general, to facilitate VT from n_a APs to n_u users, both the $(n_u \times n_a)$-element DC attenuation matrix and the users' data have to be shared amongst the n_a APs [172]. For VLC channels, the requirements may be readily satisfied, since the VLC users are predominantly stationary. This is similar to the successful employment of ZF-based transmit pre-coding techniques, which is referred to as VT in the state-of-the-art digital subscriber line based G.fast system (Recommendation ITU-T G.9701) invoked for coping with the far end cross talk between twisted pairs.

As an example, in Figure 2.2(d), A and B form a VT-aided 2-AP cell and two users are served simultaneously in the originally ICI-infested areas. For the paired points shown in Figure 2.2(d), the SINRs are given by

$$\xi_{\text{JT-2}}^{\bullet} = \frac{\gamma^2 P_t^2 \omega^2}{N_0 B}; \quad \xi_{\text{JT-2}}^{\blacktriangle} = \frac{\gamma^2 P_t^2 \omega^2}{N_0 B + \gamma^2 (P_{r,\text{C}}^2 + P_{r,\text{D}}^2)}. \tag{2.10}$$

2.2.4 Area Spectral Efficiency

To gain further quantitative insights, Figure 2.3 illustrates both the classic BE surface and the mean bandwidth efficiency (MBE) of different VLC cell formations. The BE is calculated as

$$\begin{aligned} &\eta_{\text{UFR}} = \log_2(1 + \xi_{\text{UFR}}); \quad \eta_{\text{FR-2}} = \frac{1}{2}\log_2(1 + \xi_{\text{FR-2}}); \\ &\eta_{\text{CT}} = \hbar \log_2(1 + \xi_{\text{CT-2}}); \quad \eta_{\text{JT}} = \log_2(1 + \xi_{\text{JT}}); \end{aligned} \tag{2.11}$$

where $\hbar$ accounts for the loss of resource under utilisation of CT, which is 0.9122 and 0.8737 when the FoV is 120° and 125° under our simulation setup, respectively. In Figure 2.3(c), $\hbar$ is given by

$$\hbar = \frac{1}{2} \cdot \frac{D_s}{D_{mc}} + \frac{D_{mc} - D_s}{D_{mc}}, \tag{2.12}$$

[2] Since the interference power received by the merged cell under consideration is influenced by the ZF-based VT within its neighbouring merged cells, for simplicity, we assume that the interference imposed is always equal to its maximum value, which characterises the worst-case situation in our VT cell formation scenario.

where D_s and D_{mc} denote the area of the shaded areas within the merged 2-AP cell and the total area of the merged cell, respectively. In our simulations, a 15m$\times$15m$\times$3m room model is considered, including 4$\times$4 uniformly distributed optical APs at a height of 2.5m. The parameters of the VLC APs are summarised in Table 2.1. Compared to UFR as shown in Figure 2.3(a), a FR of two sufficiently reduces the ICI-contaminated areas, but results into a significantly reduced BE as shown in Figure 2.3(b). By contrast, all of our proposed merged cell formations shown in Figures 2.3(c), 2.3(d), 2.3(e) improve the MBE, as suggested by Figure 2.3(f). More explicitly, when a 2-AP cell is created, the MBE of VT is only marginally better than that of CT. However, when forming all VLC APs as a single cell, a substantial MBE improvement can be achieved with the aid of VT, since the resultant system becomes reminiscent of a large-scale MIMO system.

2.3 Methodology for Finding the Optimum Load Balancing

Let us now determine the optimum LB for a set of users in this hybrid VLC/WiFi system by taking into account various VLC cell formations. We would like to introduce some notations first. Let $\mathcal{V}_A$ be the set of the single-AP or multi-AP VLC cells, where $|\mathcal{V}_A|$ is the number of cells. In this section, we illustrate our methodology in the UFR scenario, which can be readily extended to other cell formations. $\mathcal{V}_W$ denotes the set of the WiFi APs and we have $|\mathcal{V}_W| = 1$. At the same time, the users of the set $\mathcal{V}_U$ are assumed to be uniformly distributed at random in this hybrid VLC/WiFi system. Since each user has a limited FoV, they can only communicate with each other using VLC, if one or more optical APs reside within the FoV of the user. Let R^{VLC} be the matrix of throughput between the VLC cells a and the user u, which is defined as $R^{\text{VLC}} = (r_{au} : a \in \mathcal{V}_A, u \in \mathcal{V}_U)$. Let furthermore $R^{\text{WiFi}} = (r_{au} : a \in \mathcal{V}_W, u \in \mathcal{V}_U)$ be the matrix of throughput allocated by the WiFi AP to the user u.

The LB problem is a connection level issue, which can be performed according to the connection level statistics [20]. Since no fast-fading is experienced in VLC propagation, as long as the users' positions remain static, the channel information does not change. When considering a low-mobility indoor scenario, the coherence time of WiFi propagation is sufficiently long. Hence, both the VLC and WiFi propagation changes slowly in the given period. The required channel information only has to be collected infrequently before activating this optimisation procedure. As a result, we consider a static system without the arrival of new users and the departure of existing users. In general, this resorts to the NUM framework [120] and three methodologies will be employed in this section. We commence with an exact non-linear formulation and then discretize this non-linear formulation. Furthermore, we come to the classic distributed algorithm, which is capable of approaching the performance of the near-optimal centralised solution.

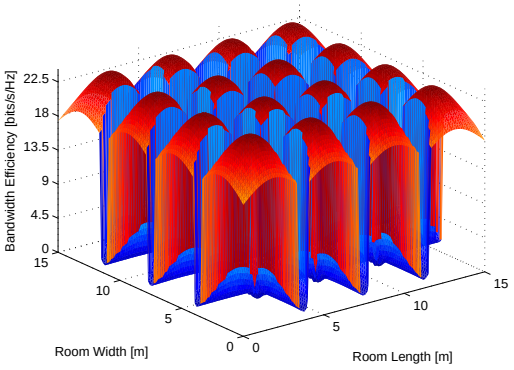

(a) UFR

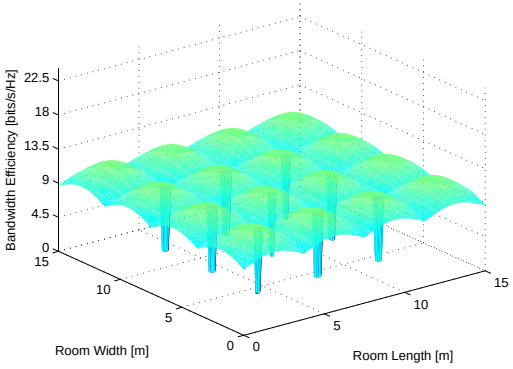

(b) FR-2

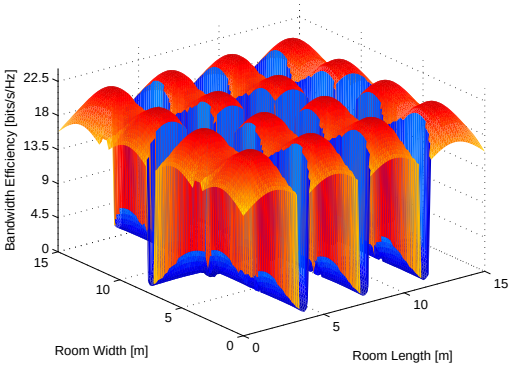

(c) CT-2

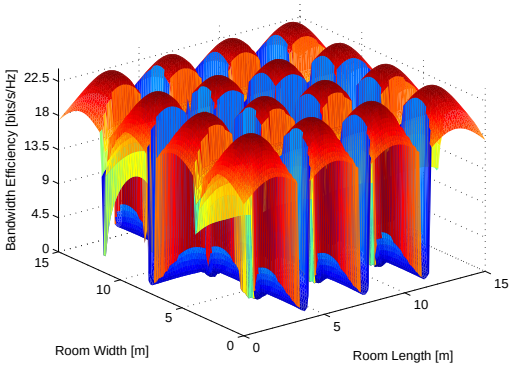

(d) VT-2

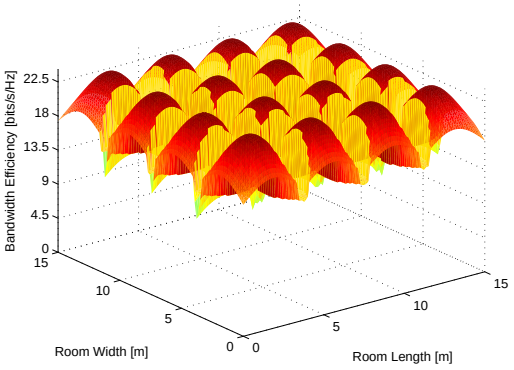

(e) VT-16

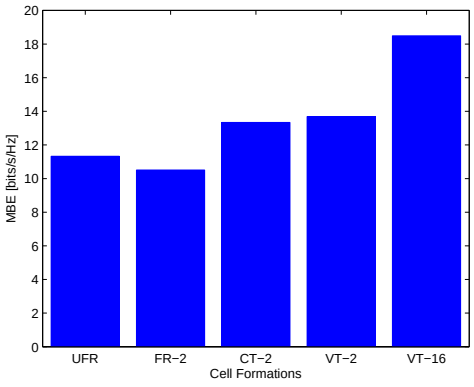

(f) MBE

Figure 2.3: BE surface and the MBE of different VLC cell formations. (a) is a regular UFR cell formation, (b) has a FR factor of two, (c) represents merged 2-AP cells with CT, (d) shows merged 2-AP cells with VT, (e) is a merged 16-AP cell with VT and (f) shows the MBE of (a)-(e), where the receivers' FoV is 120°. The corresponding simulation parameters are summarised in Table 2.1.

2.3.1 Centralised Approach

Our objective is to find the optimal LB using the objective function (OF) of maximizing the sum of all users' utility functions under the PF constraints [114] in this hybrid VLC/WiFi system, which is ultimately a *joint association control and resource allocation* problem. In this context, the authors of [173] have shown that we can achieve proportional allocation by optimizing the OF of:

$$\text{maximize} \qquad \sum_{u \in \mathcal{V}_U} \log(\beta_u), \tag{2.13}$$

where β_u is the actual throughput allocated to a user u. The logarithm of β_u may be interpreted as the utility function of a user, as argued for example in [157].

At this stage, a binary variable x_{au} is introduced to indicate, whether the user u is assigned to the AP a, where we have $x_{au} = 1$ if u and a do have a connection, while 0 otherwise. Note that a may denote either a certain VLC cell or the WiFi AP, namely $a \in \mathcal{V}_A \cup \mathcal{V}_W$ in this section. Hence, the actual throughput β_{au} of the user u allocated by the AP a may be expressed as $x_{au} r_{au} p_{au}$, where p_{au} is a fractional variable between 0 and 1, which is denoted as the proportion of time that a is allocated to u. For a given user u, the total actual throughput becomes

$$\beta_u = \sum_{a \in \mathcal{V}_A \cup \mathcal{V}_W} x_{au} r_{au} p_{au}. \tag{2.14}$$

By substituting (2.14) into the OF of (2.13), we have

$$\Gamma(\boldsymbol{x}, \boldsymbol{p}) = \sum_{u \in \mathcal{V}_U} \log \sum_{a \in \mathcal{V}_A \cup \mathcal{V}_W} x_{au} r_{au} p_{au}. \tag{2.15}$$

Since only a single AP a' is assigned to a given user, i.e. we have $x_{a'u} = 1$, we can write: $\log \sum_a x_{au} r_{au} p_{au} = \sum_a x_{au} \log(r_{au} p_{au})$. Therefore Equation (2.15) may equivalently be written as

$$\Gamma(\boldsymbol{x}, \boldsymbol{p}) = \sum_{u \in \mathcal{V}_U} \sum_{a \in \mathcal{V}_A \cup \mathcal{V}_W} x_{au} \log(r_{au} p_{au}), \tag{2.16}$$

Several optimisation constraints may be formulated based upon various assumptions as well as on a range of practical limitations. The mathematical formulation of this maximisation problem becomes:

$$\begin{aligned}
\text{maximize} \quad & \Gamma(\boldsymbol{x}, \boldsymbol{p}) && && (2.17)\\
\text{subject to} \quad & \sum_{a \in \mathcal{V}_A \cup \mathcal{V}_W} x_{au} = 1 && \forall u \in \mathcal{V}_U;\\
& \sum_{u \in \mathcal{V}_U} x_{au} p_{au} \leq 1 && \forall a \in \mathcal{V}_A;\\
& \sum_{u \in \mathcal{V}_U} x_{au} p_{au} \leq p_{\text{DL}} && \forall a \in \mathcal{V}_W;\\
& x_{au} \in \{0,1\} && \forall a \in \mathcal{V}_A \cup \mathcal{V}_W, \forall u \in \mathcal{V}_U;\\
& 0 \leq p_{au} \leq 1 && \forall a \in \mathcal{V}_A \cup \mathcal{V}_W, \forall u \in \mathcal{V}_U.
\end{aligned}$$

Firstly, for each user u, there is one and only one AP a' in order to satisfy $x_{a'u} = 1$ for an extended period of time. At this stage, we do not impose any constraint on the users' resource demand, hence all the users may either connect to the VLC APs or to the WiFi AP. Secondly, each AP has to request resources confined to its maximum capacity. By contrast, for the DL WiFi AP, the available normalised capacity is assumed to be less than p_{DL} instead of 1, because it may allocate $(1 - p_{\mathrm{DL}})$ of its total resources for example to the uplink. Furthermore, p_{DL} may be set up as any feasible value between 0 and 1 according to the specific system design and traffic requirements. Finally, the variable x_{au} should be binary, while p_{au} is a real value between 0 and 1. As a result, the above problem represents an MINLP problem that may be solved directly by using the OPTI Toolbox, albeit this would be time-consuming.

2.3.2 Discretized Linear Programming Approximation

Instead of solving the MINLP directly, we might opt for a linear relaxation of the original problem. Following the work in [114], we discretize the scheduling time period of each access point into T discrete intervals, where T is κ times the number of the users. In practice, $\kappa = 10$ turns out to be sufficient to obtain an acceptable approximation of the non-linear problem. A new binary variable y_{aut} is introduced. If and only if the access point a is associated with the user u and allocates t $(0 \leq t \leq T)$ time slots to user u, we arrive at $y_{aut} = 1$. Thus, we arrive at the linear OF of

$$\Gamma_D(\boldsymbol{y}) = \sum_{u \in \mathcal{V}_U} \sum_{a \in \mathcal{V}_A \cup \mathcal{V}_W} \sum_{t=1}^{T} y_{aut} \cdot \log(r_{au} \frac{t}{T}). \tag{2.18}$$

Accordingly, our linear program is then formulated as

$$\begin{aligned}
&\text{maximize} && \Gamma_D(\boldsymbol{y}); && && (2.19)\\
&\text{subject to} && \sum_{a \in \mathcal{V}_A \cup \mathcal{V}_W} \sum_{t=1}^{T} y_{aut} = 1 && \forall u \in \mathcal{V}_U;\\
& && \sum_{u \in \mathcal{V}_U} \sum_{t=1}^{T} y_{aut} \cdot \frac{t}{T} \leq 1 && \forall a \in \mathcal{V}_A;\\
& && \sum_{u \in \mathcal{V}_U} \sum_{t=1}^{T} y_{aut} \cdot \frac{t}{T} \leq p_{\mathrm{DL}} && \forall a \in \mathcal{V}_W;\\
& && y_{aut} \in \{0,1\} && \forall a \in \mathcal{V}_A \cup \mathcal{V}_W, \forall u \in \mathcal{V}_U.
\end{aligned}$$

The first constraint of Equation (2.19) states that only one and exactly one AP is assigned to each user. The second and third indicate that each AP restricts its time-resource allocation to capacity. This discretized linear problem has been solved with the aid of the CPLEX solver. Then we translate the solution in Equation (2.19) to the non-linear program Equation (2.17) as follows:

$$x_{au} = \sum_{t=1}^{T} y_{aut}, \qquad p_{au} = \sum_{t=1}^{T} \frac{t}{T} y_{aut}. \tag{2.20}$$

2.3.3 A Dual Decomposition Method

We now conceive an efficient and scalable distributed algorithm for Equation (2.17).

2.3.3.1 Transformation

According to [114], when the AP/user association matrix $\boldsymbol{x}$ is given, the unique optimal solution becomes $p_{au} = x_{au}/N_a$, where $N_a = \sum_{u\in\mathcal{V}_U} x_{au}$ is the number of users associated with the access point a. As a result, the optimisation in Equation (2.17) may be transformed to a pure association control problem, hence we now have the primal OF of:

$$\Gamma_{de}(\boldsymbol{x},\boldsymbol{\mathcal{N}}) = \sum_{u\in\mathcal{V}_U}\sum_{a\in\mathcal{V}_A\cup\mathcal{V}_W} x_{au}\log(\frac{r_{au}}{N_a}). \tag{2.21}$$

Additionally, we have three constraints as well:

$$\sum_{u\in\mathcal{V}_U} x_{au} = N_a \qquad \forall a \in \mathcal{V}_A\cup\mathcal{V}_W; \tag{2.22}$$

$$\sum_{a\in\mathcal{V}_A\cup\mathcal{V}_W} x_{au} = 1 \qquad \forall u \in \mathcal{V}_U; \tag{2.23}$$

$$x_{au} \in \{0,1\} \qquad \forall a \in \mathcal{V}_A\cup\mathcal{V}_W, \forall u \in \mathcal{V}_U. \tag{2.24}$$

Furthermore, the dual objective $g(\boldsymbol{\nu})$ is formulated as

$$g(\boldsymbol{\nu}) = \sup_{\boldsymbol{x},\boldsymbol{\mathcal{N}}} L(\boldsymbol{x},\boldsymbol{\mathcal{N}},\boldsymbol{\nu}), \tag{2.25}$$

where $L(\boldsymbol{x},\boldsymbol{\mathcal{N}},\boldsymbol{\nu})$ is the Lagrangian function for Equation (2.21) using the constraints of Equation (2.22) after relaxation of (2.24), yielding

$$\begin{aligned} &L(\boldsymbol{x},\boldsymbol{\mathcal{N}},\boldsymbol{\nu}) \\ &= \underbrace{\sum_{u\in\mathcal{V}_U}\sum_{a\in\mathcal{V}_A\cup\mathcal{V}_W} x_{au}(\log r_{au} - \nu_a)}_{\mathbb{S}_a} + \underbrace{\sum_{a\in\mathcal{V}_A\cup\mathcal{V}_W} N_a(\nu_a - \log N_a)}_{\mathbb{S}_b}, \end{aligned} \tag{2.26}$$

where $\boldsymbol{\mathcal{N}} = (N_a : a \in \mathcal{V}_A\cup\mathcal{V}_W)$ constitutes a set, whose elements are given by the number of users associated with each AP, while $\boldsymbol{\nu} = (\nu_a : a \in \mathcal{V}_A\cup\mathcal{V}_W)$ is the vector of Lagrangian multipliers corresponding to the constraint of Equation (2.22).

2.3.3.2 Decomposition

The problem of Equation (2.25) is further partitioned into two sub-problems in a distributive - rather than centralised - fashion.

- On the user's side, we solve the sub-problem of maximizing $\mathbb{S}_a$. Since we have $x_{au} \in \{0,1\}$ and $\sum_{a\in\mathcal{V}_A\cup\mathcal{V}_W} x_{au} = 1$, for each $u \in \mathcal{V}_U$ we find

$$a^* = \underset{a\in\mathcal{V}_A\cup\mathcal{V}_W}{\operatorname{argmax}} (\log r_{au} - \nu_a). \tag{2.27}$$

Then we set $x_{a^*u} = 1$. Hence we could compute the number of users $\boldsymbol{\mathcal{N}}^{(1)}$ associated with each AP corresponding to $\mathbb{S}_a$.

- On the AP's side, upon applying the Karush-Kuhn-Tucker (KKT) conditions [122], for each $a \in \mathcal{V}_A \cup \mathcal{V}_W$ we have

$$\frac{\partial g^{(2)}}{\partial N_a} = \nu_a - \log N_a + 1 = 0 \Rightarrow N_a = \exp(\nu_a - 1);$$

Then we can obtain $\boldsymbol{\mathcal{N}}^{(2)}$ corresponding to $\mathbb{S}_b$.

A variable $\boldsymbol{\delta}$ is introduced to reflect the difference between the resource demand $\mathbb{S}_a$ and resource supply $\mathbb{S}_b$, defined as

$$\boldsymbol{\delta} = |\boldsymbol{\mathcal{N}}^{(1)} - \boldsymbol{\mathcal{N}}^{(2)}|. \tag{2.28}$$

An acceptable target difference of δ_{target} is pre-set before iteratively solving the sub-problems. If each element of $\boldsymbol{\delta}$ is smaller than the target gap, the iterations will be curtailed and the allocation result of $(\hat{\boldsymbol{x}}, \hat{\boldsymbol{\mathcal{N}}})$ is obtained; otherwise $\boldsymbol{\nu}$ will be adjusted for the next iteration according to the gradient method, which is given as

$$\nu_a(i+1) = \nu_a(i) - \varepsilon(i)(N_a - \sum_{u \in \mathcal{V}_U} x_{au}), \tag{2.29}$$

where $\varepsilon(i)$ is a sufficiently small step size in the ith iteration. In this chapter, we set $\varepsilon(i) = \varepsilon_0 \cdot i^{-\frac{1}{2}+\tau}$, where ε_0 and τ are positive constants appropriately chosen for satisfying $\lim_{i\to\infty} \varepsilon(i) = 0$ and $\sum_{i=0}^{i=\infty} \varepsilon(i) = \infty$ for achieving the convergence of the gradient algorithm towards the optimal solution.

2.3.4 Optimality Analysis

Although the convergence of the distributed algorithm may be proved analytically, e.g. in [119], it is difficult to theoretically study how far the converged solution found is away from that of the true original problem, since the original problem contains a binary integer. Upon comparing the solutions provided by LP approximation, we experimentally study the optimality of the solution provided by the distributed algorithm, which has not been discussed in the literature.

2.3.4.1 Justification

Let us now consider the relationship between the OF value Γ of the original MINLP problem Equation (2.17), the LP OF value Γ_D for Equation (2.19) and the solution $\hat{\Gamma}_{de}$ provided by the distributed algorithm. Since the distributed algorithm is performed after relaxing Equation (2.24), which prevents us from theoretically proving the optimality of the solution $\hat{\Gamma}_{de}$ of the problem Equation (2.21), we opt for an empirical analysis of the optimality of Γ, Γ_D and $\hat{\Gamma}_{de}$.

(i) *NLP vs. LP:* The authors of [114] have characterised the relationship between the NLP and LP formulations for any feasible solution ($\boldsymbol{y}$) and its corresponding translation ($\boldsymbol{x}, \boldsymbol{p}$), which may be written as

$$\Gamma_D \leq \Gamma. \tag{2.30}$$

(ii) *NLP vs. Distributed:* We would like to introduce the notation (2.21') for the relaxation of the problem of Equation (2.21). Furthermore, we know that $\hat{\Gamma}_{de}$ upper bounds (2.21') [122]. Intuitively, $\hat{\Gamma}_{de}$ may also upper bound Equation (2.21), since the solution of x_{au} always satisfies the constraint Equation (2.24) in the process of solving (2.21').

(iii) *NLP, LP and Distributed:* Combing (i) and (ii) above, for any feasible pair, we may use $\hat{\Gamma}_{de}$ and Γ_D as the upper bound and the lower bound for the original MINLP problem, respectively. Please note that all the above discussions are here related to the resource allocation lemma detailed at the beginning of Section III-C [114]. Under this lemma Equation (2.17) may be written as Equation (2.21).

Figure 2.4 shows the empirical optimality of our distributed algorithm with the aid of simulations relying on the parameters discussed in Section 2.4.1. The discretized LP approximation is implemented in our simulation scenarios and the near-optimal solution of the LP OF is shown by the dashed line in Figure 2.4. We obtain a fairly accurate solution of the distributed OF within a dozen of iterations, which is within a margin of about 1.5% from the sub-optimal LP solution. Since we may derive from (iii) that the optimal NLP OF value Γ may be between Γ_D and $\hat{\Gamma}_{de}$, the difference between $\hat{\Gamma}_{de}$ and Γ may be even smaller. This demonstrates that the distributed algorithm is capable of converging to the optimal value of the original NLP problem, whilst providing a near-optimal solution within a few dozens of iterations.

2.3.4.2 Implementation

As a benefit of the above optimality analysis, we opt for the distributed algorithm. Indeed, the distributed algorithm converges to a near-optimal solution significantly faster than the centralised approaches. In each iteration, each AP initialises and broadcasts a feasible price value ν_a to all the users within its coverage. Here we assume that different APs use pre-allocated orthogonal frequency bands for simultaneously broadcasting ν_a. Each user finds the optimal AP a^* according to Equation (2.27) and sends its user-identifier back to a^*. Thus each AP becomes capable of calculating the user demand $\boldsymbol{\mathcal{N}}^{(1)}$. At the same time, the supply vector $\boldsymbol{\mathcal{N}}^{(2)}$ can also be calculated by the APs. Each AP compares its supply and user demand. When the difference between the demand and supply becomes sufficiently small, the iterations are curtailed and a near-optimal solution has been found. In this way, each AP becomes capable of performing its own resource allocation. The total number of information exchange operations is proportional to $(n_a + n_u)$, where n_a and n_u denote the number of APs and users, respectively. Let us now provide an overview of the dual decomposition algorithm in form of Algorithm 1, which has been verified using our simulations.

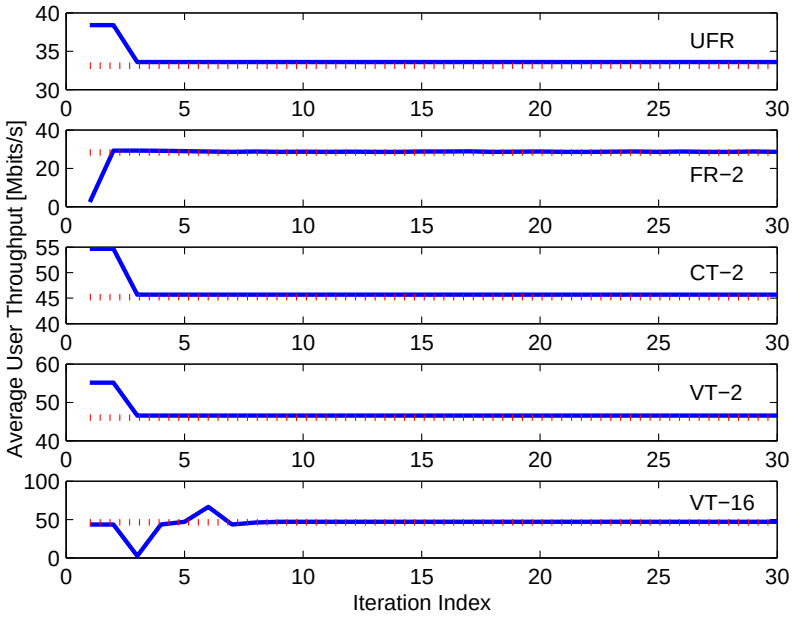

Figure 2.4: Empirical optimality of the distributed algorithm relying on the simulation parameters discussed in Section 2.4.1. The solid line shows the average user throughput in each iteration, while small vertical tick-marks show the solution of the LP problem provided by CPLEX. The corresponding simulation parameters are summarised in Table 2.1.

2.4 Performance Evaluation of the Hybrid System

In this section, we will present our simulation results for the LB problem, with special emphasis on the various aforementioned VLC cell formations in our hybrid VLC/WiFi system, since we know from Figure 2.3 that the performances of the different cell formations may be significantly different. We commence by studying the user's average throughput for different FoVs and LoS blocking probabilities, followed by investigating the fairness both from the system's and the individual users' perspectives for the sake of characterizing the quality of service experienced by the users under different cell formation schemes. Finally, different WiFi standards are introduced and compared in the hybrid system.

2.4.1 Simulation Setup

A 15m×15m×3m room model is considered, which is only covered by a VLC system including 4×4 uniformly distributed optical APs at a height of 2.5m. Additionally, the room is entirely covered by an IEEE Std 802.11n WiFi AP supporting a data rate as high as 120 Mbits/s within 25m. The parameters of the LED lamps are summarised in Table 2.1. The normalised WiFi DL capacity p_{DL} is assumed to be 0.8 and 50 users are assumed to be distributed uniformly at random

Algorithm 1: Dual Decomposition Algorithm for solving our association control problem

Input: R^{VLC}, R^{WiFi}, δ_{target};
Initialisation: $\boldsymbol{\nu}$, $i \leftarrow 0$, ε_0;
while $max(\delta) \geq \delta_{target}$ **do**
  for *each* $u \in \mathcal{V}_U$ **do**
    find $a^* = \underset{a \in \mathcal{V}_A \cup \mathcal{V}_W}{\text{argmax}} (\log r_{au} - \nu_a(i))$;
  end
  calculate *demand* $\boldsymbol{\mathcal{N}}^{(1)}$;
  for *each* $a \in \mathcal{V}_A \cup \mathcal{V}_W$ **do**
    $N_a = \exp(\nu_a(i) - 1)$;
    $\nu_a(i+1) = \nu_a(i) - \varepsilon(i)(N_a - \sum_{u \in \mathcal{V}_U} x_{au})$
  end
  calculate *supply* $\boldsymbol{\mathcal{N}}^{(2)}$;
  $\delta = \boldsymbol{\mathcal{N}}^{(2)} - \boldsymbol{\mathcal{N}}^{(1)}$;
  $\varepsilon(i) \leftarrow \varepsilon_0 \cdot i^{-\frac{1}{2}+\tau}$;
  $i \leftarrow i + 1$;
end
Calculate $\boldsymbol{x}$, $\boldsymbol{p}$;

during each simulation run. All of the results shown are averaged over 50 simulation runs. To be more realistic, we introduce specific modulation schemes for calculating the users' achievable throughput. For simplicity, we consider baseband transmissions without subcarrier modulation at this stage. PAM having an order of M (M-PAM) is used. Based on our BER performance results, given a certain target BER, SNR and signal to interference ratio (SIR), the maximum affordable M-PAM order capable of maintaining the target-BER can be determined [3]. Thus the attainable throughput becomes $r_{au} = 2B \log_2 M/(1+\rho)$, where the roll-off factor of the raised-cosine pulses is assumed to be $\rho = 1$.

[3] We could also consider the joint effects of noise and interference. According to [10], the relationship between the BER and ξ for M-PAM signals is given by

$$\text{BER}_{M-\text{PAM}} \cong \frac{M-1}{M} \frac{2}{\log_2 M} Q\left(\frac{\sqrt{\xi}}{M-1}\right).$$

Given a certain target BER and the above-mentioned SINR value ξ, this is an alternative technique of determining the maximum PAM order M, which agrees with our simulation results.

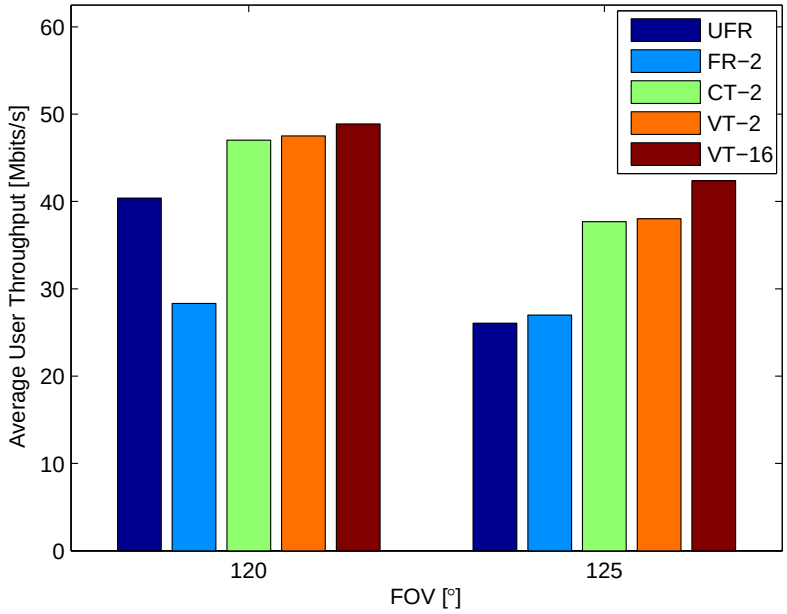

Figure 2.5: Average user throughput of various cell formations with different FoV after performing LB in the hybrid VLC/WiFi system. The corresponding simulation parameters are summarised in Table 2.1.

2.4.2 Throughput Investigations

2.4.2.1 Throughput Investigations for Different Field-of-View

The FoV is one of the factors that is expected to significantly influence the ICI in VLC-based networks. Increasing the FoV leads to the expansion of the ICI-contaminated areas and correspondingly the employment of ICI reduction techniques may become more important. Figure 2.5 shows the average user throughput of different cell formations with different FoV after performing LB in the hybrid VLC/WiFi system. We can see that the throughput provided by the merged cells is higher than the regular cell formations for both FoV values. Since the increase of FoV may result in 1. an increased probability of having user in the ICI-contaminated areas and 2. an decease of received signal power and an increase of received noise power, the average throughput is reduced in all cell formation scenarios for FoV = 120°, 125°. In particular, the UFR scheme is the most badly affected one upon increasing the FoV, which supports the lowest throughput, when the FoV is increased to 125°. Furthermore, FR-2 does not change much.

2.4.2.2 Line-of-Sight Blocking Analysis

As mentioned in Section 2.1, the WiFi AP is also capable of providing seamless DL coverage, when the LoS VLC-DL receptions are blocked. We introduce the LoS blocking probability P_{block} to represent the probability that the LoS VLC path is blocked, which may lead to a reduction of the

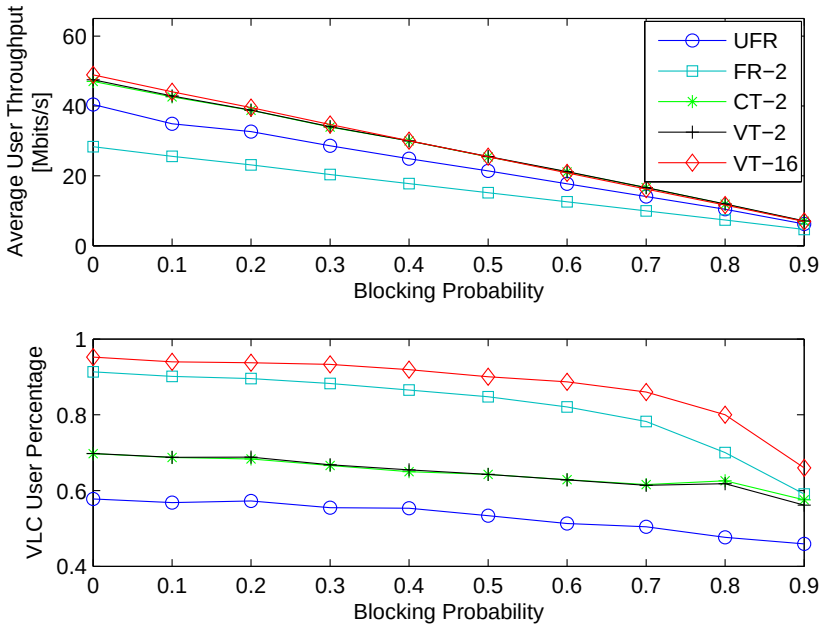

Figure 2.6: Average user throughput and proportion of VLC users under various LoS blocking probabilities, FoV = 120°. The corresponding simulation parameters are summarised in Table 2.1.

data rate experienced by some VLC users. Then the VLC DL data rate becomes $\widetilde{\mathrm{R}} = P_{\text{block}} \cdot 0 + (1 - P_{\text{block}}) \cdot \mathrm{R}$. At this stage, we assume that all LoS paths are blocked with an equal probability. Figure 2.6 indicates that, as expected, the average user throughput and the proportion of VLC users is reduced upon increasing the LoS blocking probability in all cell formation scenarios, hence more users are allocated to the WiFi AP. This demonstrates that the WiFi AP plays an important role in this hybrid system, especially when the LoS paths may be blocked.

2.4.3 Fairness Grade Investigations

2.4.3.1 Average Fairness

Next we will analyse both the network's average fairness as well as the individual user's fairness, given a certain total throughput. The grade of fairness (GoF) for the network is defined as

$$\sigma_{a\text{-VLC}} = \left| 1 - \frac{\text{VLC-fraction of total throughput}}{\text{fraction of VLC-users}} \right|. \tag{2.31}$$

For example, in the UFR scenario, the VLC throughput proportion of the total VLC/WiFi throughput is 95.25%, while 57.76% of the users is supported by the VLC APs, rather than by WiFi. Hence the grade of the average fairness becomes $\sigma_a = |1 - 95.25\%/57.76\%| \approx 0.649$. The system provides the highest grade of average fairness, when the VLC (WiFi) throughput accounts for a certain proportion of the total throughput and at the same time, the number of the VLC (WiFi) users accounts for the same proportion of the total number of users in the hybrid system. Hence for the highest

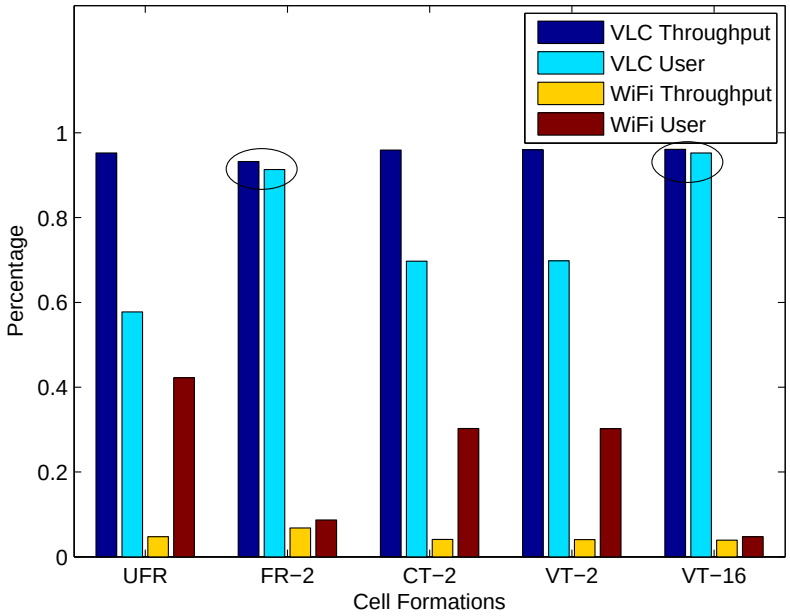

Figure 2.7: Throughput and user percentage in different cell formations, FoV = 120°. The corresponding simulation parameters are summarised in Table 2.1.

possible GoF we have $\sigma_a = 0$. It is plausible that the system will provide a higher grade of average fairness, when σ_a is closer to zero, provided that no multi-service requirements are considered at this stage [170]. Since the sum of VLC throughput (users) and WiFi throughput (users) constitutes the total throughput (users) of the system, the VLC system and the WiFi system provide a similar grade of average fairness. When the difference between the VLC (WiFi) throughput proportion and the fraction of VLC (WiFi) users is smaller, σ_a is also reduced, i.e. the hybrid system provides a higher grade of average fairness.

We know that the size of ICI-contaminated areas is significantly smaller when the FR factor is two and no ICI occurs when all the VLC APs are merged into a 16-AP cell employing VT. Hence more users are expected to be supported by VLC APs in these two scenarios compared to the UFR, CT-2 and VT-2 schemes. We can see from Figure 2.7 that the VLC (WiFi) network throughput and the corresponding user-proportion are closest to each other, since the FR-2 and VT-16 scenario have a higher percentage of VLC users, as indicated by the circles in Figure 2.7. Specific values of σ_a are plotted in Figure 2.8.

2.4.3.2 Individual Fairness

We will use the service fairness index (SFI) of [174] to reflect the individual fairness experienced by the users. The objective of ensuring fairness amongst the users is to guarantee that all users benefit from the same throughput within a given period, provided that the users' data rate requirements are identical. However, this is often unrealistic. The SFI of [174] is introduced to represent the

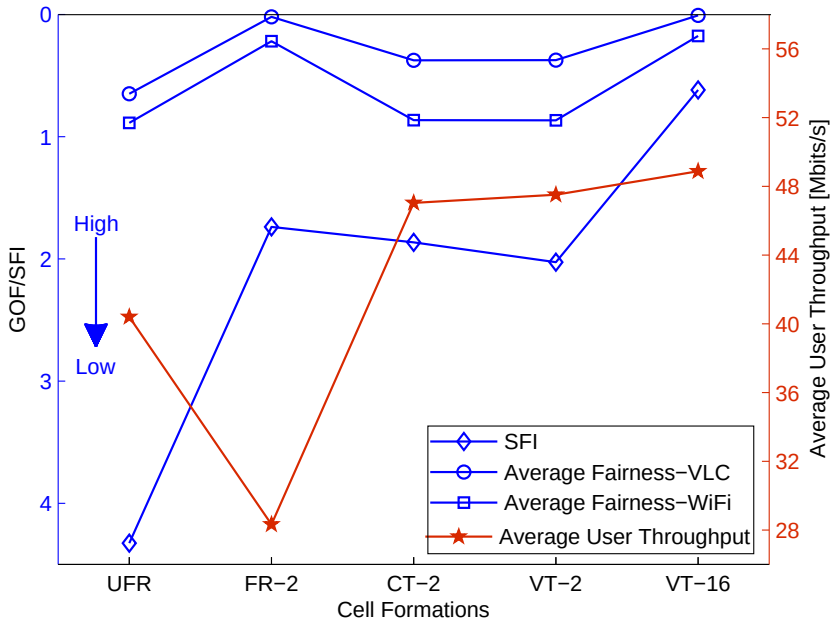

Figure 2.8: The GoF, SFI and average user throughput, FoV = 120°. The GoF/SFI perceived is reduced upon increasing its value. The corresponding simulation parameters are summarised in Table 2.1.

difference between the maximum and the minimum amongst all the users' throughput. When the SFI is low, the throughput-difference of different users is small, hence they are served fairly. By contrast, if the SFI is high, the users experiencing a lower data rate may complain about their unfair treatment. Therefore a lower SFI means a higher grade of individual fairness. The specific SFI values of the different cell formation scenarios considered are plotted in Figure 2.8. It can be clearly seen that the users' throughput-difference is the smallest in the VT-16 scheme, which is expected on the basis of Figure 2.3(e), where VT-16 provides the smoothest BE distribution.

Considering the average user throughput and fairness performance comprehensively in Figure 2.8, the merged 16-AP cell relying on VT is the most attractive one having the highest throughput as well as the highest GoF and SFI. However, its implementation complexity is also significantly higher than that of the regular designs and of CT.

2.4.4 1Gbits/s-Data-Rate WiFi

Since 802.11ac may support a data rate over 1Gbits/s, it is realistic to investigate a hybrid system having a WiFi data rate of 1Gbits/s. Figure 2.9 shows the average user throughput, the throughput and user percentages in the different cell formations having a WiFi data rate as high as 1Gbits/s and FoV = 120°. The average user throughput is increased in all the scenarios considered. Both the percentage share of WiFi throughput and the proportion of its users are increased with the improvement of the WiFi data rate. The merged cells still provide a higher throughput, however the

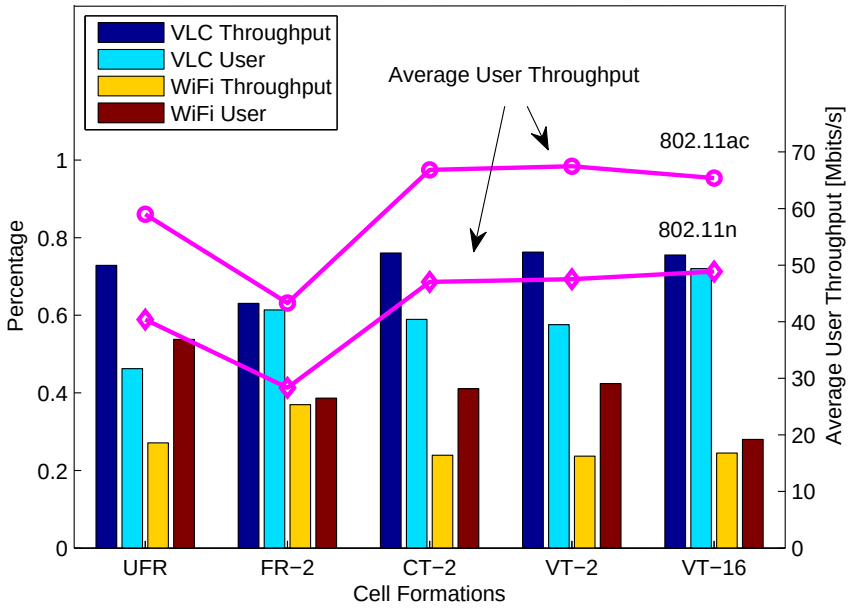

Figure 2.9: Throughput and user percentage in different cell formations, FoV = 120°. WiFi data rate is set to 1Gbits/s. The corresponding simulation parameters are summarised in Table 2.1.

single 16-AP cell relying on VT may no longer have the absolute advantage in terms of its average throughput. This may provide some insights for this hybrid systems' design, when the WiFi data rate is increased.

2.5 Chapter Conclusions

In this chapter, various VLC cell formation schemes and a heterogeneous system constituted by WLANs and VLC networks were investigated. We studied the regular design concept borrowed from cellular networks relying on different FR factors in VLC environments as well as of merged multi-AP cells employing either CT or ZF-based VT. To solve the essential LB problem in the context of our VLC/WiFi hybrid system, both centralised and distributed algorithms were invoked for implementing a PF scheduler. We analysed the MBE of different VLC cell formations as well as the throughput and fairness of the hybrid VLC/WiFi system. By employing a sophisticated VT among all the 16 VLC APs, the VLC network becomes capable of providing a higher MBE, while the hybrid system is capable of providing a higher average throughput without any sacrifice of the fairness, when the WiFi data rate is modest.

In Table 2.2, we compared the percentage of the VLC throughput, VLC users, WiFi throughput, WiFi users and the average user throughput with respect to different cell formations and different WiFi standards, which were extracted from Figure 2.7 and Figure 2.9. Comparing the two different WiFi standards, when the WiFi AP is capable of supporting as high a data rate as 1Gbps, the average

802.11 n					
	UFR	FR-2	CT-2	VT-2	VT-16
VLC throughput	95.25%	93.22%	95.92%	95.96%	96.08%
VLC user	57.76%	91.32%	69.72%	69.80%	95.24%
WiFi throughput	4.75%	6.78%	4.08%	4.04%	9.92%
WiFi user	42.24%	8.68%	30.28%	30.20%	4.76%
Ave. throughput [Mbps]	42.39	28.32	47.03	47.50	48.88
802.11 ac					
	UFR	FR-2	CT-2	VT-2	VT-16
VLC throughput	72.87%	63.06%	76.06%	76.29%	75.53%
VLC user	46.24%	61.36%	58.92%	57.60%	72.00%
WiFi throughput	27.13%	36.94%	23.94%	23.71%	24.47%
WiFi user	53.76%	38.64%	41.08%	42.40%	28.00%
Ave. throughput [Mbps]	58.99	43.31	66.83	67.47	65.38

Table 2.2: The percentage of the VLC throughput, VLC users, WiFi throughput, WiFi users and the average user throughput for different cell formations and for different WiFi standards, which were extracted from Figure 2.7 and Figure 2.9. The percentage of the VLC/WiFi throughput indicates the ratio of the throughput provided by the VLC/WiFi network and the total throughput of the system. Similarly, the percentage of the VLC/WiFi users denotes the ratio of the number of the VLC/WiFi users and the total number of the users in the hybrid system. The corresponding simulation parameters are summarised in Table 2.1, where users' FoV is 120°.

user throughput is increased in all the cell formation scenarios considered. In the meantime, the WiFi AP provides a higher fraction of the throughput in the range spanning from about 10% to around 30%. The fraction of the users supported by the WiFi network is increased correspondingly when employing the 802.11ac standard. Furthermore, as observed from Table 2.2, both changing the cell structure and increasing the WiFi data rate is capable of improving the system performance in terms of throughput.

In the following chapters, we will focus our attention on the *user-centric* cell formation of the VLC network, which is dynamically changed according to the user's information.

Chapter 3

Users First: User-Centric Cluster Formation for Interference-Mitigation in Visible-Light Networks

In Chapter 2, VLC was discussed as the complementary link of the existing RF network, along with its traditional NC cell formation. In this chapter, we will introduce a radically new *user-centric* design principle for the VLC network, which is capable of significantly improving the attainable system performance. We mainly focus our attention on the UC cluster formation and on the MUS problem in Chapter 3, while in Chapter 4, an energy-efficient scalable video provision will be conceived for the UC-VLC network. Figure 3.1 shows the outline of this chapter. The motivation of our UC design and the chapter contributions are briefly introduced in Section 3.1. In Section 3.2, a graph based model is constructed for finding the optimal UC cluster formation and the transmission scheme associated with each cluster is also discussed. The joint cluster formation and MUS problem is formulated and solved in Section 3.3. Section 3.4 offers the performance characterisation of the UC-VLC network from various perspectives. Finally, Section 3.5 provides our chapter conclusions.

3.1 Chapter Introduction

3.1.1 Background and Motivation of User-Centric Design

Owing to its huge unlicensed bandwidth, high data rate potential, energy-efficient illumination etc., the research of VLC intensified during the past decade or so [4]. As a complementary extension of classic radio frequency communications, extensive investigations have been dedicated to the point-to-point transmission and reception techniques in VLC networks [10, 15, 36, 37, 43, 72, 175–177], as also indicated by the IEEE 802.15.7 standard ratified for short-range visible light wireless

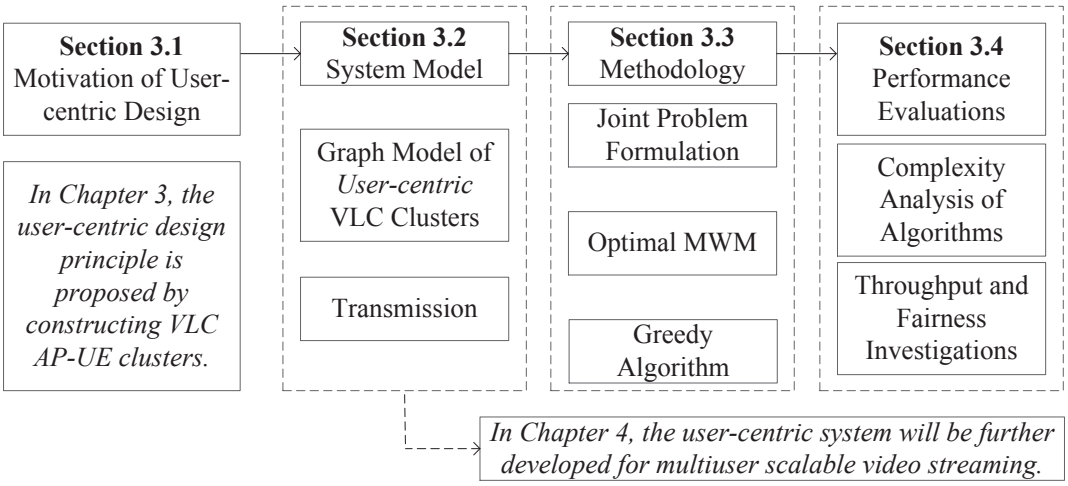

Figure 3.1: Outline of this chapter.

communication [39]. Apart from their multi-fold advantages, naturally, VLC systems also exhibit several potential drawbacks, such as reduced performance in non-line-of-sight scenarios, lack of native up-link support, a confined coverage compared to cellular radio frequency networks etc.

Amongst all the design challenges, the performance degradation imposed by ICI at the cell edge may lead to dramatic reduction of the QoS in a VLC DL system. As a result, careful VLC cell formation becomes crucial, since it is the salient design stage of the entire system design cycle. Traditional designs conceived for VLC cells operating both with and without FR or fractional frequency reuse planning, have been studied in [49, 168, 170], where each optical AP illuminates a small confined cell. As a further advance, a multi-AP joint transmission scheme relying on CT and VT [1] were also investigated in [49]. In contrast to the above-mentioned NC design philosophy, a novel UC cell formation regime was proposed in [47,61,62], where amorphous user-specific multi-AP cells are constructed for jointly transmitting data to a single [2] by employing CT, which we referred to as UC-CT. By definition, UC design is different from the NC design, where the network configuration is fixed, regardless of the tele-traffic. In order to further improve the achievable bandwidth efficiency of the previously proposed UC-CT and to allow each multi-AP cell simultaneously serve multiple UEs as discussed in [49], we propose the *UC-VT-based* cluster formation principle in this chapter. UC-VT cluster formation may be defined as forming the UC-VT clusters, where each UC-VT cluster is served by a set of VLC APs, which simultaneously serve multiple UEs by employing VT. More explicitly, a UC-VT cluster includes a set of APs and UEs as well as the

[1] In [49], relying on CT, each individual VLC AP of a multi-AP cell conveyed the same information on the same visible carrier frequency in their overlapping areas and served a single user at a time. In order to eliminate the bandwidth efficiency reduction imposed by CT, ZF-based VT techniques were employed for serving multiple users at the same time in the overlapping area, which will be exemplified in Section 3.2.2.

[2] A single UE represents a communication device equipped with a VLC receiver in our DL VLC system, which could be a smart phone, a personal computer, a tablet, a printer, etc.

transmission links between them. Note that the previously proposed UC-CT-based cell formation of [47, 61, 62] may be regarded as a special case of our UC-VT-based cluster formation, when only a single UE resides within the coverage of the UC-VT cluster.

When multiple UEs are present in a VLC network, efficient resource allocation and MUS constitutes one of the salient problems, which in fact affects all multi-user networks. However, the problem of VLC-based networks has remained to a large extent hitherto unexplored in the open literature, although recently some valuable studies were disseminated in the context of NC single-AP VLC cells [83–86]. In particular, the authors of [83] proposed a heuristic scheme for allocating interference-constrained sub-carriers in a multiple access VLC system relying on DMT modulation, in order to improve the aggregate throughput. The authors of [84] carefully designed a logical framework aiming to localise, access, schedule and transmit in VLC systems, which was capable of achieving a substantial throughput at a modest complexity. However, similar to most of the literature studying resource allocation in VLC-based systems, both [83] and [84] endeavour to improve the attainable throughput without giving any cognisance to the fairness experienced by the UEs. By taking fairness into account, the authors of [85] proposed an incremental scheduling scheme ISS, where the global scheduling phase is responsible for assigning the resources to the UEs, while the local scheduling phase regularly adjusts the resource allocation by backtracking the UEs' movements. Furthermore, the authors of [86] proposed a PF based scheduling algorithm for a centrally controlled VLC system, which outperformed the maximum-rate scheduling policy in terms of balancing the achievable throughput against the fairness experienced by the UEs. Broadly speaking, most studies of the MUS problem encountered in VLC systems are based on single-AP VLC cells. By contrast, we are going to tackle the problems of MUS and UC-based cluster formation relying on VT.

3.1.2 Chapter Contributions

Against the above-mentioned background, in this chapter,

- we investigate the MUS problem relying on the UEs' PF as a measure by assigning each UE a specific scheduling priority, which is inversely proportional to its anticipated resource consumption [156] and then maximizing a carefully selected network utility function [157], when jointly considering amorphous UC-VT cluster formations for the VLC DL.
- More explicitly, the optimal solution of this joint UC-based cluster formation and MUS problem is first found by a high-complexity exhaustive search, which may have an overwhelming complexity even for a modest-scale system. In order to reduce the computational complexity, the original problem is formulated as a MWM problem and multiple UEs are scheduled by solving the KM algorithm [158–162].
- To further improve the grade of practicability, a greedy algorithm is proposed, which operates

at a considerably lower complexity, despite taking into account the dynamics of the UC-VT clusters.

- Moreover, the computational complexity of both the exhaustive search and of the proposed schemes is analysed and various cluster formations are evaluated for diverse VLC characteristics, such as the FoV, the LoS) blocking probabilities, the optical AP arrangement, etc.

VLC can be considered as a new member in the small-cell family of the HetNets landscape for complementing the overloaded radio frequency band [47]. The UC cluster formation principle designed for VLC environments constitutes a novel and competitive design paradigm for the super dense multi-tier cell combinations of HetNets, where the sophisticated UEs can actively participate in cell planning, resource management, mobility control, service provision, signal processing, etc. Considering the large-scale multi-input-multi-output systems for example, the antenna selection scheme or beamforming techniques may be designed in a similar UC manner, according to the UEs' geo-location and service requirements. As a result, the UC concept may be expected to become one of the disruptive techniques to be used in the forthcoming 5G era [47].

3.2 System Model of the User-Centric VLC Network

The VLC DL is considered, which is constituted by a set of VLC APs and each of them relies on an LED array constructed from several LEDs. The essence of our UC-VT cluster formation is to assign the UEs and optical APs to each other for the sake of maximizing the total utility after employing VT in each of the UC-VT cluster. This procedure is entirely based on the UEs' specific conditions and thus leads to UC clusters. In this section, we first construct the graph model of our UC cluster formation, before investigating how to select the UE set supported by a specific AP set in a multi-user system. Let us recall the link characteristics of the VLC system discussed in Section 1.2.2, where the LoS and the first reflected light path's DC attenuation were given by Equation 1.4 and by Equation 1.6, respectively. Furthermore, we use the VLC parameters summarised in Table 2.1 in this chapter.

3.2.1 Cluster Formation

Following the traditional cellular design principle, each optical AP illuminates an individual cell and adopts UFR across all cells, where the ICI is imposed by the LoS ray of neighbouring cells and consequently the UE may experience dramatic performance degradation at the cell edge. In order to reduce the ICI, appropriate FR patterns may be employed as an appealingly simple solution, while the system has to obey the classic trade-off between reduced bandwidth efficiency and improved cell-edge SINR, when using a FR factor higher than one, as investigated in our previous work [49]. Apart from the single-AP cells, we studied multi-AP merged cells, where several neigh-

bouring VLC APs cooperate by employing either CT or VT techniques. The above-mentioned cell designs, including regular UFR/FR and merged multi-AP cells with CT/VT, rely on a fixed cell-shape, regardless of the traffic requirements, which are referred to as NC formations. In contrast to the fixed-shape NC cell formation designs, the UC design philosophy was proposed in [47, 61, 62], which was capable of supporting irregular-shape elastic cell formations that were capable of accommodating dynamic traffic requirements. By employing CT, each multi-AP UC-CT cell of [62] is only capable of supporting a single UE in a specific time slot. In order to serve multiple UEs at the same time, we propose the VT aided UC cluster formation, which is referred to as a UC-VT cluster in this chapter. Let us now discuss the model of our system in more detail.

Figure 3.2(a) shows the example of a particular VLC DL network having $N_A = 16$ optical APs and $N_U = 10$ UEs, where all LoS links are denoted by dotted lines and for simplicity, the reflections are not shown. Let us first construct the link's bipartite graph $\mathcal{G}(\mathcal{V}, \mathcal{E})$, as shown in Figure 3.3(a), for the network of Figure 3.2(a). The vertex set $\mathcal{V}$ denoting the communication nodes is divided into two subsets, i.e. the optical AP set $\mathcal{V}_A$ as well as the VLC UE set $\mathcal{V}_U$, where we have

$$\mathcal{V} = \mathcal{V}_A \cup \mathcal{V}_U = \{a_i | i = 1, 2, \cdots, N_A\} \cup \{u_j | j = 1, 2, \cdots, N_U\}, \tag{3.1}$$

with a_i and u_j denoting the index of VLC APs and UEs, respectively. Hence, the number of vertices in $\mathcal{G}$ is given by $(N_A + N_U)$. Furthermore, when a UE can receive data from an AP, either via the direct LoS path or via the reflected path, a link may be established between them, which is said to be an *edge*, and these two vertices are said to be *adjacent*. The edge set $\mathcal{E}$ represents all possible links between APs and UEs with one of the endpoints in $\mathcal{V}_A$ and the other one in $\mathcal{V}_U$, which may be written as

$$\mathcal{E} = \{e_{a_i,u_j} | a_i \in \mathcal{V}_A, u_j \in \mathcal{V}_U\}, \tag{3.2}$$

where e_{a_i,u_j} denotes the link between AP a_i and UE u_j. Since the placement of the VLC APs is fixed, the edge set is determined by the UEs' specific conditions, such as their FoV, position, etc. Therefore, the network graph is said to be UC.

Still referring to Figure 3.3(a), the graph $\mathcal{G}$ is not fully *connected*, since not all pairs of vertices are joined by a path. Further scrutiny reveals that $\mathcal{G}$ has three independent components, which are said to be partially *connected components*, as explicitly shown in Figure 3.3(b), marked by $\mathcal{Q}_1$, $\mathcal{Q}_2$ and $\mathcal{Q}_3$. There are no adjacent AP-UE vertices amongst these distinctive components of $\mathcal{Q}_1$, $\mathcal{Q}_2$ and $\mathcal{Q}_3$, which indicates that UEs cannot receive data from the optical APs belonging to the other components, only from their own. Thus, the ICI is totally eliminated. Explicitly, since none of the individual components is affected by the others, the proposed cluster formation algorithms may be executed within every single component, as it will be discussed in Section 3.3. On the other hand, in order to simultaneously serve multiple UEs, ZF-based VT techniques are introduced in our system. The underlying principle of ZF-based VT is to totally eliminate the interference at the multiple AP transmitters, so that all the UEs receive mutually interference-free signals. In general, when employing VT the maximum number of UEs supported in a single time slot should

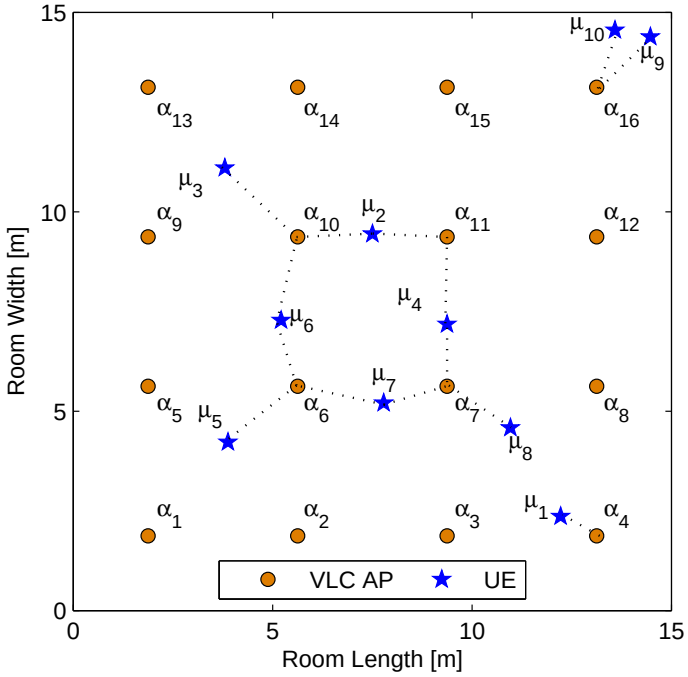

(a)

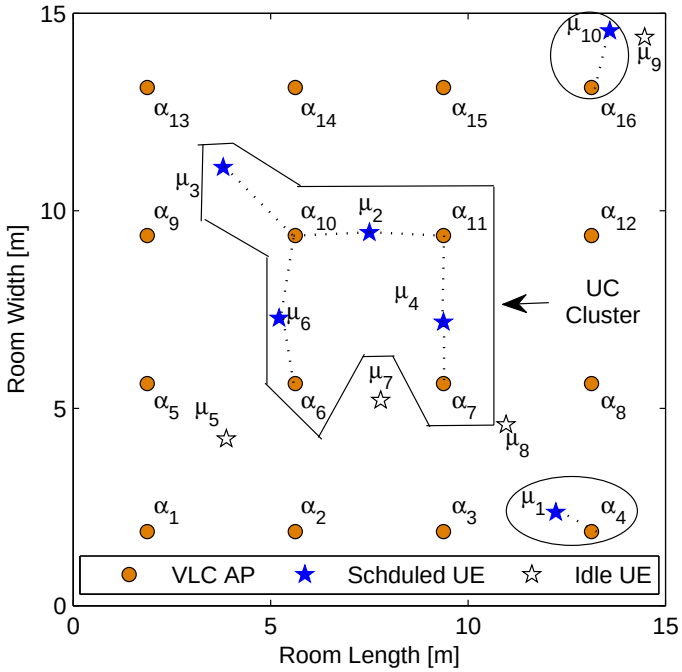

(b)

Figure 3.2: (a) Layout of the VLC APs and UEs projected on the horizontal plane, where a_i and u_j represent the VLC APs and UEs, respectively. All LoS links are denoted by dotted lines and for simplicity, the reflections are not shown in this figure. There are $(4 \times 4) = 16$ APs and 10 UEs. (b) The cluster formation result provided by Figure 3.6(d) for the VLC system of (a).

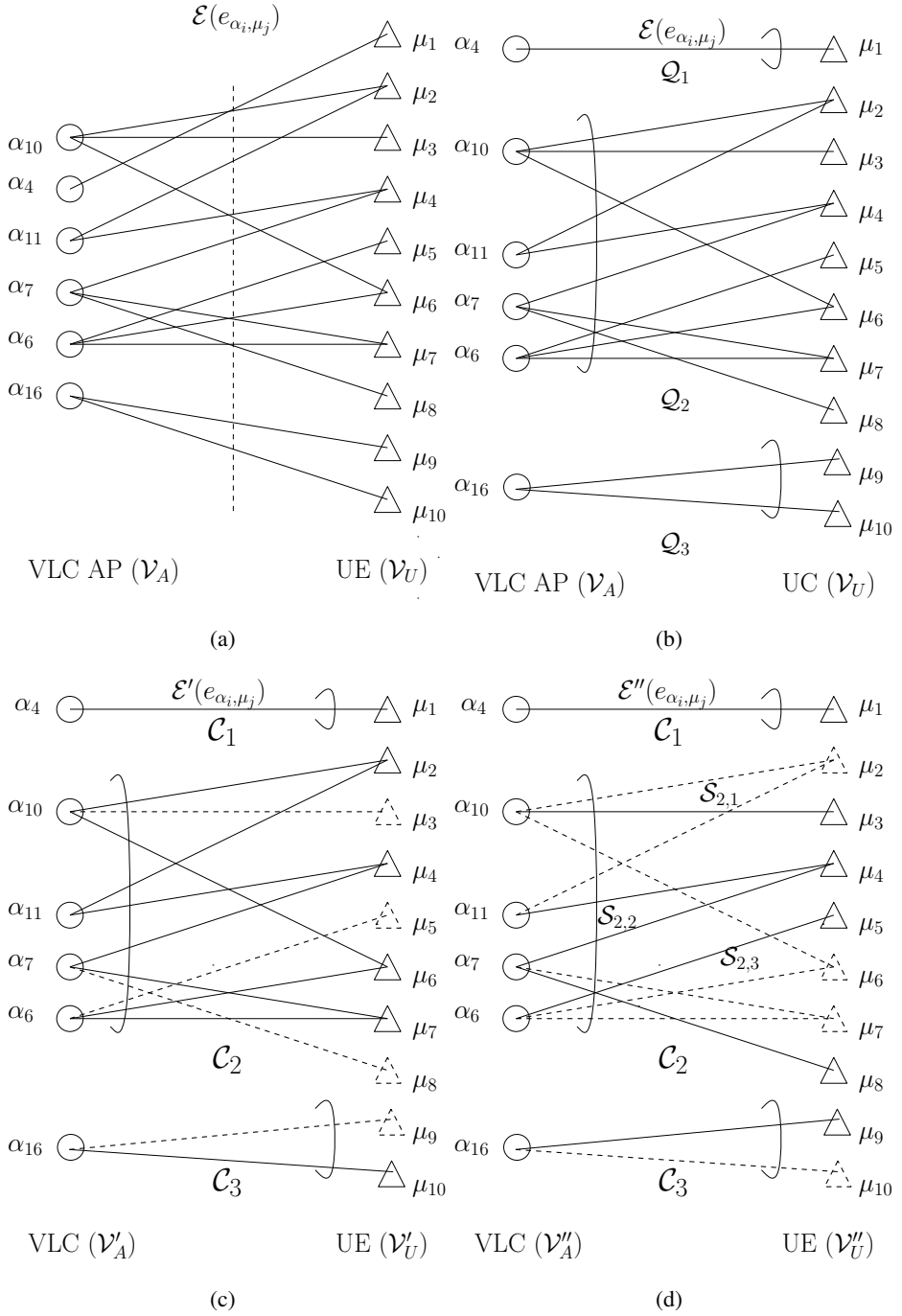

Figure 3.3: (a) A graph model $\mathcal{G}(\mathcal{V}, \mathcal{E})$ of the VLC DL seen in Figure 3.2(a). (b) The three independent components of $\mathcal{G}$, i.e. $\mathcal{Q}_1$, $\mathcal{Q}_2$ and $\mathcal{Q}_3$. (c) and (d) Possible UC-VT cluster formations of the network. In (d), $\mathcal{S}_{2,1}$, $\mathcal{S}_{2,2}$ and $\mathcal{S}_{2,3}$ are disjoint, but they are regarded as a merged large cluster $\mathcal{C}_2$.

be no more than the number of APs. Hence, the ZF-based VT may not be employed directly by each component in Figure 3.3(b). For example, the number of UEs is almost twice as high as the number of APs in $\mathcal{Q}_2$. Therefore, we eliminate the interference by ensuring that only some of the UEs will be scheduled and we solve this problem by constructing a UC-VT cluster with the aid of the serving APs. There are various options for scheduling the UEs shown in Figure 3.3(c) and 3.3(d), where the UEs denoted by the dashed triangle boundary are not scheduled and the edges denoted by dashed lines are not established during the current slot. Furthermore, the UC-VT clusters formed are denoted by $\mathcal{C}_n$, i.e. by $\mathcal{C}_1$, $\mathcal{C}_2$ and $\mathcal{C}_3$ in Figure 3.3(c) and 3.3(d). Before investigating how to schedule the UEs, let us first discuss the VT within each UC-VT cluster formed.

3.2.2 Transmission within Each Cluster

After scheduling the UEs, each UC-VT cluster is formed, as shown for example in Figure 3.3(c), where the clusters are denoted by $\mathcal{C}_1$, $\mathcal{C}_2$ and $\mathcal{C}_3$, respectively. Within $\mathcal{C}_1$ or $\mathcal{C}_3$, only a single UE is supported by a single AP, which is a similar scenario to the regular NC design. However, in order to allow $\{a_{10}, a_{11}, a_7, a_6\}$ to simultaneously serve all the UEs $\{u_2, u_4, u_6, u_7\}$ within $\mathcal{C}_2$, we employ the ZF-based VT techniques of Section 2.2.3.2 for the VT-aided multi-AP cells. Let us now elaborate further concerning the UC cluster formation based on our graph model notations. More explicitly, we may write the channel's attenuation $\boldsymbol{H}_{\mathcal{C}_2}$ between the multiple APs and UEs within $\mathcal{C}_2$ as:

$$\boldsymbol{H}_{\mathcal{C}_2} = \begin{array}{c} \\ u_2 \\ u_4 \\ u_6 \\ u_7 \end{array} \begin{array}{c} \begin{array}{cccc} a_{10} & a_{11} & a_7 & a_6 \end{array} \\ \begin{pmatrix} h_{11} & h_{12} & 0 & 0 \\ 0 & h_{22} & h_{23} & 0 \\ h_{31} & 0 & 0 & h_{34} \\ 0 & 0 & h_{43} & h_{44} \end{pmatrix} \end{array}. \tag{3.3}$$

In order to attain mutually interference-free signals at the receivers, the transmitted signals $\boldsymbol{X}_{\mathcal{C}_2} = [x_1, x_2, x_3, x_4]$ are precoded as $(\boldsymbol{P}_{\mathcal{C}_2} \cdot \boldsymbol{X}_{\mathcal{C}_2})$ and we may write $\boldsymbol{P}_{\mathcal{C}_2} = (\boldsymbol{G}_{\mathcal{C}_2} \cdot \boldsymbol{\Omega}_{\mathcal{C}_2})$, where the matrix $\boldsymbol{G}_{\mathcal{C}_2} = \boldsymbol{H}_{\mathcal{C}_2}^H \cdot (\boldsymbol{H}_{\mathcal{C}_2} \cdot \boldsymbol{H}_{\mathcal{C}_2}^H)^{-1}$ obeys the ZF criterion for the sake of obtaining an interference-free identity matrix for $\boldsymbol{H}_{\mathcal{C}_2} \cdot \boldsymbol{G}_{\mathcal{C}_2} = \boldsymbol{I}_4$ and $\boldsymbol{\Omega}_{\mathcal{C}_2}$ is introduced in order to satisfy the power constraint. Hence, the ICI can be totally eliminated at the multiple AP transmitters and as a result, all the UEs receive mutually interference-free signals. Let us now elaborate on the VT techniques a little further in general terms and derive the formations of $\boldsymbol{G}$ and $\boldsymbol{\Omega}$.

Each UC-VT cluster $\mathcal{C}_n$ is constituted by a set of APs $\mathcal{V}_{A,\mathcal{C}_n}$ with a cardinality of $N_{A,\mathcal{C}_n}$ and a set of UEs $\mathcal{V}_{U,\mathcal{C}_n}$ with a cardinality of $N_{U,\mathcal{C}_n}$. Let further $\boldsymbol{X}_t \in \mathbb{R}^{N_{U,\mathcal{C}_n} \times 1}$ and $\boldsymbol{Y}_r \in \mathbb{R}^{N_{U,\mathcal{C}_n} \times 1}$ denote the vectors of transmitted and received signals, respectively. Upon using VT, we have

$$\boldsymbol{Y}_r = \gamma \cdot P_t \cdot \boldsymbol{H} \cdot \boldsymbol{G} \cdot \boldsymbol{\Omega} \cdot \boldsymbol{X}_t + \boldsymbol{N}, \tag{3.4}$$

where γ and P_t denote the optical/electronic (O/E) conversion efficiency and the transmitted optical power, respectively. Furthermore, $\boldsymbol{N}$ denotes the noise, while the channel-matrix $\boldsymbol{H} \in \mathbb{R}^{N_{U,\mathcal{C}_n} \times N_{A,\mathcal{C}_n}}$

hosts the DC attenuations between the $N_{U,\mathcal{C}_n}$ UEs and the $N_{A,\mathcal{C}_n}$ APs, while the matrix $\boldsymbol{G} = \boldsymbol{H}^H \cdot (\boldsymbol{H} \cdot \boldsymbol{H}^H)^{-1}$ obeys the ZF criterion, which hence results in a beneficial interference-free identity matrix for $\boldsymbol{H} \cdot \boldsymbol{G} = \boldsymbol{I}_{N_{U,\mathcal{C}_n}}$. Finally, the matrix $\boldsymbol{\Omega}$ is introduced to enforce the per-AP power constraints, hence we have

$$\boldsymbol{\Omega} = \varphi \boldsymbol{I}_{N_{U,\mathcal{C}_n}}, \quad \varphi = \min_{i=1,2,\ldots,N_{A,\mathcal{C}_n}} \sqrt{\frac{1}{\|\boldsymbol{G}(i,:)\|_F^2}}, \tag{3.5}$$

where $\boldsymbol{G}(i,:)$ is the ith row of $\boldsymbol{G}$. To elaborate a little further, assuming that we have the per-AP optical power constraint of P_t, the signal transmitted with the equal power from the ith AP is $\varphi^2 \|\boldsymbol{G}(i,:)\|_F^2$. Note that we have $P_e = \pi P_t^2$, when considering the ACO-OFDM [37]. Hence, we have $\varphi^2 \|\boldsymbol{G}(i,:)\|_F^2 \leq \pi P_t^2 \Rightarrow \varphi \leq \pi P_t^2 / \sqrt{\|\boldsymbol{G}(i,:)\|_F^2}$. In order to let each AP satisfy the power constraint, we have $\varphi = \min_i \pi P_t^2 / \sqrt{\|\boldsymbol{G}(i,:)\|_F^2}$, as indicated in Equation (3.5). Furthermore, let us define the SINR as the aggregate electronic power over the noise power in a bandwidth of B [MHz] [10] plus the sum of the electronic power received from other optical sources in the vicinity. Since the corresponding electronic power is proportional to the square of the electronic current's amplitude and both the intra-cluster and inter-cluster LoS interferences are mitigated, we may express the SINR for a particular UE u_j within the cluster $\mathcal{C}_n$ as

$$\xi = \frac{\gamma^2 P_t^2 \varphi^2 \pi}{N_0 B + I_r}, \tag{3.6}$$

where I_r is the interference imposed by the reflected light. Since the interference power received by the cluster under consideration is influenced by the ZF-based VT within other clusters, for simplicity, we assume that the interference imposed is always equal to its maximum value, which characterises the worst-case situation in our VT cluster formations. Furthermore, N_0 [A^2/Hz] is the noise power spectral density dominated by the shot noise N_{shot} [15] given by $N_0 \cong N_{\text{shot}} = q I_a(P_r) \sim 10^{-22}$, where q denotes the electron charge and $I_a(P_r)$ is the photo-current at the receiver [10].

Note that there are two popular techniques of constructing white LEDs, namely either by mixing the red-green-blue (RGB) frequencies using three chips, or by using a single blue LED chip with a phosphor layer. We consider the latter one, which is the favoured commercial version. Although the terminology of 'white' LED gives the impression of having all frequency components across the entire visible light spectrum, in fact only the blue frequency-range is detected. More explicitly, not even the entire blue frequency-range is detected, since the less responsive phosphorescent portion of the frequency-band is ignored. Hence, the modulation bandwidth is typically around 20 MHz, albeit this measured bandwidth depends on the specific LED product used. Given this 20 MHz bandwidth, we are now ready to employ ACO-OFDM and partition it into arbitrary frequency reuse patterns.

3.3 Methodology of Finding User-Centric Cluster Formation

Let us now schedule multiple UEs in the VLC system in a PF manner by taking into account our UC-VT cluster formation, which is ultimately a joint UC-VT cluster formation and MUS problem. In this section, we commence with a general formulation of this joint problem and then propose an exhaustive search method, which finds the optimal solution maximizing the aggregate utility of the VLC system considered. In order to reduce the computational complexity imposed, the original problem is reformulated as an MWM problem, whose optimal solution is provided by the classic KM-algorithm-based [158] approach. For further simplifying the MUS process, we propose a greedy scheduling algorithm for finding a suboptimal solution for our original joint problem, whilst imposing a significantly reduced complexity. Note that for simplicity, we only consider LoS links in terms of constructing UC-VT clusters. By contrast, in addition to the LoS component, the effect of the first reflection will also be considered, when calculating both the UEs' SINR and the achievable data rate, as indicated in Equation (3.6). However, our algorithm is a generic one, which may be readily applied, when considering the reflected light for UC-VT cluster formation.

3.3.1 Joint Multiuser Scheduling and Cluster Formation Problem

Our goal is to find the optimal UC-VT cluster formation for maximizing the long-term network-wide utility, while scheduling UEs in a PF manner, which is ultimately a joint cluster formation and MUS problem. In order to implement a PF scheduler, the weight of each link between APs and UEs may be defined as

$$\omega(e_{a_i,u_j}) = \frac{r_{a_i,u_j}}{\hat{r}_{u_j}}, \quad e_{a_i,u_j} \in \mathcal{E}, \tag{3.7}$$

where r_{a_i,u_j} denotes the achievable data rate of the UE u_j from the AP a_i during the current slot. Since the SINR ξ experienced by a particular UE is determined by the channel attenuation matrix Equation (3.3) between the APs and UEs within the cluster, r_{a_i,u_j} should be a function of the cluster formation, which may be written as:

$$r_{a_i,u_j} = f(\mathcal{E}'), \quad e_{a_i,u_j} \in \mathcal{E}', \mathcal{E}' \subseteq \mathcal{E}, \tag{3.8}$$

where $\mathcal{E}'$ is the set of established links, after the UEs have been scheduled and the UC-VT clusters have been constructed. Furthermore, $\hat{r}_{u_j}$ denotes the long-term average throughput of the UE u_j, which may be obtained over a time window T_F as a moving average according to [113]:

$$\hat{r}_{u_j}^{(t)} = \begin{cases} (1 - \frac{1}{T_\mathrm{F}})\hat{r}_{u_j}^{(t-1)} + \frac{1}{T_\mathrm{F}} r_{a_i,u_j}^{(t)}, & \text{if scheduled,} \\ (1 - \frac{1}{T_\mathrm{F}})\hat{r}_{u_j}^{(t-1)}, & \text{if not scheduled.} \end{cases} \tag{3.9}$$

For a given UC-VT cluster formation $\{\mathcal{C}_n\}$, the aggregate utility may be formulated by taking into account the weight of each edge, where again, the weight physically represents the PF scheduling

priority of the link [113], which is formulated as:

$$W = \sum_{e_{a_i,u_j} \in \mathcal{E}'} \omega(e_{a_i,u_j}) = \sum_{a_i \in \mathcal{V}'_A} \sum_{u_j \in \mathcal{V}'_U} \frac{r_{a_i,u_j}}{\hat{r}_{u_j}}, \quad \mathcal{E}' \subseteq \mathcal{E}, \tag{3.10}$$

where $\mathcal{V}'_A$ and $\mathcal{V}'_U$ denote the serving APs and the scheduled UEs set, respectively. It is plausible that various UC-VT cluster formations may lead to different total utility. The maximum value of the aggregate utility W may be achieved by finding the optimal cluster formation. Thus, our problem may be described as selecting an appropriate set of edges $\mathcal{E}^*$ from $\mathcal{E}$ and then forming several UC-VT clusters, which maximises Equation (3.10). Hence, our OF may be formulated as:

$$\mathcal{E}^* = \arg\max_{\mathcal{E}' \subseteq \mathcal{E}}(W) = \arg\max_{\mathcal{E}' \subseteq \mathcal{E}} \left(\sum_{a_i \in \mathcal{V}'_A} \sum_{u_j \in \mathcal{V}'_U} \frac{r_{a_i,u_j}}{\hat{r}_{u_j}} \right). \tag{3.11}$$

Note that in Equation (3.11) we focus our attention on the aggregate utility of the entire system and do not distinguish, which particular APs and UEs belong to which UC-VT clusters. Let us now discuss the constraint of Equation (3.11), from the perspective of a single UC-VT cluster. As mentioned in Section 3.2.1, the number of scheduled UEs should not exceed the service capability of a cluster employing VT, where again, the maximum number of UEs supported is equal to the number of APs. Hence, within a single UC-VT cluster $\mathcal{C}_n$ we have

$$N_{A,\mathcal{C}_n} \geq N_{U,\mathcal{C}_n}. \tag{3.12}$$

For solving Equation (3.11) under the constraint of Equation (3.12) and finding the optimal cluster formation, we have to know the weight of all edges in $\mathcal{E}$. However, according to Equation (3.7), the weight $\omega(e_{a_i,u_j})$ of a particular link is defined as a function of the data rate achieved by one of its endpoints u_j during its reception from the other endpoint a_i, which can only be determined after all clusters have been formed, as briefly introduced in Section 3.2.2. To the best of our knowledge, the optimal solution of this joint problem may only be found via exhaustive search.

3.3.2 Optimisation of the Joint Problem

Given a VLC network topology having N_A optical APs and N_U UEs, it may be composed of some independent components, for example as shown in Figure 3.3(b). Note that these naturally disjoint components of the network may not constitute the final formations of the UC-VT cluster. More explicitly, there is no limitation concerning the number of APs and UEs within each single component of the network, apart from the fact that within a UC-VT cluster the cardinality of the actively served UE vertex set should be no larger than that of the AP set, as indicated by Equation (3.12). Each UC-VT cluster should be an independent component of the network, where no ICI is imposed on the neighbouring clusters. Furthermore, each individual network component should be connected at the outset, but each may become disconnected and partitioned into several sub-components/clusters throughout the process of scheduling the UEs, as shown in Figure 3.3(d), where $\mathcal{S}_{2,1}$, $\mathcal{S}_{2,2}$ and $\mathcal{S}_{2,3}$ will be regarded as a large merged cluster.

Still referring to Figure 3.3(b), in order to find the optimal cluster formation for maximizing Equation (3.10), the optimisation is performed separately in $\mathcal{Q}_1$, $\mathcal{Q}_2$ and $\mathcal{Q}_3$, which are independent network components. Within $\mathcal{Q}_1$, only a single UE u_1 is capable of connecting with the AP a_4, where a_4 either supports u_1 or it will be turned off. Therefore, there are two AP-UE combination scenarios for $\mathcal{Q}_1$. Within $\mathcal{Q}_2$, there are three UEs, i.e. u_2, u_3 and u_6, which are within the coverage of the AP a_{10}. Hence, a_{10} may either select one of them to support or become inactive. Thus, there are $(3+1)$ choices for a_{10}. Similarly, the other APs a_{11}, a_7 and a_6 have $(2+1)$, $(3+1)$ and $(3+1)$ choices, respectively. Therefore, the number of possible AP-UE combinations within $\mathcal{Q}_2$ is $(4 \times 3 \times 4 \times 4 = 192)$. $\mathcal{Q}_3$ has an easier situation, where the AP a_{16} may either select one UE from $\{u_9, u_{10}\}$ or opts for providing no services. For the entire network of Figure 3.3(b), the number of possible AP-UE combinations becomes $((2-1)+(192-1)+(3-1) = 194)$. Finally, we take into account the undesired scenario, where all APs are out of service by subtracting 1. Generally speaking, our exhaustive search-based approach of finding the optimal UC-VT cluster formation is detailed below.

i) For each separate network component $\mathcal{Q}_m$ relying on $N_{A,\mathcal{Q}_m}$ APs and $N_{U,\mathcal{Q}_m}$ UEs, let $N_{U,\mathcal{Q}_m}^{a_i}$ denote the number of possible links between a certain AP a_i with the UEs within its coverage, where $i = 1, 2, \cdots, N_{A,\mathcal{Q}_m}$.

ii) Note that not the entire set of APs has to be active during the scheduling process. In other words, we do not limit the number of active APs or scheduled UEs, when aiming for finding the optimal cluster formation. Thus the concept of a *virtual* link is introduced for each AP, which theoretically exists, but it is turned off. Hence, the number of possible AP-UE combinations in $\mathcal{Q}_m$ may be expressed as

$$\prod_{i=1}^{N_{A,\mathcal{Q}_m}} (N_{U,\mathcal{Q}_m}^{a_i} + 1) - 1, \tag{3.13}$$

where we have $1 \leq N_{U,\mathcal{Q}_m}^{a_i} \leq N_{U,\mathcal{Q}_m}$. Note that in Equation (3.13), subtracting 1 implies that we have removed the undesired scenario, where all APs are turned off.

iii) For each possible UC-VT cluster formation in $\mathcal{Q}_m$, the aggregate utility can be calculated and the optimal formation associated with the maximum utility is found correspondingly. Since each network component $\mathcal{Q}_m$ is independent, the optimal cluster formation is separately found in each of them. Hence, for finding the optimal solution of Equation (3.11) for the entire system, we need to repeat the process of ii) in each $\mathcal{Q}_m$. Thus the total number of possible AP-UE combinations is the summation of Equation (3.13) for each $\mathcal{Q}_m$, which may be expressed as

$$\sum_{m} \left(\prod_{i=1}^{N_{A,\mathcal{Q}_m}} (N_{U,\mathcal{Q}_m}^{a_i} + 1) - 1 \right). \tag{3.14}$$

The number of all possible cluster formations within a single scheduling time slot at a ms-based scale is given by Equation (3.14), which is jointly determined by the number of APs ($N_{A,\mathcal{Q}_m}$) and number of UEs ($N_{U,\mathcal{Q}_m}$) as well as by the specific distribution of the UEs ($N_{U,\mathcal{Q}_m}^{a_i}$). For a network associated with a low density of UEs and a small number of APs, a desirable cluster formation

solution may be achieved by exhaustively searching all the possibilities. For example, when 16 APs support 10 UEs, the optimal association will be found after searching $\sim 10^4$ possible cluster formations. However, this search-space may become excessive within a time slot at a ms-based scale even for a modest-scale network, which makes the exhaustive search strategy unacceptable owing to its computational complexity. For example, as many as $\sim 10^7$ cluster formations have to be searched within a single processing time slot, when there are 20 UEs supported by 16 APs. Hence, instead of solving the joint problem directly, we update the definition of the weight for each link and reformulate the original problem with the goal of significantly reducing the complexity, as it will be detailed in Section 3.4.

3.3.3 Distance-based Weight and Problem Reformulation

In Equation (3.7), the weight of each link is related to the UE's achievable data rate, which cannot be determined before the UC-VT clusters have finally been constructed. Our ultimate goal is that of finding the optimal cluster formation based on the sum weight attained by appropriately scheduling the UEs, as indicated by Equation (3.11). In other words, the cluster formation and MUS problems were originally coupled. Hence, we opt for simplifying the original problem by adopting a deterministic weight for each AP-UE link. Thus, the maximisation of the sum weight may be realised before the UC-VT clusters are constructed, and as a benefit, the joint cluster formation and MUS problem becomes decoupled.

As mentioned in Section 3.3.2, the weight of each link between the AP and the UE is non-deterministic, which is influenced by how the UC-VT clusters are constructed, while the optimal cluster formation solution is determined by maximizing the sum weight of all the scheduled links. Hence, we opt for bypassing the non-deterministic weight assignment and instead, we opt for selecting active links according to their optical channel quality, which is significantly affected by the UE's position, according to Equation (1.4). We directly adopt each UE's position information for determining the weight of each link and introduce a new weighted bipartite graph $\mathcal{G}_d(\mathcal{V},\mathcal{E})$, which is constructed based on the original graph $\mathcal{G}(\mathcal{V},\mathcal{E})$ and they have the same vertex and edge sets. However, the weight of each edge is redefined as

$$\omega_d(e_{a_i,u_j}) = \frac{1/l^3_{a_i,u_j}}{\hat{r}_{u_j}}, \quad e_{a_i,u_j} \in \mathcal{E}, \tag{3.15}$$

where l_{a_i,u_j} represents the distance between the AP a_i and the UE u_j. Given that the APs are fixed, the weight is determined by the specific position of each UE u_j. It can be readily seen from Equation (1.4) that the VLC links having a shorter length have a better channel quality. Therefore, the weight is inversely proportional to the distance and thus the links associated with better channels have a higher weight. Note that if the UE u_j is too far away from the AP a_i, namely u_j is not within the coverage of a_i, it is reasonable to assume having $\omega_d(e_{a_i,u_j}) = 0$.

Our problem becomes that of selecting a subset of links $\mathcal{E}_d^*$ having a better channel quality,

and along with their endpoints they represent our UC-VT cluster formation. In general, within a UC-VT cluster, multiple APs serve multiple UEs and there may not be a one-to-one relationship. Nonetheless, in the first MUS step, we could select the one-to-one AP-UE pairs according to their distance-based weight, where the serving APs and the scheduled UEs are determined. Then, in the cluster formation step, the cluster may be constructed by adding other possible links between the selected AP-UE set. Thus the MUS and cluster formation problem is decoupled and solved separately. Note that in the MUS step, a specific set of the links between all the AP-UE pairs, which do not share the same AP or UE, is said to represent independent edges and they constitute a *matching* $\mathcal{M}$ defined over the graph. For example, in Figure 3.3(b) we have 6 AP vertices plus 10 UE vertices as well as 14 edges. In order to construct a matching, 6 UEs are selected and each of them matches a specific AP associated with one edge, e.g. $\{a_4 \rightarrow u_1, a_{10} \rightarrow u_3, a_{11} \rightarrow u_4, a_7 \rightarrow u_7, a_6 \rightarrow u_6, a_{16} \rightarrow u_9\}$. Furthermore, we have $\mathcal{M} \subseteq \mathcal{E}_d^* \subseteq \mathcal{E}$. To elaborate a litter further in general terms, let us first formally define the matching over a graph. As mentioned in Section 3.3.2, the network graph model may be disconnected and divided into multiple independent components. For an individual component, denoted by $\mathcal{Q}_m(\mathcal{V}_{\mathcal{Q}_m}, \mathcal{E}_{\mathcal{Q}_m})$, which is a subgraph of $\mathcal{G}_d$ associated with the vertex set $\mathcal{V}_{\mathcal{Q}_m}$ and the edge set $\mathcal{E}_{\mathcal{Q}_m}$, a matching $\mathcal{M}_{\mathcal{Q}_m}$ may be defined as a specific subset of the edge set $\mathcal{E}_{\mathcal{Q}_m}$, where no pair of edges shares a vertex within $\mathcal{M}_{\mathcal{Q}_m}$. It is plausible that the cardinality of the edge-subset $\mathcal{M}_{\mathcal{Q}_m}$ is given by the number of the $\mathcal{M}_{\mathcal{Q}_m}$-saturated AP/UE vertices, which belongs to the edges of $\mathcal{M}_{\mathcal{Q}_m}$. Otherwise, the vertices not belonging to the edges of $\mathcal{M}_{\mathcal{Q}_m}$ are said to be $\mathcal{M}_{\mathcal{Q}_m}$-unsaturated. Hence, if we allow as many UEs as possible to be scheduled, $\mathcal{M}$ should have the highest possible cardinality. Furthermore, considering the weight of each edge, our cluster formation problem may be further reformulated as a MWM problem, where the OF may be written as:

$$\mathcal{M}_{\mathcal{Q}_m}^* = \arg\max_{\mathcal{M}_{\mathcal{Q}_m}}(W_{\mathcal{Q}_m}) = \arg\max_{\mathcal{M}_{\mathcal{Q}_m}} \left(\sum_{a_i \in \mathcal{V}_{\mathcal{Q}_m}, u_j \in \mathcal{V}_{\mathcal{Q}_m}} \omega_d(e_{a_i,u_j}) \right). \tag{3.16}$$

Upon solving Equation (3.16) within each individual network component, a set of APs as well as UEs is selected in order to form a UC-VT cluster along with all links between them. Thus, the solution of the MWM problem is expected to provide a suboptimal result for our original joint MUS and UC-VT cluster formation problem, which is however found at a significantly reduced complexity.

3.3.4 Optimal Maximum Weighted Matching

If we construct a $(N_{A,\mathcal{Q}_m} \times N_{U,\mathcal{Q}_m})$-element weight matrix $(\omega_d(e_{a_i,u_j}))$ for each of the individual component $\mathcal{Q}_m$, the problem of Equation (3.16) may be viewed as being equivalent to finding a set of independent elements from $(\omega_d(e_{a_i,u_j}))$, in order to maximise the sum of these elements. The definition of independent elements indicates that none of them occupies the same row or column, where a row represents an AP and a column represents a UE. To be more explicit, the selected set

of the independent elements in the weight matrix corresponds to a matching of the graph, since a single element represents an edge of the graph and no pair of these elements shares the same AP or UE. Thus our MWM problem has also been interpreted in a matrix form. Before finding the optimal solution of the afore-mentioned MWM problem, let us first introduce Theorem 1.

Theorem 1. *Given the* $(n_r \times n_r)$*-element matrix* (a_{ij}) *and* (b_{ij})*, as well as the column vector* (c_i) *and the row vector* (r_j)*, satisfying* $b_{ij} = c_i + r_j - a_{ij}$*, provided the permutation* p $(p_i : i = 1, \cdots, n_r)$ *of the integers* $1, \cdots, n_r$ *minimises* $\sum_{i=1}^{n_r} a_{ip_i}$*,* p *then also maximises* $\sum_{i=1}^{n_r} b_{ip_i}$*.*

Proof. Let p be a permutation of the integers 1,2, $\cdots$, n minimizing $\sum_{i=1}^{n_r} a_{ip_i}$, then we have

$$\sum_{i=1}^{n_r} b_{ip_i} = \sum_{i=1}^{n_r} c_i + \sum_{i=1}^{n_r} r_{p_i} - \sum_{i=1}^{n_r} a_{ip_i}.$$

Since the first two terms are constant and independent of p, $\sum_{i=1}^{n_r} b_{ip_i}$ is maximised, when $\sum_{i=1}^{n_r} a_{ip_i}$ is minimised by p. □

Hence, if we want to find the optimal assignment solution for maximizing $\sum_{i=1}^{n} b_{i,p_i}$, what we have to do is to transform (b_{ij}) into (a_{ij}) as mentioned above and then find the optimal solution minimizing $\sum_{i=1}^{n} a_{i,p_i}$, where (a_{ij}) and (b_{ij}) are said to be *equivalent*. For a rectangular $(n_r \times n_c)$-element matrix (a'_{ij}), we can obtain a square matrix (a_{ij}) by attaching $|n_r - n_c|$ lines of zero elements to (a'_{ij}). Thus, (a'_{ij}) and (a_{ij}) have the same optimal assignment solution and Theorem 1 can be readily applied for non-square rectangular matrices, where we have $n_r \neq n_c$.

In order to solve our MWM problem, which is derived from our joint cluster formation and MUS problem, we introduce the classic KM algorithm [158, 159], which is an efficient method of solving the matching problems of bipartite graphs and may be readily applied in a symmetric graph. However, the number of VLC UEs is usually higher than that of the optical APs within a single network component $\mathcal{Q}_m$, which results in an asymmetric bipartite graph. Owing to the efforts of Bourgeois and Lassalle [160], an extension of the KM algorithm was developed for non-square rectangular matrices. Relying on this approach, we introduce a KM-algorithm-based technique of solving our UC-VT cluster formation problem. The mathematical formulation of the extended KM algorithm of [160] may be described as that of finding a set of k independent elements $k = \min\{n_r, n_c\}$ from a given $(n_r \times n_c)$-element matrix $(b_{i,j})$, in order to minimise the sum of these elements. However, our problem is not a minimisation, but a maximisation problem associated with the OF of Equation (3.16). Therefore, we first transform our MWM problem into an equivalent assignment problem based upon Theorem 1 and then invoke the KM algorithm for finding the optimal solution of the equivalent problem, which is also optimal for our MWM problem. Furthermore, since the MWM result of each naturally disjoint network component is mutually independent, the matching algorithm is executed within each individual component in a parallel manner.

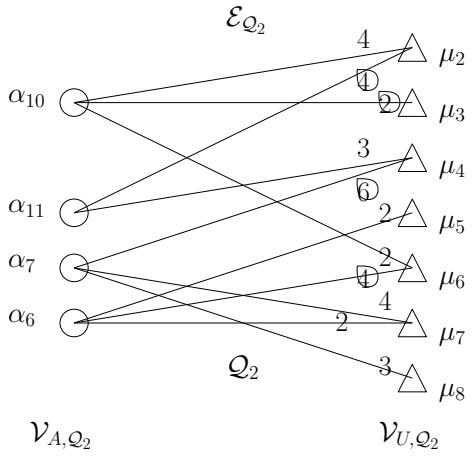

(a)

a_{10}	a_{11}	a_7	a_6	$W_{\mathcal{Q}}$	a_{10}	a_{11}	a_7	a_6	$W_{\mathcal{Q}}$
u_2	u_4	u_7	u_5	13	u_3	u_4	u_7	u_5	11
u_2	u_4	u_7	u_6	15	u_3	u_4	u_7	u_6	13
u_2	u_4	u_8	u_5	12	u_3	u_4	u_8	u_5	10
u_2	u_4	u_8	u_6	14	u_3	u_4	u_8	u_6	12
u_2	u_4	u_8	u_7	12	u_3	u_4	u_8	u_7	10
u_3	u_2	u_4	u_5	14	u_6	u_2	u_4	u_5	14
u_3	*u_2*	*u_4*	*u_6*	*16*	u_6	u_2	u_4	u_7	14
u_3	u_2	u_4	u_7	15	u_6	u_2	u_7	u_5	12
u_3	u_2	u_7	u_5	12	u_6	u_2	u_8	u_5	11
u_3	u_2	u_7	u_6	14	u_6	u_2	u_8	u_7	11
u_3	u_2	u_8	u_5	11	u_6	u_4	u_7	u_5	11
u_3	u_2	u_8	u_6	13	u_6	u_4	u_8	u_5	10
u_3	u_2	u_8	u_7	11	u_6	u_4	u_8	u_7	10

(b)

Figure 3.4: (a) A component of $\mathcal{G}_d$, $\mathcal{Q}_2$, where the distance-based weight of each link is assumed to be as seen in (a), which is inversely proportional to the AP-UE distances in Figure 3.2(a) with the UEs' being randomly distributed. (b) List of all possible AP-UE matchings in $\mathcal{Q}_2$ and the corresponding sum weight $W_{\mathcal{Q}}$. The best matching associated with the circled weights of (a) is the one in the grey-shaded line 7.

As shown in Figure 3.4(a), $\mathcal{Q}_2$ is an independent network component and also a subgraph of our weighted graph $\mathcal{G}_d$, which also shows the individual weights of the $\{a_i - u_j\}$ links. In order to schedule the maximum number of UEs, given the four APs in $\mathcal{Q}_2$, four of them will be selected and each one is paired with a specific AP, where the possible matchings and the corresponding sum weight values are shown in Figure 3.4(b). For example, bearing in mind Figure 3.4(a), the first matching of the first row in Figure 3.4(b) may represent $\{a_{10} \rightarrow u_2, a_{11} \rightarrow u_4, a_7 \rightarrow u_7, a_6 \rightarrow u_5\}$, which leads to a sum weight of $W_{\mathcal{Q}} = \sum_{l=1}^{4} \omega_l = 4+3+4+2 = 13$. The specific matching of the seventh row in Figure 3.4(b) is $\{a_{10} \rightarrow u_3, a_{11} \rightarrow u_2, a_7 \rightarrow u_4, a_6 \rightarrow u_6\}$, which is represented by the shaded row of Figure 3.4(b). This achieves the largest sum weight of $W_{\mathcal{Q}} = \sum_{l=1}^{4} \omega_l = 2+4+6+4 = 16$. The corresponding weights in Figure 3.4(a) are circled. Hence they represent the optimal matching in the scenario considered.

Instead of listing all matchings, we now proceed by constructing an equivalent minimisation problem for our MWM and invoke the KM algorithm [158, 160] for finding the optimal solution, which is described in detail in Appendix A. As shown in Figure 3.5(a), the KM-algorithm-based approach provides the optimal solution for the MWM problem Equation (3.16), with its UE-AP distance-based weight defined by Equation (3.15). The matched AP-UE pairs form a UC-VT cluster and the aggregate utility in Equation (3.10) can be calculated according to the matching result. However, by employing VT among the set of APs and UEs, the actual cluster may be formed with the aid of more links, as seen in Figure 3.5(b). Thus, the UC-VT cluster formation provided by the single-to-single matching solution may not be optimal for Equation (3.11), but it is capable of offering an acceptable suboptimal solution attained at a lower complexity than that of the exhaustive search. Explicitly, it has a complexity order of $O(k^2 \times l)$ [160], where we have $k = \min\{N_{A,\mathcal{Q}_m}, N_{U,\mathcal{Q}_m}\}$ and $l = \max\{N_{A,\mathcal{Q}_m}, N_{U,\mathcal{Q}_m}\}$. The complexity of both the exhaustive search and KM algorithm will be investigated in Section 3.4 in the context of our VLC-based network.

3.3.5 Proposed Greedy Cluster Formation/Multiuser Scheduling Algorithm

In order to further simplify the procedures of scheduling the UEs in our UC-VT cluster formation, in this section we propose a greedy cluster formation/MUS algorithm operating at a low complexity, which is also capable of achieving a near-optimal solution for our original cluster formation problem of Equation (3.11). Before discussing our proposed MUS problem, let us first introduce some notations. Explicitly, $\mathcal{V}_{U,a_i}$ denotes the set of UEs within the coverage of a specific AP a_i with a UE-cardinality of N_{U,a_i}. Each UE u_j is assumed to have a scheduling priority corresponding to each AP a_i, which is given by the weight in Equation (3.15). Let $\mathcal{P}_{a_i} = (\omega_d(e_{a_i,u_j} : u_j \in \mathcal{V}_{U,a_i})$ denote the priority of each element of $\mathcal{V}_{U,a_i}$ representing the AP a_i. Furthermore, if a UE does not receive any connection request from any AP during the slot considered, it is said to be an idle UE; otherwise, it is an active UE. Let us now introduce our algorithm by considering Figure 3.6(a), for

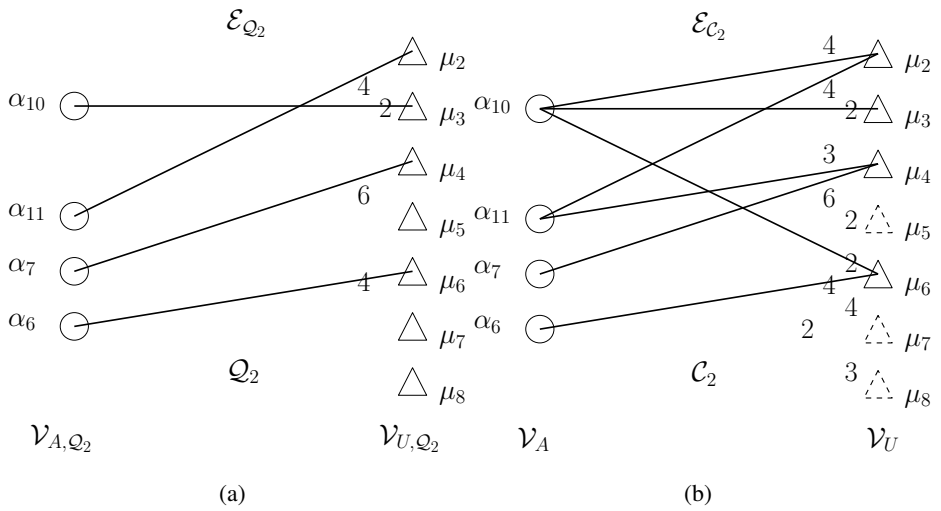

Figure 3.5: (a) The optimal solution for the MWM problem Equation (3.16) relying on the distance-based weight defined by Equation (3.15), which is provided by the KM-algorithm-based assignment. (b) The UC-VT cluster formation based on the matching result of Figure 3.4(a), where more links are added for employing VT and thus the multiple APs $\{a_{10}, a_{11}, a_7, a_6\}$ are capable of supporting all the scheduled UEs $\{u_2, u_3, u_4, u_6\}$ simultaneously. The triangle with a dashed boundary denotes the specific UE, which is not scheduled during the current slot.

example.

i) *Initial selection.* Each VLC AP a_i selects the specific UE $u_j^{a_i}$ from $\mathcal{V}_{U,a_i}$ associated with the highest distance-based priority, which satisfies

$$u_j^{a_i} = \arg \max_{u_j \in \mathcal{V}_{U,a_i}} (\mathcal{P}_{a_i}). \tag{3.17}$$

If the UE $u_j^{a_i}$ receives an assignment request exclusively from the AP a_i, this AP-UE pair is referred to as a single-to-single matching (SSM), which may be formally defined as

$$\mathcal{M}_{\text{SSM}} = \{a_i \to u_j^{a_i} : \forall a_{i'} \neq a_i \Rightarrow u_j^{a_{i'}} \neq u_j^{a_i}\}. \tag{3.18}$$

For example, as shown in Figure 3.6(b), u_4 only receives an assignment request from a_7, although it also falls within the coverage of a_{11}, since u_2 has the largest scheduling weight of 4 for a_{11} and therefore the $\{a_{11} \to u_4\}$ link of weight 3 is ignored. Similarly the $\{a_6 \to u_6\}$ link of weight 4 is also a SSM, because the $\{a_6 \to u_5\}$ and $\{a_6 \to u_7\}$ links have a lower weight of 2. Hence, the AP-UE association after this initial selection is shown in Figure 3.6(b), where the low-weight links are only shown with dotted lines.

ii) *Tentative-cluster construction.* If a UE is offered multiple connection opportunities by different APs, this is said to be a multiple-to-single matching (MSM), which may be defined as

$$\mathcal{M}_{\text{MSM}} = \{(a_i, a_{i'}, a_{i''}, \cdots) \to u_j^{a_i} : u_j^{a_i} = u_j^{a_{i'}} = u_j^{a_{i''}} = \cdots\}, \tag{3.19}$$

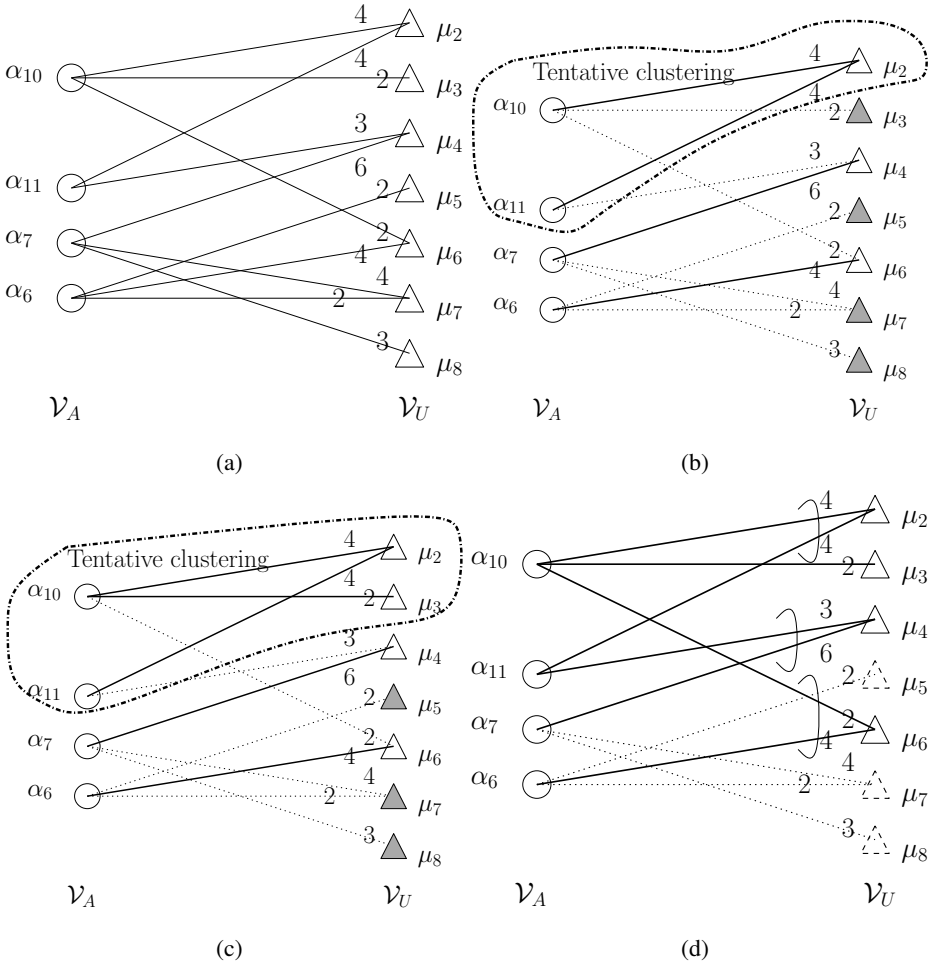

Figure 3.6: (a) The network component considered. (b) Initial selection and tentative-cluster construction. The shaded triangles indicate the hitherto unsupported UEs. (c) Expansion of the tentative-cluster. (d) UC-VT cluster formation, where the incomplete ellipsoids indicate the specific UC-VT cooperation requests of the UEs and the finally unscheduled UEs are denoted by the triangles with dashed boundary.

where we have $\mathcal{M}_{\text{MSM}} = \{(a_{10}, a_{11}) \rightarrow u_2\}$ in the example of Figure 3.6(b), since u_2 has the highest priority for both a_{10} and a_{11}. Furthermore, each MSM is assumed to construct a *tentative-cluster*, as also shown in Figure 3.6(b), where the shaded triangles indicate the hitherto unsupported UEs.

iii) *Expansion of the tentative-cluster.* Within a tentative-cluster $(a_i, a_{i'}, a_{i''}, \cdots) \rightarrow u_j^{a_i}$, each AP a_i reselects a hitherto unsupported UE to be supported with the highest priority, provided that there are still unsupported UEs in $\mathcal{V}_{U,a_i}$. Accordingly, as indicated by Figure 3.6(c), a_{10} reselects the unsupported UE u_3, since the set $\mathcal{V}_U^{a_{10}} \setminus (u_2, u_6) = u_3$ is non-empty and u_3 is the only unsupported UE within the coverage of a_{10}. However, since the set $\mathcal{V}_U^{a_{11}} \setminus (u_2, u_4) = \emptyset$ is empty, a_{11} does not have any additional UE to support.

iv) *Cluster formation.* In order to mitigate the inter-cluster interference, the scheduled UEs found in the overlapping areas of some neighbouring APs determine the cooperation of these APs.

More explicitly, if a particular scheduled UE has the benefit of a LoS ray from several different APs, then the UE sends a cooperation request to these APs. For example, in Figure 3.6(d) u_2 sends its cooperation request to $\{a_{10}, a_{11}\}$, while u_4 and u_6 request cooperation with $\{a_{11}, a_7\}$ and $\{a_{10}, a_6\}$, respectively, as indicated by the incomplete ellipsoids. Thus all the cooperating APs and their matching UEs construct a single UC-VT cluster in the examples of Figure 3.2(b).

Recall that N_A APs are only capable of simultaneously supporting at most the same number of UEs according to Equation (3.12). Therefore, during the expansion of the tentative-cluster, the number of active UEs becomes $(N_A + 1)$, provided that all APs can connect with an idle UE. Hence, the UE having the smallest priority is removed. Let us now provide an overview of the greedy cluster formation/MUS technique in form of Algorithm 2.

Algorithm 2: Proposed cluster formation/MUS Algorithm

Input: $\mathcal{V}_A$, $\mathcal{V}_U$;
for *each time slot* **do**
  Update: $\{\mathcal{P}_{a_i} : a_i \in \mathcal{V}_A\}$;
  Initial selection:
  for *each VLC AP* $a_i \in \mathcal{V}_A$ **do**
    select $u_j^{a_i} = \arg\max_{u_j \in \mathcal{V}_{U,a_i}} (\mathcal{P}_{a_i})$;
  end
  Tentative-cluster construction:
  if $\mathcal{M}_{MSM} \neq \emptyset$ **then**
    construct tentative-clusters;
  end
  Tentative-cluster expansion:
  for *each tentative-cluster* **do**
    for *each AP* $a_i \in$ *tentative-cluster* **do**
      select the idle UE with the largest priority from $\mathcal{V}_{U,a_i}$;
    end
  end
  Cluster formation:
  Establish cooperation and construct UC-VT cluster formation;
  Vectored transmission and resource allocation;
end

Parameter	Value
Half of the receiver's FoV (ψ_F)	55°/57.5°/60°/62.5°
Reflectance factor (ρ)	0.8
Power of circled-LED lamp: 17×17 LEDs with 50mW per LED	14.4 [W]
Power of cornered-LED lamp: 23×32 LEDs with 50mW per LED	36.8 [W]
Transmitted optical power per LED lamp (P_t): 20×20 LEDs with 50mW per LED	20 [W]

Table 3.1: Simulation parameters of the UC-VLC system. Other VLC parameters used are as listed in Table 2.1.

3.4 Performance Evaluation of the User-Centric VLC Network

In this section, we will present our simulation results characterising the MUS and cluster formation algorithms, with a special emphasis on our UC-VT cluster formation. A 15m×15m×3m room model is considered, which is covered by a VLC DL including (4×4) uniformly distributed optical APs at a height of 2.5m. The parameters of the LED arrays are summarised in Table 3.1. Our investigations include both the LoS and the first reflected light-path, where the channel's DC attenuation is given by Equation (1.4) and Equation (1.6), respectively. Furthermore, as mentioned in Section 3.2, ACO-OFDM is considered and the associated capacity is given as $R = \frac{B}{4}\log_2(1+\xi)$ according to [36], where ξ is the SINR of Equation (3.6). Our simulation results were averaged over 50 independent snapshots and each snapshot is constituted by 50 consecutive time slots having a length of 1ms. The UEs at a height of 2.5m are random uniformly distributed at the beginning of each snapshot and they move randomly during the consecutive 50 time slots at a speed of 1m/s. The locations of the UEs are reported every time slot, i.e. every 1ms.

3.4.1 Complexity Analysis

As shown in Figure 3.7(a), when the number of UEs is less than 5, the exhaustive search may be an appealing low-complexity approach of finding the optimal solution for our joint optimisation problem. However, the number of possible cluster formations found by employing the exhaustive search may become excessive with the number of UEs increased. Even if there are only 16 UEs supported by 16 APs, the average number of possible formations becomes as high as 5×10^6 in a single simulation run. By contrast, the complexity of the KM-algorithm based approach may become inadequate in low-UE-density scenarios. However, when the number of UEs is higher than that of the APs, the complexity is only linearly increased with the number of UEs, according to [160].

Figure 3.7(b) shows both the normalised throughput and the sum utility of various cluster/cell

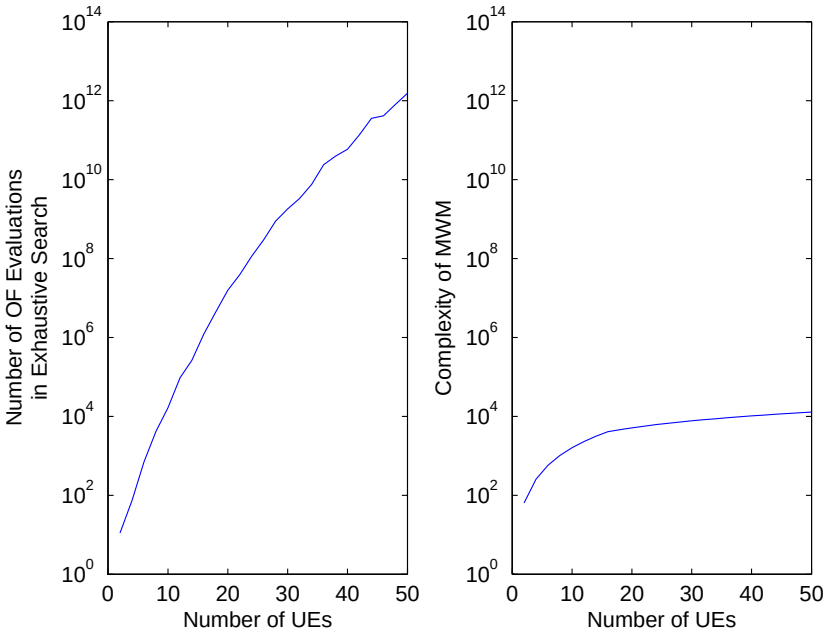

(a)

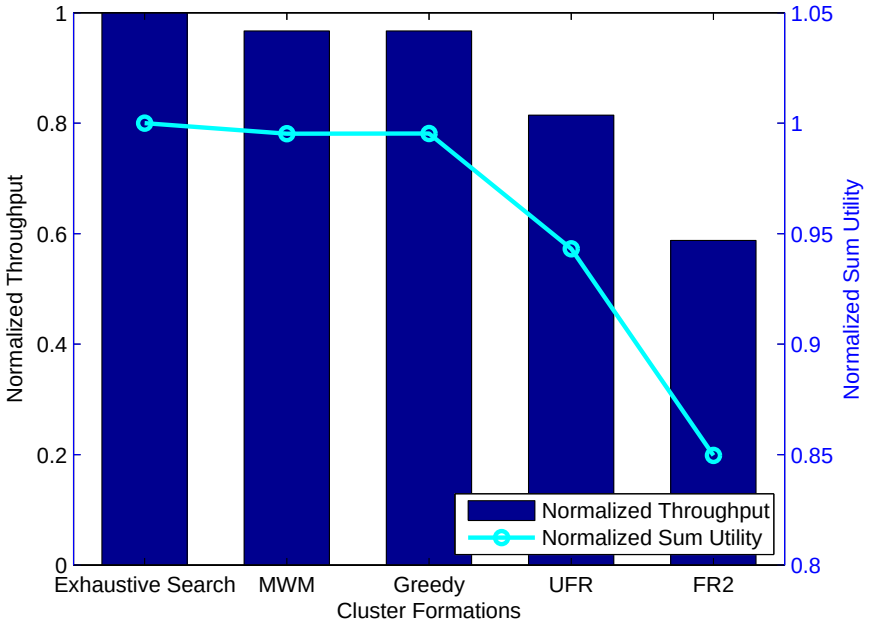

(b)

Figure 3.7: (a) Complexity of the exhaustive search for finding the optimal UC-VT cluster formations and the complexity of KM-algorithm based MWM for finding a suboptimal cluster formation solution. (b) Normalised throughput and the normalised sum utility/OF value, where FoV = 110° and 10 UEs are assumed moving randomly at a speed of 1m/s. The corresponding simulation parameters are summarised in Table 2.1 and Table 3.1.

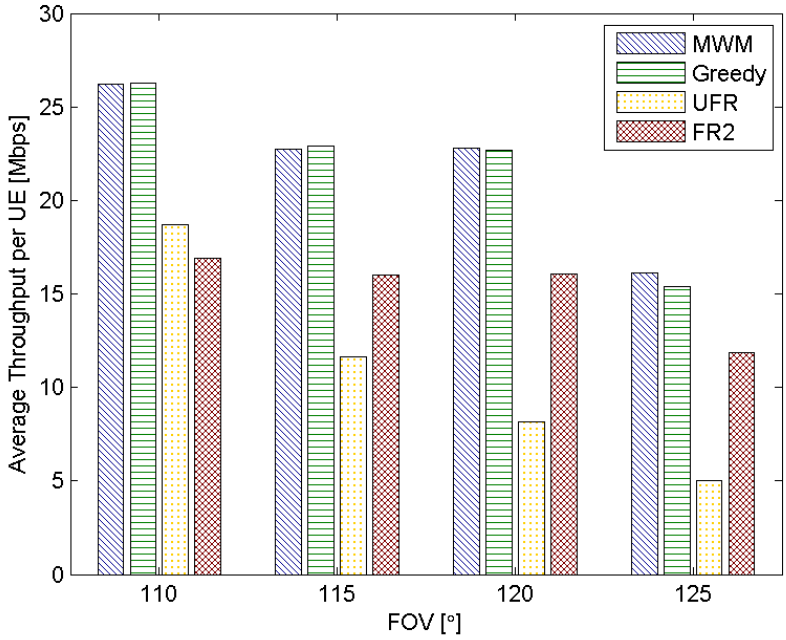

Figure 3.8: Average throughput per UE provided by different cluster formation/cell formation schemes for various FoVs and for 25 UEs. The corresponding simulation parameters are summarised in Table 2.1 and Table 3.1.

formations, where the traditional NC cell formation designs relying on UFR and on the FR factor of two (FR-2) are considered as our benchmarkers. We adopt the MUS algorithm for the UFR and FR-2 discussed in our previous work [62]. Both the highest throughput attained and the sum utility are quantified for the proposed UC-VT cluster formation, whose optimal solution is found by the exhaustive search. The optimal MWM provides a similar solution as our proposed greedy algorithm, both of which are about 90% of the optimal exhaustive search-based value in the scenario considered. Therefore, we will omit the optimal exhaustive search in the rest of this treatise and we opt for the MWM solution as well as for the more practical greedy algorithm for finding the UC-VT cluster formation solution.

3.4.2 Throughput Investigations

3.4.2.1 Throughput Investigations for Various Field-of-View and User Equipment Density

Since the FoV is an influential parameter in VLC networks in Figure 3.8, we consider its effect on the system's performance. The average throughput per UE is reduced, when the FoV [3] is increased,

[3]In order to evaluate the system's performance for various FoVs, we selected 110°/115° and 120°/125°. In the former scenario, the UE is capable of receiving data from two neighboring APs and the area contaminated by potential interference is modest. When the FoV is increased to 120°/125°, the UE is capable of receiving data from four APs and the potential interference-contaminated area is also increased. These four FoVs correspond to different interference levels, although their absolute values are quite similar.

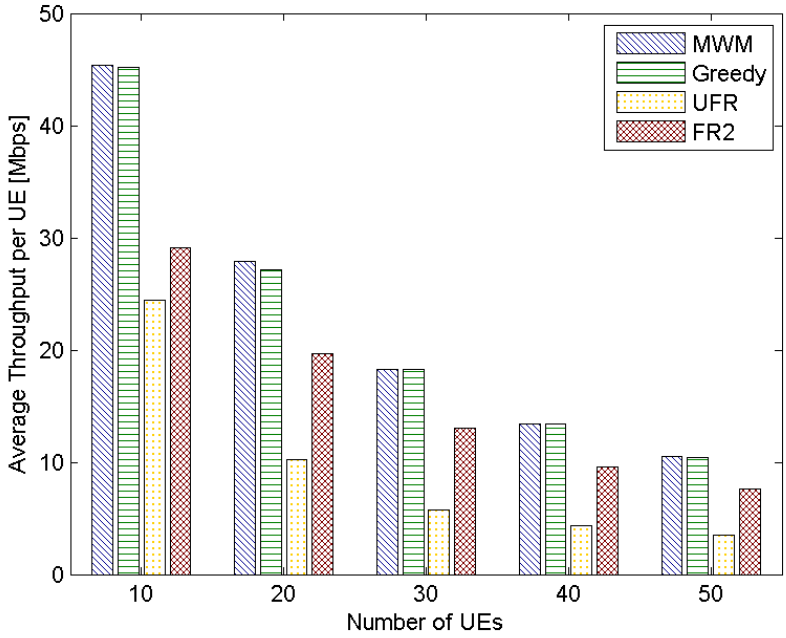

Figure 3.9: Average throughput per UE provided by different cluster formation/cell formation schemes for various UE densities, where the FoV is 120° and the number of UEs is 25. The corresponding simulation parameters are summarised in Table 2.1 and Table 3.1.

due to the increased interference, while our proposed UC-VT cluster formation remains superior in all scenarios considered. In particular, observe in Figure 3.8 that the UFR design exhibits the worst interference immunity and offers the lowest throughput, when the FoV is higher than 115°.

Figure 3.9 shows the average throughput per UE provided by different cluster formation/cell formation schemes associated with various UE densities, where the FoV is 120°. As expected, our proposed UC-VT cluster formation is capable of providing the highest average throughput for all the UE densities considered.

3.4.2.2 Throughput Investigations for Various Line-of-Sight Blocking Probabilities

As mentioned in Section 3.1, the performance of VLC systems is expected to be seriously degraded in NLoS scenarios. In order to investigate the NLoS behaviour of this VLC system, we introduce the LoS blocking probability P_b and assume that the achievable data rate $\tilde{R}$ obeys a Bernoulli distribution [170], with the probability mass function of:

$$f(\tilde{R}) = \begin{cases} 1 - P_b, & \text{if} \quad \tilde{R} = R_s, \\ P_b, & \text{if} \quad \tilde{R} = R_r, \end{cases} \tag{3.20}$$

where R_s and R_r denote the achievable data rate of the UE either in the presence or absence of LoS reception. Then the VLC DL data rate may be written as $\tilde{R} = P_b \cdot R_r + (1 - P_b) \cdot R_s$. At this stage,

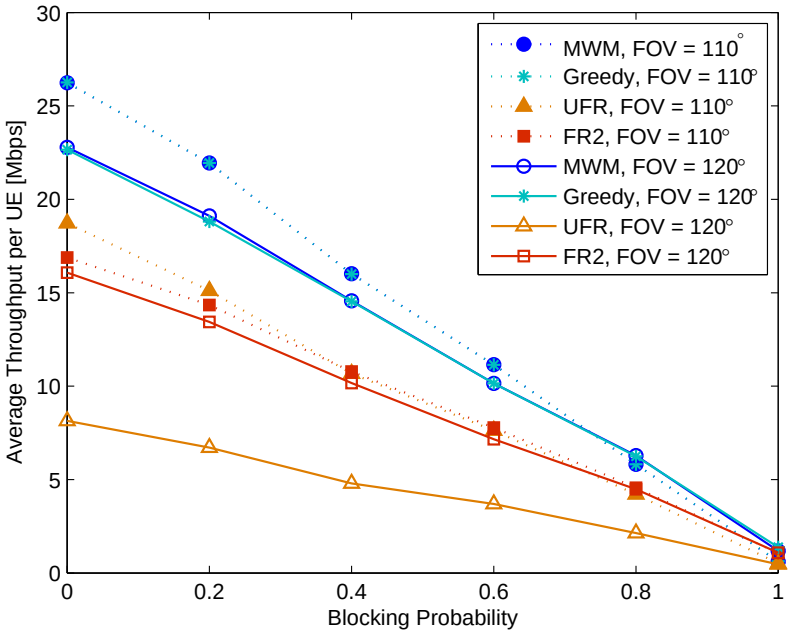

Figure 3.10: Average UE throughput of our VLC system for various blocking probabilities and FoVs supporting 25 UEs in each scenario. The corresponding simulation parameters are summarised in Table 2.1 and Table 3.1.

we assume that all LoS paths are blocked with an equal probability. As shown in Figure 3.10, the average UE throughput attained is reduced upon increasing the LoS blocking probability in all the scenarios considered, but our UC-VT cluster formation still achieves a higher throughput. Furthermore, the system performance of the MWM approach and of our proposed greedy cluster formation/MUS algorithm remains quite similar, regardless of the specific blocking probability and FoV.

3.4.3 Fairness Investigations

In order to investigate the grade of fairness experienced by the UEs, the SFI of [174] is introduced. The objective of ensuring fairness amongst the UEs is to guarantee that all UEs benefit from the same throughput within a given period, provided that the UEs' data rate requirements are identical [49], which is often unrealistic. The SFI was defined as [174]:

$$\text{SFI} = \frac{\max |\tilde{R}_{u_j} - \tilde{R}_{u_{j'}}|}{\sum_j \tilde{R}_{u_j} / N_U}, \tag{3.21}$$

which reflects the maximum throughput-difference of different UEs. If the SFI is low, the throughput-difference is low and the UEs are served fairly, while if the SFI is high, the UEs experiencing a lower data rate may complain about their unfair treatment. Furthermore, by jointly considering the throughput, we may define

$$\Delta = \frac{\text{Average throughput per UE}}{\text{SFI}}. \tag{3.22}$$

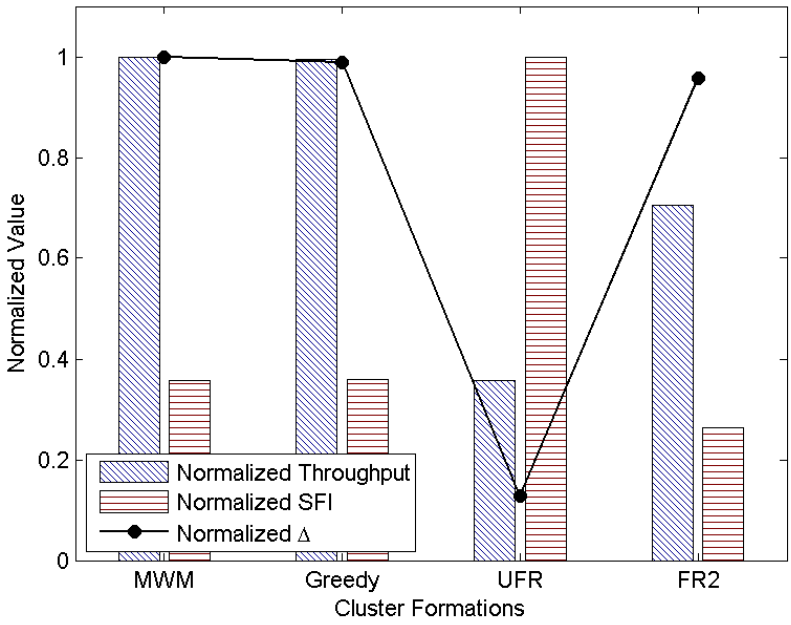

Figure 3.11: The normalised average throughput and the SFI of various cluster formation/cell formation schemes. The corresponding simulation parameters are summarised in Table 2.1 and Table 3.1.

Hence, Δ constitutes a comprehensive system performance metric, joint characterising both the throughput as well as the service fairness. If Δ is low, the system either provides a low throughput or a poor fairness; and vice versa.

Figure 3.11 shows the normalised throughput and SFI of various cell formations and cluster formations, where the UFR design has the worst performance associated with the lowest Δ. Moreover, the cumulative distribution function (CDF) of the UE throughput is shown in Figure 3.12. It can be seen that the UE may have as high as 40% probability of remaining unserved during each time slot in all the scenarios considered.

3.4.4 Irregular VLC Access Point Arrangements

Our proposed UC-VT cluster formation and MUS scheme may be readily applied to arbitrary topologies. Let us consider Figure 3.13(a), for example. This specific VLC AP arrangement was advocated in [51] for reducing the SNR fluctuation and was also employed in [61] for implementing a scheduling algorithm. As shown in Figure 3.13(a), 12 LED lamps constitute a circle and 4 LED lamps are placed in the corners at a height of 2.5m, which are referred to here as the circular-LED arrangement and corner-LED arrangement, respectively. The power of each LED array is 14.4W and 36.8W in the circular- and corner-arrangements of our simulations. Thus the total number of optical APs remains 16 and the sum of their transmission power is at most 320W, which is the same as that of the regular (4×4) LED array arrangement. Figure 3.13(b) shows the average throughput

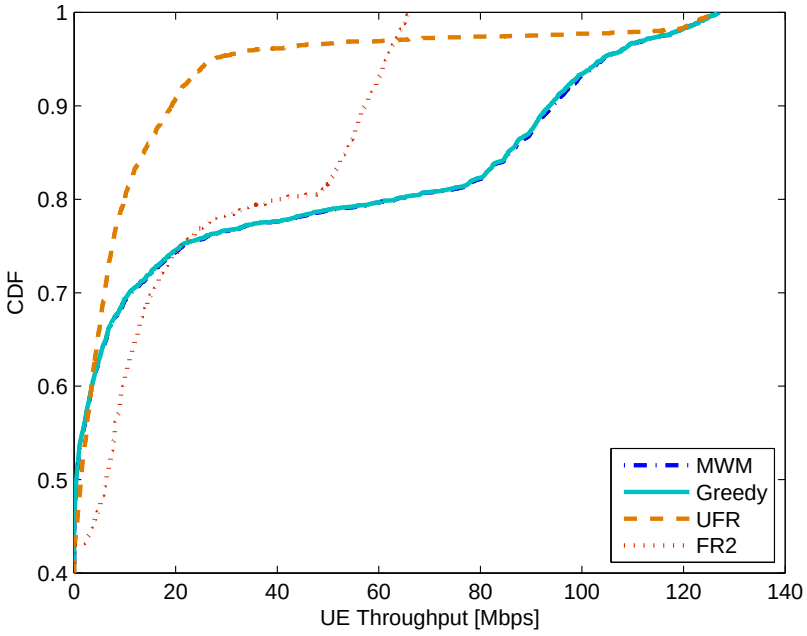

Figure 3.12: CDF of the UE throughput, where the number of UEs is 25 and we have FoV = 120°. The corresponding simulation parameters are summarised in Table 2.1 and Table 3.1.

per UE for the LED arrangement of Figure 3.13(a). The average throughput is slightly reduced, when the radius of the LED circle is increased from 4m to 4.5m, but our proposed UC-VT cluster formation still outperforms the traditional cell formation design in all scenarios of this circular LED arrangement.

3.5 Chapter Conclusions

In this chapter, an amorphous UC-VT cluster formation was proposed for mitigating the ICI and to allow a single cluster to support multiple UEs. The MUS problem combined with our UC-VT cluster formation was investigated and the optimal solution was found by an exhaustive search approach. Since the exhaustive search may become complex, the original joint problem was reformulated as a MWM problem, which was solved by the classic KM-algorithm-based method. In order to further reduce the computational complexity, an efficient greedy MUS algorithm was proposed for constructing our UC-VT clusters. The average UE throughput and the grade of fairness of different cluster/cell formation schemes relying on various parameters, which were extracted from Figure 3.8, Figure 3.9, Figure 3.10 and Figure 3.11, are summarised in Table 3.2. Our simulation results demonstrated that the UC-VT cluster formation is capable of providing a higher average UE throughput than the traditional NC cell designs in all the scenarios considered.

Despite the promise of the UC-VT cluster formation, some further challenges arise when

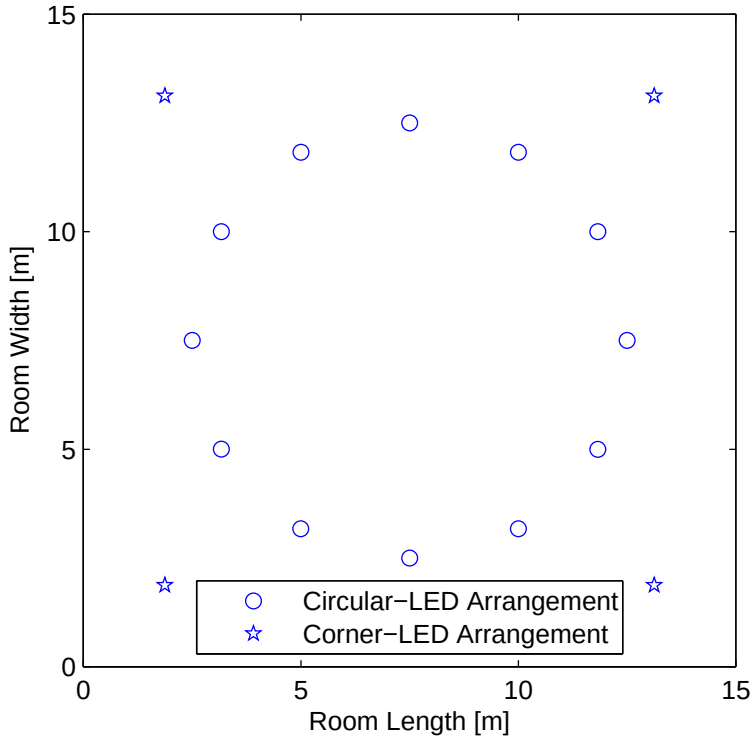

(a)

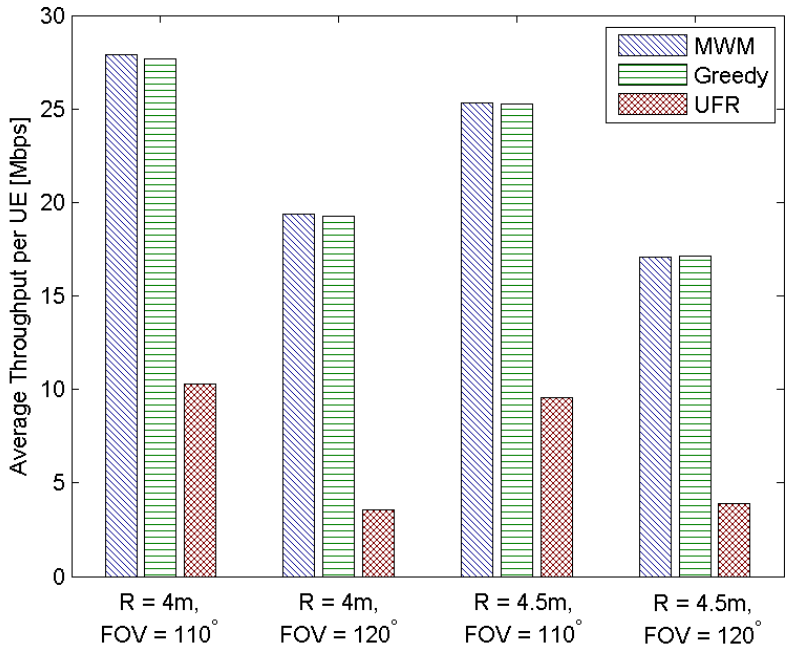

(b)

Figure 3.13: (a) The irregular LED-arrangement, where the LED circle has a radius of 4.5m and the corner LEDs are at 1.875m from the walls. (b) System performance of the LED arrangement seen in Figure 3.13(a) for 25 UEs. The corresponding simulation parameters are summarised in Table 2.1 and Table 3.1.

Parameter		UC (greedy)	UFR	FR-2	Notes
FoV	110°	26.53	19.37	16.98	Throughput per UE [Mbps], 25 UEs, no blocking.
	115°	23.24	11.86	16.14	
	120°	22.57	7.92	15.82	
	125°	17.08	5.15	11.93	
Number of UEs	10	45.21	24.48	29.16	Throughput per UE [Mbps], FoV = 120°, no blocking.
	20	27.17	10.25	19.64	
	30	18.29	5.72	13.04	
	40	13.42	4.36	9.57	
	50	10.41	3.51	7.62	
Blocking probability	0	22.66	8.14	16.08	Throughput per UE [Mbps], 25 UEs, FoV = 120°.
	0.2	18.81	6.71	13.43	
	0.4	14.54	4.80	10.17	
	0.6	10.15	3.69	7.16	
	0.8	6.24	2.14	4.48	
	1	1.37	0.46	1.08	
Fairness	SFI	0.36	1.00	0.26	25 UEs, FoV = 120°, no blocking.
	Δ	0.99	0.13	0.96	

Table 3.2: The average UE throughput and the grade of fairness of different cluster/cell formation schemes with various parameters, which were extracted from Figure 3.8, Figure 3.9, Figure 3.10 and Figure 3.11. The corresponding simulation parameters are summarised in Table 2.1 and Table 3.1.

incorporating our system-level UC design into VLC environments. The open challenges may be highlighted from various perspectives, including the acquisition of accurate location information [65, 134–139, 141], the research of robustness to LoS blocking, the specific RF technology counterpart to be used for up-link support, etc. In the next chapter, we will explore the energy efficiency of the UC-VLC network.

Chapter 4

User-Centric Visible Light Communications for Energy-Efficient Scalable Video Streaming

In Chapter 3, the UC cluster formation combing multiuser scheduling was shown to outperform the conventional cells in the context of visible-light networks both in terms of its throughput and fairness. To further explore the energy efficiency of this novel design, we conceive a scalable video-streaming solution for our UC-VLC networks, which may be considered a compelling application of the next-generation networks.

Figure 4.1 shows the organisation of this chapter, which commences with the portrayal of the background and of the motivation of our UC design conceived for scalable video-streaming in Section 4.1. Our distance-based UC system model and the scalable video architecture considered are presented in Sections 4.2 and 4.3, respectively. Furthermore, our problem formulation and its 3-tier dynamic-programming-based algorithm are described in Sections 4.4 and 4.5, respectively, where the proposed 3-tier dynamic-programming-based algorithm is constituted by the user/layer-level AM mode assignment, the AP-level PA and the cluster-level EE optimisation. In Section 4.6, our simulation results - including the EE and video quality investigations - are presented. Finally, Section 4.7 offers our chapter conclusions. Note that the distance-based UC cluster formation considered in this chapter is oblivious to the specifics of the MUS problem, while one of the possible MUS solutions was discussed in the last chapter. In this chapter, we focus our attention on the EE characterisation of our UC-VLC network, while supporting high-quality video transmission.

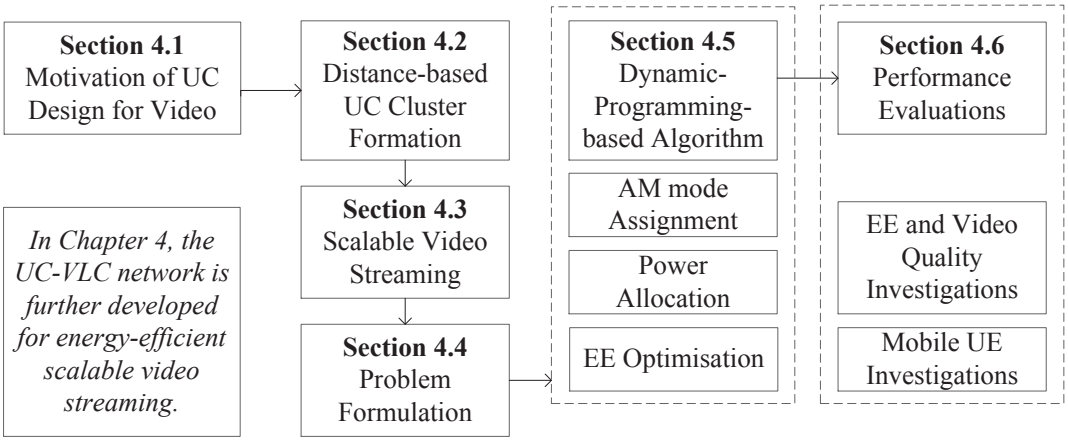

Figure 4.1: Outline of this chapter.

4.1 Chapter Introduction

4.1.1 Chapter Background

Following the launch of the global 5G research initiatives [2] conceived for tackling the explosive escalation of wireless tele-traffic, the horizon of communication spectrum has been expanded from the conventional RF band both to the millimetre wave [3] and to the visible light [4] frequency band spanning from 400 to 700 THz. Hence, the pursuit of 'green' communications has motivated both the academic as well as the industrial community to continuously explore future technologies, in order to improve the achievable EE of the entire network infrastructure [178]. As a promising complimentary extension to the well-established indoor RF networks [49, 170], VLC is becoming an additional promising enabler for providing indoor coverage, owing to its energy-efficient nature simultaneously supporting both communications and illumination. Hence, a careful design of both functions is required for fully realising the EE potential of VLC.

To elaborate, the LED transmitters are primarily used for illumination with the aid of a constant DC power, which also provides sufficient forward biasing voltage across the LEDs for wireless communications. Hence, the additional communication function should not perturb the illumination specifications, nor should it violate the LEDs' physical limits. Ideally, the extra communication-related power consumption should be as low as possible, while maintaining a minimum required QoS. To this end, in addition to the extensive efforts invested in improving the attainable throughput of the VLC networks by utilising sophisticated optical devices [179, 180], by employing novel modulation schemes [181, 182], and by employing powerful multi-input-multi-output techniques [75, 183], valuable research has also been dedicated to the improvement of link-level EE, focusing on brightness and dimming control with the aid of both modulation-related [44, 184] as well as coding-related techniques [185, 186].

Whilst there are valuable link-level studies, there is a lack of system-level investigations on designing energy-efficient VLC networks supporting multiple users, which may require a radically new design approach. When considering VLC networks supporting multiple users, the performance degradation imposed by the escalating inter-cell interference at the cell edge may lead to dramatic reduction of the QoS as well as to the EE reduction of the VLC networks. As a result, careful VLC cell formation design becomes crucial, since it crucially influences the entire system design cycle. The authors of [187] proposed a joint link scheduling and brightness control scheme for energy-efficient multi-user VLC networks with the aid of a novel light source structure, which however still relies on the classic cellular design. By contrast, in [47] we conceived a novel UC design principle for VLC, where the resultant user-to-network association structure is based on amorphous cell-shapes. More explicitly, in our UC design, the cell formation is constructed by grouping the UE and associating APs to each UE-group based on the UEs' location information. Our recent work has demonstrated that the UC design principle leads to a higher system throughput and a more uniform user fairness [63] as well as to a reduced power consumption [64], when compared to the conventional VLC cell formation relying on either UFR or on FR-2 [1].

4.1.2 Motivation of the User-Centric VLC Design for Video Streaming

Owing to these exciting findings, we further develop the UC-VLC design philosophy for video streaming, which is believed to be the killer-application for VLC [94], since video services account for much of the tele-traffic in modern wireless communications systems [92, 93]. Given the rapid development of video coding techniques [96, 107], the advanced scalable extension of the so-called SHVC techniques [97] has gained popularity, as a benefit of its scalable nature, because it is capable of offering diverse visual qualities by promptly adapting to the time-variant channel conditions of different UEs. The SHVC-based layered video stream is constituted by multiple unequal-importance layers, which are generated by using carefully designed source codecs [103,104] as well as adaptive modulation and channel coding schemes [105, 106]. According to [107], if the subsets of the original video sequence may lead either to video reconstruction at a reduced picture size or at a reduced frame rate compared to the original one, then this video scheme exhibits either spatial or temporal scalability, respectively. Another popular scalability mode is the so-called quality-scalability, where the subsets of bits may provide a reduced video fidelity. Explicitly, the fidelity is often represented by the PSNR. As a further advance, the afore-mentioned modes of scalability may be supported by a single scalable video sequence. The benefits of scalable video are multi-fold, amongst others, allowing for example the video decoder to progressively refine the reconstructed

[1] Conventional VLC cell formation follows the traditional cellular design principle, where each optical AP illuminates an individual cell and adopts UFR across all cells. As a result, inter-cell interference is imposed by the line-of-sight ray of neighbouring cells and the UEs may experience dramatic performance degradation at the cell edge. In order to reduce the inter-cell interference, appropriate frequency reuse patterns may be employed as an appealingly simple solution, while the system has to obey the classic trade-off between reduced bandwidth efficiency and improved cell-edge signal-to-interference-plus-noise-ratio, when using a frequency reuse factor higher than one.

visual quality, as the channel-quality improves. The hierarchical structure of the video-stream also facilitates energy-efficient video communications by jointly considering the scalable video quality and the power consumption, as demonstrated for traditional RF networks in [108–110]. This motivated us to support energy-efficient scalable video streaming in the radically new context of UC-VLC networks.

4.1.3 Chapter Contributions

We design an energy-efficient scalable video system relying on dynamic UC cluster formation in VLC networks, while jointly considering AM mode assignment and PA. To be more specific,

- we propose a distance-based UC cluster formation technique and employ two different joint transmission schemes within the clusters, which we refer to as CT and VT [2]. The beneficial construction of UC clusters constitutes the basis of a structurally energy-efficient VLC network;
- we design an energy-efficient scalable video scheme and carefully formulate its EE maximisation problem by taking into account its unique video-related characteristics, such as the base- and enhancement video layers etc.;
- we propose a heuristic 3-tier dynamic-programming-based algorithm, including the user/layer-level AM mode assignment, the AP-level PA and the cluster-level EE optimisation, for maximising the system-level EE of our UC-VLC network;
- we evaluate the proposed EE scheme by transmitting a SHVC sequence and compare our UC design- in terms of its achievable EE, throughput, and video quality- to the conventional cells utilising both UFR and FR-2. For our simulations results of the full video clips, please refer to `http://www.ecs.soton.ac.uk/research/projects/924`.

4.2 System Model of the Distance-based User-Centric Cluster Formation

In contrast to the conventional cellular design leading to circular cells, in our UC-VLC network each UC cluster is served by a set of VLC APs, which simultaneously serve multiple UEs. More explicitly, a UC cluster includes a set of APs and UEs. In this section, we highlight the distance-based UC cluster formation philosophy. Furthermore, we still use the link characteristics of the

[2] In [49], relying on CT, each individual VLC AP of a multi-AP cell conveyed the same information on the same visible carrier frequency in their overlapping areas and served a single UE at a time. In order to eliminate the bandwidth efficiency reduction imposed by CT, zero-forcing-based VT techniques were employed for serving multiple users at the same time in the overlapping area, which will be exemplified in Section 4.3.3.

VLC system discussed in Section 1.2.2, where the LoS and the first reflected light path's DC attenuation were given by Equation 1.4 and by Equation 1.6, respectively. Furthermore, we continue to use the VLC parameters summarised in Table 2.1 and Table 3.1 of this chapter.

4.2.1 Preliminaries

Let us introduce some notations first before constructing the UC clusters. Figure 4.2 shows the DL of a particular VLC network having $(N_A = 64)$ optical APs and $(N_U = 25)$ UEs, which are randomly distributed in the room of size 15m×15m×3m. Let $\mathcal{V}_A$ and $\mathcal{V}_U$ denote the AP set and UE set, respectively. Each UC cluster $\mathcal{C}_n$ is constituted by two subsets, i.e. the AP subset denoted by $\mathcal{V}_{A,n}$ as well as the UE subset denoted by $\mathcal{V}_{U,n}$, where $n = 1, \cdots, N$ and N denotes the total number of UC clusters. Hence, we have

$$\mathcal{C}_n = \mathcal{V}_{A,n} \cup \mathcal{V}_{U,n},\ \mathcal{V}_{A,n} \cap \mathcal{V}_{A,n'} = \emptyset,\ \mathcal{V}_{U,n} \cap \mathcal{V}_{U,n'} = \emptyset, \tag{4.1}$$

$$\{\mathcal{V}_{A,n} : n = 1, \cdots, N\} \subseteq \mathcal{V}_A,\ \{\mathcal{V}_{U,n} : n = 1, \cdots, N\} \subseteq \mathcal{V}_U. \tag{4.2}$$

Note that N may not be determined before all UC clusters have been formed, because it is influenced by the various UEs' location, FoV, etc. Furthermore, since some UEs may not have information to transmit and some APs may not be active during the current cluster formation round, we have (4.2).

Since the VLC channels are pre-dominantly static, the channel knowledge can be characterised by a single attenuation factor. Hence, the channel's impulse response can be readily estimated at the user side and then fed back to the AP side at the cost of a modest overhead. After acquiring the channel knowledge, the distances between APs and UEs may be inferred from Equation (1.4). As a result, classical positioning and tracking may be used for determining the users' positions [65, 188, 189]. Thus the mutual distances $d_{u,u'}$ between any pair of UEs as well as the mutual distances $d_{a,u}$ between any AP-UE pair may be calculated. Since our UC cluster formation is ultimately based on the UEs' locations, in order to control the size of the clusters, the distance constraints are pre-set as d_μ for the UEs and d_α for the APs within a single cluster. In other words, the distance between the UE and its cluster centre is no more than d_μ and the distance between the AP and its cluster centre is no more than d_α. Let us now discuss, how to determine the cluster centre in the following detailed cluster formation steps. In this way, various forms of the UC clusters may be constructed by adjusting the value of d_μ or d_α. For example, a larger d_μ and d_α may improve the area spectral efficiency of the network according to [49], but as its price, the signal processing complexity within each cluster is increased. Hence, upon adjusting the value of d_μ or d_α, diverse requirements of the system design may be satisfied.

4.2.2 Implementation

Let us now carry out the UC cluster formation step by step. The UE subsets $\{\mathcal{V}_{U,n}\}$ are first constructed during Step 1 - Step 3, while the corresponding AP subsets $\{\mathcal{V}_{A,n}\}$ are determined during Steps 4 and 5. Finally, the UC clusters $\{\mathcal{C}_n\}$ are formed in Step 6.

Step 1) *Initial UE selection:* During this step, a UE $u \in \mathcal{V}'_U$ is randomly selected as the starting point for constructing a tentative single-UE subset denoted by $\mathcal{V}^t_{U,n}$ as part of the new cluster $\mathcal{C}_n$, where $\mathcal{V}'_U$ is referred to as the idle UE set including all the UEs not belonging to any of the clusters constructed. Furthermore, the tentative centre c^t_n of $\mathcal{V}^t_{U,n}$ is the location of u denoted by (x_u, y_u), as shown in Figure 4.2(a).

Step 2) *Tentative UE-set expansion:* The initial tentative UE set $\mathcal{V}^t_{U,n}$ in Step 1 is expanded by including the nearby UEs within a certain range d_μ, which may be expressed as

$$\mathcal{V}^t_{U,n} = \left(\mathcal{V}^t_{U,n} \cup \{u' \in \mathcal{V}'_U : |(x_{u'}, y_{u'}) - c^t_n| \leq d_\mu\}\right), \tag{4.3}$$

as also seen in Figure 4.2(a). Hence, the centre c^t_n of $\mathcal{V}^t_{U,n}$ should also be updated by averaging the locations of all UEs in $\mathcal{V}^t_{U,n}$, which may be calculated as

$$c^t_n = \left(\frac{\max_{u\in\mathcal{V}^t_{U,n}}\{x_u\} + \min_{u\in\mathcal{V}^t_{U,n}}\{x_u\}}{2}, \frac{\max_{u\in\mathcal{V}^t_{U,n}}\{y_u\} + \min_{u\in\mathcal{V}^t_{U,n}}\{y_u\}}{2}\right), \tag{4.4}$$

as explicitly shown in Figure 4.2(b). Then the idle UE set $\mathcal{V}'_U$ should exclude all the UEs satisfying (4.3), i.e. $\mathcal{V}'_U = (\mathcal{V}'_U \setminus \{u' \in \mathcal{V}'_U : |(x_{u'}, y_{u'}) - c^t_n| \leq d_\mu\})$. Repeat checking the condition (4.3), until no more UEs are found in the proximity of the tentative UE subset $\mathcal{V}_{U,n}$.

Step 3) *UE set formation:* Following Step 2, the UE subset $\mathcal{V}_{U,n}$ is deemed to be determined, with its centre denoted as c_n, as long as no UE is close enough to the UE subset $\mathcal{V}_{U,n}$. Upon repeating Step 1 and 2, all the UE subsets $\{\mathcal{V}_{U,n}\}$ have been constructed, as shown in Figure 4.2(c).

Step 4) *Anchor AP selection:* Let us now find the corresponding AP subsets $\{\mathcal{V}_{A,n}\}$ for $\{\mathcal{V}_{U,n}\}$. In order to guarantee the number of APs is no less than the number of UEs within each UC cluster [3], each UE u first finds its closet AP denoted by $\mathrm{AP}(u)$, which is referred to as the anchor AP, hence we have

$$\mathrm{AP}(u) = \arg\min_{a\in\mathcal{V}_A}(d_{a,u}), \tag{4.5}$$

as shown in Figure 4.2(d). If more than one UEs select the same anchor AP, this AP selects its closest UE and the other UEs have to select their next nearest APs, until each UE selected a unique anchor AP satisfying $\mathrm{AP}(u) \neq \mathrm{AP}(u')$ for any two UEs u and u'. The unique anchor AP of the

[3]The UC cluster formation process proposed in this chapter should be operated after the multiple UE scheduling process, which should satisfy two requirements: i) the total number of the scheduled UEs does not exceed that of the VLC APs; ii) the scheduled UEs are not confined to a small area. This guarantees that the number of the APs is no less than that of the UEs within each cluster. However, the scheduling process is beyond our current scope.

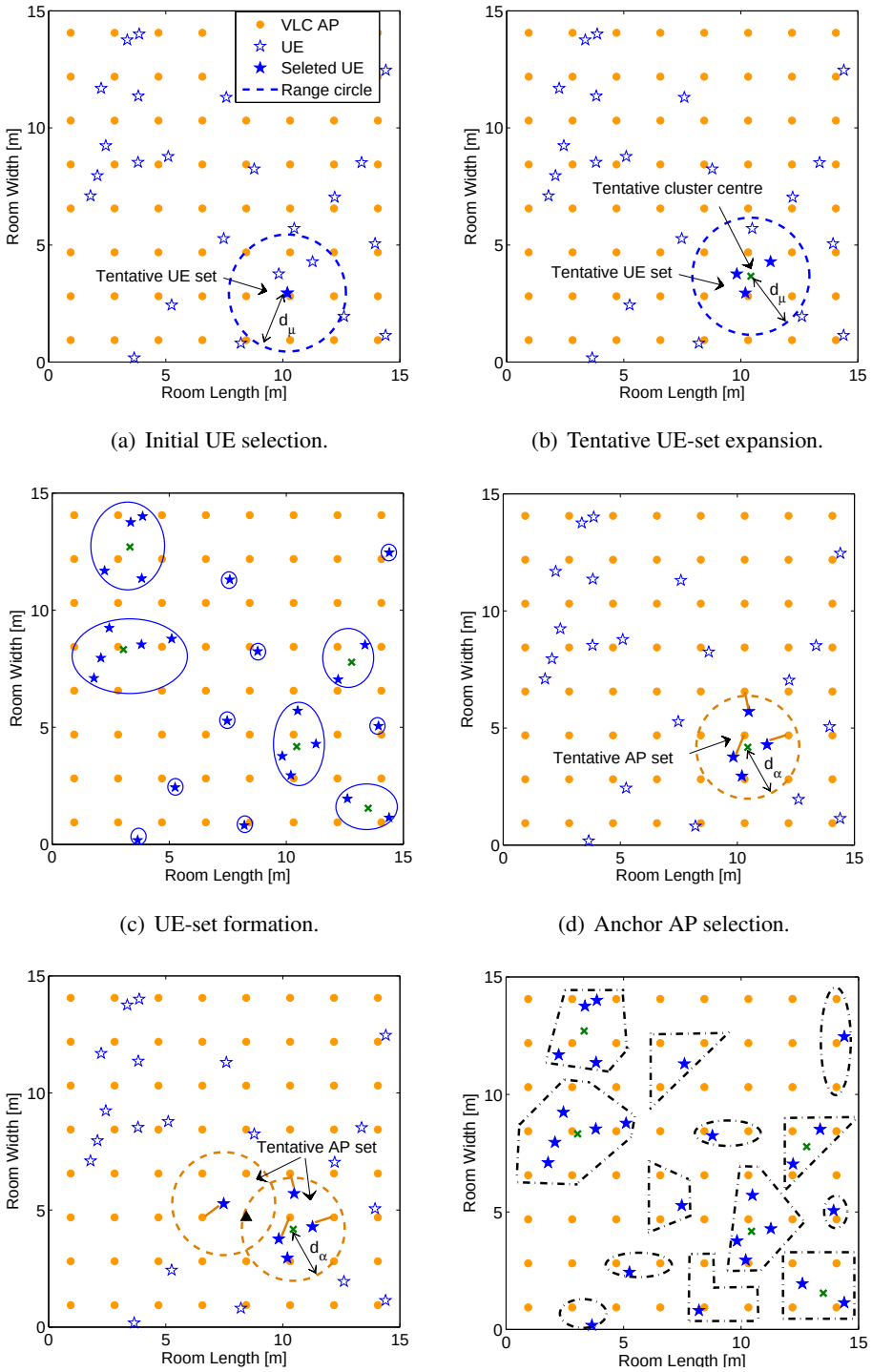

(a) Initial UE selection.

(b) Tentative UE-set expansion.

(c) UE-set formation.

(d) Anchor AP selection.

(e) Tentative AP-set adjustment.

(f) UC cluster formation.

Figure 4.2: Steps of UC cluster formation. The subfigures (a)-(c) illustrate the formation of the UE set for a specific UC cluster. (d) and (e) show the formation of the AP set for an example UC cluster, where a UE is connected by a short line with its anchor AP. Note that these steps are carried out after all UE sets are formed. In (f), multiple UC clusters are finally constructed. Note that the area of the closed irregular shapes do not represent the coverage of each cluster and the inter-cluster interference is not illustrated.

UE u is denoted as $\mathrm{AP}^*(u)$. Hence, the tentative AP set for a specific cluster $\mathcal{C}_n$ may be written as

$$\mathcal{V}^t_{A,n} = \{\mathrm{AP}^*(u) : u \in \mathcal{V}_{U,n}\}. \tag{4.6}$$

After all the tentative AP sets have been determined, similarly to the definition of the idle UE set $\mathcal{V}'_U$, let $\mathcal{V}'_A$ denote the idle AP set including all APs not belonging to any tentative AP set.

Step 5) *Tentative AP-set adjustment:* During this adjustment step, each tentative AP set is expanded first by including the nearby idle APs within a certain range d_α, which may be expressed as

$$\mathcal{V}^t_{A,n} = \left(\mathcal{V}^t_{A,n} \cup \{a \in \mathcal{V}'_A : |(x_a, y_a) - c_n| \leq d_\alpha\}\right), \tag{4.7}$$

where (x_a, y_a) denotes the position of the AP a. Furthermore, after gradually expanding all the tentative AP sets following the rules of (4.7), if a specific AP a was included in several $\mathcal{V}^t_{A,n}$ and in the meantime, a is not the anchor AP of any UE, i.e. if we have $a \in (\mathcal{V}'_A \cap \mathcal{V}^t_{A,n} \cap \mathcal{V}^t_{A,n'})$, then AP a is set to its idle mode, which is shown as the solid triangle in Figure 4.2(e). This measure is taken for the sake of avoiding any extra interference as well as for saving energy. Thus, after the process of exclusive assignment based expansion, all tentative AP subsets $\{\mathcal{V}_{A,n}\}$ are determined.

Step 6) *UC cluster formation:* Upon combining the corresponding AP subset and UE subset, the UC clusters $\{\mathcal{C}_n\}$ are finally constructed, as shown in Figure 4.2(f). In order to distinguish the single-UE and the multi-UE clusters, the former is denoted as $\mathcal{C}^{\mathrm{CT}}_n$, while the latter as $\mathcal{C}^{\mathrm{VT}}_n$, corresponding to the link-level transmission techniques CT and VT, respectively, which will be introduced next in Section 4.3.3. The overview of our proposed UC cluster formation approach is detailed in Algorithm 3.

4.3 Scalable Video Streaming

In this section, the scalable multiuser video streaming is introduced. The design aspects of the UC cluster formation and the video streaming are intricately inter-linked, where we adaptively assign AM modes to each video layer of the transmitted video stream and simultaneously allocate 'just sufficient' power to each optical AP.

4.3.1 Multiuser Video Broadcast and Scalable Extension of the High-Efficiency Video Coding

Since the UC clusters have now been constructed, let us introduce our energy-efficient scalable video system relying on the UC-VLC aided network. To elaborate, we consider a general video service scenario operating in a typical room having the dimensions of 15m$\times$15m$\times$3m, where each UE requests different video content. Supporting video multicast services is beyond the scope of this chapter. Furthermore, we employ the appealing SHVC technique [96, 107], where the video

Algorithm 3: UC Cluster Formation Algorithm

Input: $\mathcal{V}_A$, $\mathcal{V}_U$;

Initialisation: $\mathcal{V}'_U = \mathcal{V}_U$, $\mathcal{V}'_A = \mathcal{V}_A$, $n = 1$;

while $\mathcal{V}'_U \neq \emptyset$ **do**

  Initial UE selection: select $u \in \mathcal{V}'_U$; $\mathcal{V}^t_{U,n} = u$; $c^t_n = (c_u, y_u)$;

  Tentative UE-set expansion:

  while $\{u' \in \mathcal{V}'_U : |(c_{u'}, y_{u'}) - c^t_n| \leq d_\mu\} \neq \emptyset$ **do**

    include the idle UEs satisfying Equation (4.3);

    update: c^t_n;

  end

  UE-set formation: $\mathcal{V}_{U,n} = \mathcal{V}^t_{U,n}$; $c_n = c^t_n$; $\mathcal{V}'_U = (\mathcal{V}'_U \setminus \mathcal{V}_{U,n})$; $n = n + 1$;

end

Anchor AP selection:

for *each UE* $u \in \{\mathcal{V}_{U,n}\}$ **do**

  find its unique anchor AP $\mathrm{AP}^*(u)$;

end

determine all tentative AP sets as Equation (4.6) and the idle AP set $\mathcal{V}'_A = (\mathcal{V}'_A \setminus \{\mathrm{AP}^*(u)\})$;

Tentative AP-set adjustment:

for *each* $\mathcal{V}^t_{A,n}$ **do**

  expand following the rule of Equation (4.7);

end

For $n \neq n'$, if $\mathcal{V}^t_{A,n} \cap \mathcal{V}^t_{A,n'} = a$, the AP a is shut down and correspondingly determine each $\mathcal{V}_{A,n}$;

UC cluster formation

sequence is encoded into multiple layers. This allows us to progressively refine the reconstructed video quality at the receiver, when the channel quality is improved. Given a specific UC cluster, where $N_{A,n}$ optical APs simultaneously support $N_{U,n}$ UEs, $N_{U,n}$ different scalable video sequences are requested, each of which is encoded into multiple layers at the transmitter side, as shown in Figure 4.3. According to the channel conditions and to the specific video quality requirement of the UEs, the highest affordable-quality subset of transmitted video layers is decided for each video sequence and then it is assigned the appropriate AM modes by employing the 1st-tier of our proposed 3-tier dynamic-programming-based algorithm. Then, upon using the 2nd-tier PA and 3rd-tier EE optimisation algorithm, the EE of the system is maximised. In order to mitigate the intra-cluster interference, the video signals are preprocessed by exploiting the knowledge of the channel state information before transmission. At the receiver side, the UEs receive mutually interference-free video signals, which constitute a channel-quality-dependent subset of their requested video

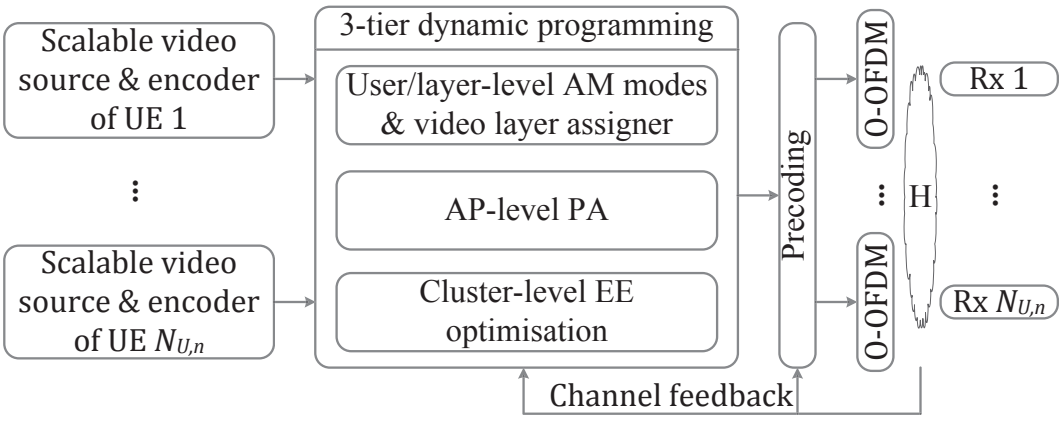

Figure 4.3: The scalable video streaming of a specific UC cluster $\mathcal{C}_n$, where $N_{A,n}$ optical APs supports $N_{U,n}$ UEs simultaneously.

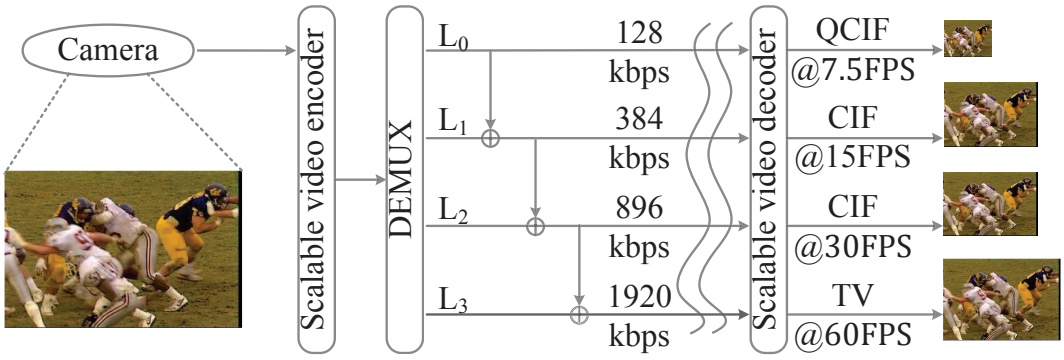

Figure 4.4: The example of a 4-layer video sequence requested by a specific UE u in the UC cluster $\mathcal{C}_n$, where the video quality is gradually refined according to the video quality demand and the channel conditions of the UE u [93].

sequence, which leads to diverse visual qualities.

To elaborate a little further, Figure 4.4 shows an example of the 4-layer video sequence downloaded by a specific UE u within the above-mentioned UC cluster $\mathcal{C}_n$ in Figure 4.3, where the video sequence exhibits both the spatial as well as the temporal scalability. In general, the base layer L_0 is the most important one amongst them, whilst the less-important video layers are termed as enhancement layers. Gradually increased video qualities are associated with receiving the higher order layers L_1, L_2 and L_3, as seen in the stylised illustration of Figure 4.4. Each enhancement layer relies on both the base layer and on all the previous enhancement layers having lower orders. If either the base layer or any of the previous enhancement layers is lost or corrupted during their transmission, the dependent layers must be dropped by the decoder. For example, observe in Figure 4.4 that layer L_1 is dependent on the base layer L_0, while layer L_3 depends on both the base layer

L_0 as well as on all the lower layers L_1 and L_2.

As far as the video streaming seen in Figure 4.3 is concerned, the video sequence of the UE u in the right subfigure is first encoded and a subset of its layers is pre-processed for transmission. Then the UE u may experience different visual qualities, depending both on its QoS requirements as well as on its channel conditions. For example, upon receiving only the base layer, the decoder is only capable of reconstructing the video at a quarter common intermediate format (QCIF) at 7.5 frame per second (FPS). By contrast, a common intermediate format (CIF) based video sequence scanned at 15 FPS and 30 FPS can be reconstructed with the aid of the layers $\{L_0, L_1\}$ and $\{L_0, L_1, L_2\}$, respectively. In order to further improve the video quality for a high-resolution TV screen at 60 FPS, all the four layers $\{L_0, L_1, L_2, L_3\}$ must be flawlessly streamed. In practice, the different video broadcast scenarios mentioned above require different throughput, which rely on the assignment of different modulation schemes to different layers. Therefore, in order to provide the highest possible video quality for all UEs and at the same time to guarantee energy-efficient scalable video provision, the various modulation schemes have to be adaptively assigned and the power has to be appropriately allocated to each video layer requested by the different UEs.

4.3.2 Adaptive Modulation

There are two popular techniques of constructing white LEDs, namely either by mixing the red-green-blue frequencies using three chips, or by using a single blue LED chip with a phosphor layer. We consider the latter one, which is the favoured commercial version. Hence, the modulation bandwidth B is typically around 20 MHz, albeit this measured bandwidth depends on the specific LED product used. Given this 20 MHz bandwidth, we are now ready to employ ACO-OFDM. To elaborate, ACO-OFDM is an energy-efficient scheme, which allows us to invoke AM modes relying on complex symbols, since the careful selection of a video-layer-specific AM mode guarantees scalable video provision.

A total of M different AM modes are adopted in our UC-VLC network, where the AM mode m provides a data rate of r^m, once its SINR threshold of ξ_{thr}^m is satisfied. According to [190], given a target BER and m-ary QAM, the minimum SINR required can be determined from:

$$\text{BER} = \frac{\sqrt{m}-1}{\sqrt{m}\log_2\sqrt{m}}\text{erfc}\left(\sqrt{\frac{3\xi_{\text{thr}}^m}{2(m-1)}}\right), \tag{4.8}$$

where $\text{erfc}(\cdot)$ denotes the complementary error function. Furthermore, we rank the M AM modes, such that if $m' \geq m$, we have $r^{m'} \geq r^m$ and $\xi_{\text{thr}}^{m'} \geq \xi_{\text{thr}}^m$.

4.3.3 Transmission Schemes

In order to simultaneously provide video services to multiple UEs within each UC cluster constructed in Section 4.2, ZF-based VT techniques are introduced, where the intra-cluster interference

is eliminated at the multiple AP transmitters, as indicated Figure 4.3. Hence, all the UEs receive mutually interference-free signals.

To elaborate a little further, for a given UC cluster $\mathcal{C}_n^{\mathrm{VT}}$, let $N_{A,n}$ and $N_{U,n}$ be the number of optical APs and the number of the UEs, respectively. Furthermore, let Z_t and Y_r denote the vectors of transmitted and received signals, respectively, where the entries of Z_t will be selected from a particular AM mode for the different video layers discussed in Section 4.3.2. Upon employing VT techniques, the received signals may be obtained by

$$Y_r = \gamma \cdot H \cdot G \cdot \widetilde{\mathcal{P}}_n \cdot Z_t + \tau, \tag{4.9}$$

where γ denotes the O/E conversion efficiency, while τ includes both the noise and the inter-cluster interference imposed by the neighbouring clusters. The channel matrix $H \in \mathbb{R}^{N_{U,n} \times N_{A,n}}$ hosts the channel attenuations between the $N_{A,n}$ APs and the $N_{U,n}$ UEs. In order to receive mutually interference-free signals at the receivers, the transmitted signals $Z_t = [z_1, z_2, \cdots, z_{N_{U,n}}]^T$, where each z_u entry satisfies that $\mathrm{E}[|z_u|^2] = 1$, are precoded as $(G \cdot Z_t)$, where the $(N_{A,n} \times N_{U,n})$-element matrix $G = H^H \cdot (H \cdot H^H)^{-1}$ obeys the ZF criterion for the sake of obtaining an interference-free identity matrix for $H \cdot G = I_{N_{U,n}}$. Furthermore, the PA matrix $\widetilde{\mathcal{P}}_n$ is a diagonal matrix and we have $\widetilde{\mathcal{P}}_n = \mathrm{diag}(p_1, \cdots, p_{N_{U,n}})$, where each diagonal entry p_u denotes the electronic power allocated to the signal z_u. Considering the AM mode m and the video layer l, where we have $l = 0, 1, \cdots, L-1$, let us furthermore denote the power allocated to the l-th video layer of the UE u associated with the AM mode m in the electronic domain by $p_{u,l}^m$, which is a specific function of the power p_u.

Let us furthermore define the SINR as the aggregated electronic power over the noise power in a bandwidth of B [MHz] [10] plus the sum of the electronic power received from other optical sources in the vicinity. Still considering ACO-OFDM, we may express the SINR for the UE u within a multi-UE cluster $\mathcal{C}_n^{\mathrm{VT}}$ as

$$\xi_{u,l}^m = \frac{(\gamma^2/2) \cdot p_{u,l}^m}{N_0 B + I_u}, \qquad u \in \mathcal{V}_{U,n^{\mathrm{VT}}}, \tag{4.10}$$

where $N_0 \sim 10^{-22}$ [A^2/Hz] [10] denotes the noise power spectral density. I_u is the interference imposed by the reflected light as well as the LoS rays from the other clusters in the vicinity. Since the interference power received by the cluster under consideration is influenced by the PA within other clusters, for simplicity, we assume the interference imposed is always equal to its maximum

value formulated as [4]

$$I_u = \gamma^2 \pi \sum_{a \notin \mathcal{V}_{A,n}} h^2[u,a] \cdot (p_{\max}^{\text{tx}})^2, \tag{4.11}$$

where $p_{\max}^{\text{tx}}$ is the maximum optical transmit power allowed for each optical AP and we have $h[u,a] = h_d[u,a] + \sum dh_r[u,a]$. (4.11) characterises the worst-case situation in our VT cluster formation.

Furthermore, for the multi-UE VT cluster, the total electronic transmit power may be expressed as

$$p_{u,l}^{\text{tx}} = \sum_{a=1}^{N_{A,n}} g_{\text{VT}}^2[a,u] \cdot p_{u,l}^m \qquad u \in \mathcal{V}_{U,n^{\text{VT}}}, \tag{4.12}$$

where $g_{\text{VT}}[a,u]$ denotes the $[a,u]$th entry of the TPC matrix G in (4.9). Given a specific UE u, the AM mode m may be assigned to it, provided that the SINR received is at least ξ_{thr}^m. Hence, the minimum power required by employing AM mode m for the UE u receiving the l-th video layer may be expressed as:

$$p_{u,l}^m = \xi_{\text{thr}}^m \cdot (N_0 B + I_u)/(\gamma^2/2). \tag{4.13}$$

Having obtained the relationship between the power required and the AM mode of the video layers of different UEs, let us now formulate the PA problem in the UC-VLC network for our energy-efficient scalable video scheme in Section 4.4.

Remark 1. When considering the single-UE cluster $\mathcal{C}_n^{\text{CT}}$ employing CT, each AP is assumed to emit the same amount of electronic power [5]. Hence the total electronic transmit power $p_{u,l}^{\text{tx}}$ of the UE u receiving the l-th video layer within the CT cluster $\mathcal{C}_n^{\text{CT}}$ may be written as

$$p_{u,l}^{\text{tx}} = \frac{N_{A,n} \cdot p_{u,l}^m}{\left(\sum_{a=1}^{N_{A,n}} h[u,a]\right)^2} = \sum_{a=1}^{N_{A,n}} \frac{p_{u,l}^m}{\left(\sum_{a=1}^{N_{A,n}} h[u,a]\right)^2} = \sum_{a=1}^{N_{A,n}} g_{\text{CT}}^2[a,u] \cdot p_{u,l}^m, \qquad u \in \mathcal{V}_{U,n^{\text{CT}}}, \tag{4.14}$$

where $h[u,a]$ denotes the $[u,a]$th entry of the channel matrix H of the single-UE CT cluster and $g_{\text{CT}}^2[a,u] = 1/\left(\sum_{a=1}^{N_{A,n}} h[u,a]\right)^2$. Hence, a unified expression derived for the CT and the VT clusters may be written as

$$p_{u,l}^{\text{tx}} = \sum_{a=1}^{N_{A,n}} g^2[a,u] \cdot p_{u,l}^m, \tag{4.15}$$

[4] Since our proposed cluster formation technique is distance-based, the distribution of the clusters constructed should be dispersed. Hence, for a specific UE, the distances to most of the APs in the neighbouring clusters should be sufficiently high compared to its anchor AP and consequently the interference imposed should be low due to the high-attenuation interference channels. Therefore, the differences between the maximum value of the interference and its actual value may be small. Furthermore, this assumption can support a more scalable and efficient solution within each cluster discussed in Section 4.4, hence avoiding the potentially excessive complexity imposed by a centralised algorithm, when true interference level is used.

[5] Since our objective is to allocate an appropriate power to each video layer of *multiple* UEs under the power constraint of each VLC AP, for the sake of maximising the achievable EE of the entire system, for simplicity, the equal power assumption was invoked in the single-UE scenarios. Hence, the optimisation in VT and the CT clusters can be operated in the same framework in Section 4.4 and 4.5.

where

$$g[a,u] = \begin{cases} g_{\mathrm{CT}}[a,u], & u \in \mathcal{V}_{U,n^{\mathrm{CT}}}, \\ g_{\mathrm{VT}}[a,u], & u \in \mathcal{V}_{U,n^{\mathrm{VT}}}, \end{cases} \tag{4.16}$$

while the SINR received by the UE u may both be expressed as in (4.10).

4.4 Energy-Efficient Video Streaming Problem

In this section, the design problem of our energy-efficient scalable video scheme is formulated and both the video-related and power-related constraints are discussed.

4.4.1 Objective Function

Let us now formulate the problem of energy-efficient scalable video streaming in our UC-VLC aided network. A general function $\mathcal{E}_{u,l}^{m}(\mathcal{P})$ is used for denoting the EE of the UE u receiving the video layer l associated with the AM mode m, where $\mathcal{P}$ represents the PA strategy of all UEs. For simplicity, we assume that the video chips requested by the different UEs have the same number of layers, but our algorithm can be readily applied, when considering different number of video layers for the different UEs. Formally, our goal is to maximise the sum EE of all UEs, which may be written as:

$$\begin{aligned} \max_{\mathcal{P}} \quad \Gamma &= \max_{\mathcal{P}} \quad \sum_{\mathcal{C}_n} \sum_{u \in \mathcal{V}_{U,n}} \sum_{l=0}^{L-1} \sum_{m=1}^{M} \mathcal{E}_{u,l}^{m}(\mathcal{P}) \\ &= \max_{\mathcal{P}} \quad \sum_{\mathcal{C}_n} \sum_{u \in \mathcal{V}_{U,n}} \sum_{l=0}^{L-1} \sum_{m=1}^{M} \frac{\Delta_{u,l}^{m}(\mathcal{P})}{p_{u,l}^{\mathrm{tx}}}, \end{aligned} \tag{4.17}$$

where $\Delta_{u,l}^{m}(\mathcal{P})$ is a general utility function assumed to be non-negative and non-decreasing in order to adequately reflect our QoS metric [106] and $p_{u,l}^{\mathrm{tx}}$ denotes the total electronic power consumption as indicated in (4.15), when the UE u receives the lth video layer. Note that the expression of (4.17) supports a more scalable and efficient distributed solution, when compared to simply maximising the system-based global EE, which is usually defined as the aggregated throughput of all UEs divided by the aggregated power consumption. Furthermore, (4.17) may be maximised independently within a cluster, provided that the interference received is conservatively assumed to be always at its maximum value, which constitutes the worst-case scenario.

Moreover, we introduce a binary indicator $x_{u,l}^{m}$. If the AM mode m is assigned to transmit the video layer l of the UE u, we have $x_{u,l}^{m} = 1$; otherwise, $x_{u,l}^{m} = 0$. Therefore, our problem is a joint AM mode assignment and PA problem, where the OF of (4.17) may be reformulated as

$$\max_{\mathcal{P}_n, \mathcal{X}_n} \quad \Gamma_n = \max_{\mathcal{P}_n, \mathcal{X}_n} \quad \sum_{u \in \mathcal{V}_{U,n}} \sum_{l=0}^{L-1} \sum_{m=1}^{M} \frac{\Delta_{u,l}^{m}(\mathcal{P}_n)}{\sum_{a=1}^{N_{A,n}} g^2[a,u] \cdot p_{u,l}^{m}} \cdot x_{u,l}^{m}, \tag{4.18}$$

where we have $\mathcal{X}_n = \{x_{u,l}^{m} : u \in \mathcal{V}_{U,n}, m = 1, \cdots M, l = 0, \cdots, L-1\}$ and $\mathcal{P}_n$ denotes the PA strategy within the cluster $\mathcal{C}_n$. Furthermore, $\Delta_{u,l}^{m}(\mathcal{P}_n)$ denotes the achievable QoS utility

corresponding to the AM mode assignment m for the video layer l of the UE u, which is a function of $\mathcal{P}_n = \{p^m_{u,l} : u \in \mathcal{V}_{U,n}, m = 1, \cdots M, l = 0, \cdots, L-1\}$. Hence, after solving $\mathcal{P}_n$ in (4.17) within each cluster, the optimal solution of the EE maximisation problem in (4.17) is found by combining all $\mathcal{P}_n$.

4.4.2 Video-related and Power-related Constraints

Let us now elaborate on the associated constraints, including both our video-related constraints and power-related constraints. During a video frame, the constraints imposed on video transmission may be formulated as follows:

$$\sum_{l=0}^{L-1} \sum_{m=1}^{M} t^m_{u,l} \cdot x^m_{u,l} \leq T, \qquad \forall u \in \mathcal{V}_{U,n}; \tag{4.19}$$

$$\sum_{m=1}^{M} x^m_{u,l} = 1 : \prod_{l'=0}^{l-1} \sum_{m=1}^{M} x^m_{u,l'} = 1, \qquad \forall l > 0; \tag{4.20}$$

$$\sum_{m=1}^{M} x^m_{u,l} \leq 1, \qquad \forall u \in \mathcal{V}_{U,n}, \forall l; \tag{4.21}$$

$$x^m_{u,l} \in \{0, 1\}, \qquad \forall u \in \mathcal{V}_{U,n}, \forall l, \forall m, \tag{4.22}$$

where $t^m_{u,l} = S_{u,l}/r^m$ denotes the time required for transmitting the lth video layer constituted by $S_{u,l}$ bits to the UE u using the AM mode m. Note that ":" represents the condition. For example, $f(x) : g(x)$ means that $f(x)$ is true provided that $g(x)$ is true. The constraint in (4.19) guarantees that the time required for transmitting a video frame does not exceed its upper limit T. Note that our scalable video scheme only has a single-video-frame delay, but it can be generalised to various video services having different delay tolerance by loosening the constraint of (4.19). Furthermore, (4.20) states the nested dependence among the different layers of the SHVC-encoded video, which ensures once the $(l+1)$st video layer is received, all the previous lower video layers must have been received as well, provided that we assume a linear dependency model for the scalable video, where the video layers of the current frame are independent of those of the other frames. Moreover, (4.21) guarantees each video layer is assigned a specific AM mode.

In addition, since the transmit power of each AP should not exceed its maximum value of $p^{\text{tx}}_{\max}$, the power-related constraints in the electronic domain of both the VT and CT clusters may be written as

$$\sqrt{\sum_{u=1}^{N_{U,n}} g^2[a,u]\bar{p}_u/2\pi} \leq p^{\text{tx}}_{\max}, \quad \forall a \in \mathcal{V}_{A,n}, \tag{4.23}$$

where $\bar{p}_u$ denotes the average power allocated to the UE u, which may be formulated as

$$\bar{p}_u = \frac{\sum_{l=0}^{L-1} \sum_{m=1}^{M} t^m_{u,l} \cdot x^m_{u,l} \cdot p^m_{u,l}}{\sum_{l=0}^{L-1} \sum_{m=1}^{M} t^m_{u,l} \cdot x^m_{u,l}}. \tag{4.24}$$

Note that we only consider the transmission power as the sole reason for power dissipation in (4.23). In our future work, other sources of power consumption, such as signal processing costs, back-haul

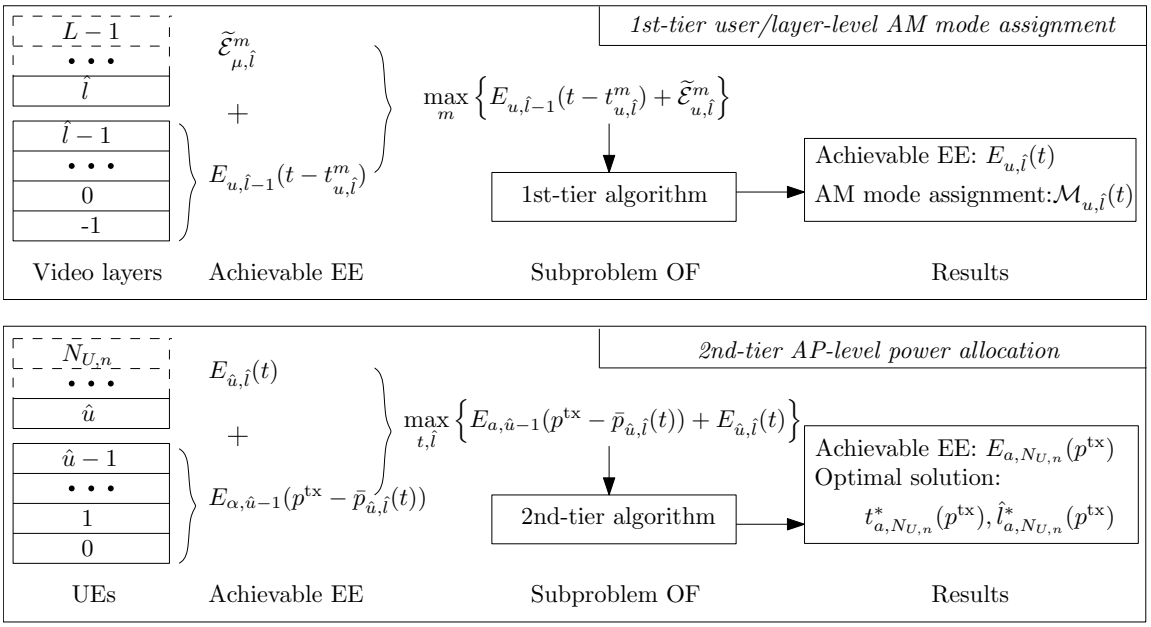

Figure 4.5: The mind map of the 1st-tier user/layer-level AM mode assignment and the 2nd-tier AP-level PA.

power consumption etc. would also be taken into account in order to paint a holistic picture in terms of the overall network's power consumption. However, at the time of writing, quantifying the network's power consumption in case of VLC systems remains an open issue, since integrating our scheme with a certain VLC back-haul deserves dedicated treatment.

In order to solve our mixed integer non-linear non-convex problem of (4.18)-(4.23), we propose a heuristic 3-tier dynamic-programming-based algorithm, which is constituted by the 1st-tier user/layer-level AM mode assignment, the 2nd-tier AP-level PA and the 3rd-tier cluster-level EE optimisation. The user/layer-level AM mode assignment step mainly copes with the constraints in (4.19)-(4.22), which are determined by the video characteristics, regardless of the power-level budget of (4.23). All the solutions provided by the user/layer-level AM mode assignment step will be regarded as the input to the following AP-level PA step, where all the feasible solutions satisfying both the video characteristic constrains of (4.19)-(4.22) as well as the power constraint (4.23) can be found. Finally, during the cluster-level EE optimisation step, the solution of our problem (4.18)-(4.23) can be obtained based on our previous discussions.

4.5 Dynamic-Programming-based Algorithm

In this section, a 3-tier dynamic-programming-based algorithm is proposed for solving our problem formulated in Section 4.4, including its user/layer-level AM mode assignment, the AP-level PA and the cluster-level EE optimisation.

4.5.1 User/Layer-Level Adaptive Modulation Mode Assignment

In this step, we first deal with the constraints (4.19)-(4.22) imposed by the video characteristics, which are determined by each individual UE, but are transparent to how the clusters are formed. Thus, let us bypass the PA across the given cluster and consider the problem on the basis of a single UE with the aid of the mind map of our proposed algorithm in Figure 4.5.

4.5.1.1 Objectives of the Adaptive Modulation Mode Assignment Subproblem

Given a specific UE u, the user/layer-level AM mode assignment problem may be formulated similar to a multi-choice knapsack problem [191], which is NP-hard. The classic multi-choice knapsack problem may be described as follows. Multiple groups of items are considered and each item has a value and a resource cost. The objective is to select exactly one item from each group into the knapsack and to maximise the total value of the selected items, whilst not exceeding the resource capacity available. In our problem, the L video layers may be viewed as the multiple groups, where the M AM modes are the items. The achievable EE and the corresponding transmission time costs may be interpreted as the value and the resource cost. Our goal is to select a specific one AM mode for each transmitted video layer in order to maximise the EE within the single-video-frame delay budget. We assume furthermore that if a video layer is not transmitted, no AM mode will be assigned to it. In contrast to the classic multi-choice knapsack problem, not all the video layers have to be transmitted by selecting an AM mode, but if the video layer l is transmitted, all the lower-order video layers must be transmitted and be assigned a specific AM mode as well. Note that the video layers' order requirement (4.20) is readily satisfied by employing our dynamic-programming-based algorithm as detailed below, since the proposed algorithm is implemented in accordance with the video layers' order, i.e. from layer 0 to layer $L-1$.

Before introducing our dynamic-programming-based algorithm, let us define an auxiliary function $E_{u,\hat{l}}(t)$ first, which may be interpreted as the maximum EE for the given UE u, when receiving the video layers from 0 to $\hat{l}$ and the transmission time duration is limited to t, where we have $0 \leq \hat{l} \leq L-1$ and $0 \leq t \leq T$. Since the time resource t has a continuous value, it is further decomposed into σ discrete values, which may be written as $t = 0, T/\sigma, 2T/\sigma, \cdots, T$. Following the basic principles of the dynamic programming approach, we consider the sub-problem under a specific transmission time limit t. Hence, $E_{u,\hat{l}}(t)$ may be written as

$$E_{u,\hat{l}}(t) = \max_{x^m_{u,l}} \left\{ \sum_{l=0}^{\hat{l}} \sum_{m=1}^{M} \frac{\Delta^m_{u,l}(p^m_{u,l}) \cdot x^m_{u,l}}{\sum_{a=1}^{N_{A,n}} g^2[a,u] \cdot p^m_{u,l}} : t_{u,\hat{l}} \leq t, \right. \\ \left. \sum_{m=1}^{M} x^m_{u,l} \leq 1,\ x^m_{u,l} \in \{0,1\},\ \forall l = 0,1,\ldots,\hat{l} \right\}, \tag{4.25}$$

where $t_{u,\hat{l}}$ is the total transmission time required for transmitting all the video layers up to $\hat{l}$ and we have $t_{u,\hat{l}} = \sum_{l=0}^{\hat{l}} \sum_{m=1}^{M} t^m_{u,l} \cdot x^m_{u,l}$. Note that during this user/layer-level AM mode assignment

procedure, we focus our attention on each single UE and the PA strategy $\mathcal{P}_n$ across the entire cluster may be treated in the next step. Hence, the achievable QoS utility has been written as $\Delta^m_{u,l}(p^m_{u,l})$ in (4.25), instead of $\Delta^m_{u,l}(\mathcal{P}_n)$ as in (4.18).

4.5.1.2 Methodologies for Assigning the Adaptive Modulation Mode

Given a specific video layer having the length of $S_{u,l}$ bits, the lower the order of the AM mode, the longer the transmission time becomes, since the lower-order AM mode provides a lower data rate. We start the recursion of $E_{u,\hat{l}}(t)$ from the virtual base layer, which may be referred to as the '-1st' video layer. Since transmitting the virtual base layer represents no transmission, for any transmission time limit t, we have

$$E_{u,-1}(t) = 0, p^m_{u,-1} = 0, t^m_{u,-1} = 0, \forall t, \forall m, \tag{4.26}$$

where $p^m_{u,-1}$ denotes the power allocated for the virtual base layer with the mth AM mode assigned to the UE u, which should be zero, since no power is consumed. Similarly, the corresponding time duration is also zero. In order to obtain a general recursion formulation for $E_{u,\hat{l}}(t)$, let us consider the base layer transmission as an explicit example. As mentioned above, if a certain video layer is transmitted, all the lower-order video layers must have been transmitted. Hence, when transmitting the base layer, as its lower video layer, the virtual '-1st' video layer must be transmitted. It is plausible that $(t^M_{u,0} + t^M_{u,-1})$ is the least time required for transmitting the base layer by employing the highest-order AM mode M for the '-1st' and 0th video layer. If the time limit t is even shorter than $(t^M_{u,0} + t^M_{u,-1})$, there will be no feasible solution for maximising $E_{u,0}(t)$, where $E_{u,0}(t)$ is assumed to be $-\infty$ and hence no AM mode will be assigned. Otherwise, for all $t \geq (t^M_{u,0} + t^M_{u,-1})$, if the base layer is assigned an AM mode m, we need a duration of $t^m_{u,0}$ to transmit, when we have associated EE value of $\Delta^m_{u,0}(p^m_{u,0})/p^m_{u,0}$. In this case, the time allocated to the virtual base layer is reduced to $(t - t^m_{u,0})$. Hence, the problem of the AM mode assignment for transmitting the '-1st' and the 0th video layers may be formulated as

$$E_{u,0}(t) = \begin{cases} -\infty, & \text{for } 0 \leq t < t^M_{u,0} + t^M_{u,-1}; \\ \max\limits_m \left\{ E_{u,-1}(t - t^m_{u,0}) + \dfrac{\Delta^m_{u,0}(p^m_{u,0})}{\sum_{a=1}^{N_{A,n}} g^2[a,u] \cdot p^m_{u,0}} : t^m_{u,0} \leq t, 1 \leq m \leq M \right\}, & \\ & \text{for } t^M_{u,0} + t^M_{u,-1} \leq t \leq T. \end{cases} \tag{4.27}$$

Similarly, for the other video layers $\hat{l} = 1, 2, \ldots, L-1$, as shown in the top subfigure of Figure 4.5, a general formulation of $E_{u,\hat{l}}(t)$ may be written as

$$E_{u,\hat{l}}(t) = \begin{cases} -\infty, & \text{for } 0 \leq t < \sum\limits_{l=-1}^{\hat{l}} t^M_{u,l}; \\ \max\limits_m \left\{ E_{u,\hat{l}-1}(t - t^m_{u,\hat{l}}) + \widetilde{\mathcal{E}}^m_{u,\hat{l}} : t^m_{u,\hat{l}} \leq t, 1 \leq m \leq M \right\}, & \text{for } \sum\limits_{l=-1}^{\hat{l}} t^M_{u,l} \leq t \leq T, \end{cases} \tag{4.28}$$

where the EE increment $\widetilde{\mathcal{E}}^m_{u,\hat{l}} = \Delta^m_{u,\hat{l}}(p^m_{u,\hat{l}})/(\sum_{a=1}^{N_{A,n}} g^2[a,u]\cdot p^m_{u,\hat{l}})$. Note that $(t - t^m_{u,\hat{l}})$ may not be equal to any of the specific time durations of $0, T/\sigma, 2T/\sigma, \cdots, T$. In this case, we assume that $(t - t^m_{u,\hat{l}})$ corresponds to its nearest lower time-duration. For example, if the exact value of $(t - t^m_{u,\hat{l}})$ is approximately $2.66T/\sigma$, we round it to $2T/\sigma$ and substitute $E_{u,\hat{l}-1}(2T/\sigma)$ into (4.28).

4.5.1.3 Adaptive Modulation Mode Assignment Results

Relying on the relationships formulated above, we obtain the AM mode assignment for each video layer of a specific UE u under various time limits. To elaborate with the aid of the top subfigure of Figure 4.5, let $\mathcal{M}_{u,\hat{l}}(t)$ be an $(1 \times L)$-element vector of the AM mode assigned for each video layer under the time-resource t and the highest-order transmitted video layer $\hat{l}$. Since no AM mode is assigned to the video layers spanning from $\hat{l}+1$ to $L-1$, the corresponding elements in $\mathcal{M}_{u,\hat{l}}(t)$ are set to zero. Thus, the corresponding achievable EE value $E_{u,\hat{l}}(t)$ can be obtained from (4.28). Correspondingly, the power allocated for transmitting each video layer is known according to (4.13). Hence, corresponding to each $\mathcal{M}_{u,\hat{l}}(t)$ under the time limit t, the average PA $\bar{p}_{u,\hat{l}}(t)$ can be calculated according to (4.24).

Following the user/layer-level AM mode assignment step, we can obtain the $(\sigma \times L)$-element time-guaranteed EE matrix $E_u = \{E_{u,\hat{l}}(t) : t = T/\sigma \cdots, T, \hat{l} = 0, \cdots L-1\}$. Furthermore, each UE u has the time-guaranteed $(L \times \sigma \times L)$-element AM mode assignment matrix $\mathcal{M}_u$, which may be expressed as $\mathcal{M}_u = \{\mathcal{M}_{u,\hat{l}}(t) : t = T/\sigma, \cdots, T, , \hat{l} = 0, \cdots L-1\}$, which is referred to as the time-guaranteed AM mode matrix of the UE u. Correspondingly, the $(\sigma \times L)$-element average PA matrix $\bar{p}_u = \{\bar{p}_{u,\hat{l}}(t) : t = T/\sigma, \cdots, T, \hat{l} = 0, \cdots L-1\}$ can also be obtained. Since all the results obtained so far are time-guaranteed and on a per-UE basis, we only have to find the highest achievable EE from E_u and its corresponding AM mode assignment, whilst avoiding the violation of the power constraint (4.23) imposed by the optical APs within each cluster.

4.5.2 Access-Point-Level Power Allocation

Let us now introduce the 2nd-tier AP-level PA algorithm, which is carried out within each UC cluster. Our objective in this step is to find the appropriate AM mode assignment solutions for each UE from its time-guaranteed AM mode assignment matrix $\mathcal{M}_u$, which further satisfies the power constraint (4.23) and maximises the achievable EE.

4.5.2.1 Objectives of the Power Allocation Subproblem

Similarly to the previous section, we first define an auxiliary function $E_{a,\hat{u}}(p^{\text{tx}})$, which may be interpreted as the maximum EE, when supporting a total of $\hat{u}$ UEs within a specific cluster $\mathcal{C}_n$ and the given AP $a \in \mathcal{V}_{A,n}$ with a maximum power limit p^{tx}, where we have $0 \leq \hat{u} \leq N_{U,n}$ and $0 \leq p^{\text{tx}} \leq p^{\text{tx}}_{\max}$. Then we further discretize the transmit power into J levels, which may be written as

$p^{\text{tx}} = p^{\text{tx}}_{\max}/J, 2p^{\text{tx}}_{\max}/J, \cdots, p^{\text{tx}}_{\max}$. Hence, considering the cluster supporting $\hat{u}$ UEs, for a given AP a with a power limit p^{tx} within the cluster, $E_{a,\hat{u}}(p^{\text{tx}})$ may be formulated as

$$E_{a,\hat{u}}(p^{\text{tx}}) = \max_{t,\hat{l}} \left\{ \sum_{u=1}^{\hat{u}} \sum_{t=0}^{T} \sum_{\hat{l}=0}^{L-1} E_{u,\hat{l}}(t) \cdot x_{u,\hat{l}}(t) : \sum_{t=T/\sigma}^{T} \sum_{\hat{l}=0}^{L-1} x_{u,\hat{l}}(t) = 1, \forall u = 1, \cdots, \hat{u}, \right.$$
$$\left. \sqrt{\sum_{u=1}^{\hat{u}} \sum_{t=T/\sigma}^{T} \sum_{\hat{l}=0}^{L-1} \frac{g^2[a,u] \cdot \bar{p}_{u,\hat{l}}(t) \cdot x_{u,\hat{l}}(t)}{2\pi}} \leq p^{\text{tx}}, x_{u,\hat{l}}(t) \in \{0,1\} \right\}, \quad (4.29)$$

where $x_{u,\hat{l}}(t)$ is a binary indicator. If the AM mode assignment $\mathcal{M}_{u,\hat{l}}(t)$ is selected for the UE u, we have $x_{u,\hat{l}}(t) = 1$; otherwise, $x_{u,\hat{l}}(t) = 0$.

4.5.2.2 Methodologies for Allocating Power

Next, we find the solution in an iterative manner. Let $\bar{p}^{\min}_u$ denote the minimum average power required, when transmitting video to the UE u, where we have $\bar{p}^{\min}_u = \min\{\min\{\bar{p}_u\}\}$. Similarly to the concept of the virtual base layer, we assume a virtual scenario, in which no UE is served, so that we have:

$$E_{a,0}(p^{\text{tx}}) = 0, \bar{p}_{0,\hat{l}}(t) = 0, \quad \forall p^{\text{tx}}, \forall t, \forall \hat{l}. \quad (4.30)$$

Hence, the basic principle of the general recursion for the AP-level PA step is similar to (4.28) of the previous section, as shown in the bottom subfigure of Figure 4.5, which furthermore may be written as

$$E_{a,\hat{u}}(p^{\text{tx}}) = \begin{cases} -\infty, & \text{for } 0 \leq p^{\text{tx}} < \sqrt{\sum_{u=1}^{\hat{u}} g^2[a,u] \cdot \bar{p}^{\min}_u/(2\pi)}; \\ \max\limits_{t,\hat{l}} \left\{ E_{a,\hat{u}-1}(p^{\text{tx}} - \bar{p}_{\hat{u},\hat{l}}(t)) + E_{\hat{u},\hat{l}}(t) : \sqrt{g^2[a,u] \cdot \bar{p}_{\hat{u},\hat{l}}(t)/(2\pi)} \leq p^{\text{tx}} \right\}, & \\ & \text{for } \sqrt{\sum_{u=1}^{\hat{u}} g^2[a,u] \cdot \bar{p}^{\min}_u/(2\pi)} \leq p^{\text{tx}} \leq p^{\text{tx}}_{\max}. \end{cases} \quad (4.31)$$

Similar to (4.28) again, $(p^{\text{tx}} - \bar{p}_{\hat{u},\hat{l}}(t))$ is rounded down to its nearest lower power level, when it is not equal to any of the legitimate power levels.

4.5.2.3 Power Allocation Results

By iteratively solving (4.31), the potential PA schemes are found, when separately considering the power limit of each AP. Since all the UEs within a single cluster must be fully supported, $E_{a,N_{U,n}}(p^{\text{tx}})$ is the achievable EE corresponding to the AP a subjected to a power constraint p^{tx}, as shown in the bottom subfigure of Figure 4.5. Correspondingly, the solution of (4.31) for achieving $E_{a,N_{U,n}}(p^{\text{tx}})$ is denoted as $(t^*_{a,N_{U,n}}(p^{\text{tx}}), \hat{l}^*_{a,N_{U,n}}(p^{\text{tx}}))$, where $t^*_{a,N_{U,n}}(p^{\text{tx}})$ and $\hat{l}^*_{a,N_{U,n}}(p^{\text{tx}})$ are both $(1 \times N_{U,n})$-element vectors. Thus, the PA scheme may be obtained by find the corresponding

element $\bar{p}_{u,\hat{l}^*_{a,N_{U,n}}(p^{\text{tx}})[1,u]}(t^*_{a,N_{U,n}}(p^{\text{tx}})[1,u])$ from the previous time-guaranteed PA matrix $\bar{p}_u$ for each of the UE u.

We further obtain the $(1 \times J)$-element vector $E_a = \{E_{a,N_{U,n}}(p^{\text{tx}}) : p^{\text{tx}} = p^{\text{tx}}_{\max}/J, \cdots, p^{\text{tx}}_{\max}\}$ to denote the achievable EE under various power limits and also the $(J \times N_{U,n})$-element PA matrix $\bar{p}_a$ at the AP a, where each row represents an PA scheme for the cluster $\mathcal{C}_n$ and we have J PA schemes. Considering all the $N_{A,n}$ APs, we now have a total of $(N_{A,n} \times J)$ PA schemes for a cluster $\mathcal{C}_n$. Next let us determine the final solution of the PA in the following section.

4.5.3 Cluster-level Energy Efficiency Optimisation

4.5.3.1 Solutions of Optimising Energy Efficiency

Given a specific cluster $\mathcal{C}_n$, we have obtained both the $(N_{A,n} \times J)$ PA schemes denoted as a $(J \times N_{U,n} \times N_{A,n})$-element matrix $\{\bar{p}_a : a = 1, \cdots, N_{A,n}\}$ and the corresponding $(J \times N_{A,n})$-element EE matrix $\{E_a : a = 1, \cdots, N_{A,n}\}$. Then the solution of the PA problem formulated for achieving the maximum EE may be found by

$$\{a*, p^{\text{tx}*}\} = \arg\max_{a, p^{\text{tx}}} \{\{E_a\}\}, \tag{4.32}$$

where the solution $\{a*, p^{\text{tx}*}\}$ corresponds to a row of the PA matrix $\bar{p}_{a*}$, which may be written as $\bar{p}_{a*}[j,:]$ and we have $j = J \cdot p^{\text{tx}*}/p^{\text{tx}}_{\max}$. It is plausible that the PA scheme $\bar{p}_{a*}[j,:]$ selected satisfies the power constraint (4.23) of the AP $a*$, but we have to check if it violates other APs' power limits. If $\bar{p}_{a*}[j,:]$ is feasible for all APs, it is the final solution of the PA for our energy-efficient video scheme. Otherwise, $\bar{p}_{a*}[j,:]$ and its corresponding EE $E_{a*,N_{U,n}}(p^{\text{tx}*})$ are set to zero and we repeat (4.32) until we find a feasible PA scheme satisfying (4.23) for all APs within the cluster. Finally, each element of $\bar{p}_{a*}[j,:]$ corresponds to a specific layer-level PA $\bar{p}_{u,\hat{l}}(t)$ and to a specific AM mode assignment vector $\mathcal{M}_{u,\hat{l}}(t)$.

4.5.3.2 Complexity of the Proposed Dynamic-Programming-based Algorithm

The complexity imposed by our 3-tier dynamic-programming-based algorithm is much lower than that of the optimal exhaustive search, which is on the order of $O(L^{(M \cdot N_{U,n})})$ for a specific cluster $\mathcal{C}_n$. By contrast, during the 1st-tier AM mode assignment of the proposed algorithm, the complexity for each UE is on the order of $O(\sigma ML)$. Then in the PA step, the complexity imposed by each AP is $O(\sigma N_{U,n} J)$ and the last EE optimisation has a complexity of $O(N_{A,n} J)$. Furthermore, the complexity of our 1st-tier AM mode assignment algorithm may be reduced by using the following rule.

Remark 2. For any $\bar{p}_u$, if there exist two elements p_i and $p_{i'}$ such that $p_i \geq p_{i'}$ and the corresponding EE obeys $E_i < E_{i'}$, where $E_i, E_{i'} \in E_u$, then E_i is set to zero.

Video parameters	
Video sequence	RaceHorses
QPs/Frame	40,26,16
Resolution	416 × 240
Video codec	SHVC
FPS	30
No. of video layers	3
Bits per pixel	8
Error-free Y-PSNR	28.3, 36.9, 44.7 [dB]
Bitrate	5.1 [Mbits/s]
Representation	YUV 4:2:0
Error concealment	Frame-copy
No. of frames	30, 300
Coding structure	IPPPIPPP...
Algorithm parameters	
The range of each AP subset (d_α)	15 [m]
No. of discrete time values (σ)	100
No. of power level (J)	10

Table 4.1: Simulation parameters of the scalable video system.

4.6 Performance Evaluation of the Energy-efficient Video Streaming Scheme

In this section, we will present our simulation results characterising the 3-tier dynamic-programming-based scheme conceived for energy-efficient scalable video transmission in the VLC system, with a special emphasis on our UC cluster formation. Before presenting our simulation results, let us elaborate further on the implementation of our energy-efficient video system. Relying on the positioning and tracking module, distance-based cluster formation is constructed. Within each cluster, our proposed optimisation algorithm is activated upon the UEs' requests. The solution gives the appropriate video layer selection, the adaptive mode assignment as well as the power allocation for the sake of maximising the EE. Thus different transmission strategies, i.e. VT and CT, are employed in multi-UE clusters and single-UE clusters correspondingly, based on the solution. Regarding the video implementation, at the transmitter side, only the carefully selected layers of the scalable SHVC stream are transmitted. At the decoder side, all the received layers will be decoded. Then, the error-infested layers will be discarded together with their dependent layers. This will result in a decodable bitstream, which is then passed to the SHVC decoder for reconstructing the final YUV clip.

As in Chapter 2 and Chapter 3, a 15m×15×3m room model is considered, which is covered by the VLC DL, including (8×8) uniformly distributed optical APs at a height of 2.5m. The parameters of the LED arrays are summarised in Table 4.1. Our investigations include both the LoS and the first reflected light-path, where the channel's DC attenuation is given by (1.4) and (1.6). As for the AM mode, we consider binary phase-shift keying (BPSK), 4-QAM, 16-QAM, 64-QAM and 256-QAM in our simulations, while our algorithm is a general one, which is not limited to the specific AM modes considered in this chapter. Furthermore, advanced SHVC techniques are employed in our VLC system, where the 3-layer video sequence "RaceHorses" is transmitted at 30 FPS. The error-free Y-PSNR is 28.3dB, 36.9dB and 44.7dB, respectively, when the first, second and third video layer is received. At this stage, we assume that if a video layer is allocated power and assigned a specific AM mode, it can be successfully received, provided that a sufficiently low BER requirement is satisfied in the indoor VLC environment considered. If a frame is not transmitted, the low-complexity error concealment technique of frame-copying is used, where the lost frame is replaced by the most recent successfully decoded frame. The general QoS metric of $\Delta_{u,l}^{m}(p_{u,l}^{m})$ is assumed to be the achievable throughput corresponding to the specific AM mode assignment m for the video l of the UE u, i.e. we have $\Delta_{u,l}^{m}(p_{u,l}^{m}) = r^{m}$. The parameters of the video sequence are detailed in Table 4.1. Each of our simulation results are averaged over 50 independent simulation runs, where the UEs are randomly distributed in the room.

4.6.1 Energy Efficiency versus Video Quality Investigations

4.6.1.1 Investigations for Various Field-of-View and User Equipment Density

Since the FoV is one of the most influential parameters in VLC networks, we consider various FoVs and their effects on the attainable system performance, as shown in Figure 4.6 [6]. The system's EE is reduced, when the FoV is increased, since a higher transmit power is required, when the interference is increased, while our UC clusters remain superior in all the scenarios considered. As for the average throughput (TP) and for the video PSNR per UE, which is used for quantifying the reconstructed video quality at the receiver side, they all reach a peak at FoV $= 75^{\circ}$ considering the UC design, due to having the lowest number of UEs in outage, according to the right subfigure of Figure 4.6. When the FoV is further increased, the UEs suffer from more interference and some of them may experience an outage as a result. Note that in this case, increasing the transmitted power may not be an appealing solution, since according to (4.11) the interference is also increased proportionally. The traditional cell designs of UFR and FR-2 have quite similar performances in terms of their video quality and the percentage of UEs in outage, although UFR provides a higher

[6] In Figure 4.6, we observed the FoVs from 70° to 90°. With the FoV 70°/75°, the UE is capable of receiving data from two neighbouring APs and the area contaminated by potential interference is modest. When the FoV is increased to 80°/85°/90°, the UE is capable of receiving data from four APs and the potential interference contaminated area is also increased. Although the five FoVs considered have quite similar absolute values, but they correspond to different interference levels

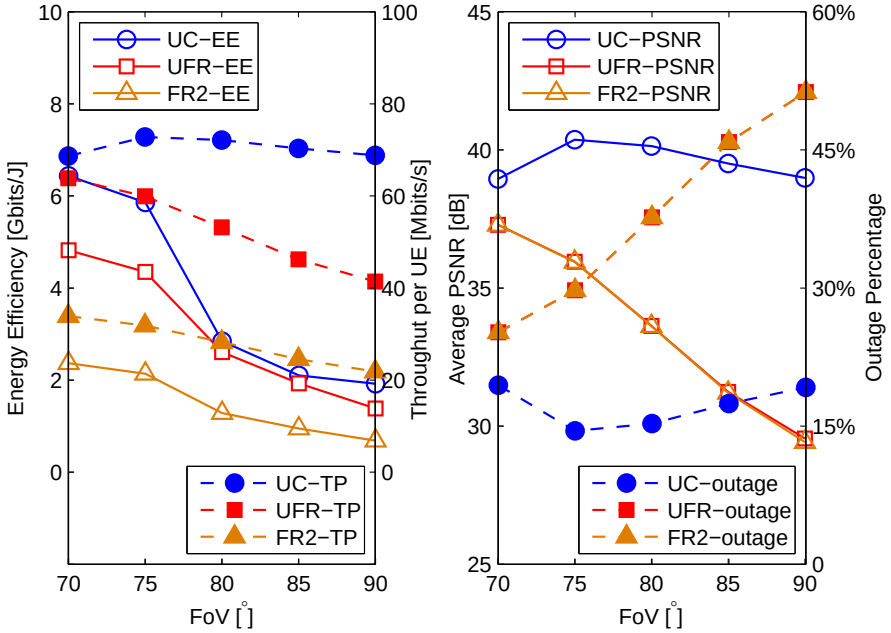

Figure 4.6: Left: EE of the VLC network and average TP per UE for various FoVs. Right: Average PSNR and the UE outage percentage. The optical power is 0.3862W for maintaining the illuminance requirement of our room model as a typical work place.

EE and TP. Hence using traditional frequency reuse may not be a desirable solution for interference mitigation in our VLC networks.

Figure 4.7 shows the attainable system performance for various UE densities, ranging from a low-density scenario of 10 UEs to a high-density scenario of 40 UEs, where the FoV is 90 ° and the maximum transmitted optical power is 0.3862W. This power was calculated according to the illumination constraint of maintaining an average illuminance of 600lx, a minimum of 200lx and a maximum of 800lx, which are typical values for the work place. As expected, our proposed UC clusters are capable of offering the highest EE, TP and PSNR in most of the scenarios considered, whilst simultaneously supporting more UEs at a given UE outage percentage, as seen in the right subfigure of Figure 4.7.

4.6.1.2 Investigations for User-Centric Cluster Edge Distance d_μ and Maximum Transmitted Optical Power

As mentioned in Section 4.2, the various characteristics of the UC clusters may be satisfied upon adjusting the value of the atto-cell edge distance d_μ. For example, a large d_μ may improve the area spectral efficiency of the system according to our previous work [49]. Figure 4.8 illustrates the system's performance for different d_μ values in terms of the EE, TP, PSNR and the outage percentage. As expected, upon increasing the value of d_μ, both the EE and TP are increased. Similarly, the average video quality is also enhanced for larger d_μ. Although a larger d_μ results

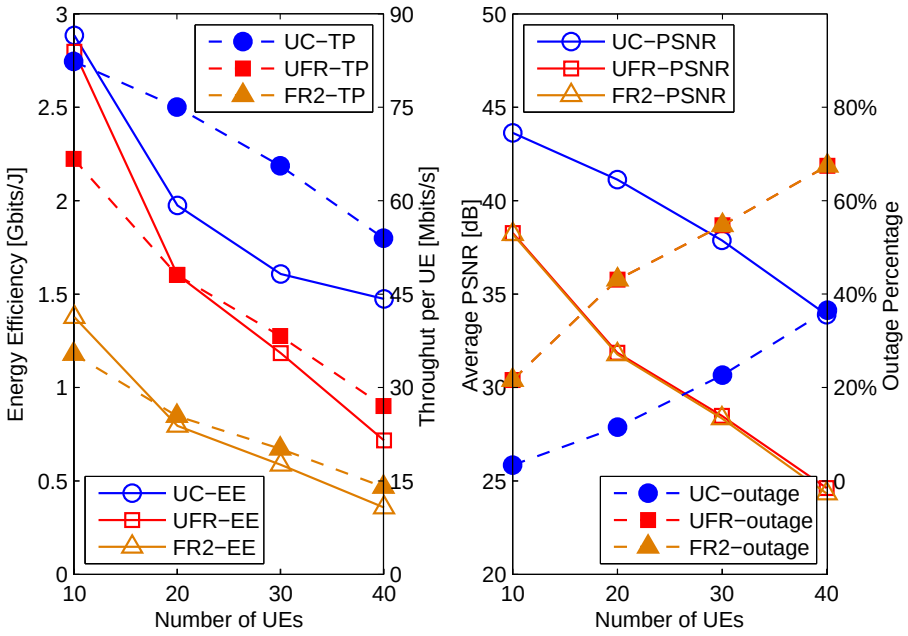

Figure 4.7: Left: EE of the VLC network and average TP per UE for various UE densities. Right: Average PSNR and the UE outage percentage, where FoV = 90°. The optical power is 0.3862W for maintaining the illuminance requirement of our room model as a typical work place.

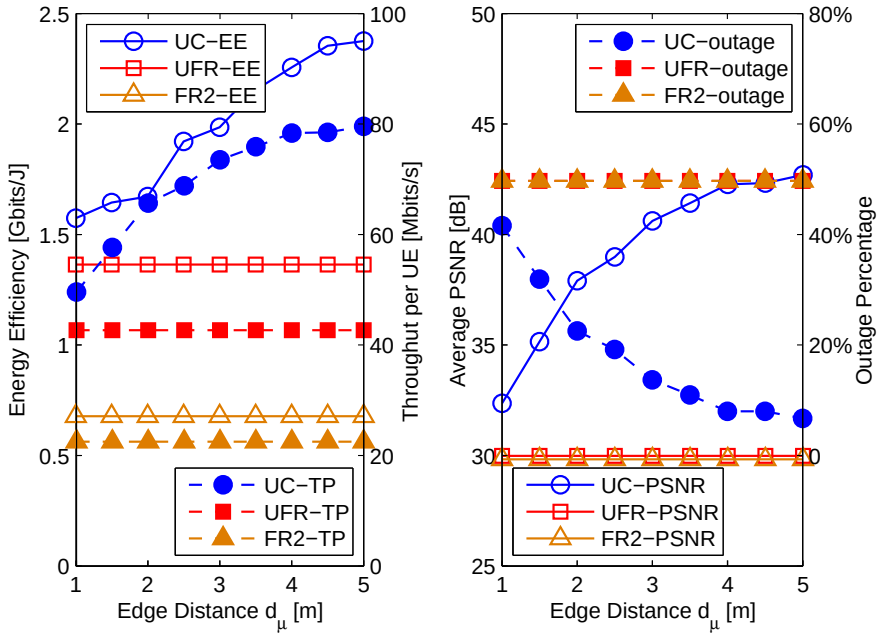

Figure 4.8: Left: EE of the VLC network and average TP per UE for various UC cluster edge distance d_μ. Right: Average PSNR and the UE outage percentage, where FoV = 90°. The optical power is 0.3862W for maintaining the illuminance requirement of our room model as a typical work place.

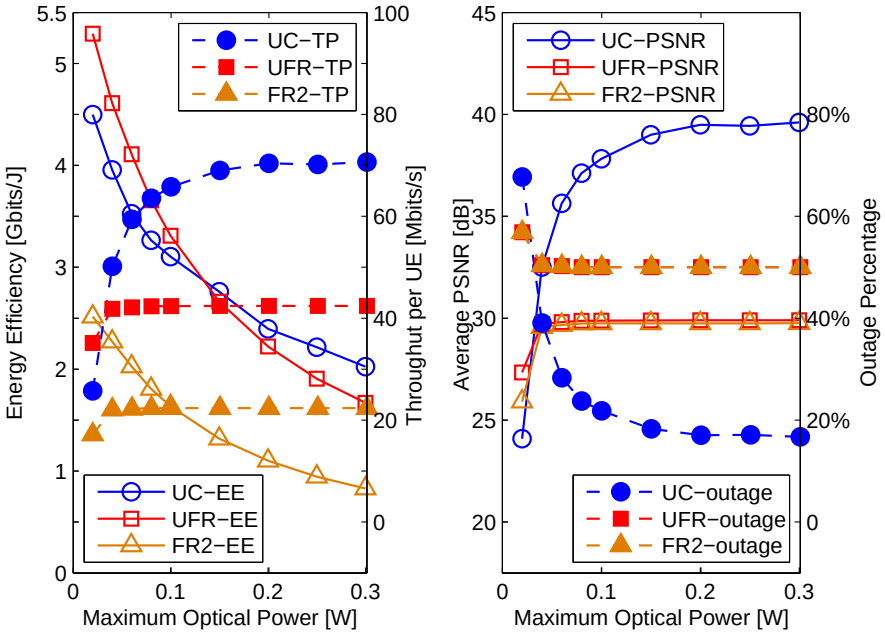

Figure 4.9: Left: EE of the VLC network and average TP per UE for various transmitted optical power thresholds. Right: Average PSNR and the UE outage percentage, where FoV = 90°.

in large-scale UC clusters, they potentially incur additional signal processing costs, such as the inversion of a large matrix at the distributed APs as required by the ZF based transmit pre-coding. Furthermore, sharing data amongst the APs of large UC clusters may require a more capable back-haul. Hence, we have to determine the most beneficial edge-distance d_μ of our UC cluster in order to minimise the network's power consumption by additionally considering the power-dissipation of the signal processing as well as of the back-haul.

Figure 4.9 shows the system's performance for different optical transmit power thresholds. Although the UC clusters are not as efficient as the traditional UFR design, when the maximum transmitted optical power is limited to 0.1W, it is capable of providing a higher TP as well as better video quality in most of the scenarios considered. Upon increasing the optical power threshold, the EE becomes lower, but the TP and video quality improvements of the system remain slow in all the scenarios considered. Note that the various optical transmit power thresholds may be realised by appropriately adjusting the LED array of each specific optical AP, in order to maintain the associated illuminance requirement.

4.6.2 Mobile User Equipment Investigations

Our proposed UC clusters and the corresponding PA algorithm are now further investigated, when the UEs are mobile. Let the UE with index '1' move at 1.25m/s following a trajectory shown in Figure 4.10, where its UC cluster is dynamically constructed. The location of the UE is reported

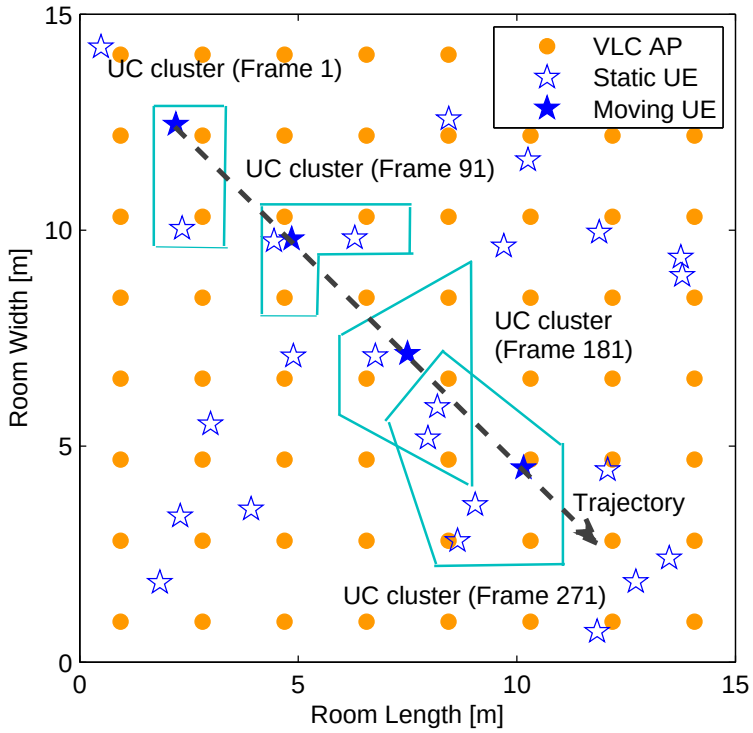

Figure 4.10: The trajectory of the moving UE and dynamic UC cluster formation.

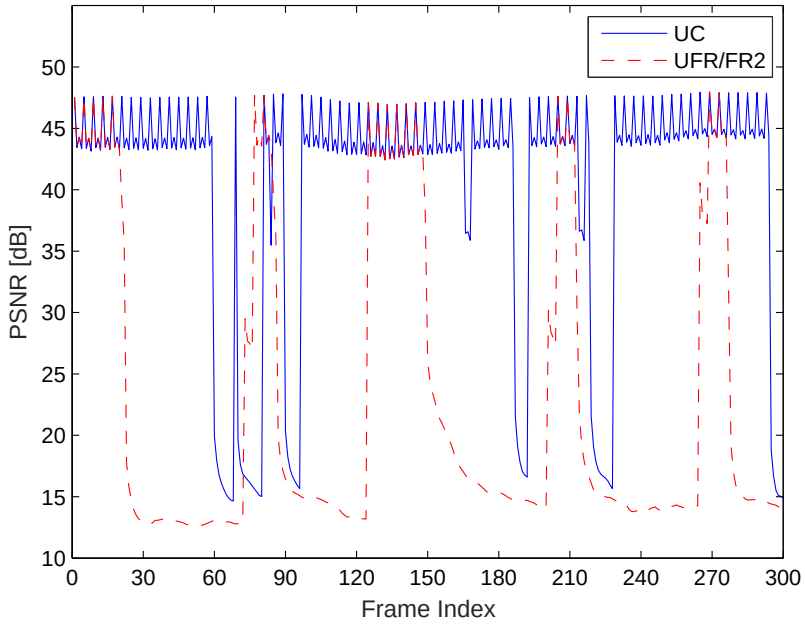

Figure 4.11: PSNR of each frame for the moving UE.

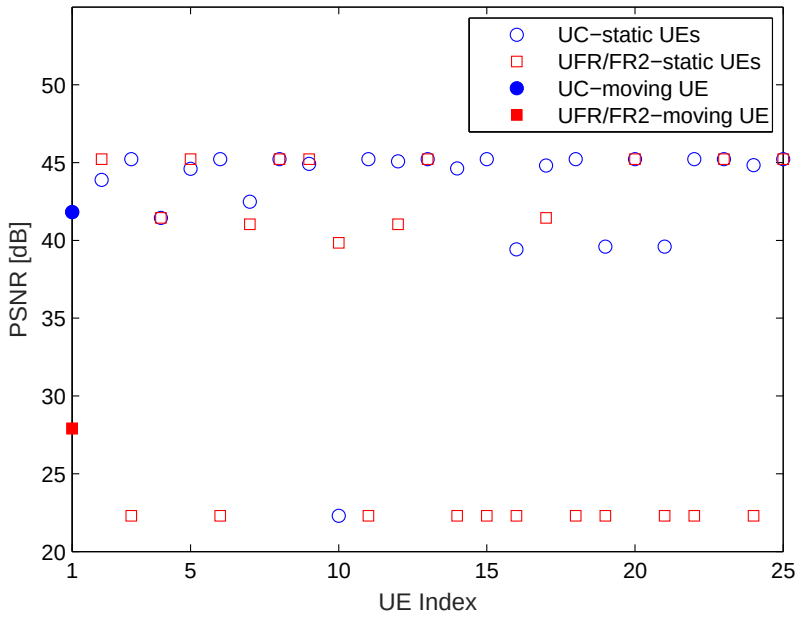

Figure 4.12: Average PSNR of each UE over 300 frames.

at the beginning of every video frame, i.e. every 1/30 s. The UC clusters for Frame 1, Frame 91, Frame 181 and Frame 271 are shown in Figure 4.10, respectively. Each frame's PSNR is shown in Figure 4.11 for UE 1, where most frames have a high PSNR and a high subjective video quality, when UE 1 is moving and the UC clusters are dynamically updated. However, almost half of the 300 frames have very poor quality or have been lost, when employing the traditional UFR/FR-2 design. Furthermore, the 5 dB or so PSNR fluctuations on top of the curves seen in Figure 4.11 are due to the coding structure of intra-coded frames (I) and predictively-coded frames (P) 'IPPPIPPP...' frames in our simulations. Explicitly, the I frames are inserted every 4 frames, which are capable of providing a higher PSNR at the cost of an increased TP requirement. Moreover, Figure 4.12 portrays the PSNR averaged over 300 frames for each UE, where the UC design remains capable of serving more UEs at a higher video quality compared to the traditional cell designs.

Figure 4.13 shows the video frames reconstructed by the moving UE, where the 60th, 120th, 180th and 240th video frames have been extracted from the original video sequence (first column), UC (second column) and UFR (third column) schemes, respectively. Observe from the second column that the quality of the video frames is only slightly degraded compared to the original lossless video frames (first column). However, the visual quality provided by the UFR design is very poor, as shown in the third column. Three out of four frames have been lost and replaced by the previously successfully decoded frames. Hence, the video frames in the third column are quite different from the original frames. For our simulation results of the full video clips, please refer to `http://www.ecs.soton.ac.uk/research/projects/924`.

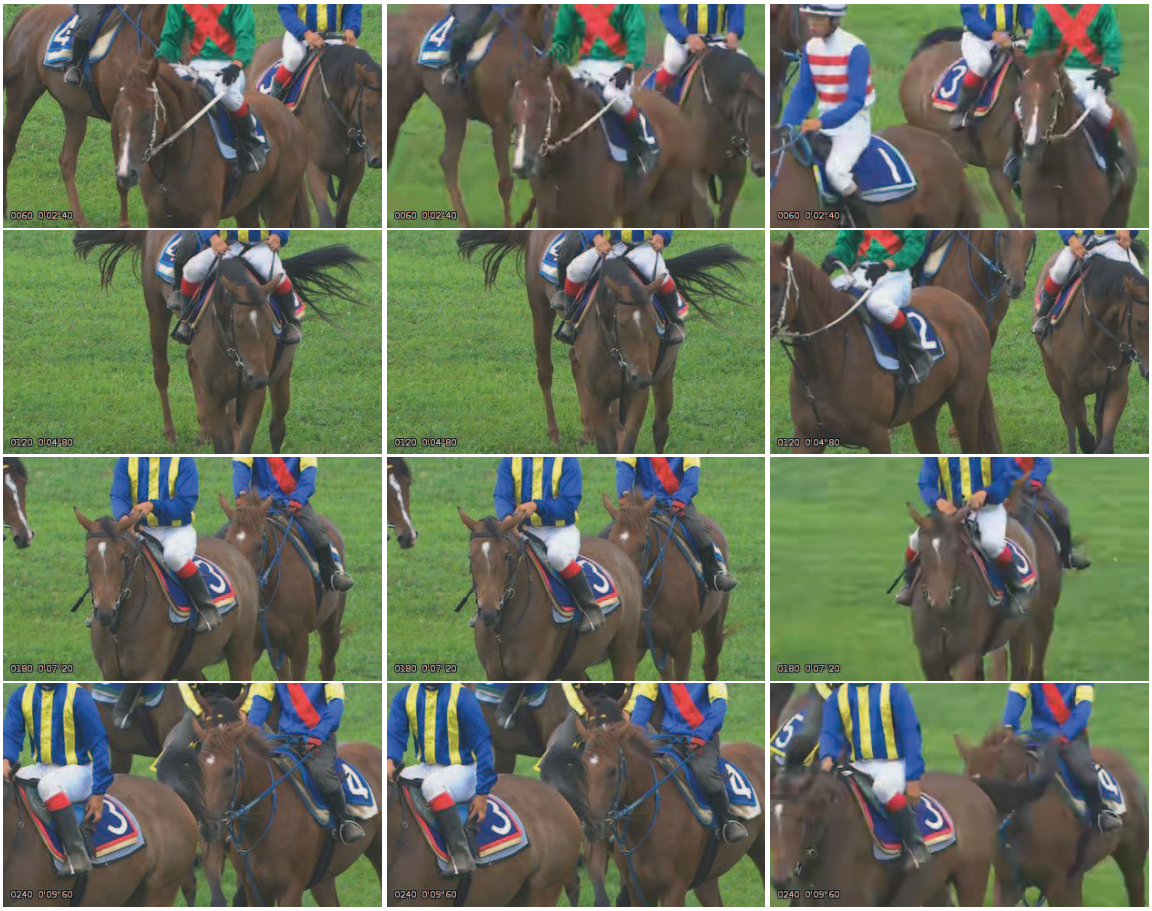

Figure 4.13: Four video frames of the Racehorses video sequence transmitted in the UC-VLC network, where the 60th, 120th, 180th and 240th video frames have been extracted from the original video sequence (first column), UC (second column) and UFR (third column) schemes, respectively.

4.7 Chapter Conclusions

In order to conceive an energy-efficient VLC system, a beneficial UC cluster formation was designed from a radically new perspective. Then a 3-tier dynamic-programming-based algorithm was proposed for transmitting the advanced scalable H.265-encoded video sequence, whilst relying on user/layer-level AM mode assignment, AP-level PA and cluster-level EE optimisation. Table 4.2, Table 4.3 and Table 4.4 summarise our main numerical results from various perspectives for characterising the attainable system performance. Observe from the result tables that there are a range of different techniques, which are capable of improving the system performance, such as

- selecting appropriate FoVs for the UEs, where a large FoV may result in increased interference and hence imposes some system performance degradation;
- limiting the total number of UEs;
- setting an appropriate edge distance d_u, since simply increasing its value may lead to unaf-

fordable computational complexity;

- increasing the optical transmit power within a certain range, just to name a few.

Overall, our numerical results demonstrated that the UC design constitutes an energy-efficient VLC system solution by providing a higher EE, improved average TP and enhanced video quality compared to the conventional cells. Despite the promise of the UC cluster formation, some open challenges arise, including the acquisition of accurate location information [65, 134–139, 141], the research of robustness under channel estimation uncertainties, the provision of up-link support, etc, which may be considered as our future research topics.

Parameter			EE [Gbits/J]	Throughput [Mbits/s]	PSNR [dB]	Outage
FoV	70°	UC	6.44	68.65	38.95	19.44%
		UFR	4.82	63.83	37.29	25.20%
		FR-2	2.37	33.91	37.29	25.20 %
	75°	UC	5.86	72.81	40.37	14.48%
		UFR	4.35	59.94	35.95	29.76%
		FR-2	2.14	31.84	35.94	29.76%
	80°	UC	2.85	72.14	40.14	15.28%
		UFR	2.61	53.18	33.63	37.68%
		FR-2	1.28	28.25	33.62	37.68%
	85°	UC	2.10	70.32	39.51	17.44%
		UFR	1.93	46.22	31.24	45.84%
		FR-2	0.95	24.52	31.20	45.84%
	90°	UC	1.92	68.81	38.99	19.20%
		UFR	1.38	41.39	29.55	51.28%
		FR-2	0.69	21.84	29.42	51.28%
Number of UEs	10	UC	2.88	82.36	43.63	3.40%
		UFR	2.80	66.71	38.27	21.60%
		FR-2	1.38	35.37	38.20	21.60%
	20	UC	1.97	75.03	41.13	11.50%
		UFR	1.60	48.07	31.87	43.10%
		FR-2	0.79	25.43	31.78	43.10%
	30	UC	1.61	65.60	37.87	22.67%
		UFR	1.18	38.28	28.49	54.73%
		FR-2	0.59	20.17	28.34	54.73%
	40	UC	1.47	53.97	33.89	36.55%
		UFR	0.72	27.03	24.62	67.45%
		FR-2	0.36	14.03	24.32	67.45%

Table 4.2: The EE, average throughput, PSNR and the outage percentage of the system for various FoVs and different UE densities, which were extracted from Figure 4.6 and Figure 4.7. The illuminance requirement of the room model is maintained as a typical work place, where the maximum transmit optical power is 0.39W. The edge distance d_u is 2.5m. When the FoV changes, the total number of UEs is 25; when the UE density changes, the FoV is assumed to be 90° . Other corresponding simulation parameters are summarised in Table 2.1, Table 3.1, and Table 4.1.

Parameter		EE [Gbits/J]	Throughput [Mbits/s]	PSNR [dB]	Outage
d_u	1	1.57	49.58	32.36	41.60%
	1.5	1.64	57.67	35.15	31.92%
	2	1.67	65.70	37.91	22.56%
	2.5	1.92	68.81	38.99	19.20%
	3	1.99	73.53	40.61	13.68%
	3.5	2.15	75.89	41.42	10.96%
	4	2.26	78.34	42.27	8.00%
	4.5	2.35	78.49	42.32	8.00%
	5	2.38	79.58	42.70	6.72%
UFR		1.36	42.66	29.98	49.70%
FR-2		0.68	22.49	29.83	49.70%

Table 4.3: The EE, average throughput, PSNR and the outage percentage of the system for various cell sizes, which were extracted from Figure 4.8. The illuminance requirement of the room model is maintained as a typical work place, where the maximum transmit optical power is 0.39W. The total number of UEs is 25 and the FoV is 90°. Other corresponding simulation parameters are summarised in Table 2.1, Table 3.1, and Table 4.1.

Parameter			EE [Gbits/J]	Throughput [Mbits/s]	PSNR [dB]	Outage
$p_{\max}^{\text{tx}}$	0.02	UC	4.50	25.75	24.09	67.70%
		UFR	5.29	35.13	27.34	56.88%
		FR-2	2.51	17.17	25.91	56.88%
	0.04	UC	3.96	50.18	32.51	39.04%
		UFR	4.61	41.83	29.72	50.40%
		FR-2	2.27	22.05	29.57	50.40%
	0.06	UC	3.52	59.39	35.64	28.32%
		UFR	4.11	42.13	29.81	50.24%
		FR-2	2.03	22.22	29.67	50.24%
	0.08	UC	3.27	63.53	37.11	23.76%
		UFR	3.66	42.34	29.87	50.00%
		FR-2	1.81	22.34	29.74	50.00%
	0.10	UC	3.10	65.77	37.82	21.83%
		UFR	3.31	42.37	29.88	50.00%
		FR-2	1.64	22.35	29.74	50.00%
	0.15	UC	2.76	69.00	39.00	18.82%
		UFR	2.66	42.40	29.89	50.00%
		FR-2	1.32	22.36	29.75	50.00%
	0.20	UC	2.40	70.40	39.49	17.04%
		UFR	2.22	42.41	29.90	50.00%
		FR-2	1.10	22.36	29.75	50.00%
	0.25	UC	2.21	70.18	39.44	17.12%
		UFR	1.91	42.42	29.90	50.00%
		FR-2	0.95	22.36	29.75	50.00%
	0.30	UC	2.02	70.63	39.61	16.72%
		UFR	1.67	42.42	29.90	50.00%
		FR-2	0.83	22.37	29.76	50.00%

Table 4.4: The EE, average throughput, PSNR and the outage percentage of the system for different transmit optical power, which were extracted from Figure 4.9. The total number of UEs is 25 and the FoV is 90°. The edge distance d_u is 2.5m. Other corresponding simulation parameters are summarised in Table 2.1, Table 3.1, and Table 4.1.

Chapter 5

Thesis Conclusions and Future Research

In this chapter, the overall summary and conclusions of this treatise will be provided in Section 5.1, several potential research topics will be discussed briefly as future research directions in Section 5.2.

5.1 Summary and Conclusions

- **Chapter 2:** In Chapter 2, we focused our attention on the hybrid VLC/WiFi DL, where the essential LB problem was investigated with special emphasis on diverse cell formations. Firstly, in Section 2.1, the development of VLC was portrayed and the disadvantages of the stand-alone VLC systems were discussed, which had also been the motivation of integrating VLC and WiFi. Then some valuable existing contributions regarding VLC cell formations as well as the techniques of solving LB in RF networks were reviewed.

  Before investigating the LB problem, the system model of the hybrid VLC/WiFi DL was introduced in Section 2.2. More explicitly, given the optical channel's DC attenuation in Equation (1.4), the general form of the SINR for a specific UE was derived in Equation (2.3). Then the regular cell formations both with and without FR were discussed in Section 2.2.2. As depicted in Figure 2.2(a) and 2.2(b), the potential ICI-infested areas were reduced, when the FR factor was increased from one to two. However, when using an FR factor of higher than one, the system has to obey the classic trade-off between reduced BE and improved cell-edge SINR, which can be clearly seen in Figure 2.3(a) and 2.3(b). Another potential drawback of employing non-unity FR was that mobility management would become more challenging, since switching between frequencies every few metres during the users' movement potentially degrades the user experience. In order to reduce the ICI and improve mobility, the multi-AP cells of Figure 2.2(c) and 2.2(d) were designed and both the CT and VT transmission techniques were employed in Section 2.2.3. The corresponding SINRs of a particular UE were formulated in Equation (2.6) and (2.7), respectively. Figure 2.3

Sections	Contributions
Section 2.1	Discussed the background of VLC and the motivation of VLC/WiFi integration, reviewed the approaches for solving LB in existing literature.
Section 2.2	Introduced the system model, discussed regular cell formations with FR, designed merged multi-AP cells with the aid of CT and VT, compared the BE of various cell formations in VLC systems.
Section 2.3	Formulated the LB problem, relaxed the original problem to a linear one, proposed and evaluated a distributed algorithm for reducing complexity.
Section 2.4	Presented our simulation results and the corresponding analysis.

Table 5.1: Summary of the contributions of Chapter 2.

illustrated both the classic BE surface and the MBE of different VLC cell formations, where a substantial MBE improvement was achieved relying on VT, since the resultant system became reminiscent of a large-scale MIMO system.

In Section 2.3, the LB problem between the VLC network and WiFi network was investigated. The original problem was firstly formulated in Equation (2.17). Instead of solving the MINLP problem of Equation (2.17), we relaxed the original problem by discretising the scheduling time period and obtained a linear formulation in Equation (2.19), which was solved by the CPLEX solver. In order to further reduce the computational complexity, a dual-decomposition-based distributed algorithm was proposed in Section 2.3.3. Furthermore, in Section 2.3.4, the optimality of the proposed algorithms was analysed. Observe from Figure 2.4 that the distributed algorithm is capable of converging to the optimum of the original problem and a fairly accurate solution of the distributed approach was obtained within as few as a dozen of iterations.

The performance results of the hybrid VLC/WiFi DL were detailed in Section 2.4. The throughput investigations conducted for different FoV and blocking probabilities were provided in Figure 2.5 and 2.6, receptively. As expected, the VT-aided multi-AP cells were superior in all scenarios considered. Apart from the throughput, we also investigated the fairness of different cell formations in Figure 2.7 and 2.8, where both the average fairness and the individual UE's fairness were considered. The VT-aided multi-AP cells were still the most attractive one having the highest throughput as well as the highest grade of fairness, but this was achieved at the highest implementation complexity. Additionally, in Section 2.4.4, a WiFi data rate of 1Gbps stipulated, where the VT-aided multi-AP cells lost their absolute advantages. We have summarised the major contributions of Chapter 2 in Table 5.1.

- **Chapter 3**: We then shifted our attention from the VLC-based HetNets to a VLC-only network in Chapter 3, where the investigations of cell formation conducted in Chapter 2 were extended. In order to further reduce the ICI, we proposed a radically new design principle

for VLC cells and at the same time solved the associated MUS problem. In Section 3.1, conventional designs conceived for mitigating the ICI in VLC networks were discussed first, ranging from FR to merged multi-AP cells, which were referred to as the NC design. By contrast, the UC cluster formation was then defined and briefly introduced. Furthermore, we reviewed the MUS approaches proposed for VLC networks and listed the main contributions in Chapter 3.

To commence, the example of a particular VLC DL scenario and its UC cluster formation result were depicted in Figure 3.2(a) and 3.2(b) of Section 3.2, respectively. Upon using the graph theory, a bipartite graph was then constructed between the VLC APs and UEs, as shown in Figure 3.3(a). The potential cluster formations were intuitively discussed in the context of Figure 3.3(b), 3.3(c) and 3.3(d). Before investigating how to schedule transmissions to the multiple UEs, the VT techniques were introduced in Section 3.2.2, where the SINR of a particular UE within a specific cluster was derived in Equation (3.6).

In Section 3.3, the joint UC cluster formation and MUS problem was investigated in a PF manner. Firstly, the problem was formulated in Equation (3.11) under the constraint of Equation (3.12). Since the cluster formation and the scheduling priority were mutually affected, there may not be any readily available algorithm for solving this joint problem. Therefore, we first proposed an exhaustive-search-based approach, whose complexity was analysed and given by Equation (3.14). Since the complexity of the exhaustive search may not be acceptable even for a modest-scale network, we reformulated the problem in Section 3.3.3. Explicitly, the weight of each edge in the graph model was weighted by the distance between an AP and a UE, as in Equation (3.15), which had been determined before the clusters were formed. Thus the original problem was reformulated as a MWM problem of Equation (3.16). The optimal solution of Equation (3.16) was then found by employing the KM-algorithm-based technique. In order to further reduce the complexity of scheduling the multiple UEs and constructing UC clusters, the efficient greedy algorithm of Figure 3.6 was proposed, which was capable of providing a similar solution to the KM-algorithm-based benchmark technique.

Our simulation results characterising the UC cluster formation and MUS algorithms were presented in Section 3.4. The complexity of the exhaustive search imposed by finding the optimal cluster formation and that of the KM-algorithm-based MWM required for finding a suboptimal solution were both analysed with the aid of Figure 3.7(a). The number of evaluations in the exhaustive search became excessive upon increasing the number of UEs. Figure 3.7(b) showed that both the optimal MWM and our proposed greedy algorithm approached the optimal solution found by exhaustive search within about 10%. Furthermore, both the throughput and fairness of our UC cluster formation were investigated compared to the conventional UFR and FR-2 schemes in Figure 3.8-3.12. As expected, the proposed UC cluster formation was capable of providing the highest average throughput and the best grade of fairness, regardless of the specific FoV, blocking probability and the number of UEs. Apart

Sections	Contributions
Section 3.1	Reviewed the approaches for mitigating ICI in NC VLC networks and MUS algorithms in existing literature, defined and briefly introduced our UC cluster formation.
Section 3.2	Constructed the graph model of the VLC DL, introduce the VT transmission techniques.
Section 3.3	Formulated the joint problem, reformulated the distance-based MWM problem, found the MWM solution by using KM algorithm, proposed a greedy algorithm for reducing complexity.
Section 3.4	Presented our simulation results and the corresponding analysis.

Table 5.2: Summary of the contributions of Chapter 3.

from the regular 4×4 APs layout, an irregular VLC AP arrangement was investigated, as shown in Figure 3.13(a).

- **Chapter 4:** In Chapter 4, we extended the investigations of Chapter 3, by designing an energy-efficient scalable video-streaming solution for our UC visible-light networks. First of all, we introduced the research background regarding the development of the UC-VLC networks in Section 4.1.1. In Section 4.1.2, we stated our motivations for developing the UC-VLC design philosophy for supporting video services, which are believed to be one of the most important applications for VLC. The chapter contributions were listed in Section 4.1.3.

  Our system model was discussed in Section 4.2. An efficient distance-based UC cluster formation approach was detailed in Section 4.2.2, as explicitly shown in Figure 4.2. After all the UC clusters were formed, our energy-efficient scalable video system was introduced in Section 4.3 with the aid of Figure 4.3 and 4.4. Figure 4.3 portrayed our UC-VLC video-steaming system, while Figure 4.4 illustrated an example of a 4-layer video sequence, which introduced the relationships between the video layers in a layered video. Additionally, different video layers may be assigned different AM modes for transmission. The minimum power required for a specific UE receiving a specific layer by employing a certain AM mode was derived in Equation (4.13).

  Relying on the preliminary knowledge mentioned above, the design of our energy-efficient scalable video-streaming solution was formulated in Section 4.4. Owing to its scalability and efficiency, the user-based EE was defined and considered in Equation (4.17) instead of the system-based global EE. Then constrains were formulated from two perspectives, i.e. regarding the video transmission and power constraints, which were formulated in Equation (4.19)-(4.23). We proposed a 3-tier dynamic-programming-based algorithm for solving the problem (4.18)-(4.23) in Section 4.5. Explicitly, the 1st-tier user/layer-level AM mode as-

Sections	Contributions
Section 4.1	Introduced the background of the UC-VLC networks, stated the motivations and contributions.
Section 4.2	Detailed UC cluster formation steps.
Section 4.3	Demonstrated multi-user video broadcast system and layered video structure, derived the minimum transmit power required.
Section 4.4	Formulated the EE maximisation problem.
Section 4.5	Proposed 3-tier dynamic-programming-based algorithm, analysed the algorithm's complexity.
Section 4.6	Presented our simulation results and the corresponding analysis.

Table 5.3: Summary of the contributions of Chapter 4.

signment operated on a per-UE scale and was formulated in Equation (4.25), as demonstrated in the top subfigure of Figure 4.5. The time-guaranteed AM mode assignment matrix was obtained for each UE relying on the recursions of Equation (4.28). The 2nd-tier AP-level PA was operated on the basis of the 1st-tier algorithm's results and it was formulated in Equation (4.29), as well as illustrated in the bottom subfigure of Figure 4.5. Then the results of Equation (4.31) were input to the 3rd-tier cluster-level EE optimisation, where the final results associated with maximising the EE of the system were generated. Finally, the complexity of our proposed algorithm was analysed in Section 4.5.3.2.

Our simulation results characterising the 3-tier dynamic-programming-based scheme conceived for energy-efficient scalable video transmission in our UC-VLC networks were presented in Section 4.6. In the meantime, the conventional cell formations, i.e. UFR and FR-2, were invoked as the benchmarkers. In Section 4.6.1, the achievable system performance was investigated under various parameters, in terms of the EE, throughput, PSNR and outage percentage. Our UC design outperformed most of the scenarios considered and was capable of achieving an energy-efficient performance without degrading the QoS. Furthermore, we also investigated mobile UEs requesting video services, where an example trajectory was shown in Figure 4.10. When the UE was moving, the UC clusters were dynamically constructed, but the quality of the video slightly fluctuated. Observe from Figure 4.11 and 4.12 that our UC design was capable of mitigating the detrimental effects of transmission dead zone in the UFR/FR-2 scenario, whilst providing a higher QoS.

5.2 Future Research

In this section, we will briefly discuss a number of future research ideas.

5.2.1 Differentiated Video Services and Multicast

In Chapter 4, we designed an energy-efficient scalable video-streaming solution for the UC-VLC networks, which imposed a single-frame delay. Therefore, the constraint in Equation (4.19) guarantees that the time required for transmitting a video frame does not exceed its upper delay-limit of T. However, Equation (4.19) may be adjusted to various video services associated with different delay tolerance. For example, for some delay-tolerant systems, Equation (4.19) may be relaxed as

$$\sum_{k=1}^{K_u} \sum_{l=0}^{L-1} \sum_{m=1}^{M} t_{u,l}^{m,k} \cdot x_{u,l}^{m,k} \leq K_u \cdot T, \quad \forall u \tag{5.1}$$

where K_u denotes the number of frames during a single optimisation slot for the UE u, which is determined by the delay requirements of the system. For example, we have all $K_u = 1$ in Equation (4.19) for real-time video services; for more delay-tolerant services, K_u may become larger. Moreover, $t_{u,l}^{m,k} = S_{u,l}^{k} / r^{m}$ is the time required for transmitting the lth video layer constituted by $S_{u,l}^{k}$ bits to the UE u using the AM mode m, where $S_{u,l}^{k}$ denotes the length of the kth frame during a processing slot. Correspondingly, the proposed dynamic-programming-based algorithm should be adjusted as well.

On the other hand, as an efficient mechanism for real-time dissemination, the scalable video multicast has attracted much attention [105, 106, 110, 192, 193]. Multicast grouping constitutes one of the fundamental problems affecting the multicast system over HetNets. The multicast groups and our UC-VT clusters are expected to be inter-linked, when supporting multicast in our UC-VLC networks, since both the operations selects a specific set of VLC APs and UEs. Thus there are two-tier clusters in the system, constituted by the multicast group and by the physical UC-VT cluster formation. The system should be carefully designed by considering the relationship between the two-tier clusters.

5.2.2 Coexistence of User-Centric VLC and Radio Frequency Networks

In Chapter 2, the essential LB problem was investigated in a hybrid VLC/WiFi network, where various NC cell formations were considered. Owing to its capability of providing a superior system performance, the UC VLC design principle may be expected to constitute the UC-VLC/RF HetNets, as studied in Chapter 3 and Chapter 4. Naturally, when integrating this radically new UC design into existing systems, some challenges may occur. Some of the open problems are listed below, which may be considered as our potential research topics:

(1) The essential MUS and LB problem between UC-VLC clusters and RF APs may be jointly reformulated and solved by taking into account the construction of the UC clusters;

(2) Given the inconvenience of VLC up-links, the readily available RF techniques may be considered as the up-link candidate, where the RA solution between the up-link and DL may be obtained, when considering the problems in (1) above;

(3) When jointly considering both indoor hybrid UC-VLC/RF and outdoor RF networks, the HetNets may be considered from a holistic perspective, where the interference imposed by the RF macro-cells may lead to a significant change of the problems in (1) and (2) above.

Appendix A

Appendix

A.1 Kuhn-Munkres-Algorithm-based Approach for Finding the Optimal Maximum Weighted Matching

Let us first rely on Lemma 1, where having independent elements indicates that none of them occupies the same row or column.

Lemma 1. *(König Theorem) [160]. If z is the maximum number of independent zero elements in the matrix (a_{a_i,u_j}), then there are z lines (rows, columns or both) containing all the zeros elements of (a_{a_i,u_j}).*

First, the weight matrix $(\omega_d(e_{a_i,u_j}))$ of Figure 3.4(a) is formulated, as shown in Figure A.1(a), where the weight is set to zero when there is no link between two vertices. Our problem is that of maximizing the sum weight, while the KM algorithm is suitable for a minimization problem. We have to construct an equivalent matrix (a_{a_i,u_j}) for $(\omega_d(e_{a_i,u_j}))$, according to Theorem 1. The maximum element $(\omega_d(e_{a_i,u_j}))$ is selected and forms (c_{a_i}), where we have $(c_{a_i}) = [4,4,6,4]^{\mathrm{T}}$ in our example. Let $(c_{a_i} - \omega_d(e_{a_i,u_j}))$ be the matrix (a_{a_i,u_j}), as shown in Figure A.1(b), and its optimal matching solution minimizing the sum weight is also optimal for our MWM problem. Next, find a zero in each column of $(c_{a_i} - \omega_d(e_{a_i,u_j}))$. If however there is no starred zero either in its row or in its column, we mark it by a star, again as shown in Figure A.1(b). Then we mark every column containing a 0^* by a vertical line and all the 0^* form a set of independent zeros, since none of them occupies the same row or column. The above-mentioned procedure is our initialization step, which may be described as:

i) *Initialization.* Generate an initial label set (c_{a_i}), where for each row a_i we have:

$$c_{a_i} = \max_{u_j}(\omega_d(e_{a_i,u_j})), \qquad u_j = 1, \cdots, N_{U,\mathcal{Q}_m}. \tag{A.1}$$

Thus, the equivalent matrix is constructed as $(c_{a_i} - \omega_d(e_{a_i,u_j}))$. Generate an initial matching $\mathcal{M}_{\mathcal{Q}_m}$

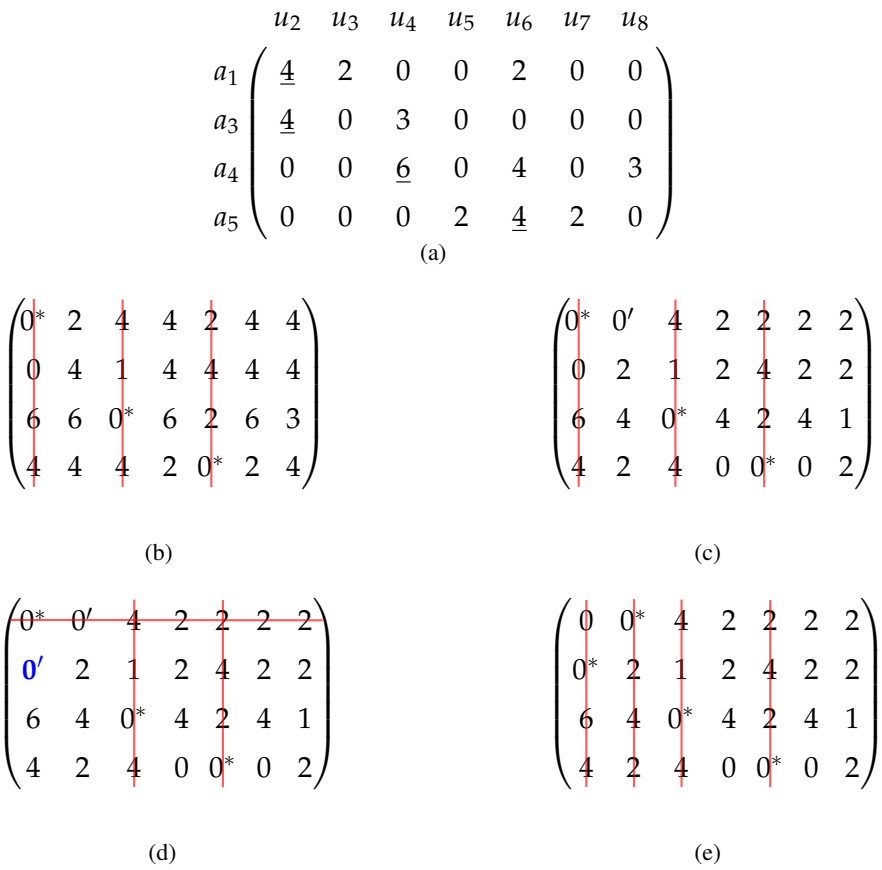

Figure A.1: (a) The weight matrix $(\omega_d(e_{a_i,u_j}))$ of $\mathcal{Q}_2$, where the maximum element of each row is underlined. (b) Initialization step. The equivalent matrix (a_{a_i,u_j}) of $(\omega_d(e_{a_i,u_j}))$ is obtained as $(a_{a_i,u_j}) = (c_{a_i} - \omega_d(e_{a_i,u_j}))$, where we have $(c_{a_i}) = [4,4,6,4]^{\mathrm{T}}$. Find and mark the zero by a star, if there are no starred zeros in its row or in its column. Cover every column containing a 0^* by a vertical line. (c) Adjustment step. (a_{a_i,u_j}) is modified as $(a_{a_i,u_j} - c_{a_i} + r_{u_j})$, where $(c_{a_i}) = [0,0,0,0]^{\mathrm{T}}$ and $(r_{u_j}) = [0,-2,0,-2,0,-2,-2]$. Mark the uncovered zeros by the upper prime. (d) Explicitly, if there is a starred zero in the primed zero's row, mark this row by a line and remove the vertical line for the column of the starred zero. (e) Starred zero and primed zero alternating. Remove all lines. Recover the columns containing 0^*. Optimal solution found.

by finding and marking independent zeros denoted by $z_j^{(a_i,u_j)}$ using a star, whose superscript corresponds to its index in $(c_{a_i} - \omega_d(e_{a_i,u_j}))$, where we have:

$$\begin{aligned} &\forall z_j^{(a_i,u_j)} \in (z_j), \quad z_{j'\neq j}^{(a_i'\neq a_i,u_j)} \notin (z_j), \\ &\forall z_j^{(a_i,u_j)} \in (z_j), \quad z_{j'\neq j}^{(a_i,p_{a_i'}\neq u_j)} \notin (z_j). \end{aligned} \tag{A.2}$$

If $|(z_j)| = \min\{N_{A,\mathcal{Q}_m}, N_{U,\mathcal{Q}_m}\}$ columns are marked, we find the desired matching, where each AP matches a specific UE and the sum weight of their links is maximized, which furthermore form a UC-VT cluster. Otherwise, the cardinality of the matching will be iteratively increased during the following steps.

If there are no unmarked zeros as shown in Figure A.1(b), the current matrix should be modified according to Theorem 1, which leads to the following adjustment step.

ii) *Adjustment.* Let h be the smallest unmarked element of the matrix and construct a column vector (c_{a_i}) and a row vector (r_{u_j}) by the following rules: if the a_ith row is covered, $c_{a_i} = h$; otherwise, $c_{a_i} = 0$. If the u_jth column is covered, $r_{u_j} = 0$; otherwise, $r_{u_j} = -h$. In our example, (a_{a_i,u_j}) is updated as $(a_{a_i,u_j} - c_{a_i} + r_{u_j})$ and $(c_{a_i}) = [0,0,0,0]^{\mathrm{T}}$ and $(r_{p_i}) = [0,-2,0,-2,0,-2,-2]$, as shown in Figure A.1(c).

Then let us choose and mark an unmarked zero by priming it. If there is a starred zero in its row, mark this row by a line and remove the line from the column of the starred zero, as shown in Figure A.1(d). Then we prime another unmarked zero in the second row indicated by the bold font, but there is no starred zero in its row. According to the starred and primed zero alternating rules of [160], we obtain the matrix seen in Figure A.1(e), where the number of independent zeros reached its maximum given by the number of rows. Correspondingly, the number of lines containing all these zeros becomes maximal, as stated by Lemma 1, where the maximum number of independent zeros is equal to the number of lines containing them. The algorithm terminates here in our scenario. However, if the number of marked columns is still insufficient, the set of independent zeros has to be increased by iteratively repeating the above-mentioned steps, commencing from the Adjustment stage. Thus, we find the optimal solution for our MWM, which is $\{a_{10} \rightarrow u_3, a_{11} \rightarrow u_2, a_7 \rightarrow u_4, a_6 \rightarrow u_6\}$, namely the same as indicated in Figure 3.4(b).

Glossary

A

ACO-OFDM Asymmetrically clipped OOFDM.

ADO-OFDM Asymmetrically clipped DC biased OOFDM.

AM Adaptive modulation.

AP Access point.

ASE Area spectral efficiency.

B

BE Bandwidth efficiency.

BER Bit-error-rate.

BPSK Binary phase-shift keying.

C

CDF Cumulative distribution function.

CIF Common intermediate format.

CSK Colour shift keying.

CT Combined transmission.

D

DC Direct current.

DCO-OFDM DC biased OOFDM.

DL Down-link.

DMT Discrete multitone.

E

EE Energy efficiency.

F

FoV Field-of-view.

FPS Frame per second.

FR Frequency reuse.

FR-2 FR factor of two.

G

GCM Generalised colour modulation.

GoF Grade of fairness.

GPS Global positioning system.

H

HetNets Heterogeneous networks.

I

I Intra-coded frame.

ICI Inter-cell interference.

IM-DD Intensity modulation direct detection.

IoT Internet of Things.

K

KKT Karush-Kuhn-Tucker.

KM Kuhn-Munkres.

L

LB Load balancing.

LEDs Light-emitting diodes.

LoS Line-of-sight.

M

MBE Mean bandwidth efficiency.

MC-LEDs Multi-chip LEDs.

MIMO Multiple input multiple output.

MINLP Mixed-integer non-linear programming.

MSM Multiple-to-single matching.

MU-MIMO Multi-user MIMO.

MU-MISO Multiuser-multiple-input-single-output.

MUS Multiuser scheduling.

MWM Maximum weighted matching.

N

NC Network-centric.

NLoS Non-LoS.

O

O/E Optical/electronic.

OF Objective function.

OLEDs Organic LEDs.

OOFDM Optical orthogonal frequency division multiplexing.

OOK On-off keying.

OW Optical wireless.

P

P Predictively-coded frame.

PA Power allocation.

PAM Pulse amplitude modulation.

PC-LEDs Phosphor converted LEDs.

PD Photodetector.

PF Proportional fairness.

PLC Power-line communication.

PPM Pulse position modulation.

PSNR Peak signal-to-noise ratio.

PWM-DMT Pulse width modulation with DMT.

Q

QAM Quadrature amplitude modulation.

QCIF Quarter common intermediate format.

QoS Quality of service.

R

RF Radio frequency.

RGB Red-green-blue.

RLL Run length limited.

S

SFI Service fairness index.

SHVC Scalable extension of the high-efficiency video coding.

SINR Signal-to-interference-plus-noise ratio.

SIR Signal to interference ratio.

SISO Single input single output.

SNR Signal-to-noise ratio.

SSM Single-to-single matching.

T

TP Throughput.

U

U-OFDM Unipolar OFDM.

UC User-centric.

UC-VT User-centric-vectored-transmission-aided.

UE User equipment.

UFR Unity FR.

V

V2I Vehicle to infrastructure.

V2V Vehicle to vehicle.

VHO Vertical handover.

VLC Visible light communications.

VOOK Variable OOK.

VPPM Variable PPM.

VT Vectored transmission.

W

WiFi Wireless fidelity.

WLAN Wireless local area network.

Bibliography

[1] A. J. Goldsmith, *Wireless communications*. Cambridge University Press, 2005.

[2] J. G. Andrews, S. Buzzi, W. Choi, S. V. Hanly, A. Lozano, A. C. K. Soong, and J. Zhang, "What will 5G be?," *IEEE Journal on Selected Areas in Communications*, vol. 32, pp. 1065–1082, June 2014.

[3] S. Rangan, T. S. Rappaport, and E. Erkip, "Millimeter-wave cellular wireless networks: Potentials and challenges," *Proceedings of the IEEE*, vol. 102, pp. 366–385, March 2014.

[4] L. Hanzo, H. Haas, S. Imre, D. O'Brien, M. Rupp, and L. Gyongyosi, "Wireless myths, realities, and futures: From 3G/4G to optical and quantum wireless," in *Proceedings of the IEEE*, vol. 100, pp. 1853–1888, May 2012.

[5] A. G. Bell, W. G. Adams, Tyndall, and W. H. Preece, "Discussion on the photophone and the conversion of radiant energy into sound," *Journal of the Society of Telegraph Engineers*, vol. 9, no. 34, pp. 375–383, 1880.

[6] Y. Tanaka, S. Haruyama, and M. Nakagawa, "Wireless optical transmissions with white colored LED for wireless home links," in *2000 The 11th IEEE International Symposium on Personal, Indoor and Mobile Radio Communications*, vol. 2, pp. 1325–1329 vol.2, 2000.

[7] C. W. Chow, C. H. Yeh, Y. F. Liu, and Y. Liu, "Improved modulation speed of LED visible light communication system integrated to main electricity network," *Electronics Letters*, vol. 47, pp. 867–868, July 2011.

[8] T. Komine, *Visible light wireless communications and its fundamental study*. PhD thesis, Ph. D. dissertation, Keio University, 2005.

[9] Cree Inc., "Cree sets new R&D performance record with 276 lumen-per-watt power LED," Feb. 2013. [Online]. Available: http://www.cree.com/News-and-Events/Cree-News/Press-Releases/2013/February/276-LPW.

[10] J. Grubor, S. Randel, K. D. Langer, and J. W. Walewski, "Broadband information broadcasting using LED-based interior lighting," *Journal of Lightwave Technology*, vol. 26, no. 24, pp. 3883–3892, Dec. 2008.

[11] D. A. Steigerwald, J. C. Bhat, D. Collins, R. M. Fletcher, M. O. Holcomb, M. J. Ludowise, P. S. Martin, and S. L. Rudaz, "Illumination with solid state lighting technology," *IEEE Journal of Selected Topics in Quantum Electronics*, vol. 8, pp. 310–320, Mar 2002.

[12] C. Yen-Chih, "Multi-chip LED," Jan. 2013. US Patent D675,169.

[13] P. E. Burrows, G. Gu, V. Bulovic, Z. Shen, S. R. Forrest, and M. E. Thompson, "Achieving full-color organic light-emitting devices for lightweight, flat-panel displays," *IEEE Transactions on Electron Devices*, vol. 44, pp. 1188–1203, Aug 1997.

[14] J. J. D. McKendry, D. Massoubre, S. Zhang, B. R. Rae, R. P. Green, E. Gu, R. Henderson, A. E. Kelly, and M. D. Dawson, "Visible-light communications using a CMOS-controlled micro-light- emitting-diode array," *Journal of Lightwave Technology*, vol. 30, pp. 61–67, Jan 2012.

[15] T. Komine and M. Nakagawa, "Fundamental analysis for visible-light communication system using LED lights," *IEEE Transactions on Consumer Electronics*, vol. 50, no. 1, pp. 100–107, Feb. 2004.

[16] D. Karunatilaka, F. Zafar, V. Kalavally, and R. Parthiban, "LED based indoor visible light communications: State of the art," *IEEE Communications Surveys Tutorials*, vol. 17, pp. 1649–1678, thirdquarter 2015.

[17] P. H. Pathak, X. Feng, P. Hu, and P. Mohapatra, "Visible light communication, networking, and sensing: A survey, potential and challenges," *IEEE Communications Surveys Tutorials*, vol. 17, pp. 2047–2077, Fourthquarter 2015.

[18] A. Zukauskas, M. S. Shur, and R. Gaska, *Introduction to solid-state lighting*. J. Wiley, 2002.

[19] C. Inc., "Cree XLamp XP-E high-efficiency white LEDs," 2015. [Online]. Available: http://www.cree.com/∼/media/Files/Cree/LED-Components-and-Modules/XLamp/Data-and-Binning/XLampXPEHEW.pdf.

[20] G. Wyszecki and W. S. Stiles, *Color science*. Wiley New York, 1982.

[21] Z. Ghassemlooy, W. Popoola, and S. Rajbhandari, *Optical wireless communications: system and channel modelling with MATLAB*. CRC Press, 2012.

[22] J. M. Kahn and J. R. Barry, "Wireless infrared communications," in *Proceedings of the IEEE*, vol. 85, pp. 265–298, Feb. 1997.

[23] F. R. Gfeller and U. Bapst, "Wireless in-house data communication via diffuse infrared radiation," in *Proceedings of the IEEE*, vol. 67, pp. 1474–1486, Nov. 1979.

[24] S. Rajagopal, R. D. Roberts, and S. K. Lim, "IEEE 802.15.7 visible light communication: modulation schemes and dimming support," *IEEE Communications Magazine*, vol. 50, pp. 72–82, March 2012.

[25] S. Zhang, S. Watson, J. J. D. McKendry, D. Massoubre, A. Cogman, E. Gu, R. Henderson, A. E. Kelly, and M. D. Dawson, "1.5 Gbit/s multi-channel visible light communications using CMOS-controlled GaN-based LEDs," *Journal of Lightwave Technology*, vol. 31, pp. 1211–1216, April 2013.

[26] H. Elgala, R. Mesleh, and H. Haas, "Indoor optical wireless communication: potential and state-of-the-art," *IEEE Communications Magazine*, vol. 49, no. 9, pp. 56–62, Sep. 2011.

[27] M. Noshad and M. Brandt-Pearce, "Application of expurgated PPM to indoor visible light communications-part I: Single-user systems," *Journal of Lightwave Technology*, vol. 32, pp. 875–882, March 2014.

[28] M. Noshad and M. Brandt-Pearce, "Application of expurgated PPM to indoor visible light communications-part II: Access networks," *Journal of Lightwave Technology*, vol. 32, pp. 883–890, March 2014.

[29] D. Shiu and J. M. Kahn, "Differential pulse-position modulation for power-efficient optical communication," *IEEE Transactions on Communications*, vol. 47, pp. 1201–1210, Aug 1999.

[30] S. H. Lee, K. I. Ahn, and J. K. Kwon, "Multilevel transmission in dimmable visible light communication systems," *Journal of Lightwave Technology*, vol. 31, pp. 3267–3276, Oct 2013.

[31] R. Singh, T. O'Farrell, and J. P. R. David, "Performance evaluation of IEEE 802.15.7 CSK physical layer," in *2013 IEEE Globecom Workshops*, pp. 1064–1069, Dec 2013.

[32] R. Singh, T. OFarrell, and J. P. R. David, "An enhanced color shift keying modulation scheme for high-speed wireless visible light communications," *Journal of Lightwave Technology*, vol. 32, pp. 2582–2592, July 2014.

[33] J. Jiang, R. Zhang, and L. Hanzo, "Analysis and design of three-stage concatenated color-shift keying," *IEEE Transactions on Vehicular Technology*, vol. 64, pp. 5126–5136, Nov 2015.

[34] P. Das, B. Kim, Y. Park, and K. Kim, "Color-independent VLC based on a color space without sending target color information," *Optics Communications*, vol. 286, pp. 69–73, Jan. 2013.

[35] P. Das, Y. Park, and K. Kim, "Performance analysis of color-independent visible light communication using a color-space-based constellation diagram and modulation scheme," *Wireless personal communications*, vol. 74, no. 2, pp. 665–682, 2014.

[36] X. Li, R. Mardling, and J. Armstrong, "Channel capacity of IM/DD optical communication systems and of ACO-OFDM," in *IEEE ICC 2007*, pp. 2128–2133, June 2007.

[37] J. Armstrong and B. Schmidt, "Comparison of asymmetrically clipped optical OFDM and DC-biased optical OFDM in AWGN," *Communications Letters, IEEE*, vol. 12, pp. 343–345, May 2008.

[38] D. Tsonev, S. Sinanovic, and H. Haas, "Novel unipolar orthogonal frequency division multiplexing (U-OFDM) for optical wireless," in *2012 IEEE 75th Vehicular Technology Conference (VTC Spring)*, pp. 1–5, May 2012.

[39] IEEE, "IEEE standard for local and metropolitan area networks–part 15.7: Short-range wireless optical communication using visible light," *IEEE Std 802.15.7-2011*, pp. 1–309, Sep. 2011.

[40] F. Yang, J. Gao, and S. Liu, "Novel visible light communication approach based on hybrid OOK and ACO-OFDM," *IEEE Photonics Technology Letters*, vol. 28, pp. 1585–1588, July 2016.

[41] Y. Yang, Z. Zeng, J. Cheng, and C. Guo, "An enhanced DCO-OFDM scheme for dimming control in visible light communication systems," *IEEE Photonics Journal*, vol. 8, pp. 1–13, June 2016.

[42] J. Armstrong and A. J. Lowery, "Power efficient optical OFDM," *Electronics Letters*, vol. 42, pp. 370–372, March 2006.

[43] S. D. Dissanayake and J. Armstrong, "Comparison of ACO-OFDM, DCO-OFDM and ADO-OFDM in IM/DD systems," *Journal of Lightwave Technology*, vol. 31, no. 7, pp. 1063–1072, Apr. 2013.

[44] K. Lee and H. Park, "Modulations for visible light communications with dimming control," *IEEE Photonics Technology Letters*, vol. 23, pp. 1136–1138, Aug 2011.

[45] J. H. Yoo, B. W. Kim, and S. Y. Jung, "Modelling and analysis of M-ary variable pulse position modulation for visible light communications," *IET Optoelectronics*, vol. 9, pp. 184–190, Oct. 2015.

[46] G. Ntogari, T. Kamalakis, J. Walewski, and T. Sphicopoulos, "Combining illumination dimming based on pulse-width modulation with visible-light communications based on discrete multitone," *IEEE/OSA Journal of Optical Communications and Networking*, vol. 3, pp. 56–65, January 2011.

[47] R. Zhang, J. Wang, Z. Wang, Z. Xu, C. Zhao, and L. Hanzo, "Visible light communications in heterogeneous networks: Paving the way for user-centric design," *IEEE Wireless Communications*, vol. 22, pp. 8–16, April 2015.

[48] H. Haas, "High-speed wireless networking using visible light," *SPIE Newsroom*, vol. 10, April 2013.

[49] X. Li, R. Zhang, and L. Hanzo, "Cooperative load balancing in hybrid visible light communications and WiFi," *IEEE Transactions on Communications*, vol. 63, pp. 1319–1329, April 2015.

[50] Y. Wang and H. Haas, "Dynamic load balancing with handover in hybrid Li-Fi and Wi-Fi networks," *Journal of Lightwave Technology*, vol. 33, pp. 4671–4682, Nov 2015.

[51] Z. Wang, C. Yu, W. Zhong, J. Chen, and W. Chen, "Performance of a novel LED lamp arrangement to reduce SNR fluctuation for multi-user visible light communication systems," *Optics Express*, vol. 20, pp. 4564–4573, Feb 2012.

[52] I. Stefan and H. Haas, "Analysis of optimal placement of LED arrays for visible light communication," in *2013 IEEE 77th Vehicular Technology Conference (VTC Spring)*, pp. 1–5, IEEE, 2013.

[53] R. Guan, J. Wang, Y. Wen, J. Wang, and M. Chen, "PSO-based LED deployment optimization for visible light communications," in *WCSP*, pp. 1–6, 2013.

[54] G. W. Marsh and J. M. Kahn, "Channel reuse strategies for indoor infrared wireless communications," *IEEE Transactions on Communications*, vol. 45, no. 10, pp. 1280–1290, 1997.

[55] B. Ghimire and H. Haas, "Self-organising interference coordination in optical wireless networks," *EURASIP Journal on Wireless Communications and Networking*, vol. 2012, no. 1, pp. 1–15, 2012.

[56] J. Sung, W. Lin, Y. Wu, C. Chow, and C. Yeh, "Design of visible light communication system for maintaining uniform data rate," in *Proceedings of SPIE*, vol. 9193, 2014.

[57] C. Chen, S. Videv, D. Tsonev, and H. Haas, "Fractional frequency reuse in DCO-OFDM-based optical attocell networks," *Journal of Lightwave Technology*, vol. 33, pp. 3986–4000, Oct 2015.

[58] G. B. Prince and T. D. C. Little, "On the performance gains of cooperative transmission concepts in intensity modulated direct detection visible light communication networks," in *2010 6th International Conference on Wireless and Mobile Communications (ICWMC)*, pp. 297–302, Sept 2010.

[59] Y. Wu, A. Yang, L. Feng, L. Zuo, and Y. Sun, "Modulation based cells distribution for visible light communication," *Optics Express*, vol. 20, pp. 24196–24208, Oct 2012.

[60] M. S. Alouini and A. J. Goldsmith, "Area spectral efficiency of cellular mobile radio systems," *IEEE Transactions on Vehicular Technology*, vol. 48, pp. 1047–1066, Jul 1999.

[61] Y. Tao, X. Liang, J. Wang, and C. Zhao, "Scheduling for indoor visible light communication based on graph theory," *Optics Express*, vol. 23, pp. 2737–2752, Feb 2015.

[62] X. Li, R. Zhang, J. Wang, and L. Hanzo, "Cell-centric and user-centric multi-user scheduling in visible light communication aided networks," in *2015 IEEE International Conference on Communications (ICC)*, pp. 5120–5125, June 2015.

[63] X. Li, F. Jin, R. Zhang, J. Wang, Z. Xu, and L. Hanzo, "Users first: User-centric cluster formation for interference-mitigation in visible-light networks," *IEEE Transactions on Wireless Communications*, vol. 15, pp. 39–53, Jan 2016.

[64] R. Zhang, H. Claussen, H. Haas, and L. Hanzo, "Energy efficient visible light communications relying on amorphous cells," *IEEE Journal on Selected Areas in Communications*, vol. 34, pp. 894–906, April 2016.

[65] S. Feng, X. Li, R. Zhang, M. Jiang, and L. Hanzo, "Hybrid positioning aided amorphous-cell assisted user-centric visible light downlink techniques," *IEEE Access*, vol. 4, pp. 2705–2713, 2016.

[66] X. Li, Y. Huo, R. Zhang, and L. Hanzo, "User-centric visible light communications for Energy-Efficient scalable video streaming," *IEEE Journal on Selected Areas in Communications - Series on Green Communications and Networking (Issue 3) (Accepted)*, Dec. 2016.

[67] S. G. Wilson, M. Brandt-Pearce, Q. Cao, and J. H. Leveque, "Free-space optical MIMO transmission with Q-ary PPM," *IEEE Transactions on Communications*, vol. 53, pp. 1402–1412, Aug 2005.

[68] T. A. Tsiftsis, H. G. Sandalidis, G. K. Karagiannidis, and M. Uysal, "Optical wireless links with spatial diversity over strong atmospheric turbulence channels," *IEEE Transactions on Wireless Communications*, vol. 8, pp. 951–957, Feb 2009.

[69] L. Zeng, D. C. O'Brien, H. Minh, G. E. Faulkner, K. Lee, D. Jung, Y. Oh, and E. T. Won, "High data rate multiple input multiple output (MIMO) optical wireless communications using white LED lighting," *IEEE Journal on Selected Areas in Communications*, vol. 27, pp. 1654–1662, December 2009.

[70] K. D. Dambul, D. C. O'Brien, and G. Faulkner, "Indoor optical wireless MIMO system with an imaging receiver," *IEEE Photonics Technology Letters*, vol. 23, pp. 97–99, Jan 2011.

[71] M. Biagi, A. M. Vegni, and T. D. C. Little, "LAT indoor MIMO-VLC — localize, access and transmit," in *2012 International Workshop on Optical Wireless Communications (IWOW)*, pp. 1–3, Oct 2012.

[72] A. H. Azhar, T. Tran, and D. O'Brien, "A gigabit/s indoor wireless transmission using MIMO-OFDM visible-light communications," *IEEE Photonics Technology Letters*, vol. 25, pp. 171–174, Jan 2013.

[73] Z. Yu, R. J. Baxley, and G. T. Zhou, "Multi-user MISO broadcasting for indoor visible light communication," in *2013 IEEE International Conference on Acoustics, Speech and Signal Processing (ICASSP)*, pp. 4849–4853, May 2013.

[74] T. Q. Wang, Y. A. Sekercioglu, and J. Armstrong, "Analysis of an optical wireless receiver using a hemispherical lens with application in MIMO visible light communications," *Journal of Lightwave Technology*, vol. 31, pp. 1744–1754, June 2013.

[75] B. Li, J. Wang, R. Zhang, H. Shen, C. Zhao, and L. Hanzo, "Multiuser MISO transceiver design for indoor downlink visible light communication under per-LED optical power constraints," *IEEE Photonics Journal*, vol. 7, pp. 1–15, Aug 2015.

[76] Q. Wang, Z. Wang, and L. Dai, "Multiuser MIMO-OFDM for visible light communications," *IEEE Photonics Journal*, vol. 7, pp. 1–11, Dec 2015.

[77] H. Shen, Y. Deng, W. Xu, and C. Zhao, "Rate-maximized zero-forcing beamforming for VLC multiuser MISO downlinks," *IEEE Photonics Journal*, vol. 8, pp. 1–13, Feb 2016.

[78] J. M. Kahn, R. You, P. Djahani, A. G. Weisbin, B. K. Teik, and A. Tang, "Imaging diversity receivers for high-speed infrared wireless communication," *IEEE Communications Magazine*, vol. 36, pp. 88–94, Dec 1998.

[79] C. Chen and L. Wang, "A unified capacity analysis for wireless systems with joint multiuser scheduling and antenna diversity in Nakagami fading channels," *IEEE Transactions on Communications*, vol. 54, pp. 469–478, March 2006.

[80] C. Chen and L. Wang, "Performance analysis of scheduling in multiuser MIMO systems with zero-forcing receivers," *IEEE Journal on Selected Areas in Communications*, vol. 25, pp. 1435–1445, September 2007.

[81] R. Morsi, D. S. Michalopoulos, and R. Schober, "Multiuser scheduling schemes for simultaneous wireless information and power transfer over fading channels," *IEEE Transactions on Wireless Communications*, vol. 14, pp. 1967–1982, April 2015.

[82] E. Castaneda, A. Silva, R. Samano-Robles, and A. Gameiro, "Distributed linear precoding and user selection in coordinated multicell systems," *IEEE Transactions on Vehicular Technology*, vol. 65, pp. 4887–4899, July 2016.

[83] D. Bykhovsky and S. Arnon, "Multiple access resource allocation in visible light communication systems," *Journal of Lightwave Technology*, vol. 32, pp. 1594–1600, April 2014.

[84] M. Biagi, S. Pergoloni, and A. M. Vegni, "LAST: A framework to localize, access, schedule, and transmit in indoor VLC systems," *Journal of Lightwave Technology*, vol. 33, pp. 1872–1887, May 2015.

[85] X. Huang, X. Fu, and W. Xu, "Incremental scheduling scheme for indoor visible light communication," *Electronics Letters*, vol. 51, pp. 268–270, Feb 2015.

[86] O. Babatundi, L. Qian, and J. Cheng, "Downlink scheduling in visible light communications," in *WCSP 2014*, pp. 1–6, Oct 2014.

[87] W. C. Kim, C. S. Bae, S. Y. Jeon, S. Y. Pyun, and D. H. Cho, "Efficient resource allocation for rapid link recovery and visibility in visible-light local area networks," *IEEE Transactions on Consumer Electronics*, vol. 56, pp. 524–531, May 2010.

[88] K. H. Park, Y. C. Ko, and M. S. Alouini, "On the power and offset allocation for rate adaptation of spatial multiplexing in optical wireless MIMO channels," *IEEE Transactions on Communications*, vol. 61, pp. 1535–1543, April 2013.

[89] H. Marshoud, V. M. Kapinas, G. K. Karagiannidis, and S. Muhaidat, "Non-orthogonal multiple access for visible light communications," *IEEE Photonics Technology Letters*, vol. 28, pp. 51–54, Jan 2016.

[90] R. Jiang, Z. Wang, Q. Wang, and L. Dai, "Multi-user sum-rate optimization for visible light communications with lighting constraints," *Journal of Lightwave Technology*, vol. 34, pp. 3943–3952, Aug 2016.

[91] Cisco, "Cisco visual networking index: Global mobile data traffic forecast update, 2015-2020 white paper," Feb. 2016. [Online]. Available: http://www.cisco.com/c/en/us/solutions/collateral/service-provider/visual-networking-index-vni/mobile-white-paper-c11-520862.html.

[92] L. Hanzo, P. Cherriman, and J. Streit, *Wireless video communications: second to third generation and beyond*. IEEE Press-John Wiley & Sons, 2001.

[93] Y. Huo, C. Hellge, T. Wiegand, and L. Hanzo, "A tutorial and review on inter-layer FEC coded layered video streaming," *IEEE Communications Surveys Tutorials*, vol. 17, pp. 1166–1207, Secondquarter 2015.

[94] J. Jiang, Y. Huo, F. Jin, P. Zhang, Z. Wang, Z. Xu, H. Haas, and L. Hanzo, "Video streaming in the multiuser indoor visible light downlink," *IEEE Access*, vol. 3, pp. 2959–2986, Dec 2015.

[95] L. Hanzo, P. Cherriman, and J. Streit, *Video compression and communications: from basics to H. 261, H. 263, H. 264, MPEG4 for DVB and HSDPA-style adaptive turbo-transceivers*. John Wiley & Sons, 2007.

[96] G. J. Sullivan, J. Ohm, W. Han, and T. Wiegand, "Overview of the high efficiency video coding (HEVC) standard," *IEEE Transactions on Circuits and Systems for Video Technology*, vol. 22, pp. 1649–1668, Dec 2012.

[97] J. M. Boyce, Y. Ye, J. Chen, and A. K. Ramasubramonian, "Overview of SHVC: Scalable extensions of the high efficiency video coding (HEVC) standard," *IEEE Transactions on Circuits and Systems for Video Technology*, vol. PP, pp. 1–1, July 2015.

[98] Y. Wang and Q. Zhu, "Error control and concealment for video communication: a review," *Proceedings of the IEEE*, vol. 86, pp. 974–997, May 1998.

[99] Y. Huo, M. El-Hajjar, and L. Hanzo, "Inter-layer FEC aided unequal error protection for multilayer video transmission in mobile TV," *IEEE Transactions on Circuits and Systems for Video Technology*, vol. 23, pp. 1622–1634, Sept 2013.

[100] P. Pahalawatta, R. Berry, T. Pappas, and A. Katsaggelos, "Content-aware resource allocation and packet scheduling for video transmission over wireless networks," *IEEE Journal on Selected Areas in Communications*, vol. 25, pp. 749–759, May 2007.

[101] Y. Li, Z. Li, M. Chiang, and A. R. Calderbank, "Content-aware distortion-fair video streaming in congested networks," *IEEE Transactions on Multimedia*, vol. 11, pp. 1182–1193, Oct 2009.

[102] M. Ismail, W. Zhuang, and S. Elhedhli, "Energy and content aware multi-homing video transmission in heterogeneous networks," *IEEE Transactions on Wireless Communications*, vol. 12, pp. 3600–3610, July 2013.

[103] Y. Huo, T. Wang, R. G. Maunder, and L. Hanzo, "Motion-aware mesh-structured trellis for correlation modelling aided distributed multi-view video coding," *IEEE Transactions on Image Processing*, vol. 23, pp. 319–331, Jan 2014.

[104] D. Vukobratovic, V. Stankovic, D. Sejdinovic, L. Stankovic, and Z. Xiong, "Scalable video multicast using expanding window fountain codes," *IEEE Transactions on Multimedia*, vol. 11, pp. 1094–1104, Oct 2009.

[105] P. Li, H. Zhang, B. Zhao, and S. Rangarajan, "Scalable video multicast with adaptive modulation and coding in broadband wireless data systems," *IEEE/ACM Transactions on Networking*, vol. 20, pp. 57–68, Feb 2012.

[106] H. Zhou, Y. Ji, X. Wang, and B. Zhao, "Joint resource allocation and user association for SVC multicast over heterogeneous cellular networks," *IEEE Transactions on Wireless Communications*, vol. 14, pp. 3673–3684, July 2015.

[107] H. Schwarz, D. Marpe, and T. Wiegand, "Overview of the scalable video coding extension of the H.264/AVC standard," *IEEE Transactions on Circuits and Systems for Video Technology*, vol. 17, pp. 1103–1120, Sept 2007.

[108] C. Singhal, S. De, R. Trestian, and G. M. Muntean, "Joint optimization of user-experience and energy-efficiency in wireless multimedia broadcast," *IEEE Transactions on Mobile Computing*, vol. 13, pp. 1522–1535, July 2014.

[109] M. Ismail, W. Zhuang, and S. Elhedhli, "Energy and content aware multi-homing video transmission in heterogeneous networks," *IEEE Transactions on Wireless Communications*, vol. 12, pp. 3600–3610, July 2013.

[110] S. Chuah, Z. Chen, and Y. Tan, "Energy-efficient resource allocation and scheduling for multicast of scalable video over wireless networks," *IEEE Transactions on Multimedia*, vol. 14, pp. 1324–1336, Aug 2012.

[111] C. E. Shannon., "A mathematical theory of communication," *ACM SIGMOBILE Mobile Computing and Communications Review*, vol. 5, pp. 3–55, Jan. 2001.

[112] J. G. Andrews, S. Singh, Q. Ye, X. Lin, and H. Dhillon, "An overview of load balancing in hetnets: old myths and open problems," *IEEE Wireless Communications*, vol. 21, pp. 18–25, April 2014.

[113] T. Bu, L. Li, and R. Ramjee, "Generalized proportional fair scheduling in third generation wireless data networks," in *Proceedings of INFOCOM 2006*, pp. 1–12, Apr. 2006.

[114] L. Li, M. Pal, and Y. Yang, "Proportional fairness in multi-rate wireless LANs," in *Proceedings of INFOCOM 2008*, pp. 1–9, Apr. 2008.

[115] K. Son, S. Chong, and G. Veciana, "Dynamic association for load balancing and interference avoidance in multi-cell networks," *IEEE Transactions on Wireless Communications*, vol. 8, pp. 3566–3576, July 2009.

[116] H. Burchardt, S. Sinanovic, Z. Bharucha, and H. Haas, "Distributed and autonomous resource and power allocation for wireless networks," *IEEE Transactions on Communications*, vol. 61, no. 7, pp. 2758–2771, Jul. 2013.

[117] F. Heliot, M. A. Imran, and R. Tafazolli, "Low-complexity energy-efficient resource allocation for the downlink of cellular systems," *IEEE Transactions on Communications*, vol. 61, no. 6, pp. 2271–2281, Jun. 2013.

[118] M. Ismail and W. Zhuang, "A distributed multi-service resource allocation algorithm in heterogeneous wireless access medium," *IEEE Journal on Selected Areas in Communications*, vol. 30, no. 2, pp. 425–432, Feb. 2012.

[119] Q. Ye, B. Rong, Y. Chen, M. Al-Shalash, C. Caramanis, and J. G. Andrews, "User association for load balancing in heterogeneous cellular networks," *IEEE Transactions on Wireless Communications*, vol. 12, pp. 2706–2716, June 2013.

[120] D. P. Palomar and M. Chiang, "A tutorial on decomposition methods for network utility maximization," *IEEE Journal on Selected Areas in Communications*, vol. 24, no. 8, pp. 1439–1451, Aug. 2006.

[121] D. P. Bertsekas, "Nonlinear programming," 1999.

[122] S. P. Boyd and L. Vandenberghe, *Convex optimization*. Cambridge University Press, 2004.

[123] H. Haas, L. Yin, Y. Wang, and C. Chen, "What is LiFi?," *Journal of Lightwave Technology*, vol. 34, pp. 1533–1544, March 2016.

[124] B. V. Quang, R. V. Prasad, and I. Niemegeers, "A survey on handoffs: Lessons for 60 GHz based wireless systems," *IEEE Communications Surveys & Tutorials*, vol. 14, pp. 64–86, First 2012.

[125] S. K. Ray, K. Pawlikowski, and H. Sirisena, "Handover in mobile WiMAX networks: The state of art and research issues," *IEEE Communications Surveys & Tutorials*, vol. 12, pp. 376–399, Third 2010.

[126] D. Xenakis, N. Passas, L. Merakos, and C. Verikoukis, "Mobility management for femtocells in LTE-Advanced: Key aspects and survey of handover decision algorithms," *IEEE Communications Surveys & Tutorials*, vol. 16, pp. 64–91, First 2014.

[127] A. M. Vegni and T. D. C. Little, "Handover in VLC systems with cooperating mobile devices," in *2012 International Conference on Computing, Networking and Communications*, pp. 126–130, Jan 2012.

[128] M. B.Rahaim, A. M. Vegni, and T. D. C. Little, "A hybrid radio frequency and broadcast visible light communication system," in *IEEE GLOBECOM Workshops 2011*, pp. 792–796, Dec. 2011.

[129] S. Liang, H. Tian, B. Fan, and R. Bai, "A novel vertical handover algorithm in a hybrid visible light communication and LTE system," in *2015 IEEE 82nd Vehicular Technology Conference*, pp. 1–5, Sept 2015.

[130] J. Hou and D. C. O'Brien, "Vertical handover-decision-making algorithm using fuzzy logic for the integrated radio-and-OW system," *IEEE Transactions on Wireless Communications*, vol. 5, pp. 176–185, Jan 2006.

[131] F. Wang, Z. Wang, C. Qian, L. Dai, and Z. Yang, "Efficient vertical handover scheme for heterogeneous VLC-RF systems," *IEEE/OSA Journal of Optical Communications and Networking*, vol. 7, pp. 1172–1180, Dec 2015.

[132] H. Wymeersch, J. Lien, and M. Z. Win, "Cooperative localization in wireless networks," *Proceedings of the IEEE*, vol. 97, pp. 427–450, Feb 2009.

[133] K. Chintalapudi, A. P. Iyer, and V. N. Padmanabhan, "Indoor localization without the pain," in *Proceedings of the Sixteenth Annual International Conference on Mobile Computing and Networking*, MobiCom '10, (New York, NY, USA), pp. 173–184, ACM, 2010.

[134] L. Li, P. Hu, C. Peng, G. Shen, and F. Zhao, "Epsilon: A visible light based positioning system," in *11th USENIX Symposium on Networked Systems Design and Implementation*, pp. 331–343, 2014.

[135] S. Y. Jung, S. Hann, and C. S. Park, "TDOA-based optical wireless indoor localization using LED ceiling lamps," *IEEE Transactions on Consumer Electronics*, vol. 57, pp. 1592–1597, November 2011.

[136] H. S. Kim, D. R. Kim, S. H. Yang, Y. H. Son, and S. K. Han, "An indoor visible light communication positioning system using a RF carrier allocation technique," *Journal of Lightwave Technology*, vol. 31, pp. 134–144, Jan 2013.

[137] J. Armstrong, Y. A. Sekercioglu, and A. Neild, "Visible light positioning: a roadmap for international standardization," *IEEE Communications Magazine*, vol. 51, pp. 68–73, December 2013.

[138] S. Yang, H. S. Kim, Y. H. Son, and S. K. Han, "Three-dimensional visible light indoor localization using AOA and RSS with multiple optical receivers," *Journal of Lightwave Technology*, vol. 32, pp. 2480–2485, July 2014.

[139] Y. Hou, S. Xiao, H. Zheng, and W. Hu, "Multiple access scheme based on block encoding time division multiplexing in an indoor positioning system using visible light," *IEEE/OSA Journal of Optical Communications and Networking*, vol. 7, pp. 489–495, May 2015.

[140] M. Yasir, S. W. Ho, and B. N. Vellambi, "Indoor position tracking using multiple optical receivers," *Journal of Lightwave Technology*, vol. 34, pp. 1166–1176, Feb 2016.

[141] W. Xu, J. Wang, H. Shen, H. Zhang, and X. You, "Indoor positioning for multiphotodiode device using visible-light communications," *IEEE Photonics Journal*, vol. 8, pp. 1–11, Feb 2016.

[142] H. Liu and G. Pang, "Positioning beacon system using digital camera and LEDs," *IEEE Transactions on Vehicular Technology*, vol. 52, pp. 406–419, March 2003.

[143] C. Li and S. Shimamoto, "An open traffic light control model for reducing vehicles CO_2 emissions based on ETC vehicles," *IEEE Transactions on Vehicular Technology*, vol. 61, pp. 97–110, Jan 2012.

[144] I. Takai, S. Ito, K. Yasutomi, K. Kagawa, M. Andoh, and S. Kawahito, "LED and CMOS image sensor based optical wireless communication system for automotive applications," *IEEE Photonics Journal*, vol. 5, pp. 6801418–6801418, Oct 2013.

[145] S. H. Yu, O. Shih, H. M. Tsai, N. Wisitpongphan, and R. D. Roberts, "Smart automotive lighting for vehicle safety," *IEEE Communications Magazine*, vol. 51, pp. 50–59, December 2013.

[146] T. Yamazato, I. Takai, H. Okada, T. Fujii, T. Yendo, S. Arai, M. Andoh, T. Harada, K. Yasutomi, K. Kagawa, and S. Kawahito, "Image-sensor-based visible light communication for automotive applications," *IEEE Communications Magazine*, vol. 52, pp. 88–97, July 2014.

[147] T. Yamazato, M. Kinoshita, S. Arai, E. Souke, T. Yendo, T. Fujii, K. Kamakura, and H. Okada, "Vehicle motion and pixel illumination modeling for image sensor based visible light communication," *IEEE Journal on Selected Areas in Communications*, vol. 33, pp. 1793–1805, Sept 2015.

[148] M. Uysal, Z. Ghassemlooy, A. Bekkali, A. Kadri, and H. Menouar, "Visible light communication for vehicular networking: Performance study of a V2V system using a measured headlamp beam pattern model," *IEEE Vehicular Technology Magazine*, vol. 10, pp. 45–53, Dec 2015.

[149] A. M. Cailean and M. Dimian, "Toward environmental-adaptive visible light communications receivers for automotive applications: A review," *IEEE Sensors Journal*, vol. 16, pp. 2803–2811, May 2016.

[150] B. Zhang, K. Ren, G. Xing, X. Fu, and C. Wang, "SBVLC: Secure barcode-based visible light communication for smartphones," *IEEE Transactions on Mobile Computing*, vol. 15, pp. 432–446, Feb 2016.

[151] J. Rufo, J. Rabadan, F. Delgado, C. Quintana, and R. Perez-Jimenez, "Experimental evaluation of video transmission through LED illumination devices," *IEEE Transactions on Consumer Electronics*, vol. 56, pp. 1411–1416, Aug 2010.

[152] T. Komine and M. Nakagawa, "Integrated system of white LED visible-light communication and power-line communication," *IEEE Transactions on Consumer Electronics*, vol. 49, pp. 71–79, Feb 2003.

[153] J. Song, W. Ding, F. Yang, H. Yang, B. Yu, and H. Zhang, "An indoor broadband broadcasting system based on PLC and VLC," *IEEE Transactions on Broadcasting*, vol. 61, pp. 299–308, June 2015.

[154] T. Nguyen, M. Z. Chowdhury, and Y. M. Jang, "A novel link switching scheme using prescanning and RSS prediction in visible light communication networks," *EURASIP Journal on Wireless Communications and Networking*, vol. 2013, no. 1, pp. 1–17, 2013.

[155] T. Komine and M. Nakagawa, "A study of shadowing on indoor visible-light wireless communication utilizing plural white LED lightings," in *1st International Symposium on Wireless Communication Systems*, pp. 36–40, Sept 2004.

[156] H. J. Kushner and P. A. Whiting, "Convergence of proportional-fair sharing algorithms under general conditions," *IEEE Transactions on Wireless Communications*, vol. 3, pp. 1250–1259, July 2004.

[157] J. Akhtman and L. Hanzo, "Power versus bandwidth-efficiency in wireless communications: The economic perspective," in *IEEE VTC 2009*, pp. 1–5, Sep. 2009.

[158] H. W. Kuhn, "The Hungarian method for the assignment problem," *Naval research logistics quarterly*, vol. 2, pp. 83–97, Mar. 1955.

[159] J. Munkres, "Algorithms for the assignment and transportation problems," *Journal of the Society for Industrial & Applied Mathematics*, vol. 5, pp. 32–38, Mar. 1957.

[160] F. Bourgeois and J. Lassalle, "An extension of the Munkres algorithm for the assignment problem to rectangular matrices," *Communications of the ACM*, vol. 14, pp. 802–804, Dec. 1971.

[161] M. M. Halldórsson and J. Radhakrishnan, "Greed is good: Approximating independent sets in sparse and bounded-degree graphs," *Algorithmica*, vol. 18, no. 1, pp. 145–163, May 1997.

[162] K. Zheng, F. Liu, Q. Zheng, W. Xiang, and W. Wang, "A graph-based cooperative scheduling scheme for vehicular networks," *IEEE Transactions on Vehicular Technology*, vol. 62, pp. 1450–1458, May 2013.

[163] X. Li, J. Vucic, V. Jungnickel, and J. Armstrong, "On the capacity of intensity-modulated direct-detection systems and the information rate of ACO-OFDM for indoor optical wireless applications," *IEEE Transactions on Communications*, vol. 60, no. 3, pp. 799–809, Mar. 2012.

[164] R. Mesleh, H. Elgala, and H. Haas, "On the performance of different OFDM based optical wireless communication systems," *IEEE/OSA Journal of Optical Communications and Networking*, vol. 3, no. 8, pp. 620–628, Aug. 2011.

[165] J. Armstrong, "OFDM for optical communications," *Journal of Lightwave Technology*, vol. 27, no. 3, pp. 189–204, Feb. 2009.

[166] H. Le-Minh, D. O'Brien, G. Faulkner, L. Zeng, K. Lee, D. Jung, Y. Oh, and E. T. Won, "100-Mb/s NRZ visible light communications using a postequalized white LED," *IEEE Photonics Technology Letters*, vol. 21, no. 15, pp. 1063–1065, Aug. 2009.

[167] Y. Wang, S. Videv, and H. Haas, "Dynamic load balancing with handover in hybrid Li-Fi and Wi-Fi networks," in *2014 IEEE 25th Annual International Symposium on Personal, Indoor, and Mobile Radio Communication (PIMRC)*, pp. 575–579, Sept 2014.

[168] C. Chen, N. Serafimovski, and H. Haas, "Fractional frequency reuse in optical wireless cellular networks," in *IEEE PIMRC 2013*, pp. 3594–3598, Sep. 2013.

[169] C. Chen, D. Tsonev, and H. Haas, "Joint transmission in indoor visible light communication downlink cellular networks," in *IEEE GLOBECOM Workshops 2013*, pp. 1127–1132, Dec. 2013.

[170] F. Jin, R. Zhang, and L. Hanzo, "Resource allocation under delay-guarantee constraints for heterogeneous visible-light and RF femtocell," *IEEE Transactions on Wireless Communications*, vol. 14, pp. 1020–1034, Feb 2015.

[171] H. Zhang and H. Dai, "Cochannel interference mitigation and cooperative processing in downlink multicell multiuser MIMO networks," *EURASIP Journal on Wireless Communications and Networking*, vol. 2004, no. 2, pp. 222–235, Dec. 2004.

[172] R. Zhang and L. Hanzo, "Cooperative downlink multicell preprocessing relying on reduced-rate back-haul data exchange," *IEEE Transactions on Vehicular Technology*, vol. 60, pp. 539–545, Feb. 2011.

[173] F. Kelly, "Charging and rate control for elastic traffic," *European Transactions on Telecommunications*, vol. 8, no. 1, pp. 33–37, 1997.

[174] B. Bensaou, D. H. K. Tsang, and K. T. Chan, "Credit-based fair queueing (CBFQ): a simple service-scheduling algorithm for packet-switched networks," *IEEE/ACM Transactions on Networking*, vol. 9, pp. 591–604, Oct. 2001.

[175] D. O'Brien, H. Haas, S. Rajbhandari, H. Chun, G. Faulkner, K. Cameron, A. V. N. Jalajakumari, R. Henderson, D. Tsonev, and M. Ijaz, "Integrated multiple-input multiple-output visible light communications systems: recent progress and results," in *SPIE OPTO*, pp. 93870P–93870P, 2015.

[176] D. Tsonev, S. Videv, and H. Haas, "Towards a 100 Gb/s visible light wireless access network," *Optics Express*, vol. 23, pp. 1627–1637, Jan 2015.

[177] D. Tsonev, H. Chun, S. Rajbhandari, J. J. D. McKendry, S. Videv, E. Gu, M. Haji, S. Watson, A. E. Kelly, G. Faulkner, M. D. Dawson, H. Haas, and D. O'Brien, "A 3-Gb/s single-LED OFDM-based wireless VLC link using a gallium nitride μLED," *IEEE Photonics Technology Letters*, vol. 26, pp. 637–640, April 2014.

[178] C. I, C. Rowell, S. Han, Z. Xu, G. Li, and Z. Pan, "Toward green and soft: a 5G perspective," *IEEE Communications Magazine*, vol. 52, pp. 66–73, February 2014.

[179] P. A. Haigh, F. Bausi, H. Minh, I. Papakonstantinou, W. O. Popoola, A. Burton, and F. Cacialli, "Wavelength-multiplexed polymer LEDs: Towards 55 Mb/s organic visible light communications," *IEEE Journal on Selected Areas in Communications*, vol. 33, pp. 1819–1828, Sept 2015.

[180] S. Zhang, D. Tsonev, S. Videv, S. Ghosh, G. A. Turnbull, I. D. W. Samuel, and H. Haas, "Organic solar cells as high-speed data detectors for visible light communication," *Optica*, vol. 2, pp. 607–610, Jul 2015.

[181] P. Haigh, A. Burton, K. Werfli, H. L. Minh, E. Bentley, P. Chvojka, W. O. Popoola, I. Papakonstantinou, and S. Zvanovec, "A multi-CAP visible-light communications system with 4.85-b/s/Hz spectral efficiency," *IEEE Journal on Selected Areas in Communications*, vol. 33, pp. 1771–1779, Sept 2015.

[182] A. Yang, Y. Wu, M. Kavehrad, and G. Ni, "Grouped modulation scheme for LED array module in a visible light communication system," *IEEE Wireless Communications*, vol. 22, pp. 24–28, April 2015.

[183] A. Nuwanpriya, S. Ho, and C. Chen, "Indoor MIMO visible light communications: Novel angle diversity receivers for mobile users," *IEEE Journal on Selected Areas in Communications*, vol. 33, pp. 1780–1792, Sept 2015.

[184] I. Din and H. Kim, "Energy-efficient brightness control and data transmission for visible light communication," *IEEE Photonics Technology Letters*, vol. 26, pp. 781–784, April 2014.

[185] S. Kim and S. Jung, "Modified Reed-Muller coding scheme made from the bent function for dimmable visible light communications," *IEEE Photonics Technology Letters*, vol. 25, pp. 11–13, Jan 2013.

[186] Y. Suh, C. Ahn, and J. K. Kwon, "Dual-codeword allocation scheme for dimmable visible light communications," *IEEE Photonics Technology Letters*, vol. 25, pp. 1274–1277, July 2013.

[187] S. Shao, A. Khreishah, and I. Khalil, "Joint link scheduling and brightness control for greening VLC-based indoor access networks," *arXiv preprint arXiv:1510.00026*, 2015.

[188] U. Hammes, E. Wolsztynski, and A. M. Zoubir, "Robust tracking and geolocation for wireless networks in NLOS environments," *IEEE Journal of Selected Topics in Signal Processing*, vol. 3, pp. 889–901, Oct 2009.

[189] A. Kushki, K. N. Plataniotis, and A. N. Venetsanopoulos, "Intelligent dynamic radio tracking in indoor wireless local area networks," *IEEE Transactions on Mobile Computing*, vol. 9, pp. 405–419, March 2010.

[190] R. Mesleh, H. Elgala, and H. Haas, "Performance analysis of indoor OFDM optical wireless communication systems," in *2012 IEEE WCNC*, pp. 1005–1010, April 2012.

[191] S. Martello and P. Toth, *Knapsack problems: algorithms and computer implementations*. John Wiley & Sons, Inc., 1990.

[192] Y. J. Yu, P. C. Hsiu, and A. C. Pang, "Energy-efficient video multicast in 4G wireless systems," *IEEE Transactions on Mobile Computing*, vol. 11, pp. 1508–1522, Oct 2012.

[193] J. B. Hwang and C. Y. Lee, "Effective video multicast using SVC with heterogeneous user demands over TDMA-based wireless mesh networks," *IEEE Transactions on Mobile Computing*, vol. 12, pp. 984–994, May 2013.

Subject Index

V

W

Z

Author Index

D

E

F

G

H

I

J

K

L

M

N

O

P

Q

R

S

X

Y

Z